Understanding the regulation of the ubiquitin-conjugating enzyme UBE2S

Die Regulation des Ubiquitin-konjugierenden Enzyms UBE2S

Doctoral thesis

for a doctoral degree at the Graduate School of Life Sciences,
Julius-Maximilians-Universität Würzburg,
Section Biomedicine

submitted by

Anna Katharina Luise Liess, née Eller
from Darmstadt, Germany

Würzburg 2020

Submitted on: ……...

Office stamp

Members of the Thesis Committee

Chairperson:	**Prof. Dr. Christoph Sotriffer**
Primary Supervisor:	Dr. Sonja Lorenz
Supervisor (Second):	Dr. Jörg Mansfeld
Supervisor (Third):	Prof. Dr. Hermann Schindelin

Date of Public Defence: ……...

Date of Receipt of Certificates: ……...

Für Andreas und meine Eltern,
in unendlicher Dankbarkeit.

Summary

The ubiquitination of proteins serves as molecular signal to control an enormous number of physiological processes and its dysregulation is connected to human diseases like cancer. The versatility of this signal stems from the diverse ways by which ubiquitin can be attached to its targets. Thus, specificity and tight regulation of the ubiquitination are pivotal requirements of ubiquitin signaling. Ubiquitin-conjugating enzymes (E2s) act at the heart of the ubiquitination cascade, transferring ubiquitin from a ubiquitin-activating enzyme (E1) to a ubiquitin ligase (E3) or substrate. When cooperating with a RING-type E3, ubiquitin-conjugating enzymes can determine linkage specificity in ubiquitin chain formation. Our understanding of the regulation of E2 activities is still limited at a structural level.

The work described here identifies two regulation mechanisms in UBE2S, a cognate E2 of the human RING-type E3 anaphase-promoting complex/cyclosome (APC/C). UBE2S elongates ubiquitin chains on APC/C substrates in a Lys11 linkage-specific manner, thereby targeting these substrates for degradation and driving mitotic progression. In addition, UBE2S was found to have a role in DNA repair by enhancing non-homologous end-joining (NHEJ) and causing transcriptional arrest at DNA damage sites in homologous recombination (HR). Furthermore, UBE2S overexpression is a characteristic feature of many cancer types and is connected to poor prognosis and diminished response to therapy.

The first regulatory mechanism uncovered in this thesis involves the intramolecular auto-ubiquitination of a particular lysine residue (Lys^{+5}) close to the active site cysteine, presumably through conformational flexibility of the active site region. The Lys^{+5}-linked ubiquitin molecule adopts a donor-like, ‘closed’ orientation towards UBE2S, thereby conferring auto-inhibition. Notably, Lys^{+5} is a major physiological ubiquitination site in ~25% of the human E2 enzymes, thus providing regulatory opportunities beyond UBE2S. Besides the active, monomeric state and the auto-inhibited state caused by auto-ubiquitination, I discovered that UBE2S can adopt a dimeric state. The latter also provides an auto-inhibited state, in which ubiquitin transfer is blocked via the obstruction of donor binding. UBE2S dimerization is promoted by its unique C-terminal extension, suppresses auto-ubiquitination and thereby the proteasomal degradation of UBE2S.

Taken together, the data provided in this thesis illustrate the intricate ways by which UBE2S activity is fine-tuned and the notion that structurally diverse mechanisms have evolved to restrict the first step in the catalytic cycle of E2 enzymes.

Zusammenfassung

Die Ubiquitinierung von Proteinen fungiert als molekulares Signal zur Kontrolle einer Vielzahl physiologischer Prozesse, wobei eine gestörte Regulation der Ubiquitinierung eng mit zahlreichen Erkrankungen, wie beispielsweise Krebs, verbunden ist. Aufgrund der verschiedenen Verknüpfungsmöglichkeiten von Ubiquitin, die das zelluläre Schicksal des Zielproteins bestimmen, sind Spezifität und stringente Regulation unabkömmliche Voraussetzungen im Ubiquitinierungsprozess.

Ubiquitin-konjugierende Enzyme (E2s) fungieren in der Mitte der Ubiquitinierungskaskade. Sie übernehmen ein Ubiquitinmolekül vom Ubiquitin-aktivierenden Enzym (E1) und übertragen es auf eine Ubiquitin-Ligase (E3) oder direkt auf das Zielprotein. Arbeiten Ubiquitin-konjugierende Enzyme mit E3s des RING-Typus zusammen, so bestimmen E2s die Art der Verknüpfung. Die Regulation der Aktivität Ubiquitin-konjugierender Enzyme auf struktureller Ebene ist jedoch bisher nur bedingt verstanden.

Die hier dargelegte Arbeit umfasst die Identifizierung zweier Regulationsmechanismen des Ubiquitin-konjugierenden Enzyms UBE2S. UBE2S arbeitet mit einem humanen E3 des RING-Typus, dem ‚Anaphase Promoting Complex/Cyclosome' (APC/C) zusammen und bildet Lys11-spezifische Ubiquitinketten auf Substraten des APC/Cs. Hierdurch werden die Substrate für den Abbau durch das Proteasom markiert, was das Fortschreiten der Mitose bedingt. Zusätzlich wird UBE2S eine Rolle in der DNS-Reparatur zugeschrieben. Hierbei verstärkt UBE2S die nicht-homologe Rekombination (NHEJ) und verhindert außerdem die Transkription an DNS-Bruchstellen, die durch Homologe Rekombination (HR) repariert werden. Die Überexpression von UBE2S ist ein Charakteristikum verschiedenster Krebsarten, vermindert den Erfolg herkömmlicher Krebstherapien, und führt somit zu schlechten Prognosen für betroffenen Patienten.

Der erste hier beschriebene Regulationsmechanismus beinhaltet die intramolekulare Ubiquitinierung eines Lysins (Lys^{+5}) nahe des katalytischen Cysteins, mutmaßlich durch strukturelle Flexibilität der Region des aktiven Zentrums. Das Lys^{+5}-verknüpfte Ubiquitin nimmt eine Donorubiquitin-ähnliche Position auf UBE2S ein, wodurch UBE2S gehemmt wird. Da ein Lysin an der Position +5 in ~25% der humanen E2-Enzyme vorhanden und eine physiologische Ubiquitinierungsstelle ist, birgt dieser Mechanismus Regulationsmöglichkeiten über UBE2S hinaus. Zusätzlich zum aktiven monomeren Zustand und dem durch Autoubiquitinierung ausgelösten inhibierten Zustand, kann UBE2S auch als Dimer vorliegen. In diesem Zustand ist es ebenfalls inaktiv, da die

Donorubiquitin-Bindestelle auf UBE2S durch ein zweites Molekül des E2s blockiert wird. Begünstigt wird die Dimerisierung durch die C-terminale Verlängerung von UBE2S und verhindert so deren Autoubiquitinierung, und folglich den proteasomalen Abbau von UBE2S. Es handelt sich hierbei somit um einen zweiten Regulationsmechanismus von UBE2S.

Zusammenfassend veranschaulichen die in dieser Arbeit dargelegten Daten die komplexen Möglichkeiten, durch die die Aktivität von UBE2S reguliert werden kann, sowie die Erkenntnis, dass strukturell unterschiedliche Mechanismen existieren, um den ersten Schritt der von Ubiquitin-konjugierenden Enzymen katalysierten Reaktion zu hemmen.

Table of contents

1. Introduction

Ever since Rudolf Virchow stated his hypothesis **"***Omnis cellula e cellula"* [1] – all cells come from cells – a main interest of life scientists has been to understand cells, the cell cycle and its regulation as well as the potential pathogenic consequences of these mechanisms on a molecular level. The discovery of the proteasomal degradation of proteins by the post-translational modification with ubiquitin, for which Aaron J. Ciechanover, Avram Hershko and Irwin Rose were awarded the Nobel Prize in Chemistry in 2004 was a milestone.

But ubiquitination does not only regulate the degradation of proteins, it plays a role in nearly every cellular process, because it controls the lifetimes, conformational dynamics, as well as the localization and interaction patterns of eukaryotic proteins [2]. Thus, its dysregulation leads to neurological diseases and is found in many cancer types, among many other human pathologies. Therefore, it is of particular importance to study the ubiquitination cascade and its regulation to ultimately understand and efficiently treat human disease.

The modification with ubiquitin proceeds through a three-step enzymatic cascade, wherein ubiquitin-conjugating enzymes (E2s) cooperate with their respective ubiquitin ligases (E3s), to mediate the isopetide formation of the C-terminus of ubiquitin with a primary amino group of the target protein. Whereas the molecular mechanisms of many human E2s are studied at a molecular level, their regulation is incompletely understood. Thus, the question of whether the human ubiquitin-conjugating enzyme UBE2S is regulated by mechanisms other than E3-enhanced auto-ubiquitination and degradation at the end of the cell cycle [3], namely on the E2 level, was not answered.

My structural and mechanistic work on UBE2S lays the foundation for understanding the different layers of regulation of a highly important enzyme, functioning in cell cycle regulation [3–6] and DNA repair [7,8], whose upregulation is found in many cancer types and is associated with a poor response to therapeutics [8–10]. Also common principles for the regulation of ubiquitin-conjugating enzymes can be derived from my work.

1.1 The ubiquitin conjugating system

Ubiquitin is a small globular protein comprised of 76 amino acids (Figure 1A) that is ubiquitously expressed in eukaryotic cells. Ubiquitination describes the process of modifying a cellular target protein with ubiquitin by the ubiquitination machinery [11]. This machinery consists of ubiquitin-activating enzyme (E1) that activates ubiquitin and transfers it in a thioester transfer reaction to the catalytic cysteine of a ubiquitin-conjugating enzyme (E2) [12,13]. The E2 then cooperates with a ubiquitin ligase (E3), to mediate isopeptide formation of the C-terminus of ubiquitin with a primary amino group of a target protein. When the E2 interacts with a 'Homologous to the E6-AP Carboxyl Terminus' (HECT) or 'RING-between-RING' (RBR)-type E3, the ubiquitin is first transferred to the catalytic cysteine of the E3 and subsequently passed to the target protein. On the contrary, in case of 'Really Interesting New Gene' (RING)-type E3s, the E3 works as a scaffold and the ubiquitin moiety is directly transferred to the primary amino group of the target protein (Figure 1B). The target is either mono-ubiquitinated or multi-mono-ubiquitinated (I), because ubiquitin cannot only be attached to a target protein, but also to one of its seven lysine residues or its free N-terminus (Met1; Figure 1A). This allows for the formation with homotypic (II) or heterotypic (III) ubiquitin chains (Figure 1B, [14]), in which the ubiquitin molecules are linked by (iso)peptides between the primary amino group of one ubiquitin molecule and the C-terminus of another ubiquitin molecule.

The E3 mediates substrate recognition, and together with its respective E2, linkage specificity. However, the structural mechanisms are not completely understood. All components together allow for the extraordinary versatility of ubiquitin as a molecular signal because the different modification types serve as protein-protein interaction platforms that elicit distinct signaling functions [2]. It was shown that mono-ubiquitination has a function in chromatin remodeling [15] and DNA repair [16], Lys11- and Lys48-linked ubiquitin chains as well as their branched form lead to the proteasomal degradation of the target protein [17–19], and Lys27 linkages are involved in the DNA damage response [20] and in innate immunity [21]. Ubiquitin chains linked via Lys29 are found to repress Wnt/β-catenin signaling [22], although the regulation of this pathway also involves Lys48 and Lys63 linkages at several steps [23]. Lys63-linked ubiquitin chains are found to directly target proteins to the endocytotic pathway [24] and to function in the regulation of the NF-κB pathway [25], which is also regulated by liner ubiquitin chains (linked via Met1) in inflammatory and immune responses [26].

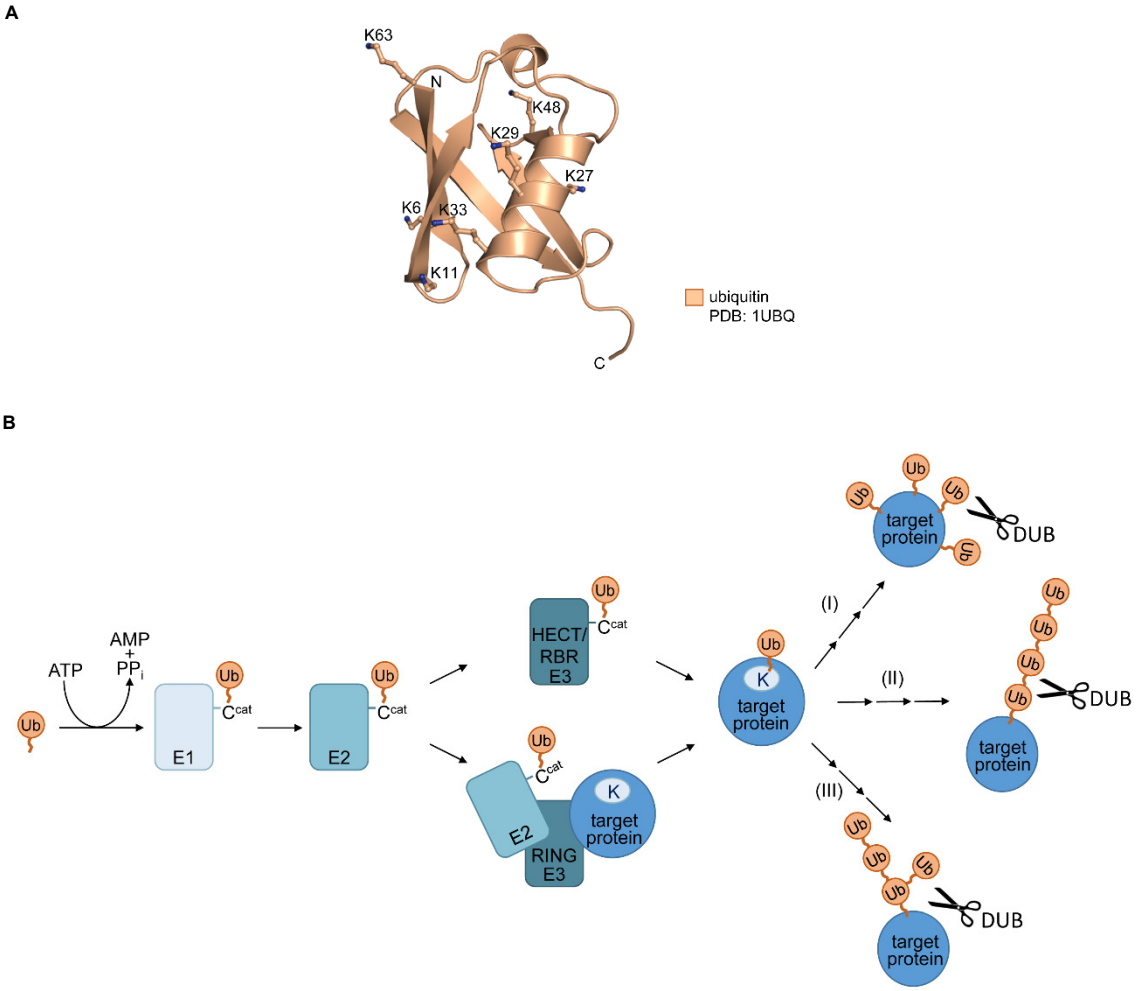

Figure 1: Ubiquitin and its conjugation system. (A) Crystal structure of ubiquitin (PDB: 1UBQ, [27]) shown in ribbon representation with the lysine side chains shown in ball-and-stick-representation. The N-terminus and the lysine side chains represent potential linkage sites with another ubiquitin molecule to form ubiquitin chains. (B) Ubiquitin is conjugated to its target by the sequential action of three enzymes. The ubiquitin-activating enzyme (E1) activates ubiquitin in an ATP-dependent manner and catalyzes the thioester formation between its catalytic cysteine (C^{cat}) and the C-terminal glycine of ubiquitin, as well as the thioester transfer to the ubiquitin-conjugating enzyme (E2). In the next step the ubiquitin ligase (E3) facilitates the ubiquitin transfer from the E2 to a substrate, either directly (in case of 'Really Interesting New Gene' (RING) ligases) or through an E3-ubiquitin intermediate (in case of 'Homologous to E6AP C-Terminus' (HECT) or 'RING-between-RING' (RBR) ligases). The target can be modified with one or multiple ubiquitin molecules. For the latter, one discriminates multi-mono-ubiquitination (I), homotopic ubiquitin chains (II) and heterotypic ubiquitin chains (III). The modification with ubiquitin can be reversed by the action of deubiquitinating enzymes (DUBs).

In addition, the diverse ubiquitin code can be expanded by other posttranslational modifications. Phosphorylation of ubiquitin at Ser65 activates the E3 Parkin allosterically [28] and affects ubiquitin chain assembly and hydrolysis [29], whereas acetylation at Lys11 of the ubiquitin-like SUMO2 modifier favors the formation of non-canonical SUMO chains under basal and stress conditions [30]. The pathogen *Legionella pneumophila* has developed a ubiquitin modification to hijack the eukaryotic ubiquitin system to establish its replicative niche. Therefore, they phosphoribosylate ubiquitin at Arg42 and attach it to a serine residue of the substrate, which is required for replication in host cells and prevents the activation of E1 and E2 enzymes of the conventional ubiquitination cascade [31,32].
Ubiquitination can be reversed by the action of deubiquitinating enzymes (DUBs, Figure 1), which makes it a highly dynamic modification, as required for the regulation of protein levels and activity [33].

Understanding the ubiquitin system mechanistically is of high importance, because components of this system can be used as drug targets [34,35]. Bortezomib (PS341, Velcade) and carfilzomib (PR-171, Kyprolis) are extraordinary potent proteasome inhibitors that are successfully used for the treatment of multiple myoloma [36–39]. Proteasome inhibitors shut down protein degradation globally. Although they are highly efficient, it can be advantageous to target E2 or E3 enzymes to generate higher specificity and fewer side effects. Examples therefore are the immune modulators (IMiDs) lenalidomide and pomalidomide that are thalidomide derivates. They reprogram Cereblon (CRBN), a substrate receptor of the E3 ligase complex $CRL4^{CRBN}$, to ubiquitinate the transcription factors IKZF1 and IKZF3 (Ikaros family zinc finger protein 1 and 3), while the ubiquitination of the endogenous substrates is assumed to be blocked [40–42].

Another promising concept in drug discovery are PROTACs, proteolysis targeting chimeras, that do not target the ubiquitination pathway in a classical way but hijack it to induce the ubiquitination and subsequent degradation of a protein of interest (POI) [43–45]. PROTACs are hetero-bifunctional molecules composed of a POI ligand and an E3 ligand, connected by a linker. The formation of a ternary complex of the POI with the PROTAC and the E3 induces the ubiquitination of the POI by the E3. The ubiquitinated POI is recognized by the 26S proteasome and subsequently degraded. This concept may allow for the targeting not only of enzymatically active proteins, but also of those, considered undruggable, such as scaffolding proteins [46].

1.2 Ubiquitin-conjugating enzymes

The family of human ubiquitin-conjugating enzymes (E2s) is comprised of ~40 members that are in average only twice the size of ubiquitin (~14-35 kDa [47]) and share a conserved catalytic core domain (UBC). They are sub-grouped into four classes: E2s in class I contain the catalytic domain only, whereas E2s in class II have an N-terminal extension. E2s in class III contain a C-terminal extension and E2s in class IV have both. An overview of the ubiquitin conjugating enzymes and their classification is shown in Figure 2.

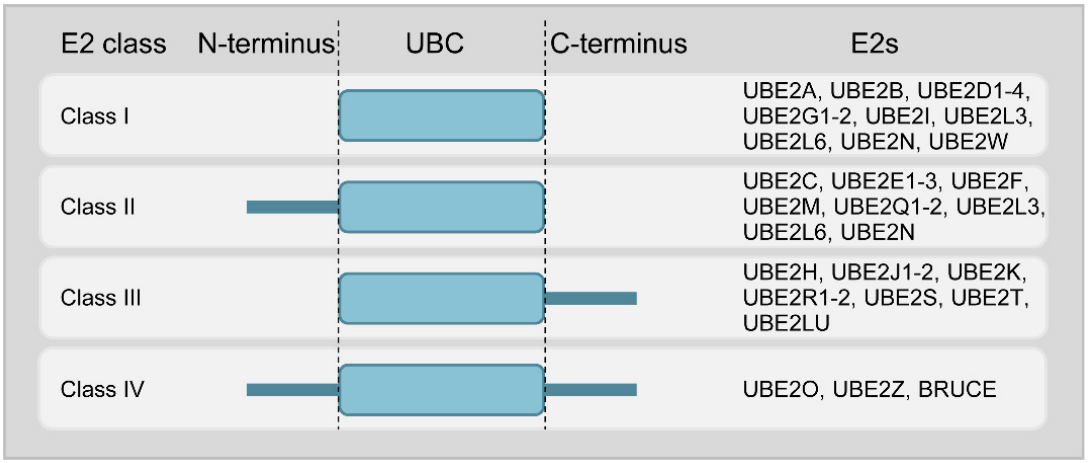

Figure 2: Classification of ubiquitin-conjugating enzymes (E2s). The E2s are classified upon the absence (class I) or presence of an N-terminal (class II) or C-terminal (class III) extension. Class IV E2s have extensions at the N- and C-terminus. The figure is adapted from [47].

The UBC domain has a canonical α/β-fold with four α-helices and four β-strands, connected by loops (Figure 3). It contains the active-site region with the catalytic cysteine residue (C^{cat}) and is therefore needed for catalytic activity. In addition, the UBC domain harbors binding sites for the E1 and E3 enzymes that are partially overlapping, thus ensuring the correct timing of the reactions carried out by the E2s [48–50]. The binding of ubiquitin also occurs via the UBC domain, including a site for non-canonical ubiquitin backside binding (grey; further discussed in 1.2.1) as well as the conserved donor ubiquitin binding site (orange circle, Figure 3).

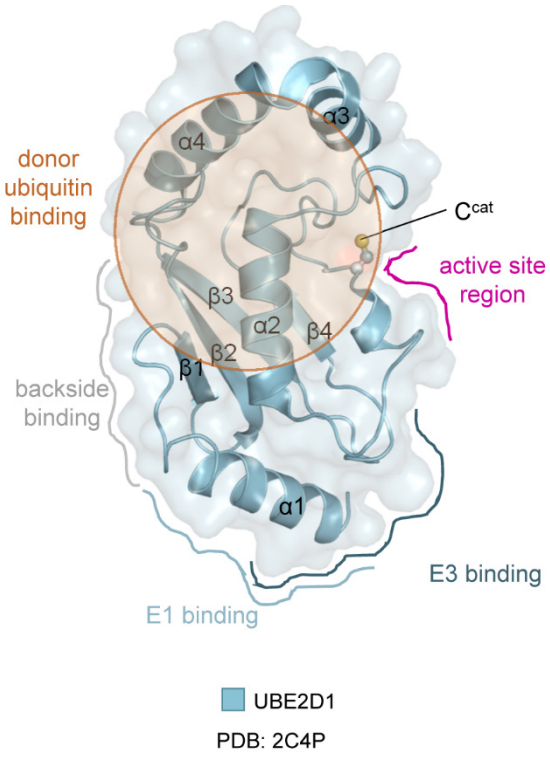

Figure 3: Structural representation of the catalytic core domain (UBC) of an E2. The crystal structure of UBE2D1 (PDB: 2C4P) is depicted in ribbon-and-surface representation. Highlighted are the active-site region (pink) with the catalytic cysteine (C^{Cat}) in ball-and-stick representation, the E1 and E3 binding sites as well as the backside for non-covalent ubiquitin binding. The orange circle represents the donor ubiquitin binding site.

The various interaction sites for ubiquitin reflect the complexity of the activity of E2 enzymes. They act in the middle of the ubiquitination cascade, where they receive a ubiquitin from the E1 and subsequently transfer it to the E3. In the first step, the C-terminal glycine of ubiquitin is thioester-linked to the catalytic cysteine of the E2. In the second step, the E2 transfers ubiquitin to the catalytic cysteine of a HECT- or RBR-E3 or it interacts with a RING E3 to transfer ubiquitin to a lysine residue of the target protein, resulting in an isopetide linkage. In the latter case, the RING E3 works as a scaffold to bring the charged E2 and the substrate in close proximity so that the ubiquitin can be transferred. When interacting with RING-type E3s, the specific interaction of ubiquitin with the catalytic domain of the E2, known as ‘closed conformation’ (Figure 4), is of immense importance. In this state, the C-terminus of ubiquitin is covalently linked to the catalytic cysteine of the E2 and there are additional, non-covalent interactions between the globular domain of ubiquitin and the UBC domain. These interactions are mediated by the hydrophobic patch of ubiquitin (around Ile44) and helix α2 of the E2 (Figure 3).

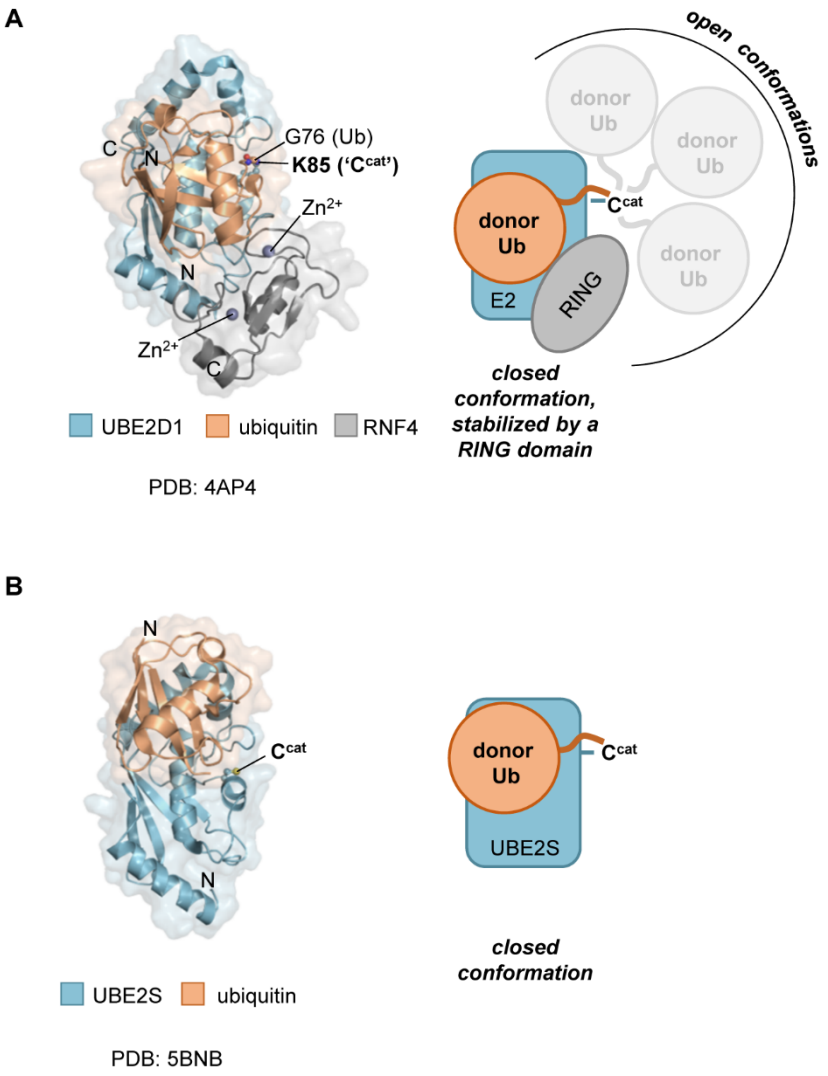

Figure 4: Conformational space of the E2-linked donor ubiquitin. (A) Crystal structure and cartoon model of a ternary ubiquitin-E2-RING E3-complex (E2: UBE2D1, E3: RING domain of RNF4, extracted from PDB: 4AP4 [51]; note that the RING domain dimerizes, but only one monomer is displayed here). In this complex, the C-terminus of the donor ubiquitin is isopeptide-linked to an engineered lysine (K85), replacing the catalytic cysteine ('C^{cat}'). The RING domain stabilizes the closed donor conformation, as opposed to open states that have no significant interface between ubiquitin and the E2. The structure is shown in a combined ribbon-and-surface representation; the side chain of K85 (UBE2D1) and main chain of G76 (Ub) in ball-and-stick mode. (B) Analogous representations of the closed state of a complex of $UBE2S^{UBC}$ with ubiquitin, extracted from PDB: 5BNB [52]. Here, the ubiquitin (G76C variant) is disulfide-linked to the catalytic cysteine of UBE2S; in the crystal, however, the closed interface is formed between neighboring molecules in *trans*. Therefore, the C-terminal tail of ubiquitin (residues 73-76) is not displayed. This figure is taken from [53].

In many cases, the closed conformation is stabilized by the RING (Figure 4A), which also enhances the reactivity of the E2. In other cases, the closed conformation does not

require the RING for the stabilization, and the RING fulfills other functions (Figure 4B, [4]).

The closed conformation of the donor is conserved among many E2s and was shown to promote thioester formation [54] as well as catalytic efficiency and processivity [4] if interacting with RING ligases. In contrast, it is not necessary for the interaction of E2s with HECT and RBR ligases [55–58]. This reflects the fact that E2s can catalyze several specific reactions. Besides thioester bond formation and (iso)petide bond formation, E2s have also been shown to drive oxyester bond formation of the C-terminus of ubiquitin with a serine or threonine. For example, UBE2J2 ubiquitinates the histocompatibility complex via hydroxyl groups, together with the viral RING E3 murine K3 [59,60].

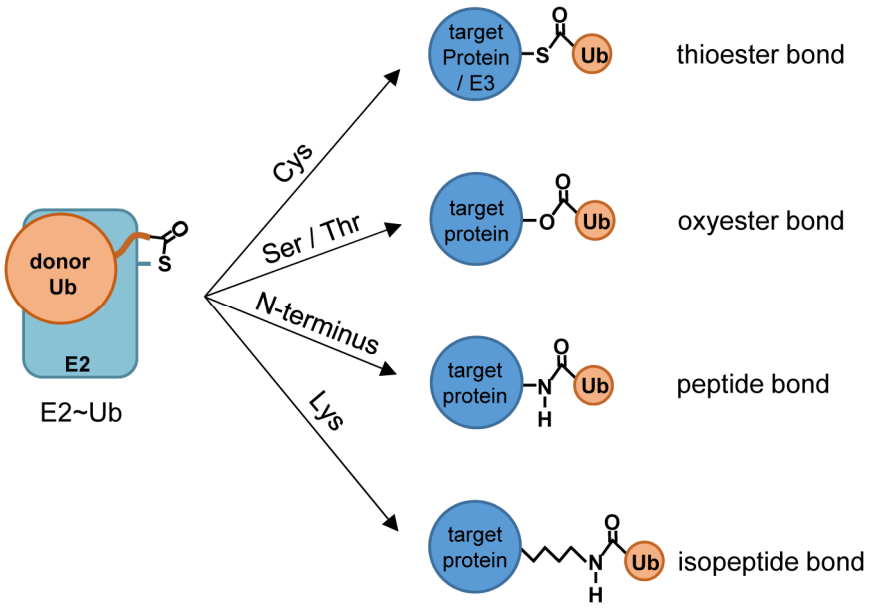

Figure 5: Reactions catalyzed by ubiquitin-conjugating enzymes. The thioester-linked E2-ubiquitin conjugate (E2~Ub, left side) can react with a cysteine e.g. of a HECT- or RBR-E3 to form a thioester bond or with a lysine residue of the target protein to form an isopetide bond. In addition, reactions with serine and threonine residues (oxyester bond formation) and with an unstructured N-terminus of a target protein are described (peptide bond formation). This figure is adapted from [61].

Taken together, the members of the E2 family are shown to catalyze at least four enzymatic reactions, as summarized in Figure 5, whereas the last two are chemically very similar.

1.2.1 Regulation of ubiquitin-conjugating enzymes

To date, many regulatory mechanisms that occur on the E3 level have been described, but it becomes more and more clear that regulation can also occur upstream of the E3s. It has also emerged that E2 enzymes are not only regulated via their levels, but are subjects to regulation at additional levels [61], such as posttranslational modifications: UBE2A, UBE2R1 and yeast *UBC2* are phosphorylated in an acidic loop, which makes the active site more accessible to ubiquitin and thereby facilitates the charging of the E2 [62–66]. Furthermore, E2s can be inhibited [53,67,68] or targeted for proteasomal degradation [6,69,70] by auto-ubiquitination, either in the conserved UBC domain or their N- or C-terminal extensions. In addition, modifications with the ubiquitin-like modifier SUMO were described for the SUMO E2 UBE2I as well as for the ubiquitin-specific UBE2K. For the latter, SUMOylation in the E1 and E3 binding site leads to inhibition [71], whereas the SUMOylation of UBE2I has different outcomes, such as increasing or decreasing activity, depending on the attachment sites [72,73].

Many E2s bind ubiquitin through their ‘backside’, the β-sheet-containing region of the UBC domain (Figure 3), in a non-covalent manner, resulting in allosterical activation of the E2s, e.g. UBE2D2, UBE2D3 and UBE2B [74–78]. In contrast, ubiquitin binding to the backside of UBE2E3 inhibits its processivity so that UBE2E3 mainly performs mono-ubiquitination of its products. Mutations disrupting the backside binding enable the formation of K63-linked ubiquitin chains by UBE2E3 [61,79].

Additionally, the activity of some ubiquitin-conjugating enzymes is influenced by their oligomeric states. *CDC34* from *Saccharomyces cerevisiae* was shown to self-associate upon thioester formation with ubiquitin and this self-association is required for its catalytic activity [80]. The dimerization of human UBE2G2 is induced by the thioester formation with ubiquitin, as well and in addition, promoted by the oligomerization of the E3 glycoprotein 78 (GP78) and is needed for ER-associated degradation of their substrates [81–83]. The SUMO-E2 UBE2I, which undergoes oligomerization [84], was speculated to enhance non-covalent interactions with SUMO, as required for poly-SOMO chain formation by dimerization [85]. However, a low-affinity homodimer of UBE2I was also found to be formed through the same interaction sites that are involved in E1 and SUMO binding. Thus, the outcome of UBE2I dimerization requires further investigation [86].

In summary, various mechanisms have evolved to regulate the level and activity of E2s, including post-translational modifications, non-covalent backside binding of ubiquitin and oligomerization. This demonstrates the importance of this enzyme family, whose dysregulation is connected to human disease.

1.2.2 Ubiquitin-conjugating enzymes in human disease

An emerging body of data on the E2 family emphasizes their role in human diseases such as genetic, immunological and neurodegenerative disorders as well as cancer [9,47,87]. One of the best studied E2s in pathology and disease is UBE2T. It mono-ubiquitinates the Fanconi anemia (FA) protein FANCD2 after aldehyde-induced DNA damage, leading to FANCD2 accumulation on chromatin and co-localization with DNA-repair factors. Defects in FANCD2 mono-ubiquitination increase chromosomal abnormalities and hypersensitivity to DNA interstrand crosslinking agents like cisplatin or reactive aldehydes [67,87–91]. These symptoms as well as bone marrow failure, mental birth defects and affected haematopoesis are characteristics of Fanconi anemia, an autosomal recessive genetic disorder in which the alleles that carry the FA genes including *FANCD2* and *FANCL* (the RING E3 of the FA complex) are mutated. Additionally, UBE2D1 [92], UBE2U [93] and UBE2W [94] are associated with genetic disorders.

Polymorphism in the genomic locus of *UBE2L3* however, is found to be a high risk factor for the development of autoimmune diseases like systemic lupus erythematosus [95,96], inflammatory bowel disease (IBD) [97] and rheumatoid arthritis [98].

Patients with the autoimmune disease Sjögren's syndrome (SS) express higher amounts of the ERAD machinery, including the E2s UBE2J1 and UBE2G2. This in turn triggers higher levels of pro-inflammatory cytokines [99]. However, the same effect was found to be triggered by the formation of auto-antibodies specific for the RING domain of TRIM21, an E3 that negatively regulates the production of pro-inflammatory cytokines. This inhibits the binding of TRIM21 to UBE2E1 in patients with SS, indicating a putative role of UBE2E1 inhibition in the development of this immunological disorder [100].

Parkinson´s disease has been associated with several ubiquitin-conjugating enzymes with biological roles in DNA repair [47]. Parkinson´s disease is mainly caused by mutations in the mitochondrial kinase PINK1 or the E3 Parkin, leading to a loss of function, causing mitochondrial dysfunction and the selective loss of dopamine-producing neurons. Normally, PINK1 activates Parkin which is activated by ubiquitin loading through UBE2L3 and UBE2D2/3. UBE2N affects the translocation of Parkin to de-energized mitochondria and mitochondrial clustering, whereas the interaction of Parkin with UBE2R1 negatively affects the translocation of Parkin [101]. Thus, Parkin is regulated by several E2s.

UBE2W and UBE2K were found to have a crucial role in Huntington´s disease, in which they modify the mutated protein huntingtin (mHTT) with ubiquitin. E2 deficient cells [102]

or those expressing an antisense sequence of the E2 [103] showed reduced mHTT aggregate formation and neurotoxicity.

Besides genetic, immunological and neurodegenerative disorders, many ubiquitin-conjugating enzymes are de-regulated in cancer as they impact cell proliferation, DNA repair and other oncogenic pathways [9,47]. This is exemplified by the tumor-promoting roles of UBE2C and UBE2O: Overexpression of the cell-cycle-regulating E2 UBE2C was identified in several cancer types, such as non-small cell lung, liver and breast cancer, where it is correlated with poor prognosis and drug resistance and thus serves as a biomarker [104–107]. UBE2O poly-ubiquitinates the activated protein kinase alpha 2 (AMPKα2), thereby targeting it for degradation. This induces the mTOR-HIF-1α pathway and promotes tumor growth and metastasis. Thus, it is not surprising that UBE2O is overexpressed in various cancer types, whereas its depletion or inhibition by arsenite inhibits tumorigenesis [9,108,109]. Together, these examples illustrate roles of E2s as biomarkers for cancer diagnosis, and possible therapeutic targets.

Understanding their biological roles and molecular mechanisms in homeostasis and disease is, therefore, of particular importance.

1.3 The human ubiquitin-conjugating enzyme UBE2S

The ubiquitin-conjugating enzyme UBE2S, also named E2-EPF, is a ~24 kDa protein that consists of a canonical catalytic domain (UBE2S^{UBC}, residues 1-156) and a C-terminal extension (residues 157-222), defining UBE2S as a class III-E2 (Figure 19 and Figure 37). The catalytic domain contains the binding sites for ubiquitin as well as the active site region (residues 95-103) with the catalytic cysteine (Cys^{cat} = Cys95). The C-terminal extension is structurally uncharacterized and predicted to be mainly unstructured with the exception of an α-helix at the C-terminus (C-helix) (Figure 6).

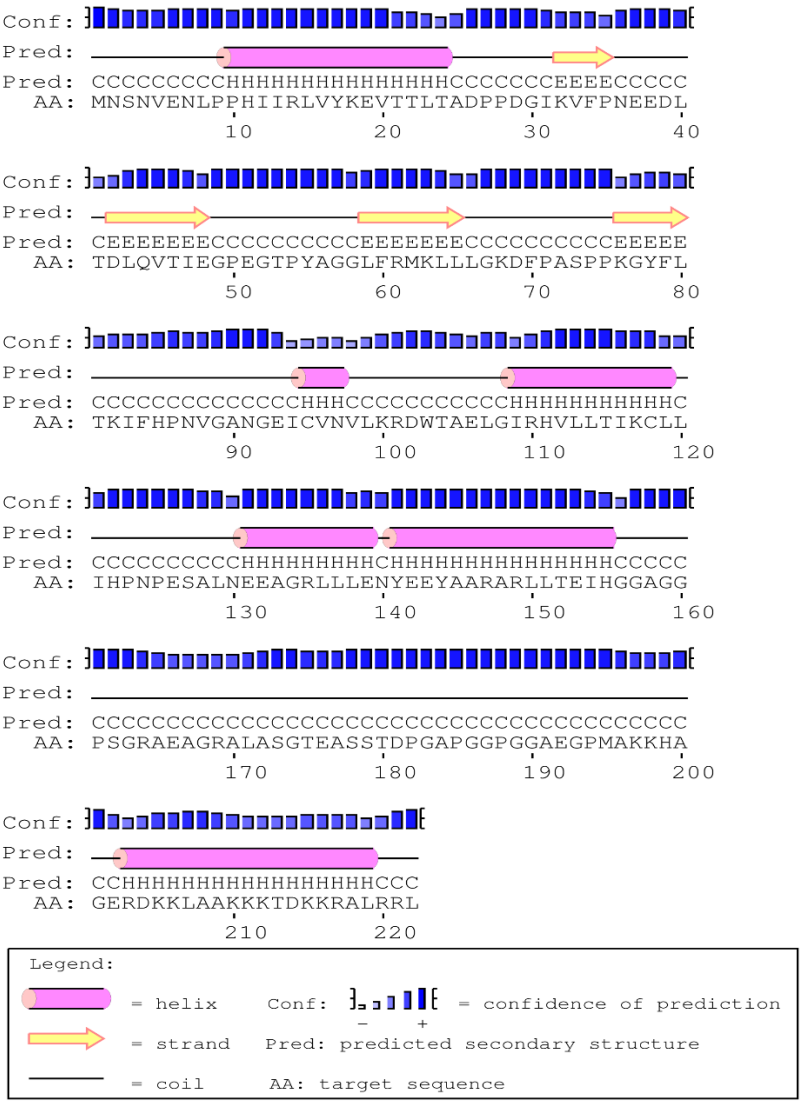

Figure 6: Secondary structure prediction of UBE2S. While the catalytic domain (UBE2S^{UBC}, residues 1-156) shows defined secondary structure regions, the C-terminal extension is predicted to be mainly unstructured. The C-terminal residues are predicted to form an α-helix (C-helix) .The prediction was conducted with the PSIPRED server [110,111].

The role of the lysine-rich C-terminal extension that is unique to UBE2S within the human E2 family, is not completely understood. It was shown that the C-terminal extension harbors the binding site for a RING-type E3, the anaphase promoting complex/cyclosome (APC/C) [112,113], with which UBE2S interacts when modifying cell-cycle regulators with Lys11-linked ubiquitin chains. This marks them for proteasomal degradation and promotes mitotic exit [3,5,114] (chapter 1.3.1). The mutation of Leu222 in UBE2S to alanine decreases its affinity for the APC/C [112] and impairs substrate ubiquitination [114]. In addition, it was shown that the C-terminal extension is auto-ubiquitinated in an E3-enhanced manner and presumed that this auto-ubiquitination leads to the proteasomal degradation of UBE2S during G1 phase, when the APC/C substrates are on the decline [3]. Whether the C-terminal extension is also needed for the interaction with the RING-type E3 RNF8 in DNA double strand break repair (chapter 1.3.2) has not been investigated. In the context of DNA repair, UBE2S was shown to form Lys11-linked ubiquitin chains on the histones H2A and H2AX and cause transcriptional arrest at the DNA lesion site [7].

The ability of UBE2S to form Lys11-linked ubiquitin chains was first described in 1996 [115], while the role of these chains and their abundance in the cell remained elusive for a decade (see the following chapters). UBE2S has been reported to have important roles in cancer: In contrary to the normal state, in primary liver, colon and breast tumors, UBE2S levels were found to correlate with the level of the α-subunit of the hypoxia-inducible factor (HIF-1α) [116]. UBE2S ubiquitinates the von Hippel-Lindau tumor suppressor protein (pVHL), targeting it for degradation [116] and thus triggering the expression of Hypoxia-inducible genes [117]. The same interplay of UEB2S and HIF-1α was found in cervical squamous cancer [118] and papillary renal cell carcinoma [119]. Additionally, UBE2S can enhance the ubiquitination of the tumor suppressor p53 in hepatocellular carcinoma [120] and presumably in lung adenocarcinoma cells [121], favoring tumor growth and colony formation [120,121]. In contrast to the proteasomal degradation of target proteins, modified by UBE2S, the UBE2S-dependant β-catenin ubiquitination was found to stabilize β-catenin. This promotes its cellular accumulation, mesendoderm specification and colorectal cancer development [122]. Most of the above studies have in common that UBE2S overexpression in cancer is associated with unfavorable patient survival [10,118–121], tumor growth and invasion [10,116,118,120,121,123] and poor response to therapy [8,10,118,124].
To provide the basis for understanding the pathogenic functions of UBE2S and evaluate therapeutic opportunities, it is of particular importance to understand the non-pathogenic roles of UBE2S and its interplay with interaction partners.

1.3.1 The role of UBE2S in cell cycle regulation

The exact timing of the cell cycle is of immense importance to avoid homeostatic imbalance. Thus, every step of the cell cycle is tightly controlled. One layer of regulation is the transition from prometaphase to anaphase, as mediated by the spindle assembly checkpoint (SAC) (Figure 7).

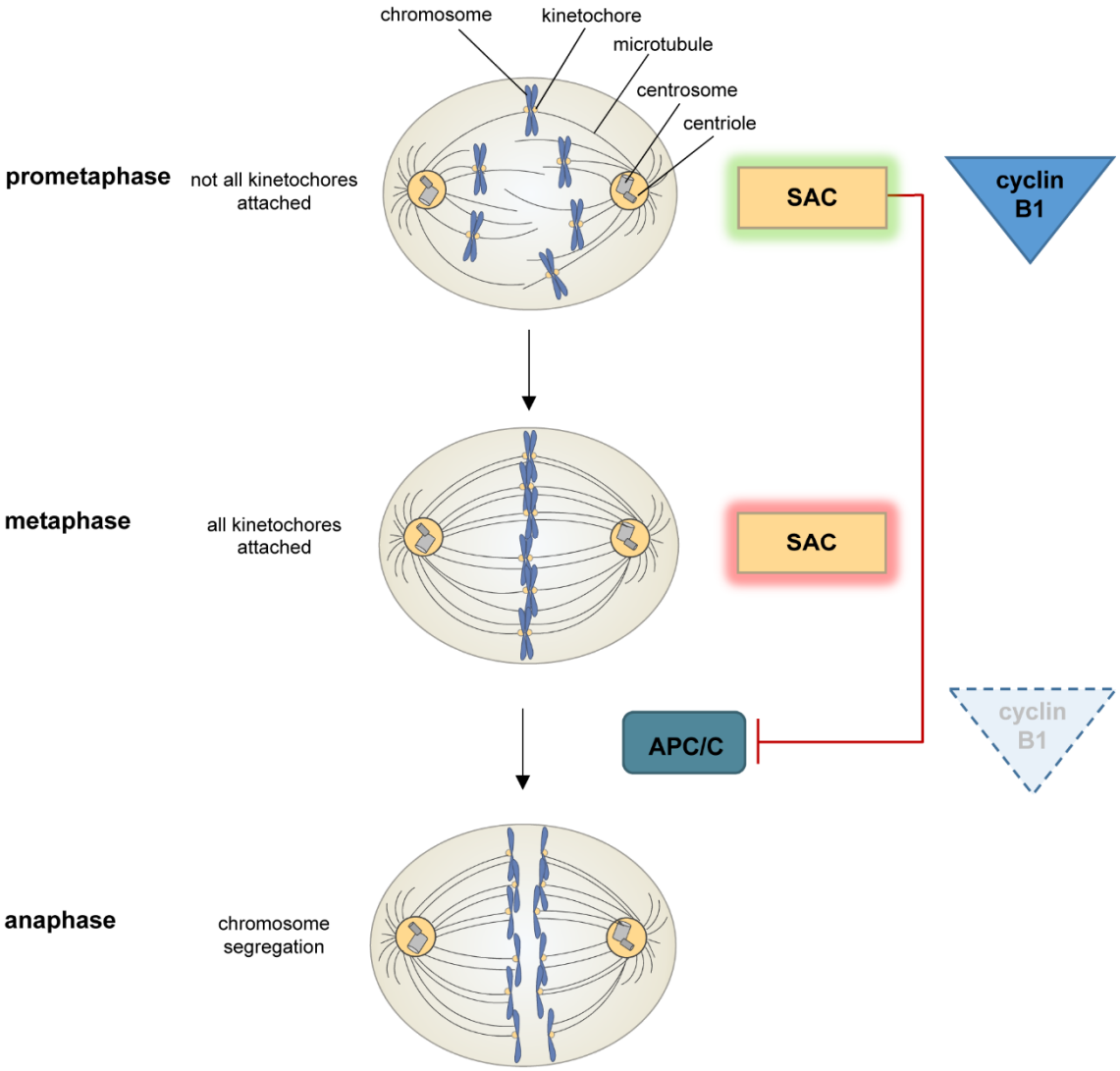

Figure 7: The transition from prometaphase to anaphase of the somatic cell cycle is regulated by the spindle assembly checkpoint (SAC). As long as not all kinetochores are attached to microtubules, the SAC generates the mitotic checkpoint complex (MCC), inactivating the APC/C. When all kinetochores are attached properly, the SAC is inactivated and the MCC disassembles. The APC/C then ubiquitinates cyclin B1 and securin, leading to their proteasomal degradation and chromosome segregation.

The SAC monitors the attachment of microtubules to kinetochores. As long as attachment is incomplete, the SAC generates the mitotic checkpoint complex (MCC) which inactivates the APC/C by blocking its substrate binding site and keeping the

APC/C in a closed conformation [125]. Once the SAC is inactivated and MCC disassembled, APC/C is activated [126]. The APC/C then ubiquitinates cell cycle mediators, such as cyclins and securin which induces their degradation by the proteasome [6,127,128].
The ~1.2 MDa APC/C comprises of 14 proteins, of which five exist in two copies (a total of 19 subunits) in humans [129,130] and a coactivator, either CDH1 or CDC20, regulating its activity and substrate specificity [129,131]. Interestingly, most of the subunits have a scaffolding function and only five are related to the catalytic function: APC2 and APC11 form the catalytic module of cullin repeats and RING-domain and APC10 and the respective coactivator form the substrate recognition module [129] which recognizes destruction (D box: (RxxLxxxxN, [132]) and KEN boxes (KENxxxN, [133]) in APC/C substrates. During mitotic exit, the APC/C interacts with the coactivator CDC20, facilitated by the phosphorylation of APC1 by cyclin-dependent kinases in prophase [134,135]. In late mitosis, the CDH1-bound APC/C is activated and remains active during G1 phase and quiescence, where it prevents unscheduled proliferation [136] by cyclin B1 degradation [137].

To modify substrates with Lys11-linked ubiquitin chains to mark them for degradation by the proteasome (Figure 8) [114,138,139], the APC/C interacts with two E2 enzymes: UBE2C for starting substrate ubiquitination and UBE2S for elongating these ubiquitin chains [4,5,114] and encoding linkage specificity [4] (chapter 1.3.3). While the depletion of UBE2S is dispensable during unperturbed mitosis, it was found to prolong mitotic exit and prevent mitotic slippage in case of drug-induced mitotic arrest [5]. In the context of UBE2C knockout, an additional knockout of UBE2S causes a more pronounced phenotype, manifesting in prolonged nuclear envelope breakdown to anaphase onset times [3,140]. Nevertheless, ΔUBE2C/ΔUBE2S cells are viable, although suffering from massively prolonged mitosis [140]. This can be explained by the ability of the APC/C to interact additionally with UBE2D1 for ubiquitin chain formation initiation *in vitro* [3,5,114,141] and to a minimal extend *in vivo*.

Cryo-electron microscopy (cryo-EM) in combination with *in vitro* analysis [112,113,125,129,130,134,135,142] have unraveled the structural architecture of the APC/C and its interplay with UBE2C and UBE2S. During chain priming, UBE2C interacts with the RING-E3 in a canonical fashion, thus favoring the closed conformation of the E2~ubiqutin complex and promoting the nucleophilic attack of an acceptor lysine [143]. UBE2C interacts not only with ubiquitin and the RING-domain (APC11), but additionally with the winged-helix B domain (WHB) of APC2 (cullin) via its backside (Figure 8A) [143].

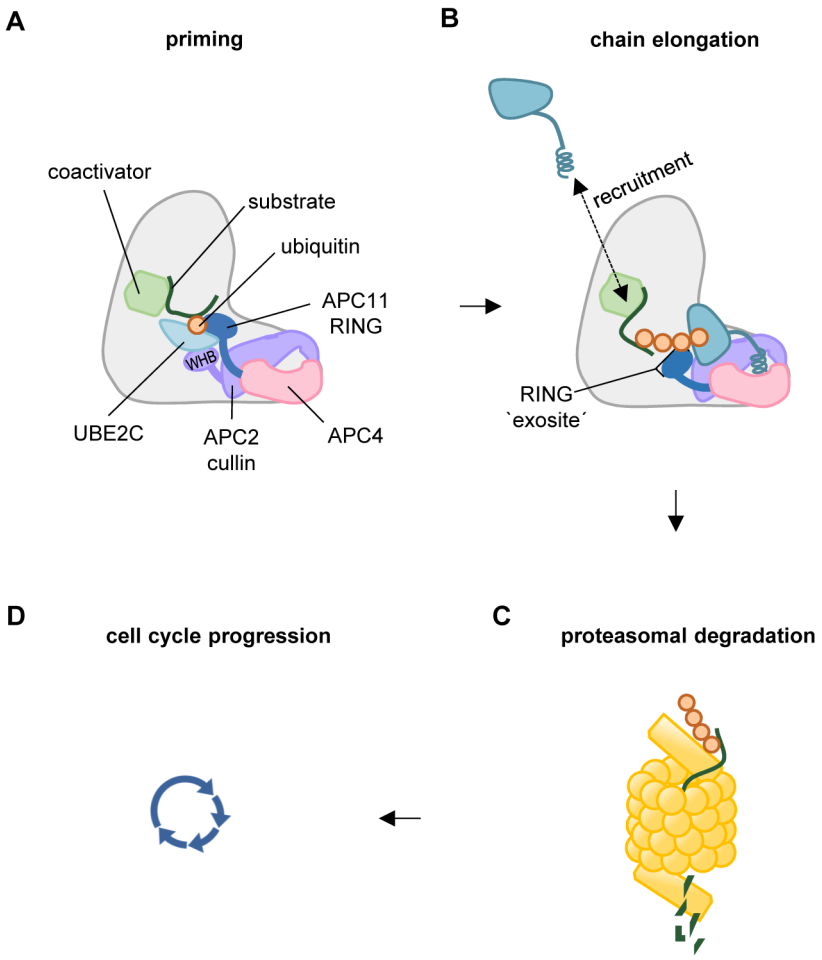

Figure 8: Substrate ubiquitination by the anaphase promoting complex/cyclosome (APC/C). In (A) and (B), the APC/C is depicted in grey, with subunits important for substrate and E2 binding, highlighted in color. (A) For chain priming, the APC/C clamps UBE2C via canonical interactions with the RING domain (APC11) and interactions between the winged-helix B domain (WHB) of APC2 and the backside of the E2. The substrate is bound to the coactivator via KEN- or D-boxes. (B) Ubiquitin chain elongation via UBE2S: UBE2S is recruited to the APC/C by interactions between the coactivator and the C-terminal extension of UEB2S that thereafter binds in the APC4/APC2 groove. A reorientation of the RING allows it to bind a substrate-linked ubiquitin with its 'exosite'. (C) Modified substrates are degraded by the proteasome to facilitate cell cycle progression (D).

In this state, substrates can be mono-ubiquitinated at several lysine residues [112] which provides an additional signal for their proteasomal degradation [144]. Without interacting partners, the catalytic core consisting of the RING and the cullin are mobile [145], pointing towards dynamic flexibility of this subunits. Indeed, the non-canonical interaction of UBE2S with the APC/C is associated with structural rearrangements of the RING-domain [112,113]. After the recruitment of UBE2S to the APC/C by interactions of the C-terminal extension of UBE2S with the coactivator [3,131,146], the C-helix of UBE2S

inserts into the groove between APC2 and APC4 (Figure 8B), placing UBE2S at the edge of the APC/C to give space for the elongation of the ubiquitin chains in a Lys11-linked manner [112]. UBE2S does not directly interact with the RING, but the exosite of the RING instead interacts with ubiquitin that is bound to the substrate. UBE2S also does not seem to interact with the WHB domain of UBE2S-bound APC2, as this domain is not visible in the cryo-EM structure of the APC/C, indicating conformational flexibility of this domain [112].

The structures of different E2-bound APC/C states highlight the conformational dynamics within the APC/C and the specific arrangements that mediate UBE2C binding, as required for priming, mono-ubiquitination or UBE2S binding, as required for ubiquitin chain elongation. Together, these substrate modifications mark them for the degradation by the proteasome to facilitate cell cycle progression (Figure 8C, D).

Interestingly, substrate degradation was shown to be enhanced by branched ubiquitin chains [18]. Such chains result from the property of UBE2C to start promiscuously-linked chains in additive to multi-mono-ubiquitination. These chains can be linked via Lys11, but also via Lys48 and Lys63 [70,147]. UBE2S elongates these chains in a Lys11-linked manner, thus synthesizes branched ubiquitin chains [18]. The development of an antibody specific for Lys11/Lys48-branched ubiquitin chains enabled the cell-based detection of these chain-type on APC/C substrates in mitosis, proving their role as proteasome-targeting signals [148].

In sum, UBE2S functions in cell cycle control by elongating Lys11-linked ubiquitin chains on cell cycle regulators in collaboration with UBE2C, targeting the substrates for proteasomal degradation and ensuring the correct timing of mitotic progression.

1.3.2 The role of UBE2S in DNA repair

Besides its role in cell-cycle regulation, UBE2S was demonstrated to have a role in the DNA repair mechanism of non-homologous end joining (NHEJ) [8]. Double strand breaks (DSBs) in DNA that are induced by ionizing radiation can lead to cell death [149]. They can be repaired by the NHEJ machinery [150]. The DSBs are recognized by the KU70/KU80 heterodimer that additionally binds to the DNA-dependent Protein Kinase catalytic subunit (DNA-PKcs) that is recruited to the damage site. Subsequent auto-phosphorylation of DNA-PKcs results in the recruitment of the DNA repair machinery, including the X-ray Repair Cross-Complementing protein 4 (XRCC4) and DNA Ligase 4 (LIG4), which initiate repair [149].

Cancer cells harboring a loss of function mutation in phosphatase and tensin homologue deleted on chromosome ten (PTEN) have a constantly active PI3K/AKT/mTOR signaling pathway, which leads to the activation of NHEJ [151]. UBE2S interacts with the activated RAC-alpha serine/threonine-protein kinase AKT1 and is phosphorylated at Thr152, what stabilizes UBE2S in those cancer cells. Additionally, UBE2S can interact with KU70. Upon double-strand breaks, the interaction of UBE2S and KU70 is enhanced and the proteins are re-localized to nuclear foci, which co-localize with foci of the phosphorylated histone H2AX (γ-H2AX), marking the DNA damage site. The knockdown of UBE2S diminishes the NHEJ efficiency by ~20%, enhances the sensitivity to DSB-inducing agents like etoposide, which results in subsequent cell death in cells and *in vivo*. Inhibition of AKT1 by inhibitors prevents UBE2S phosphorylation and the associated stabilization of UBE2S. This reduces the level of NHEJ and drug resistance (Figure 9, [8]).

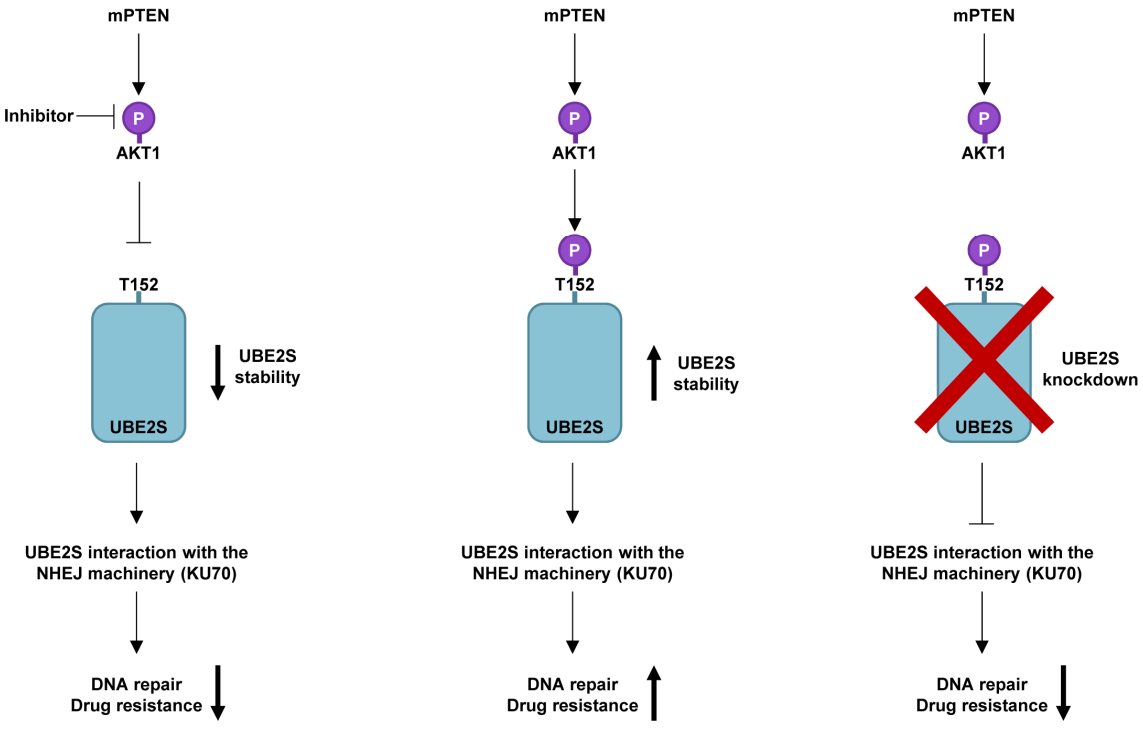

Figure 9: UBE2S is involved in NHEJ and mediates drug resistance in PTEN-mutated cancer. In cancer cells expressing mutated PTEN (mPTEN), AKT1 activation by phosphorylation causes the phosphorylation of UBE2S at Thr152. This increases UBE2S stability, leading to its interaction with the NHEJ machinery and increased DNA repair and drug resistance (middle). Interference by AKT1-inhibition (left) or UBE2S knockdown (right) reverse these effects. The figure is adapted from Hu et al. [8].

DNA double-strand breaks can also be repaired by homologous recombination (HR). This repair mechanism is based on an undamaged sister chromatid that is used as a template. After the recognition of the damage by the MRE11-RAD50-NBS-complex, ATM kinase is recruited and activated, thus leading to the formation of a 3´-single stranded DNA overhang by nucleases. Finally, RAD51 binds the single-stranded DNA in an ATP-dependent manner, searches for homology and catalyzes the strand exchange. This is followed by DNA synthesis and ligation [149].

Furthermore, ATM kinase is crucial for transcriptional arrest at double strand breaks. It phosphorylates histone H2AX (γ-H2AX) and its interactor MDC1 (mediator of DNA damage checkpoint protein 1) and then recruits the RING-type E3 RNF8. Together with UBE2N, RNF8 catalyzes the modification of histone H1 with Lys63-linked ubiquitin chains [152] and recruits the RING E3 RNF168 to the DSB [153]. RNF168 mono-ubiquitinates the histones H2A and H2AX. These modifications can be elongated in a Lys63-linkage specific manner by RNF8 [154] and lead to the recruitment of the DNA repair machinery and represses transcription [152,155,156].

Together with UBE2C and UBE2S, RNF8 can also catalyze the formation of Lys11-linked ubiquitin chains on histone H2A and H2AX at the DNA damage site. As in the APC/C-dependent mechanism, UBE2C initiates the modification of the substrates and UBE2S elongates the chains in a Lys11-specific manner what is antagonized by the Lys11-specific DUB Cezanne. It was demonstrated that the depletion of UBE2C and UBE2S results in the reduction of transcriptional silencing after DNA damage. The modification of the histones with Lys11 chains occurs as extensively as the modification with Lys63-linked ubiquitin chains, but does not interfere with it. Interestingly, in contrast to the APC/C-mediated modification of cell cycle regulators with Lys11-linked ubiquitin chains, Lys11-linked chains on histones appear not to be degradative. Instead, they may have a specific signaling function in this context, which inhibits transcription of genes close to the DNA damage site ([7], Figure 10).

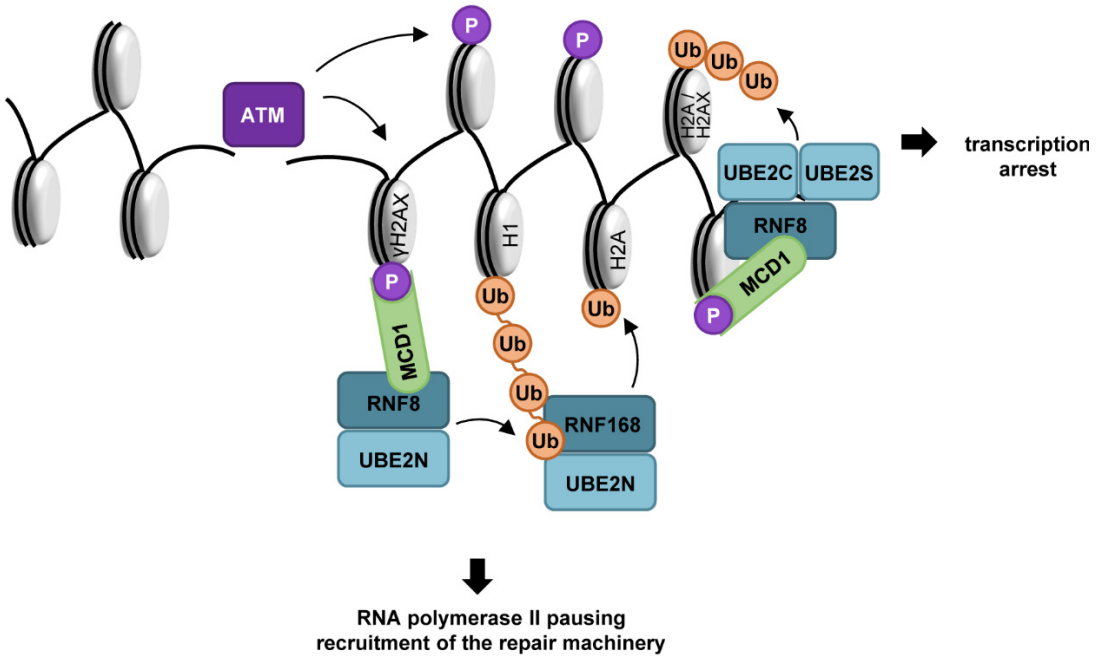

Figure 10: ATM-dependent transcription arrest after DNA double-strand breaks. Upon DSBs, the ATM kinase gets activated and phosphorylates H2AX to recruit the mediator protein MCD1 and the E3 ligase RNF8. RNF8, together with the E2 UBE2S, modifies histone H1 with Lys63-linked ubiquitin chains what recruits RNF168 that mono-ubiquitinates H2A histones. These chains can further be elongated by RNF8 and UBE2N in a Lys63-specific manner. Together, this causes RNA polymerase II pausing and the recruitment of the DNA damage repair machinery. Additionally, RNF8 can interact with UBE2C and UBE2S to catalyze the ubiquitination of the histones H2A and H2AX with Lys11-linked chains to cause transcription arrest at DNA damage sites. The figure is adapted from [149] and [7].

1.3.3 Molecular mechanism of UBE2S

An important question in the ubiquitin field is how the specificity of ubiquitinating and deubiquitinating enzymes is encoded. UBE2S is highly specific for the formation of Lys11-linked ubiquitin chains. For the formation of those chains, which are formed by UBE2S even in the absence of a ubiquitin ligase, UBE2S has to interact with two ubiquitin molecules. First, UBE2S binds a donor ubiquitin (orange) covalently via its active site cysteine (Cys95) in a closed conformation (Figure 4). Second, UBE2S interacts with an acceptor ubiquitin (yellow), which should be oriented in a way that the primary amino group of Lys11 can nucleophilically attack the thioester bond (Figure 11A).

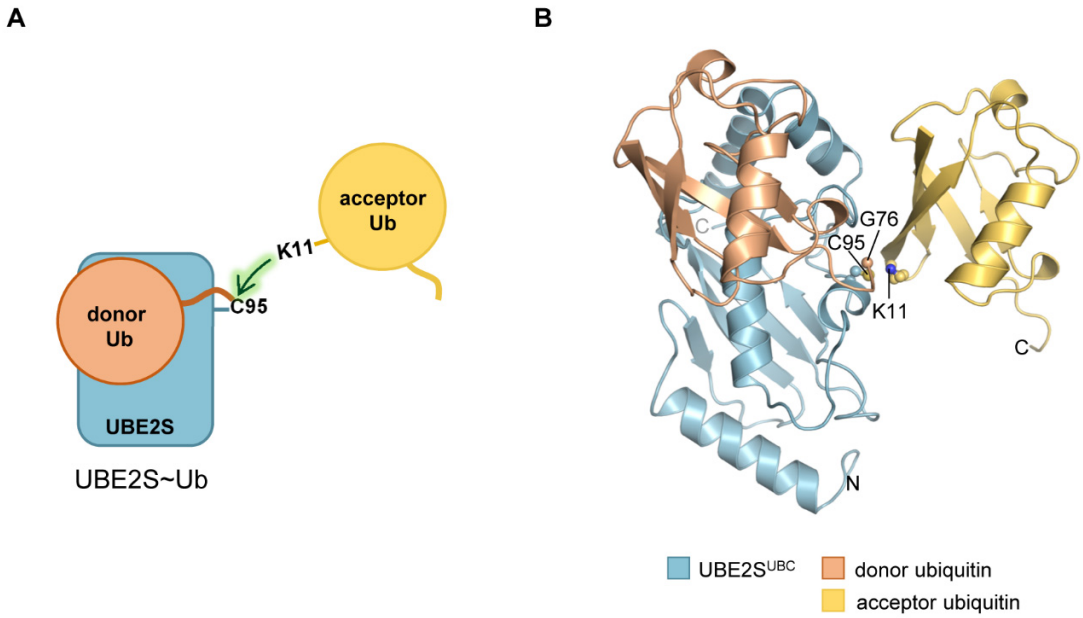

Figure 11: UBE2S interacts with the donor and acceptor ubiquitin. (A) Cartoon model of donor ubiquitin bound UBE2S (UBE2S~Ub, blue), interacting with an acceptor ubiquitin molecule (yellow) in a way that Lys11-linked ubiquitin chains can be formed. (B) NMR-derived, docked model of the ternary complex of UBE2S with donor and acceptor ubiquitin, adapted from [4].

The structural basis of the Lys11 specificity and the molecular mechanism of ubiquitin chain formation by UBE2S was explained by an NMR-derived, docked model of the ternary complex of UBE2S with donor and acceptor ubiquitin, as shown in Figure 11B [4]. Unexpectedly, NMR-experiments revealed that UBE2S already interacts with ubiquitin in a closed conformation in the absence of a thioester linkage or a RING-domain. The binding interface on ubiquitin encompass the hydrophobic patch, including residues Leu8, Ile44, Ala46, Val70 and Leu71 (Figure 12A). Those residues are interacting with residues around helix α2 (see Figure 3) on UBE2S, namely Asp29, Glu51-Thr53, Lys117, Cys118 and Ile121-Pro123 among others (Figure 12B) [4]. Although the interaction of UBE2S with donor ubiquitin in *trans* is extremely weak, with K_D-values of 1.1 mM for UBE2S^{UBC} and 1.7 mM for the full-length protein [4], they reproduce the donor-E2 interface seen in a crystal structure of a UEB2S^{UBC}-ubiquitin conjugate mimicking the thioster-linked complex. Note that the relevant interface therein is formed in *trans* [52].

Donor-ubiquitin bound UBE2S interacts highly transiently with the acceptor ubiquitin molecule in isolation, but the interaction is assisted by the APC/C [113]. Mostly electrostatic interactions between Glu139, Glu131, Arg135 and Asn97 of UBE2S and Glu34, Lys6 and Lys63 of ubiquitin orient the acceptor ubiquitin molecule in a position that brings Lys11 into close proximity of the active site region (illustrated by Cys95, pink,

Figure 12C) [4]. Interacting residues on the acceptor ubiquitin, most importantly Glu34, are crucial for Lys11-linked formation by UBE2S. In fact, Glu34 was found to suppress the pK_a of Lys11, promoting its deprotonation [4]. Thus, the Lys11-specificity of ubiquitin chain formation by UBE2S is achieved by substrate-assisted catalysis [4].

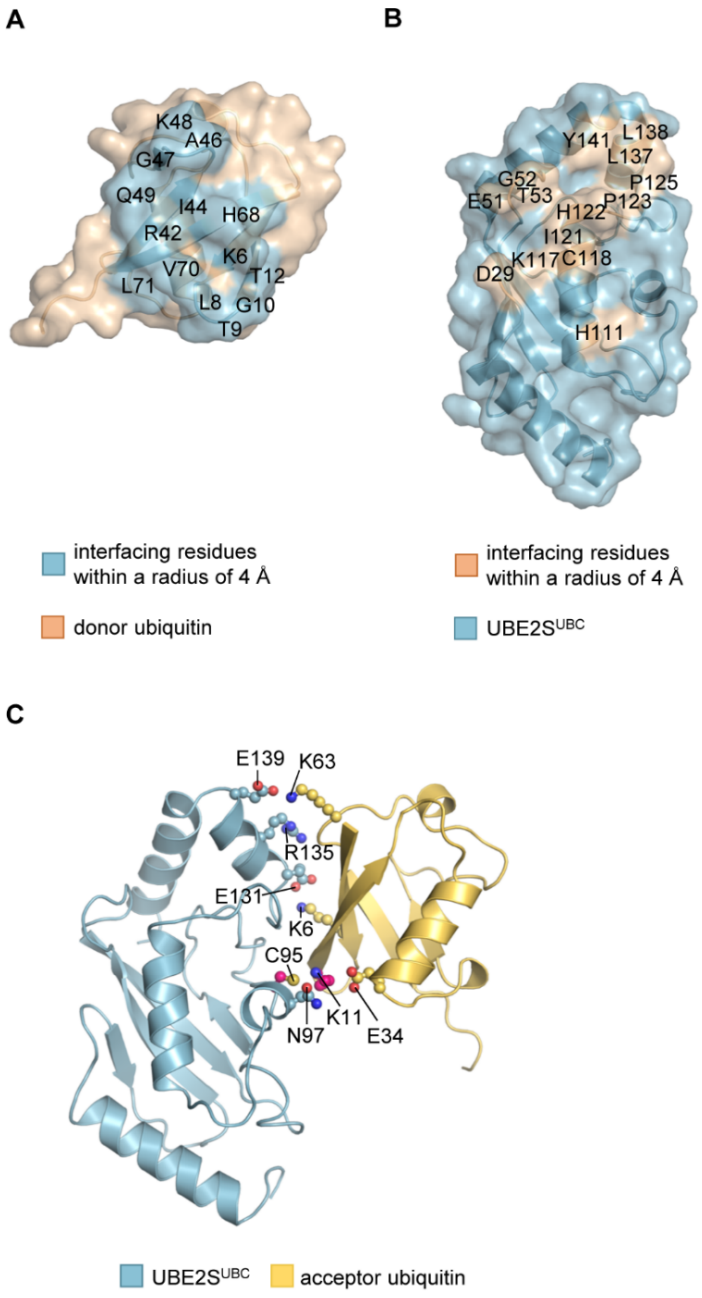

Figure 12: Interaction sites of UBE2S with the donor and acceptor ubiquitin. (A) Surface representation of ubiquitin (orange, PDB: 1UBQ) showing the interfacing residues (within a radius of 4 Å) of donor ubiquitin with UBE2S^{UBC} (blue) [4]. (B) Surface representation of UBE2S^{UBC} (blue, PDB: 1ZDN) showing the interfacing residues (within a radius of 4 Å) of UBE2S^{UBC} with the donor ubiquitin (orange) [4]. (C) Detail on the electrostatic interactions of UBE2S^{UBC} (blue) with the acceptor ubiquitin (yellow) in the NMR-derived, docked model shown in Figure 11B) [4]. Interacting residues are depicted in ball-and-stick representation and the active site cysteine of UBE2S (Cys95) and Lys11 of ubiquitin are highlighted in pink.

1.4 Objectives

Although historically simply termed ‘ubiquitin carriers’, E2s actively participate in the ubiquitination cascade, and determine linkage specificity when interacting with RING-type E3s. Emerging evidence suggests that E2s get regulated by distinct mechanisms influencing their levels, conformational dynamics and macromolecular interactions [61]. The importance of stringent control of E2 activities manifests in the severe physiological consequences of E2 dysregulation, which comprises immunological and neurodegenerative disorders as well as cancer [9,47,87]. However, the precise structural underpinnings and molecular consequences of E2 regulatory pathways are incompletely understood.

This work interrogates the regulatory mechanisms of the ubiquitin-conjugating enzyme UBE2S at the structural and mechanistic level. While UBE2S was shown to undergo (E3-enhanced) auto-ubiquitination at the C-terminal extension that presumably drives its proteasomal degradation at the end of mitosis [3], it is not understood whether auto-ubiquitination at alternative sites has regulatory consequences. Furthermore, it was reported that E2s can oligomerize with different outcomes for their function [80–86]. Therefore, I set out to investigate the potential regulation of UBE2S by dimerization and auto-ubiquitination.

To gain information about the regulatory mechanism of UBE2S on a structural level may open up avenues towards a rational therapeutic manipulation of UBE2S. After all, several studies have uncovered the severe consequences of UBE2S dysregulation (chapter 1.3). Because UBE2S overexpression is linked to poor prognosis and poor response to therapeutics [8–10] in many cancer types, it is of great importance to understand the function and regulation of this E2, to outline common principles of regulation in the E2 family and ultimately generate powerful cancer therapies.

2. Material

2.1 Primers

Oligonucleotides for site-directed mutagenesis, restriction free (RF) cloning and sequencing were purchased from Sigma-Aldrich in high purity salt free (HPSF) quality and lyophilized form and dissolved in reagent-grade water.

Table 1: Oligonucleotide sequences, used in polymerase chain reactions (PCRs). F denotes forward; R reverse

Name		Nucleotide sequence (5'-3')
T7	F	TAATACGACTCACTATAGGG
	R	GCTAGTTATTGCTCAGCGG
CMV	F	CGCAAATGGGCGGTAGGCGTG
	R	AGTAGGAAAGTCCCGTAAGG
UBE2S pMal Mod	F	ATGAACTCCAACGTGGAG
		CAGCCGCCGCAGCGCCCG
UBE2S C95S FL-His_6_RF-Cloning pMal Mod	F	TCTGCTCACAGAGATCCACGGGGGCGCCGGCGGGCCCAGC
	R	CCTAGTGGTGGTGGTGGTGGTGCAGCCGCCGCAGCGCCCG
Del G2 for $UBE2S^{UBC}$	F	GAAGGAGATATACCATGAACTCCAACGTGGAGAAC
C95S His_6 pMal Mod	R	GTTCTCCACGTTGGAGTTCATGGTATATCTCCTTC
3HA UBE2S pCCA1	F	GCTCACAGAGAACAGATTGGTGGGATGTACCCATACGATGTTCCAG
	R	TGATAGGCCTGCATTCGATGAGGTGCTACAGCCGCCGCAGCGC
3HA $UBE2S^{UBC}$ pCCA1	F	GCTCACAGAGAACAGATTGGTGGGATGTACCCATACGATGTTCCAG
	R	TGATAGGCCTGCATTCGATGAGGTGTTATTACCCGTGGATCTCTGTGAG
UBE2S C95A	F	CCAGTGGCGAGATCGCAGTCAACGTGCTCAAG
	R	CTTGAGCACGTTGACTGCGATCTCGCCACTGG
UBE2S K100R pCCA1	F	GATCTGCGTCAACGTGCTCCGTAGGGACTGGACGGCTGAG
	R	CTCAGCCGTCCAGTCCCTACGGAGCACGTTGACGCAGATC
UBE2S K100R with C95S pCCA1	F	ATCTCCGTCAACGTGCTCTGCAGGGACTGGACGGCTGAG
	R	CTCAGCCGTCCAGTCCCTGCAGAGCACGTTGACGGAGAT
K0 $UBE2S^{UBC}$ R100K	F	GAAATTTGCGTTAATGTTCTGAAACGTGATTGGACCGCAGAACTG
	R	CAGTTCTGCGGTCCAATCACGTTTCAGAACATTAACGCAAATTTC

Name		Nucleotide sequence (5'-3')
UBE2S R101A pCCA1	F	TGCGTCAACGTGCTCAAGGCGGACTGGACGGCTGAGCTG
	R	CAGCTCAGCCGTCCAGTCCGCCTTGAGCACGTTGACGCA
UBE2S D102A pCCA1	F	GTCAACGTGCTCAAGAGGGCCTGGACGGCTGAGCTGGG
	R	CCCAGCTCAGCCGTCCAGGCCCTCTTGAGCACGTTGAC
UBE2S L107A pCCA1	F	GGGACTGGACGGCTGAGGCGGGCATCCGAACGTACTG
	R	CAGTACGTGTCGGATGCCCGCCTCAGCCGTCCAGTCCC
UBE2S L114A pCCA1	F	GGCATCCGACACGTACTGGCGACCATCAAGTGCCTGCTG
	R	CAGCAGGCACTTGATGGTCGCCAGTACGTGTCGGATGCC
UBE2S L114E pCCA1	F	GGCATCCGACACGTACTGGAAACCATCAAGTGCCTGCTG
	R	CAGCAGGCACTTGATGGTTTCCAGTACGTGTCGGATGCC
UBE2S L114R pCCA1	F	CATCCGACACGTACTGCGTACCATCAAGTGCCTGC
	R	GCAGGCACTTGATGGTACGCAGTACGTGTCGGATG
UBE2S L137A pCCA1	F	AACGAGGAGGCGGGCCGCCTGGCGTTGGAGAACTACGAGGAGTAT
	R	ATACTCCTCGTAGTTCTCCAACGCCAGGCGGCCCGCCTCCTCGTT
UBE2S L138A pCCA1	F	GGGCCGCCTGCTCGCGGAGAACTACGAGGAGTAT
	R	ATACTCCTCGTAGTTCTCCGCGAGCAGGCGGCCC
UBE2S K197R/K198R pCCA1	F	GGTCCCATGGCCCGTCGTCATGCTGGAGAAAG
	R	CTTTCTCCAGCATGACGACGGGCCATGGGACC
E2insert pCDNA5 FRT/TO-MCS-IRES2-eGFP	F	GCGTTTAAACTTAAGCTTGGTACCGAGATGAATAGTAATGTCGAAAATTTGC
	R	GAGGGAGAGGGGCGGATCCCGGCTATAATCTTCTTAAGGCTCTTTTT
K/R tail pCDNA5 FRT/TO-MCS-IRES2-eGFP	F	GGGGACGGAGGCGAGTAGTACGGATCCGGGCGCGCCCGGC
	R	TTCGGCCAGTAACGTTAGGGGGGGGGGAGGGAGAGGGGCG
pCDNA5 FRT/TO-MCS-IRES2-eGFP-linear	F	AAAAAGAGCCTTAAGAAGATTATAGCCGGGATCCGCCCCTCTCCCTC
	R	GCAAATTTTCGACATTACTATTCATCTCGGTACCAAGCTTAAGTTTAAACGC
UBE2S C95Sw	F	GGCGAACGGGGAAATAAGCGTGAATGTCTTGAAACG
	R	CGTTTCAAGACATTCACGCTTATTTCCCCGTTCGCC
UBE2S K100Rw	F	GTGTGAATGTCTTGAGGCGCGATTGGACCGCG
	R	CGCGGTCCAATCGCGCCTCAAGACATTCACAC
UBE2S R101Aw	F	GTGAATGTCTTGAAAGCCGATTGGACCGCGG
	R	CCGCGGTCCAATCGGCTTTCAAGACATTCAC
UBE2S D102Aw	F	GAATGTCTTGAAACGCGCCTGGACCGCGGAATTAG
	R	CTAATTCCGCGGTCCAGGCGCGTTTCAAGACATTC
UBE2S L107Aw	F	ATTGGACCGCGGAAGCCGGGATAAGGCATGTC
	R	GACATGCCTTATCCCGGCTTCCGCGGTCCAAT

Name		Nucleotide sequence (5'-3')
UBE2S H111Aw	F	CGCGGAATTAGGGATAAGGGCCGTCTTATTAACG
	R	CGTTAATAAGACGGCCCTTATCCCTAATTCCGCG
UBE2S L114Aw	F	AGGGATAAGGCATGTCTTAGCCACGATAAAATGTTTATTAA
	R	TTAATAAACATTTTATCGTGGCTAAGACATGCCTTATCCCT
UBE2S T115Aw	F	GGGATAAGGCATGTCTTATTAGCCATAAAATGTTTATTAATAC
	R	GTATTAATAAACATTTTATGGCTAATAAGACATGCCTTATCCC
UBE2S K117Aw	F	GGGATAAGGCATGTCTTAGCCACGATAAAATGTTTAT
	R	ATAAACATTTTATCGTGGCTAAGACATGCCTTATCCC
UBE2S C118Sw	F	CATGTCTTATTAACGATAAAAAGCTTATTAATACATCCGAATCCG
	R	CGGATTCGGATGTATTAATAAGCTTTTTATCGTTAATAAGACATG
UBE2S H122Aw	F	GATAAAATGTTTATTAATAGCCCCGAATCCGGAGAGCGCC
	R	GGCGCTCTCCGGATTCGGGGCTATTAATAAACATTTTATC
FLAG-UBE2S_pCDNA5_FRT/TO-UBE2S_L114A	F	CAGATATCATGGATTACAAGGATGACGACGATAAGAACTCCAACGTGGAGAACC
	R	CCCTCTAGACTCGAGCGGCCGCCTACAGCCGCCGCAGCGC
C1ins ubiquitin_pET30a	F	GGAGATATACATTGCATGCAGATTTTCGTGAAAAC
	R	GTTTTCACGAAAATCTGCATGCAATGTATATCTCC
K11R ubiquitin_pET30a	F	GAAAACCCTTACGGGGCGTACCATCACCCTCGAGG
	R	CCTCGAGGGTGATGGTACGCCCCGTAAGGGTTTTC

Additional primers were designed by Dr. Sonja Lorenz, while working at the University of California, Berkeley, CA/USA.

2.2 Bacterial strains and expression constructs

Table 2: Bacterial strains for cloning and protein expression

Organism	Strain	Genotype	Supplier
E. coli	Top10	F- *mcr*A Δ(*mrr-hsd*RMS-*mcr*BC) Φ80*lac*ZΔM15 Δ*lac*X74 *rec*A1 *ara*D139 Δ(*ara leu*) 7697 *gal*U *gal*K *rps*L (StrR) *end*A1 *nup*G	Invitrogen
E. coli	DH5a	F- φ80*lac*ZΔM15 Δ(*lac*ZYA-*arg*F)U169 *rec*A1 *end*A1 *hsd*R17(rk -, mk +) *pho*A *sup*E44 *thi*-1 *gyr*A96 *rel*A1 λ-	Invitrogen
E. coli	BL21 (DE3)	F- *ompT hsdS*(rB – mB -) *dcm*+ gal *l* (DE3)	Invitrogen
E. coli	Rosetta (DE3) pLysS	F- *ompT hsdS*(rB – mB -) *dcm*+ gal *l* (DE3) [pLysS CamR]	Novagen

Table 3: Vectors for protein expression in bacterial and mammalian cells

Vector	Host	Affinity tag	Cleavage site	Resis-tance	Supplier
pCCA1, (*pET-28*, modified)	bacterial	N-terminal His_6-SUMO tag	ULP1	Kan	Merck
pMAL-TEV	bacterial	C-terminal His_6-taq	TEV	Amp	
pET-30a	bacterial	N-/C-terminal His_6-tag	Thrombin	Kan	Merck
pRK793	bacterial	N-terminal His_6	TEV	Amp	Addgene
pFGET19	bacterial	N-terminal His_6		Kan	Addgene
pGEX TEV	bacterial	Cleavable N-terminal GST-tag, uncleavable C-terminal His_6-tag	TEV	Amp	Prof. Brenda Schulman
pSKB2	bacterial	N-terminal His_6-tag		Kan	
pCDNA5/FRT/TO-3xFLAG	mammalian	N-terminal 3xFLAG-tag		Amp	Dr. Catherine Lindon
pCDN5/FRT/T0 3xFLAG Venus (pCDNA5/FRT/TO-3xFLAG, modified)	mammalian	N-terminal 3xFLAG-tag		Amp	Dr. Jörg Mansfeld (Dr. Catherine Lindon)

Vector	Host	Affinity tag	Cleavage site	Resis-tance	Supplier
pCS2	mammalian			Amp	
pCDNA5 FRT/TO-MCS-IRES2-eGFP (pcDNA5/FRT/TO -neo, modified*)*	mammalian			Amp	Dr. Jörg Mansfeld (Prof. Jonathon Pines)

Table 4: Expression constructs. The protein sequences are from *Homo sapiens*, expect for the ones of the proteases.

Vector	Insert	Residue number	Provided by
pCCA1	UBE2S	1-222	Dr. Sonja Lorenz [4]
pCCA1	UBE2S pointmutants	1-222	
pCCA1	$UBE2S^{UBC}$	1-156	Dr. Sonja Lorenz [4]
pCCA1	$UBE2S^{UBC}$ pointmutants	1-156	
pCCA1	$UBE2S^{1-196}$	1-196	Marie-Annick Letzelter
pCCA1	HA-UBE2S	1-222	
pCCA1	HA-UBE2S pointmutants	1-222	
pCCA1	HA-$UBE2S^{UBC}$	1-156	
pCCA1	HA-$UBE2S^{UBC}$ pointmutants	1-156	
pSKB2	His-UBE2S	1-222	Dr. Sonja Lorenz [4]
pSKB2	His-UBE2S pointmutants	1-222	
pSKB2	His-$UBE2S^{UBC}$	1-156	
pSKB2	His-$UBE2S^{UBC}$ pointmutants	1-156	
pET-30a	Ubiquitin	1-76	Dr. Sonja Lorenz [4]
pET-30a	Ubiquitin pointmutants	1-76 / -1-76	
pGEX TEV	ubiquitin-cyclin $B1^{NTD}$	Ubiquitin: 1-74 Cyclin $B1^{NTD}$: 1-95 + C-terminal Cys	Prof. Brenda Schulman [142]
pRK793	TEV protease	1-303	Prof. John Kuriyan
pFGET19	ULP1 protease	403-621	Prof. John Kuriyan

2.3 Bioreagents, kits and enzymes

Table 5: Bioreagents, enzymes and kits

Designation	Supplier
5x Q5 reaction buffer	New England Biolabs
5x Q5 High GC Enhancer	New England Biolabs
10x Standard *Taq* Reaction Buffer	New England Biolabs
Albumin Fraktion V (BSA)	Roth
DNaseI	Invitrogen
DpnI	New England Biolabs
GC buffer (PCR)	New England Biolabs
Gel Filtration Standard	Bio-Rad
GeneRulerTM 1 kb DNA Ladder	Thermo Fisher Scientific
Lysogeny broth (LB) medium	Carl Roth
Midori Green Advance DNA stain	NIPPON
NucleoSpin Gel and PRC cleanup kit	Macherey & Nagel
NucleoSpin Plasmid kit	Macherey & Nagel
PageRuler Prestained Protein Ladder	Thermo Fisher Scientific
Pierce Silver Stain Kit	Thermo Fisher Scientific
Q5 high fidelity DNA Polymerase	New England Biolabs
SignalFire ECL Reagent	Cell Signalling Technology
Taq DNA Polymerase	New England Biolabs
Terrific Broth (TB) medium	Carl Roth

2.4 Chemicals

Table 6: Chemicals

Substance	Supplier
2-Deoxyadenosine 5-triphosphate (dATP) sodium salt solution	New England Biolabs
2-Deoxycytidine 5-triphosphate (dCTP) sodium salt solution	New England Biolabs
2-Deoxyguanosine 5-triphosphate (dGTP) sodium salt solution	New England Biolabs
2-Deoxythymidine 5-triphosphate (dTTP) sodium salt solution	New England Biolabs
2-Propanol (Isopropanol)	Carl Roth
3-Morpholinopropane-1-sulfonic acid (MOPS)	Sigma-Aldrich
4-(2-Hydroxyethyl)-1-piperazineethanesulfonic acid (HEPES)	Carl Roth

Substance	Supplier
5,5-Dithiobis-2-nitrobenzoic acid (DTNB)	Carl Roth
Acetic acid	Carl Roth
Agarose NEEO ultra quality	Carl Roth
Ammonium persulfate (APS)	Carl Roth
Ammonium acetate (NH_4COOH)	Carl Roth
^{15}N-labeled Ammonium chloride ($^{15}NH_4Cl$)	Sigma-Aldrich
Ampicillin sodium salt	Carl Roth
Benzamidin hydrochloride monohydrate	Carl Roth
Beta-mercapthoethanol (β-ME)	Sigma-Aldrich
Bis-Acrylamid 29:1	Fisher Bioreagents
Bromphenol blue	Carl Roth
Calcium chloride dihydrate ($CaCl_2$)	Carl Roth
Chloramphenicol	Carl Roth
Coomassie Brilliant Blue G-250	Carl Roth
Coomassie Brilliant Blue R-250 Carl Roth	Carl Roth
Deuteriumoxid (D_2O)	Sigma-Aldrich
Dibromobimane (bBBr)	Sigma-Aldrich
Dimethylsulfoxide (DMSO)	Carl Roth
Disodium hydrogen phosphate (Na_2HPO_4)	Carl Roth
Dithiothreitol (DTT)	Carl Roth
Ethanol (EtOH)	Carl Roth
Ethylenediaminetetraacetic acid (EDTA)	Carl Roth
Ethylene glycol	Sigma-Aldrich
Glucose	Carl Roth
^{13}C-labeled glucose	Sigma-Aldrich
Glycerol	Carl Roth
Glycine	Carl Roth
Hydrochloric acid (HCl)	Carl Roth
Imidazole	Carl Roth
Iron(II) sulfate heptahydrate ($FeSO_4$)	Sigma-Aldrich
Isopropyl-β-D-thiogalactopyranoside (IPTG)	Carl Roth
Kanamycin sulfate	Carl Roth
Magnesium chloride hexahydrate	Carl Roth
Magensium sulfate heptahydrate (Mg_2SO_4)	Sigma-Aldrich
Manganese(II) chloride tetrahydrate ($MnCl_2 \cdot 4\ H_2O$)	Sigma-Aldrich
Methanol	Carl Roth
N-Ethylmaleimide (NEM)	Carl Roth
Nickel(II) sulfate hexahydrate	Carl Roth
Perchloric acid	Sigma-Aldrich

Substance	Supplier
Phenylarsine oxide (PAO)	Sigma-Aldrich
Polyethylenglycol (PEG) 3350	Sigma-Aldrich
Polyethylenglycol (PEG) 4000	Sigma-Aldrich
Potassium dihydrogen phosphate	Carl Roth
Potassium formate (KOOH)	Carl Roth
Rubidium chloride (RbCl)	Sigma-Aldrich
Sodium acetate	Carl Roth
Sodium cacodylate trihydrate	Sigma-Aldrich
Sodium chloride (NaCl)	Carl Roth
Sodium dodecyl sulfate (SDS)	Sigma-Aldrich
Sodium dihydrogenphosphate dihydrate (NaH_2PO_4)	Carl Roth
Sodium hydroxide (NaOH)	Carl Roth
Tetramethylethylenediamin (TEMED)	Carl Roth
Thiamine hydrochloride	Sigma-Aldrich
Tris-(2-carboxyethyl)-phosphine (TCEP)	Carl Roth
Tris-(hydroxymethyl)-aminoethane (Tris)	Carl Roth
Triton X-100	Sigma-Aldrich
Tween 20	Sigma-Aldrich
Yeast nitrogen base	Sigma-Aldrich
Zinc chloride ($ZnCl_2$)	FlukaBioChemica

2.5 Crystallization screens

All crystallization screens were prepared by the in-house facility, according to the composition of the commercial crystallization screens:

Table 7: Commercial crystallization screens used as templates for in-house screens.

Screen	Supplier
Additive Screen	Hampton Research
Crystal Screen, Crystal Screen 2	Hampton Research
Index Screen HT	Hampton Research
JCSG+	Molecular Dimensions
Nextal PEG Suite	Qiagen
Nucleix Suite	Qiagen
Optimix 3	Fluidigm
Optimix PEG	Fluidigm
PEGs Suite, PEGs II Suite	Qiagen

Screen	Supplier
pH Clear Suite, pH Clear II Suite	Qiagen
Protein Complex Suite	Qiagen
Silver Bullets Bio	Hampton Research
Wizard 1+2, Wizard 3+4	Emerald BioSystems

2.6 Specialized consumables

Table 8: Specialized consumables

Type	Model	Supplier
24-well hanging-drop crystallization plates	Crystalgen SuperClear Plate	Jena Bioscience
96-well sitting-drop crystallization plates	Crystalquick 1 square well, flat bottom, low profile	Greiner Bio-One
Microplate 96 well	96-well half area microplates	Greiner Bio-One
Cover slides	22 mm, siliconised	Jena Bioscience
Dialysis membranes	Spectra/Por	Spectrum Laboratories
Nickel-beads	Ni-NTA agarose	Macherey & Nagel
PVDF membrane	Roti -PVDF	Carl Roth
SDS gels	Novex 10-20% Tris-Glycine Mini Gels, Wedge Well	Thermo Fisher Scientific
Ultrafiltration units	Amicon MWCO 3-30 kDa, 0.5-20 ml	Merck Millipore

2.7 Relevant scientific equipment

Table 9: Scientific equipment

Device	Model	Company
Affinity chromatography column	HisTrap HP 1 ml/5 ml	GE Healthcare
Agarose gel electrophoresis system	Mini-Sub Cell GT System	Bio-Rad
Analytical ultra centrifuge	Optima XL-I	Beckmann Coulter
Anion exchange chromatography column	Mono Q 10/100 GL Mono Q 4.6/100 PE	GE Healthcare
Cation exchange chromatography column	HiTrap SP 5 ml	GE Healthcare
CD cuvette	QS-110	Hellma
CD spectropolarimeter	J-810	Jasco

Device	Model	Company
Chemiluminescence imager	FluorchemQ Multi image	Alpha Innotech
Crystallization loops	CryoLoop	Hampton Research
Crystallization robot	Analytic Honey Bee 963	Digilab
Differential refractometer	Optilab T-rEX	Wyatt Technologies
SEC columns	HiLoad 16/600 Superdex (SD) 75/200 pg HiLoad 26/600 Superdex 75 Superdex 75/200 10/300 GL	GE Healthcare
FPLC systems	AKTA pure 25 AKTA purifier (SEC-MALS)	GE Healthcare
Gel electrophoresis chamber (SDS-PAGE)	Mini-ProteanR 3-cell Xcell SureLock Mini-Cell	Bio-Rad Invitrogen
Liquid handling robot	LISSY 2002	Zinsser Analytik
MALS detector	DAWNR 8 + HELEOSR II	Wyatt Technologies
Microplate Reader	CLARIOstar	BMG LABTECH
Robotic sealing unit for microplates	RoboSeal	HJ-BIOANALYTIC
Scanner	Odyssey	LI-COR
Sonicator	LabsonicR B.	Braun Biotech International
Spectrophotometer	Bio-Photometer Plus	Eppendorf
Nanodrop	ND 2000c	Thermo Fisher, PEQLAB
Thermo block	Rotilabo-Block Heater250 Thermomixer Comfort	Carl Roth Eppendorf
UV imaging system	Gel Doc XR System	Bio-Rad
Western blot	Trans-Blot Turbo Transfer-System	Bio-Rad

2.8 Software, servers and databases

The software as well as server-based tools and databases were used in the latest version published at the time.

Table 10: Software, server-based tools and databases

Program	Description	Supplier / Reference
AIMLESS	Scaling and merging of diffraction data	[157,158]
AlphaView	Capturing images of the FluorchemQ system	Alpha Innotech
Astra VI	MALS control and data analysis	Wyatt Technologies

Program	Description	Supplier / Reference
blastp/ blastn	Sequence search	[159]
CCP4	Software suite for macromolecular X-ray crystallography	[160]
COOT	Model-building software	[161]
Clustal Omega	Sequence alignments	[162]
ExPASy ProtParam	Computation of physical and chemical properties of proteins	[163]
ExPASy Translate	Translation tool of nucleotide sequences to protein sequences	[163]
ImageJ	image processing program, 1.48v	[164]
Image Studio Software	image processing program	LI-COR
MARS	Clariostar data analysis software	BMG LABTECH
Microsoft Excel	Spreadsheet software	Microsoft Corporation
Microsoft Power Point	Generation of figures	Microsoft Corporation
MolProbity	Structure validation for macromolecular crystallography	[165]
NMRViewJ	Software for visualization and analysis of NMR Spectra	One Moon Scientific
ODYSSEY	Infra-red imaging software	LI-COR
OriginPro	Graphics and data analysis software	OriginLab
PDB	Protein Data Bank	[166]
PHASER	Phasing software	[167]
Phenix	Software suite for macromolecular X-ray crystallography	[168]
Phyre2	Biosequence analysis; protein 3D structure prediction	[169]
PISA	Bioinformatic characterization of interfaces	[170]
PrimerX	Automated design of mutagenic primers for site-directed mutagenesis	Lapid, 2003
PyMOL	3-dimensional visualization and graphical illustration software	DeLano Scientific LLC
Pubmed	Literature search	[171]
RF-cloning.org	automated primer design process for RF cloning	[172]
Quantity One	UV imaging system control; UV image recording and analysis	Bio-Rad
SEDFIT	Analysis of AUC data	[173]

Program	Description	Supplier / Reference
Spectra Manager	CD data acquisition and analysis	Jasco
UNICORN	FPLC instrument control; recording, analysis and management of chromatograms	GE Healthcare
XDS	indexing, and integration of diffraction images	[174]

3. Methods

Several of the listed methods in this chapter have been originally described in the associated publications by Liess et al. [53,175] and represent an original excerpt of these manuscripts, extended or adapted, as appropriate.

3.1 Molecular biology

3.1.1 Preparation of chemically competent *E. coli* cells

LB medium:	20 g/l LB medium
TFB1:	30 mM KCOOH, pH 5.8, 75 mM $CaCl_2$, 10 mM RbCl, 15% glycerol
TFB2:	10 mM MOPS, pH 6.5, 75 mM $CaCl_2$, 10 mM RbCl, 15% glycerol

The competent cells were mostly prepared by Julia Haubenreißer (TA, Lorenz lab). Therefore, a single colony of the respective *E. coli* cells was transferred into 2.5 ml of LB medium and incubated overnight at 37 °C. 1 ml of this culture was sub-cultured into 100 ml of pre-warmed LB-medium, supplemented with the appropriate antibiotic, and shaken at 37 °C until an OD_{600} of 0.4 - 0.6 was reached. Then the cells were incubated on ice for 5 min and pelleted for 5 min at 1500 x g in a cooled centrifuge. The pellet was re-suspended in 30 ml of ice-cooled transformation buffer 1 (TFB1), incubated on ice for 90 min, and pelleted as before. Thereafter, the cell pellet was re-suspended in 4 ml of ice cooled TFB2, incubated on ice for 60 min and aliquoted (50 µl fractions). The aliquots were flash-frozen in liquid nitrogen and stored at −80 °C.

3.1.2 Transformation

LB agar plates:	20 g/l LB medium, 15 g/l agar, appropriate antibiotic
Antibiotics:	100 µg/ml ampicillin
	100 µg/ml kanamycin

Bacterial cells (*E. coli* TOP 10, *E. coli* BL 21/DE3 or *E. coli* Rosetta pLysS) were thawed on ice and supplemented with 50 ng – 100 ng of the appropriate plasmid DNA and incubated for 30 min at 4 °C before the heat shock at 42 °C for 45 s. Thereafter, 600 µl of LB medium were added and the cells were incubated for 45 – 60 min at 37 °C and

1000 rpm. The cells were spun down, the pellet was dissolved in 100 µl of LB. 50 – 100 µl were plated on LB agar plates including the appropriate antibiotic for selection and incubated at 37 °C overnight.

3.1.3 DNA amplification and isolation

For DNA amplification and isolation, the respective plasmid DNA was transformed into *E. coli* TOP10 (see 3.1.2), plated on the appropriate LB agar plate and incubated overnight at 37 °C. One to three of the grown colonies were used to inoculate 5 ml of LB medium, supplemented with the appropriate antibiotics. The cultures were grown at 37 °C and 300 rpm for nine hours up to overnight. Hereafter, the DNA was isolated using the NucleoSpin plasmid kit (Macherey & Nagel), following the manufacturer´s instructions. The DNA concentration was determined as described in section 3.2.15. For DNA sequencing, the DNA was sent for sequencing to Eurofins Genomics, LGC Genomics or Microsynth Seqlab.

3.1.4 Site-directed mutagenesis via QuickChange

For single amino acid substitutions or the introduction or deletion of a few amino acids in the encoded proteins, QuickChange site-directed mutagenesis (QC) was used. Therefore, primer pairs containing the mutation of interest in the middle with an overhang of at least 16 base pairs (bp) on each site were designed using the online program PrimerX (Carlo Lapid, 2003). The amplification of the plasmid with the appropriate primer pairs was performed according to the manufacturer´s protocol (Stratagene) using Q5 high fidelity DNA polymerase (New England Biolabs), with an appropriate annealing temperature and extension time. Thereafter, the methylated, non-mutated parental DNA template was digested with *Dpn*I at 37 °C for at least 2 h and the reaction mixture transformed into competent *E. coli* (see 3.1.2). The mutation was finally verified by sequencing (see above).

3.1.5 Restriction-free cloning

Restriction-free cloning (RF cloning) was used for the insertion of longer DNA fragments or whole genes into a vector of interest [176]. Therefore, primers that contain overhangs that are homologous to the vector were designed with the online tool RF-Cloning.org [172]. In a first PCR, the desired template was amplified and purified by agarose-gel

extraction, using the NucleoSpin Gel and PCR cleanup kit (Macherey & Nagel). In a second PCR, the insert was inserted into the vector, whereas the insert and the vector were used in ratio of 10:1. The methylated parental DNA template was digested with *Dpn*I at 37 °C for at least 2 hours and the reaction mixture was transformed into competent *E. coli* cells (see 3.1.2). The DNA sequence was verified as described above.

3.1.5.1 Sequence and ligation independent cloning

For sequence and ligation independent cloning (SLIC) [177], an insert and a vector of interest need complementary ends. Thus, the primers for the insert (RF primers) were designed to contain overhangs that are homologous to the vector ends. With this method, the wobbled UBE2S sequence (provided as gene block) was inserted into the pCDNA5 FRT/TO-MCS-IRES2-eGFP vector and simultaneously a point mutation was introduced. In a first step, two polymerase chain reactions (PCRs), were performed. In the first PCR, the forward RF primer and the reverse primer to introduce the point mutation (QC primer) were used, and the second PCR was performed with the reverse RF primer and the forward QC primer. The resulting fragments were purified by agarose-gel extraction, using the NucleoSpin Gel and PCR cleanup kit (Macherey & Nagel). In the second step, the inserts of step 2 were combined, amplified by using the RF primers and purified by agarose-gel extraction, as described above. In a third step, the vector was linearized, digested with *Dpn*I at 37 °C for at least 2 hours and purified by PCR cleanup (NucleoSpin Gel and PCR cleanup kit, Macherey & Nagel). The vector as well as the insert were digested by T4 DNA polymerase (New England Biolabs, NEB), using 1 µl DNA, 5 µl NEB buffer 2, 1 µl BSA, 0.5 µl T4 DNA polymerase and 42.5 µl ddH_2O. The reaction mixture was incubated at room temperature for 30 min and was stopped by the addition of 1 µl of dGTP to a final concentration of 1 mM. For the annealing of the insert and the vector, 2 µl of the vector and 8 µl of the insert were mixed with 10 µl ddH_2O and incubated for 5 min at 75 °C and then cooled down to 30 °C. 10 µl of the reaction mixture were transformed into competent *E. coli* cells (see 3.1.2) and the DNA sequence was verified by sequencing (see above).

3.1.6 Agarose gel electrophoresis

TAE buffer: 40 mM Tris, pH 8, 20 mM acetic acid, 1 mM EDTA

DNA loading dye (6x): 4 mM urea, 10 mM EDTA, 50% (v/v) glycerol, 0.1% (w/v) bromphenol blue

For the separation of DNA fragments according to their size, agarose gel electrophoresis was used. Depending on the size of the DNA fragments 1.6% (w/v) agarose (for fragments < 1 kb) or 1% (w/v) agarose (fragments > 1kb) was resuspended in TAE buffer, supplemented with the DNA-intercalating Midori Green Advanced dye (NIPPON) and poured in a caster. The DNA samples were mixed with the DNA loading dye (1x final concentration) and the gel electrophoresis was performed in TAE buffer for 30 min at 120 V. DNA fragments were visualized by UV light and cut out for gel extraction (NucleoSpin Gel and PCR cleanup kit, Macherey & Nagel) if required. DNA concentrations were measured by UV/VIS absorbance at 260 nm with a Nanodrop ND 2000c (Peqlab).

3.1.7 Protein expression and harvesting

TB media:	50.8 g/l, 4 ml glycerol
M9 media:	47.9 mM Na_2HPO_4 x $2H_2O$, 22 mM KH_2PO_4, 8.6 mM NaCl, pH 7.4; supplemented with 0.4% (w/v) glucose, 2 mM $MgSO_4$, 0.1 mM $CaCl_2$, 1 mg/l thiamine, 10 µM $FeSO_4$, 10 µM $ZnCl_2$, 0.1% (w/v) $^{15}NH_4Cl$, 0.17% (w/v) YNB

For the expression of unlabeled Proteins, the DNA of interest was transformed into *E. coli* BL21/DE3 cells, with the expectation of UBE2S K100R, $UBE2S^{UBC}$ K100R and Ub-Cyclin B^{NTD}. These were expressed in *E. coli* Rosetta pLysS. One day prior to large-scale expression, a 100 ml pre-culture (100 ml LB media containing the appropriate antibiotic for selection) was inoculated with a single colony and incubated overnight at 37 °C and 200 rpm. The following day, 2 l of TB media, supplemented with the appropriate antibiotics, were inoculated with the pre-culture and incubated at 37 °C and 200 rpm until an OD_{600} of 0.6 – 1.0 was reached. Thereafter, expression was induced by the addition of 0.5 mM IPTG. The proteins were expressed at 20 °C and 200 rpm overnight.

^{15}N-labeled as well as ^{15}N- and ^{13}C-labeled proteins were expressed in supplemented M9-based medium. One day prior to large-scale expression, the pre-culture (50 ml M9-based medium containing the appropriate antibiotics) was inoculated with a single colony and incubated, as described above. The following day, 1 l of M9-based medium was supplemented with the appropriate antibiotics and inoculated with the pre-culture, to an OD_{600} of 0.05 was reached. The bacterial culture was incubated at 37 °C and 190 rpm,

and protein expression induced with 0.5 mM IPTG at an OD_{600} of 0.8. Expression was conducted at 20 °C and 190 rpm overnight.
Cells were generally harvested by centrifugation for 12 min at 4 °C and 4500 x g and either used directly for protein purification or stored at –80 °C.

3.2 Protein purification

3.2.1 Cell lysis

UBE2S lysis buffer:	50 mM Tris, pH 8.0, 500 mM NaCl, 5 mM benzamidine, 8 mM β-ME, 0.4% Triton X-100, protease-inhibitor cocktail (Roche)
Ub lysis buffer:	50 mM Tris, pH 7.4, 50 mM NaCl

The cell pellets were resuspended in the respective lysis buffer at 4 °C and lysed by sonification at 4 °C. The lysate was cleared by centrifugation at 57500 x g for one hour at 4 °C.

3.2.2 Affinity chromatography

3.2.2.1 Immobilized metal ion affinity chromatography

Buffer A IMAC:	50 mM Tris, pH 8.0, 500 mM NaCl, 20 mM imidazole, 8 mM β-ME
Buffer B IMAC:	50 mM Tris, pH 8.0, 500 mM NaCl, 500 mM imidazole, 8 mM β-ME
Buffer A2 IMAC:	50 mM HEPES pH 8.0, 150 mM NaCl, 8 mM β-ME
Buffer B2 IMAC:	50 mM HEPES pH 8.0, 150 mM NaCl, 500 mM imidazole, 8 mM β-ME

For the purification of His-tagged proteins, immobilized metal ion affinity chromatography (IMAC) was applied as initial purification step. This method is based on the non-biospecific interactions between exposed histidine groups and Ni^{2+} ions that are immobilized on beads via a chelating group. Therefore, a HisTrap Ni Sepharose affinity column (GE Healthcare) was used that selectively retains proteins containing a His_6-tag.

To perform IMAC, the column was equilibrated in buffer A/A2 IMAC, the filtered lysate loaded and the column and washed with buffer A/A2 IMAC for 15 - 20 column volumes (CV) to remove unbound proteins. The His_6-tagged proteins were eluted in 100% Buffer B IMAC (for UBE2S) or by a gradient from 20 - 100% buffer B2 IMAC (for Ub-Cyclin B^{NTD}).

3.2.2.2 Affinity chromatography using immobilized glutathione

GST buffer A:	PBS pH 7.4 (140 mM NaCl, 2.7 mM KCl, 10 mM $NaHPO_4$, 1.8 mM KH_2PO_4, pH 7.4), 2 mM DTT
GST buffer B:	50 mM Tris, 10 mM reduced glutathione, pH 8.0

By affinity chromatography with immobilized glutathione, glutathione S-Transferase (GST) tagged proteins can be purified.
A GSTrap HP column (GE Healthcare) was equilibrated in GST buffer A and the protein solution was loaded. After washing with 10 CV of GST buffer A, the GST-tagged proteins were eluted with GST buffer B.

3.2.3 Ion exchange chromatography

IEX buffer A1:	50 mM ammonium acetate pH 4.5
IEX buffer B1:	50 mM ammonium acetate pH 4.5, 500 mM NaCl
IEX dilution buffer:	25 mM Tris pH 7.4
IEX buffer A2:	25 mM Tris pH 7.4, 25 mM NaCl
IEX buffer B2:	25 mM Tris pH 7.4, 500 mM NaCl

For ion exchange chromatography (IEX) the protein solution was either dialyzed overnight at 4 °C, desalted by using a HiPrep 26/10 Desalting column (GE Healthcare) into the respective buffer A or diluted with the IEX dilution buffer to reach the salt concentration of the respective buffer A. Before sample application, a HiTrap SP HP column (GE Healthcare, for the purification of ubiquitin; see 3.2.10) or a MonoQ 4.6/100 PE column (GE Healthcare, for isolation and preparation of the conjugates, see 3.2.13 and 3.2.14) was washed with the respective buffer B to remove proteins sticking to the column and thereafter in the corresponding buffer A. The sample was then applied to the column and the column washed with 5 - 10 CV of 20% of buffer B in buffer A. For protein elution, an increasing gradient of buffer B was used. For details, see chapters 3.2.10, 3.2.13 and 3.2.14. According to the elution profile, selected fractions were analyzed by

SDS-PAGE and fractions containing the target protein or protein complex pooled and concentrated.

3.2.4 Tag cleavage by SMT3-specific protease ULP1 and TEV protease

Dialysis buffer UBE2S: 50 mM Tris pH 7.5, 300 mM NaCl, 2 mM DTT
Dialysis buffer Ub-Cyclin $B1^{NTD}$: 50 mM HEPES pH 7, 300 mM NaCl, 2 mM DTT

For some protein purifications the affinity tag (His_6-SUMO-tag for UBE2S and variants and the GST-tag for Ub-Cyclin $B1^{NTD}$) was removed. To this end, the proteins were dialyzed into the respective dialysis buffers using pre-treated Spectra/Pro Dialysis Membrane (Spectrum Labs) with the appropriate cut-off. After 4 h the buffer was replaced, and the protease added. To cleave His_6-SUMO-tag off UBE2S, ULP1 was used whereas the GST-tag of Ub-Cyclin $B1^{NTD}$ was cleaved by Tobacco Etch Virus (TEV) protease. The cleavage was performed at 4 °C overnight. The cleaved tags and the His-tagged proteases were subsequently removed from the protein solution by affinity chromatography.

3.2.5 Preparative size exclusion chromatography

SEC buffer 1: 25 mM Tris pH 7.4, 100 mM NaCl, 2 mM DTT
SEC buffer 2: 75 mM sodium phosphate pH 7.2, 1 mM EDTA, 5 mM DTT
SEC buffer 3: 50 mM Tris pH 7.4, 100 mM NaCl
SEC buffer 4: 50 mM HEPES pH 7, 150 mM NaCl, 2 mM DTT

The last purification step for all proteins was size exclusion chromatography (SEC). According to the molecular weight of the protein and the protein amount, a HiLoad SD 75 16/600 or HiLoad SD 75 26/600 gel filtration column (GE Healthcare) was used. Prior to sample application, the column was equilibrated in the gel filtration buffer. Thereafter the protein was loaded on the column, eluted in the respective SEC buffer, and analyzed by SDS-PAGE. Pooled fractions were concentrated with amicon ultra centrifugal filters (Merck Millipore) with a suitable MW cut-off for further use or aliquoted, flash frozen in liquid nitrogen and stored at −80 °C.

3.2.6 Purification of SMT3-specific protease ULP1

Buffer A IMAC (ULP1):	50 mM Tris pH 8.0, 500 mM NaCl, 20 mM imidazole, 10% glycerol, 5 mM β-ME
Buffer B IMAC (ULP1):	50 mM Tris pH 8.0, 500 mM NaCl, 500 mM imidazole, 10% glycerol, 5 mM β-ME
Storage buffer (ULP1):	50 mM Tris pH 8.0, 250 mM NaCl, 10% glycerol, 5 mM β-ME

The SMT3-specific protease ULP1 was mostly prepared by Julia Haubenreißer (TA, Lorenz lab). Therefore, TB medium, supplemented with the appropriate antibiotic, was inoculated with *E. coli* Rosetta pLysS, expressing His_6-tagged ULP1 protease (provided by Prof. John Kuriyan, University of California, Berkeley, CA/USA). Protein expression was induced by IPTG induction and conducted at 18 °C overnight. At the next morning, the bacteria cells were harvested, resuspended in buffer A and lysed by sonication. ULP1 protease was purified as His_6-fusion protein from the supernatant by Ni-affinity chromatography, using a HisTrap Ni Sepharose affinity column (GE Healthcare) and eluted in 50 ml of buffer B. In a final step, buffer B was exchanged against the storage buffer, using Zeba Spin Desalting Columns (Thermo Fisher Scientific) and the protein aliquoted in 200 µl aliquots of 2.5 mg/ml, flash frozen in liquid nitrogen and stored at −80 °C.

3.2.7 Purification of tobacco etch virus (TEV) protease

Lysis buffer (TEV):	25 mM Tris pH 8.0, 500 mM NaCl, 20 mM imidazole, 2 mM β-ME, 0.005% Triton X-100, 10% glycerol, Dnase, lysozyme
Buffer A IMAC (TEV):	25 mM Tris pH 8.0, 500 mM NaCl, 20 mM imidazole, 10% glycerol, 2 mM β-ME
Buffer B IMAC (TEV):	25 mM Tris pH 8.0, 150 mM NaCl, 20 mM imidazole, 10% glycerol, 2 mM β-ME
Buffer C IMAC (TEV):	25 mM Tris pH 8.0, 150 mM NaCl, 500 mM imidazole, 10% glycerol, 2 mM β-ME
Storage buffer (TEV):	25 mM Tris pH 8.0, 150 mM NaCl, 0.5 mM EDTA, 10% glycerol, 5 mM DTT

TEV protease was mostly prepared by Julia Haubenreißer (TA, Lorenz lab). The TEV protease was expressed as a His_6-tagged fusion in antibiotic-supplemented TB medium, inoculated with *E. coli* Rosetta pLysS. After the induction by IPTG, the culture was shaken at 25 °C overnight. The bacterial cells were harvested, resuspended in the lysis buffer and disrupted by sonication. The lysate was cleared by centrifugation and the supernatant loaded on a HisTrap Ni Sepharose affinity column (GE Healthcare), equilibrated in buffer A. The column was washed with buffer B and the TEV protease eluted with a linear gradient of buffer C, dialyzed overnight into the storage buffer and aliquoted in 200 µl aliquots of 2.5 mg/ml. The aliquots were flash-frozen in liquid nitrogen and stored at −80 °C.

3.2.8 Purification of the human E1 enzyme UBA1

Human UBA1 was prepared from insect cells by Dr. Sonja Lorenz, as described previously [4].

3.2.9 Purification of human UBE2S and variants

Untagged UBE2S and variants as well as HA-tagged UBE2S were purified as a His_6-SUMO-tag-UBE2S fusion from the supernatant by Ni-affinity chromatography, using a HisTrap Ni Sepharose affinity column (GE Healthcare). The column was equilibrated in buffer A IMAC and thereafter the cleared and filtered lysate loaded on the column. Unbound proteins were removed by washing with buffer A for 18 CVs. The His_6-SUMO-tag-UBE2S fusion proteins were then eluted with 5 CVs buffer B IMAC and the column was re-incubated into buffer A IMAC (see 3.2.2). To cleave off the His_6-SUMO-tag and further purify UBE2S and variants, the tagged proteins were dialyzed into the dialysis buffer for 4 h at 4 °C, using pre-treated Spectra/Pro Dialysis Membrane (MWCO 3.5 kDa; Spectrum Labs). After 4 h, His-tagged ULP1 was added and the cleavage performed overnight. The His_6-tag as well as the protease were removed by IMAC and the UBE2S-containing flow-through was injected on a HiLoad 16/600 Superdex 75 column (GE Healthcare) using the SEC buffer 1 (see 3.2.5).
Isotope-enriched UBE2S and variants were purified as described above but SEC buffer 2 was used for the final preparative size exclusion chromatography (see 3.2.5).
His_6-tagged $UBE2S^{UBC}$ and UBE2S were expressed after induction with 0.5 mM IPTG at 20 °C overnight. Cells were harvested and lysed as described in section 3.2.1. The proteins were purified by Ni-affinity chromatography (HisTrap Ni sepharose, GE

Healthcare, see 3.2.2.1), buffer-exchanged into SEC buffer 1 (see 3.2.5), and polished by gel filtration (HiLoad 16/600 Superdex 75, GE Healthcare) in the same buffer.

3.2.10 Purification of ubiquitin

Ubiquitin and variants were purified from the supernatant by precipitation with 75% perchloric acid while stirring on ice for 10 min. The mixture was centrifuged at ≥ 8 x g for 30 min and the supernatant dialyzed into 50 mM ammonium acetate pH 4.5 for at least 4 h or overnight, using pre-treated Spectra/Pro Dialysis Membrane (MWCO 3.5 kDa; Spectrum Labs). Thereafter, the solution was applied on a HiTrap SP HP column (GE Healthcare) and an ion exchange chromatography performed with IEC buffer A2 and B2. The column was washed for 5 CV with IEC buffer A2 and eluted by using a gradient from 0 - 44% IEC buffer B2 in 4 CV, 45% IEC buffer B2 for 6 CV followed by 4 CV of 100% IEC buffer B2 (see 3.2.3) The ubiquitin containing fractions were pooled and applied to a HiLoad 16/600 Superdex 75 column (GE Healthcare) in SEC buffer 3 (see 3.2.5). For NMR, SEC buffer 2 was used, while Cys-ubiquitin for labeling with IRDye 800CW Maleimide (LI-COR) was purified in SEC buffer 4 (see 3.2.5).

3.2.11 Purification of Ub-Cyclin B1^{NTD}

The preparation of the ubiquitin-cyclin B1^{NTD} fusion carrying an N-terminal GST and a C-terminal His_6-tag has also been described in [113]. In brief, Ub-Cyclin B1^{NTD} was expressed in *E. coli* Rosetta pLysS and purified by Ni-affinity chromatography, using buffer A2 IMAC and buffer B2 IMAC (see 3.2.2.1). TEV-cleavage was performed at 4 °C overnight (see 3.2.4) and the GST-tag was removed by affinity chromatography with immobilized glutathione (see 3.2.2.2). Ub-Cyclin B1^{NTD} was finally polished by size exclusion chromatography, using SEC buffer 4 (see 3.2.5).

3.2.12 IRDye 800CW maleimide-labeling of Cys-ubiquitin and Ub-Cyclin B1^{NTD}

To label ubiquitin at the N-terminus (Cys-1) and ubiquitin-cyclin B1^{NTD} at the C-terminus [113] with a fluorophore, the purified proteins were first incubated with 10 mM DTT for 10 min and desalted in 50 mM HEPES pH 7.0 and 150 mM NaCl. IRDye 800CW maleimide (LI-COR) was added to the proteins at 3-fold molar excess, the reactions incubated at room temperature for 2 h, and then quenched with 10 mM DTT. To quantitatively remove unreacted fluorophores the samples were desalted twice (HiPrep

26/10 desalting column; GE Healthcare), followed by an additional size-exclusion chromatography (Superdex 75 10/300 GL increase column; GE Healthcare) in 50 mM HEPES pH 7.0, 150 mM NaCl, and 2 mM DTT (ubiquitin-cyclin $B1^{NTD}$) and 25 mM Tris pH 7.4, 100 mM NaCl, and 2 mM DTT (ubiquitin), respectively.

3.2.13 Isolation of the $UBE2S^{UBC}$-Ub K11R-conjugate

For activity assays, a UBE2S-ubiquitin conjugate was isolated from an *in vitro* ubiquitination reaction. Therefore, 0.5 µM UBA1, 20 µM $UBE2S^{UBC}$, 120 µM ubiquitin K11R, 3 mM ATP, and 9 mM $MgCl_2$ were incubated in 25 mM Tris pH 7.0 and 100 mM NaCl at 30 °C for 1 h. The reaction was subsequently diluted in 25 mM Tris pH 7.4 and 2 mM DTT to adjust the salt concentration to 25 mM NaCl. Mono-ubiquitinated UBE2S was isolated by anion exchange chromatography (Mono Q 4.6/100 PE; GE Healthcare), using a gradient from 25 to 500 mM NaCl in 25 mM Tris pH 7.4, and 2 mM DTT and purified by size-exclusion chromatography (HiLoad 16/600 SD 75; GE Healthcare) in 25 mM Tris pH 7.4, 100 mM NaCl, and 2 mM DTT. The fraction of unmodified $UBE2S^{UBC}$ from the reaction was also recovered to serve as a control in the activity assays.

3.2.14 Preparation of $UBE2S^{UBC}$ C95S/C118M/K100C-Ub G76C conjugates

For NMR studies, disulfide-linked conjugates of ubiquitin G76C and $UBE2S^{UBC}$ C95S/C118M/K100C were prepared according to established protocols [4,52]. Briefly, the required purified protein variants were buffer exchanged into 50 mM sodium phosphate pH 7.4. Ubiquitin was activated by incubation with a 9-fold molar excess of 5,5'-dithio-bis-2-nitrobenzoic acid (DTNB) at room temperature for 40 min and the excess of DTNB removed by desalting (HiPrep 26/10 desalting column; GE Healthcare). Then the activated ubiquitin was incubated with a sub-stoichiometric amount of $UBE2S^{UBC}$ C95S/C118M/K100C at room temperature for 30 min. After exchange into 25 mM Tris pH 7.4 and 100 mM NaCl, the disulfide-linked complex was purified by anion exchange chromatography (MonoQ 4.6/100 PE; GE Healthcare) using a NaCl-gradient from 25 to 500 mM in 25 mM Tris pH 7.4 and subsequent size-exclusion chromatography (SD 75 16/600: GE Healthcare) in 75 mM sodium-phosphate pH 7.2 and 1 mM EDTA.

For chemical shift mapping studies, either the ubiquitin or the E2 in the complex was supplied in a ^{15}N-enriched form. To generate backbone resonance assignments for the complex, both components were ^{15}N- and ^{13}C-enriched.

3.2.15 Protein concentration determination

Protein concentrations of folded proteins in their reduced state were determined by UV/VIS spectroscopy based on the Lambert-Beer law.

Equation 1: The Lambert-Beer law. [c]: protein concentration / mol·l^{-1} A_{280}: measured absorption at 280 nm, ε: molar extinction coefficient / l·mol^{-1}·cm^{-1}, d: path length of light through the sample / cm

$$[c] = \frac{A_{280}}{\varepsilon \cdot d}$$

The extinction coefficient ε, that is characterized by the number of tryptophan, tyrosine and cysteine residues, was determined for each protein using the online tool ExPASy ProtParam [178]. The measurements were performed in triplicates, utilizing a Nanodrop ND 2000c spectrophotometer (Peqlab), and the values averaged.

3.3 Circular dichroism spectroscopy

CD buffer: 50 mM K_2H / H_2K-PO_4, pH 7.9

Circular dichroism (CD) spectroscopy was used to confirm the structural integrity of protein samples in solution. The measurements were recorded at a Jasco J-810 spectropolarimeter in a temperature-controlled quartz cuvette with a layer thickness of 1 mm at 20 °C. All UBE2S variants were at a concentration of 5 µM in the CD buffer and the CD spectra were recorded in the range of 190 to 260 nm in 0.1 nm steps at a scanning speed of 20 nm/min and a band width of 1 nm. To improve the signal-to-noise ratio, a total of 15 spectra were accumulated per sample and the spectrum of the reference buffer was recorded and subtracted from the protein spectra. Finally, the the molar ellipticity [Θ] was calculated according to Equation 2.

Equation 2: Calculation of the molar ellipticity [Θ]. Θ: measured ellipticity in mdeg, [c]: protein concentration in mM, d: thickness of the cuvette in cm, N_{AA}: number of amino acids of the protein

$$[\theta] = \frac{\theta \cdot 100}{[c] \cdot d \cdot N_{AA}}$$

3.4 SDS-polyacrylamide gel electrophoresis and immunoblotting

3.4.1 SDS-polyacrylamide gel electrophoresis

Separating gel:	10-15% (w/v) Bis-Acrylamide 29:1, 375 mM Tris pH 8.8, 0.1% (w/v) SDS, 0.1% APS, 0.025 TEMED
Stacking gel:	4% (w/v) Bis-Acrylamide 29:1, 125 mM Tris pH 6.8, 0.1% (w/v) SDS, 0.1% APS, 0.025 TEMED
SDS sample buffer (4x):	62.5 mM Tris pH 7.0, 40 mM EDTA, 15% (w/v) SDS, 48% (w/v) glycerol, 0.04% (w/v) bromphenol blue, ± 120 mM β-ME
SDS running buffer:	25 mM Tris pH 7.0, 192 mM glycine, 0.1% (w/v) SDS
Staining solution:	0.1% (w/v) Coomassie Brilliant Blue G-250/R-250, 25% (v/v) isopropanol, 10% (v/v) acetic acid
De-staining solution:	10% (v/v) acetic acid

Gels with an appropriate amount of Bis-Acrylamide 29:1 in the separating gel section, were prepared in Bio-Rad casting frames or stands. For SDS-PAGE of protein purifications and *in vitro* assays 12 - 15% gels were used and for SDS-PAGE followed by immunoblotting, 10 - 12% gels were used. Protein samples were mixed with SDS sample buffer to a final concentration of 1x and incubated at 95 °C for 5 min. To estimate the molecular weight of the samples, a protein standard marker (PageRuler protein ladder, Thermo Fisher Scientific) was used. The gels were inserted into a Mini-Protean electrophoresis chamber (Bio-Rad), filled with SDS running buffer and the electrophoresis was carried out at 220 V for ~50 min.

To separate proteins samples in the low, as well as in the high-molecular range, pre-cast gradient gels (Novex 10 - 20% Tris-Glycine Mini Gels, Thermo Fisher Scientific) were used according to the manufacturer´s instructions.

Gels were stained in the staining solution for 15 min, including brief heating in a microwave, and de-stained in the de-staining solution. Thereafter, the gels were scanned with an Odyssey system (LI-COR) for documentation.

If samples with low protein concentrations needed to be visualized, silver staining was performed using the Pierce Silver Stain kit (Thermo Fisher Scientific) according to the manufacturer´s instructions. For documentation, those gels were scanned with a common document scanner.

3.4.2 Immunoblotting

Transfer buffer:	25 mM Tris pH 7.5, 192 mM glycine, 20% methanol
TBS-T:	20 mM Tris pH 7.5, 150 mM NaCl, 0.1% Tween®20
Blocking buffer 1:	5% BSA in TBS-T
Blocking buffer 2:	5% milk powder in TBS-T
Blocking buffer 3:	5% BSA in PBS, 0.1% Tween®20, 0.01% SDS

Table 11: Antibodies

Antibody	Supplier	Dilution	Blocking buffer
rabbit polyclonal anti-UBE2S	self-made, Moravian Biotechnology	1:1000	2
rabbit monoclonal anti-HA tag (clone C29F4)	Cell Signaling Technology (RRID: AB_1549585)	1:1000	1
mouse monoclonal anti-ubiquitin (P4D1)	Santa-Cruz Biotechnology (RRID: AB_628423)	1:1000	2
mouse monoclonal anti-His H1029 (HIS-1)	Sigma-Aldrich (RRID: AB_260015)	1:3000	2
Horse anti-mouse IgG, HRP-linked	Cell Signaling Technology (RRID: AB_330924)	1:10000	depending on the primary antibody
Goat anti-rabbit IgG, HRP-linked	Cell Signaling Technology (RRID: AB_2099233)	1:10000	depending on the primary antibody
Donkey anti-rabbit IgG, IRDye 800CW conjugated (diluted 1:1 in PBS, pH 7.4.)	LI-COR Biosciences (RRID: AB_621848)	1:10000	3

For immunoblotting (Western blot), protein samples were separated by SDS-PAGE (3.4.1) and then the gel was incubated in transfer buffer for three times 5 min. The PVDF membrane was activated in methanol and thereafter incubated in transfer buffer. For transfer, a Trans-Blot Turbo Transfer System (Bio-Rad) was used and the transfer was carried out for 35 min at 25 V. Then the membrane was blocked in the appropriate blocking buffer for at least one hour and subsequently incubated overnight at 4 °C in the primary antibody that was diluted in the appropriate blocking buffer. Thereafter, the membrane was washed with TBS-T three times for 15 min and incubated with the secondary antibody, diluted in blocking buffer, for one hour at room temperature. If the secondary antibody was coupled to horseradish peroxidase (HRP), chemiluminescent detection with SignalFire ECL Reagent (Cell Signaling) was performed with a FluorochemQ Multi image system (Alpha Innotech). If the secondary antibody was

coupled to IRDye 800CW (LI-COR), the incubation was performed in the dark and the signals were detected by fluorescence scanning with an Odyssey system (LI-COR).

3.5 *In vitro* assays

3.5.1 *In vitro* isopetide bond formation assay

The *in vitro* isopetide bond formation activity assay was performed to monitor di-ubiquitin formation as well as auto-ubiquitination of UBE2S. 0.25 µM E1 enzyme, 2 µM E2, 30 µM ubiquitin, 3 mM ATP and 7.5 mM $MgCl_2$ were mixed in 25 mM Tris pH 7.0 and 100 mM NaCl. The activity of the dimer interface mutants was tested at the concentrations described above and at 0.5 µM E1, 100 µM and 150 µM ubiquitin, supplemented with 3 mM ATP and 7.5 mM $MgCl_2$ in the same reaction buffer as before. The reaction was incubated for 1 h at 30 °C, stopped by adding SDS-loading dye containing DTT, separated via SDS-PAGE and visualized by Coomassie staining. To enhance the sensitivity, IR-dye-labelled ubiquitin was used. In those cases, the activity of the proteins was monitored by SDS-PAGE and fluorescence scanning (Odysse System, LI-COR) in addition to Coomassie staining.
The quantification of di-ubiquitin formation and auto-ubiquitination was performed with Image Studio Lit2 Ver 5.2 (LI-COR).

3.5.2 *In vitro* charging assay

The E2 charging assay was performed by mixing 0.25 µM E1 enzyme, 30 - 60 µM ubiquitin, 3 mM ATP and 9 mM $MgCl_2$ in 25 mM Tris pH 7.5 and 100 mM NaCl. The reaction mixture was incubated for 3 min on ice, 2 - 5 µM of the appropriate E2 enzyme were added and thereafter the reaction mixture was incubated at room temperature for 2 - 10 min. Afterwards, the reaction was quenched with non-reducing SDS-loading dye to monitor thioester-formation between the E2 enzyme and ubiquitin. As a control, the samples were quenched with DTT-containing SDS-loading dye. All samples were analyzed by SDS-PAGE and Coomassie staining.

3.5.3 *Cis-trans* assay

To discriminate auto-ubiquitination of UBE2S in *cis* and *trans*, 0.25 µM UBA1, 1 µM HA3-UBE2S C95A (catalytically dead), 1 µM or 5 µM untagged UBE2S WT, 60 µM ubiquitin, 3 mM ATP, and 7.5 mM $MgCl_2$ were mixed in 25 mM Tris pH 7.0 and 100 mM NaCl. The reaction was incubated at 30 °C for 30 min and 1 h, respectively, and quenched by adding SDS-PAGE loading dye that contained 100 mM DTT. The samples were analyzed by SDS-PAGE and Western blotting using an HA-antibody (C29F4, Cell Signaling).

3.6 Protein interaction analyses

3.6.1 Size exclusion chromatography coupled to multi-angle light scattering (SEC-MALS)

SEC-MALS was performed at room temperature using a Superdex 75 10/300 GL column (GE Healthcare) coupled to a Dawn 8+ MALS detector and Optilab T-rEX refractive index detector (Wyatt Technology). Proteins were injected at a concentration of 300 µM in a buffer containing 25 mM Tris pH 6.8 and 100 mM NaCl. The total volume was 100 µl. MWs were determined at the absorbance peak tips using the ASTRA 6 software (Wyatt Technology).

3.6.2 *In vitro* pull-down

Washing buffer: 500 mM NaH_2PO_4 pH 7.5, 500 mM NaCl, 30 mM imidazole, 2 mM DTT

For *in vitro* pull-down experiments, 500 µg of His-tagged UBE2S / $UBE2S^{UBC}$ were incubated with 500 µg of HA-tagged UBE2S / $UBE2S^{UBC}$ in 25 mM Tris pH 7.4, and 100 mM NaCl for 1 h on ice and Ni-NTA agarose beads were pre-washed 3x with the washing buffer. Thereafter, the protein mixture was incubated with the Ni-NTA agarose beads at 20 °C for 12 min. The mixture was washed at least five times with the washing buffer and the supernatant removed. Proteins were eluted in SDS-loading dye and heated for 5 min at 95 °C. The samples were separated by SDS-PAGE and analyzed by anti-HA and anti-His Western blotting (see 3.4).

3.6.3 Crosslinking

3.6.3.1 Crosslinking with phenylarsine oxide

Phenylarsine oxide (PAO) reacts with vicinal thiol groups and therefore can be used for cysteine selective crosslinking approaches. For crystallization, UBE2S^{UBC} was buffer-exchanged into 25 mM Tris pH 7.4 and 100 mM NaCl and concentrated to 10 mg/ml. PAO was dissolved in DMSO (150 mM) and added to the protein solution in the molar ratios 1:1 and 1:5, either without or with the addition of 1 mM TCEP (see 3.8).

3.6.3.2 Crosslinking with dibromobimane

Dibromobimane (bBBr) was purchased from Sigma-Aldrich and dissolved in DMSO.
End-point assay: For analytical size-exclusion chromatography, 40 µM of the proteins were incubated with 60 µM bBBr in 25 mM Tris pH 6.8 and 100 mM NaCl for 40 min at room temperature. The reaction was quenched with 5 mM *N*-ethylmaleimide (NEM, Sigma-Aldrich) for 10 min and subsequently used for analytical SEC.
To isolate the bBBr-linked UBE2S dimer, 600 µM UBE2S WT were mixed with bBBr in a ratio of 3:1 for 30 min on ice and 15 min at room temperature, using 25 mM Tris pH 6.8 and 100 mM NaCl as reaction buffer. The reaction was quenched by the addition of 2 mM DTT and loaded onto the size-exclusion column (see analytical size-exclusion chromatography 3.6.4).
To visualize dimerization via SDS-PAGE, 40 µM of the proteins were incubated with 40 µM bBBr in 25 mM Tris pH 6.8 and 100 mM NaCl for 40 min at room temperature. The reaction was quenched by the addition of DTT-containing SDS-loading dye separated by SDS-PAGE and visualized by Coomassie staining.
Kinetic analyses: Dimerization of UBE2S via bBBr crosslinking was followed by detecting the fluorescence of reacted bBBr (excitation: 315 - 390 nm, emission: 420 - 480 nm). Therefore, 20 µM UBE2S WT and variants were mixed with bBBr in a ratio of 1:1.5 in 25 mM Tris pH 6.8 and 100 mM NaCl. After 2 mins of mixing at 500 rpm, the fluorescence was measured with a CLARIOstar (BMG LABTECH) microplate reader. Reaction rates detected after the first 5 min of the experiment in the linear region were fitted by linear regression using OriginPro 2016G (OriginLab).

3.6.4 Analytical size-exclusion chromatography

Proteins at indicated concentrations were subjected to analytical SEC. A Superdex 75, 10/300 GL column (GE Healthcare) was used and the runs were performed at 4 °C in 25 mM Tris pH 6.8 and 100 mM NaCl.

3.6.5 Analytical ultracentrifugation (AUC)

Sedimentation velocity runs were conducted with UBE2S at a concentration of 160 µM in 25 mM Tris pH 7.4, 100 mM NaCl and 2 mM DTT in a Beckman Optima XL-I analytical ultracentrifuge (Beckman Coulter) using an eight-hole An-50 Ti rotor at 40,000 rpm and 20 °C, with 400 µl samples in standard double-sector charcoal-filled Epon centerpieces equipped with sapphire windows. Data were collected using interference detection and analyzed using the software SEDFIT to determine continuous distributions for solutions to the Lamm equation c(s), as described previously [173]. Analysis was performed with regularization at confidence levels of 0.68 and floating frictional ratio (f/f0), time-independent noise, baseline, and meniscus position to root mean square values of <0.016. The performance of the experiment and data processing and analysis was kindly assisted by Dr. Bodo Sander and Dr. Ingrid Tessmer.

3.7 Nuclear magnetic resonance

All NMR measurements were done at the North Bavaria Center for High Resolution NMR Spectroscopy, Bayreuth/Germany. A Bruker Avance IIIHD 700 MHz spectrometer equipped with a $^{1}H/^{15}N/^{13}C$ cryo-probe was used. All samples were in 75 mM sodium phosphate pH 7.2, 1 mM EDTA, 5 mM DTT, and 2 mM TCEP except for the disulfide-linked conjugates, which were kept in non-reducing conditions. NMR data were processed using the University of Bayreuth´s in-house routines (Kristian Schweimer, unpublished). For visualization and chemical shift analysis, NMRViewJ [179] was used. The backbone chemical shift assignments were transferred from Biological Magnetic Resonance Data Bank (BMRB) entry 17437 ($UBE2S^{UBC}$, [4]), BMRB entry 17439 (ubiquitin at pH 7.2, [4]), BMRB entry 27768 ($UBE2S^{UBC}$ C95S/C118M/K100C, [53]) and BMRB entry 27799 (disulfide-linked $UBE2S^{UBC}$ C95S/C118M/K100C-ubiquitin G76C-complex, [53])

3.7.1 Relaxation rate measurements

For the determination of the transverse relaxation (R_2) rates (κ) of amide protons located in structured regions of the UBE2S^{UBC} two-point spin-echo experiments were performed with UBE2S^{UBC} as well as full-length UBE2S at three different concentrations in the range of 0.2 - 2 mM. The transverse relaxation rate was calculated according to the following equation:

Equation 3: Transverse relaxation (R_2) rate κ. T1: longitudinal relaxation time; T2: transverse relaxation time

$$k = \frac{\ln\left(\frac{T1}{T2}\right)}{0.01}$$

^{15}N longitudinal (R_1) and transverse (R_2) relaxation rates were measured as previously described [180]. The temperature was controlled by a Bruker NMR thermometer which makes use of the difference in the ^{2}H signals of HDO and 50 mM sodium acetate-d_3 in the NMR sample. The relaxation delays were fitted to a mono-exponential decay (NMRViewJ). Data acquisition and analyses was performed by Dr. Kristian Schweimer (University of Bayreuth, Bayreuth/Germany).

3.7.2 ^{1}H-^{15}N HSQC titrations

To determine the dissociation constant (K_D) of donor ubiquitin binding to UBE2S WT and variants and to map this interaction on UBE2S, ^{1}H-^{15}N-TROSY spectra of ^{15}N-labeled UBE2S WT or variants without (*apo*) or with unlabeled ubiquitin were collected. Ubiquitin was titrated in a concentration range of 0.25 - 6.5 mM. Weighted combined chemical shift perturbations, $\Delta\delta(^{1}H^{15}N)$, were calculated according to the following equation:

Equation 4: Calculation of the chemical shift perturbations, $\Delta\delta$ ($^{1}H^{15}N$). $\delta(^{1}H)/(^{15}N)$: $^{1}H/^{15}N$ chemical shift perturbations of the perturbed spectrum; $\delta(^{1}H)_0/(^{15}N)_0$: $^{1}H/^{15}N$ chemical shift perturbations of the unperturbed spectrum (*apo* spectrum, without ligand)

$$\Delta\delta(^{1}H^{15}N) = \sqrt{(\delta(^{1}H) - \delta(^{1}H)_0)^2 + 0.04 \cdot (\delta(^{15}N) - \delta(^{15}N)_0)^2}$$

The K_D was derived by fitting the binding curves for defined resonances globally to a single-site model with Origin (OriginLab):

Equation 5: Determination of K_D-values. $\Delta\delta$ ($^1H^{15}N$): weighted combined chemical shift perturbation; $[P_{tot}]$: concentrations of ^{15}N-enriched protein; $[L_{tot}]$: concentration of the unlabeled ligand

$$\Delta\delta(^1H^{15}N) = \frac{\Delta\delta(^1H^{15}N)_{sat}(([P_{tot}] + [L_{tot}] + K_D) \pm \sqrt{([P_{tot}] + [L_{tot}] + K_D)^2 - 4[P_{tot}][L_{tot}]})}{2[P_{tot}]}$$

The dissociation constant is defined by Equation 6, if the protein P interacts with the ligand L in a simple binding equilibrium:

Equation 6: Definition of the dissociation constant K_D. [P]: concentration of the free protein, [L]: concentration of the free ligand, [PL]: concentration of the protein-ligand complex.

$$K_D = \frac{[P] \cdot [L]}{[PL]}$$

The concentration of the free (unbound) protein and ligand are not known, [P] can be replaced by ($[P_{tot}]$-[PL]), where $[P_{tot}]$ describes the total amount of protein (bound and unbound), and [L] can be replaced by $[L_{tot}]$ respectively. Thus, the concentration of the protein-ligand complex is given by Equation 7:

Equation 7: Calculation of the concentration of the protein-ligand complex [PL].

$$[PL] = \frac{([P_{tot}] + [L_{tot}] + K_D) \pm \sqrt{([P_{tot}] + [L_{tot}] + K_D)^2 - 4 \cdot [P_{tot}] \cdot [L_{tot}]}}{2}$$

Due to the fast exchange of the bound and free states in the conducted NMR experiments of the UBE2S-ubiquitin complex at 75 MHz resonance frequency, the binding-induced chemical shift perturbations $\Delta\delta$ ($^1H^{15}N$) are linearly dependent on the fraction of protein in the ligand-bound state (Equation 8).

Equation 8: Linear dependency of the binding induced weighted combined chemical shift perturbations on the protein-ligand complex. $\Delta\delta(^1H^{15}N)_{max}$: maximum experimental signal, observed at 100% saturation of the protein with ligand, $\Delta\delta(^1H^{15}N)_0$: signal of the protein in absence of the ligand

$$\Delta\delta(^1H^{15}N) = \Delta\delta(^1H^{15}N)_0 + (\Delta\delta(^1H^{15}N)_{max} - \Delta\delta(^1H^{15}N)_0) \cdot \frac{[PL]}{[P_{tot}]}$$

Thus, Equation 6 to Equation 8 form the basis for the estimation of the K_D as described in Equation 5.

To study the UBE2S^{UBC}-ubiquitin interactions in the context of the disulfide-linked conjugate, ^{1}H-^{15}N-HSQC spectra of samples containing 200 µM conjugate, in which either UBE2S^{UBC} C95S/C118M/K100C or ubiquitin G76C was ^{15}N-enriched were recorded and compared to the corresponding spectra for the *apo* protein components. Weighted combined chemical shift perturbations, $\Delta\delta(^{1}H^{15}N)$ were calculated based on Equation 4.

3.7.3 *De novo* backbone-assignment of ^{13}C-^{15}N-labeled proteins

The *de novo* backbone assignments of UBE2S^{UBC} C95S/C118M/K100C and the UBE2S^{UBC} C95S/C118M/K100C-ubiquitin G76C conjugate were generated by Dr. Kristian Schweimer (University of Bayreuth, Bayreuth/Germany). Therefore, BEST-TROSY-based triple resonance data [181] of a uniformly ^{15}N, ^{13}C protein sample (600 µM for the triple mutant of UBE2S and 400 µM of the complex) were recorded using non-linear sampling (NUS) with 25% of the total data points. Data processing was performed with in-house software (Kristian Schweimer, unpublished). The signals of the disulfide-linked complex with ubiquitin G76C were assigned by comparison of the HSQC and HNCA spectra with the corresponding data from ubiquitin and the UBE2S^{UBC} C95S/C118M/K100C variant. Due to missing signals, the following residues of the UBE2S^{UBC} C95S/C118M/K100C variant could not be assigned: S3, N4, N11, and A90. Additionally, K18, E19, I31, H111, T115, R135 and L150 could not unambiguously be assigned in the context of the UBE2S^{UBC}-Ub conjugate, due to signal overlap.

3.8 X-ray crystallography

3.8.1 Protein crystallization

Crystal growth was achieved by vapor diffusion. Therefore, freshly purified protein was concentrated to 8 - 30 mg/ml and centrifuged for 15 min at 16,000 x g and 4 °C. Initial screens (see chapter 2.5) were set up at room temperature using the HoneyBee 963 crystallization robot (Digilab). The robot prepared 96-well crystallization plates in sitting drop format containing 40 µl of reservoir solution and a sitting drop consisting of 0.3 µl of the same reservoir solution mixed with 0.3 µl of the protein solution in each well. Plates were sealed with an adhesive film and stored at 20 °C.

The initial crystallization screens were used for screening (see Table 7) and fine screens in the 24-well hanging drop format were pipetted manually with 500 µl reservoir solution and 0.5 µl - 1 µl of the reservoir, mixed with the protein solution in the ratios of 0.5:1, 1:1 and 2:1 (v/v) on a cover slip that was placed headfirst onto the respective well and sealed with silicon grease. Plates were stored at 20 °C.
Crystals were cryo-protected if needed and flash frozen in liquid nitrogen. To test whether a cryo-protection is needed, the corresponding mother liquor and mother liquor including 5 - 30% glycerol were pipetted onto a cover slip and flash frozen. If the drop stayed clear, the solution was considered sufficiently cryo-protected. When needed, the crystal was transferred into a drop of the cryo-protected solution before freezing.

The crystallization and cryo-protection conditions for UBE2S^{UBC}/UBE2S crystals are listed in Table 12.

Table 12: Crystallization and cryo-protection conditions

Crystal name	Growing condition	Cryo-protection
UBE2S^{UBC} WT (PDB: 6S98)	11.7 mg/ml in 0.2 M sodium acetate trihydrate, 0.1 M Tris pH 8.5, and 30% PEG 4000; 20 °C; in sitting drops	0.2 M sodium acetate trihydrate, 0.1 M Tris pH 8.5, and 30% PEG 4000, 10% glycerol
UBE2S^{UBC} WT (PAO-linked, PDB: 6QHK)	12 mg/ml in 0.2 M $MgCl_2$, 0.1 M Tris pH 8.5, 30% PEG 4000, 1 mM TCEP, 0.67 mM phenylarsine oxide (PAO) 20 °C; in sitting drops	0.2 M $MgCl_2$, 0.1 M Tris pH 8.5, 30% PEG 4000, 1 mM TCEP, 0.67 mM PAO, 10% glycerol
UBE2S^{UBC} C118M (PDB: 6QH3)	18 mg/ml 0.2 M $MgCl_2$, 0.1 M HEPES pH 7.5, and 25% PEG 3350 20 °C in sitting drops	0.2 M $MgCl_2$, 0.1 M HEPES pH 7.5, and 25% PEG 3350, 20% glycerol
UBE2S^{UBC} C118A (PDB: 6S96)	22.0 mg/ml 2.5 M potassium formate and 0.1 M sodium cacodylate pH 6.5 20 °C in sitting drops	2.5 M potassium formate and 0.1 M sodium cacodylate pH 6.5, 20% glycerol
UBE2S^{UBC} L114E `monomer´	11 mg/ml 1 M sodium citrate tribasic, 0.1 M ches pH 9.4 20 °C in hanging drops	1 M sodium citrate tribasic, 0.1 M ches pH 9.4, 20% glycerol
UBE2S^{UBC} L114E dimer	11 mg/ml 1.33 M magnesium formate dihydrate, 15% PEG 3350 20 °C in sitting drops	1.33 M magnesium formate dihydrate, 15% PEG 3350, 20% glycerol
UBE2S T115A	15 mg/ml 1.33 M $MgCl_2$, 0.1 M Tris pH 8.5, 18% PEG 3350, 0.625 mM PAO 20 °C in sitting drops	1.33 M $MgCl_2$, 0.1 M Tris pH 8.5, 18% PEG 3350, 0.625 mM PAO, 20% glycerol

3.8.2 Data collection, processing and refinement

Diffraction data were collected at the European Synchrotron Radiation Facility (ESRF), Grenoble/France, beamline ID30A-3 (UBE2S^{UBC} WT, PDB: 6S98 and UBE2S^{UBC} WT PAO-linked, PDB: 6QHK), at the Deutsches Elektronen-Synchrotron (DESY), Hamburg/Germany, beamline P14 (UBE2S^{UBC} C118M, PDB: 6QH3) and P13 (UBE2S^{UBC} C118A, PDB: 6S96) and at the Berliner Elektronenspeicherring-Gesellschaft für Synchrotronstrahlung (BESSY), Berlin/Germany at beamline 14.1 (UBE2S T115A, UBE2S^{UBC} L114E monomer and dimer).
The data were processed with XDS [174]; molecular replacement was performed with Phaser [167], as implemented in the Collaborative Computational Project No. 4 (ccp4) suite [160], using an available structure of UBE2S^{UBC} (PDB: 1ZDN [182]) as a search model. Refinement was performed with Phenix [168] and manual model building with Coot [161]. Data collection, processing and refinement was kindly assisted by Dr. Christian Feiler.

3.9 MD simulations

The MD simulations were performed by Mathias Diebold and Prof. Dr. Christoph Sotriffer, University of Würzburg, as described in [53].

3.10 Backbone RMSD calculations

All backbone RMSD calculations were performed by Mathias Diebold and Prof. Dr. Christoph Sotriffer, University of Würzburg using CPPTRAJ V4.14.0 [190]

3.11 p*K*a measurements

The pK_a-values of the thiol groups of the catalytic cysteine (Cys95) and Cys118 of UBE2S were derived from the kinetics of the reaction of single-cysteine variants of UBE2S (C95S and C118S) with 5,5'-dithiobis (2-nitrobenzoic acid) (DTNB) at 10 °C by Marie-Annick Letzelter. The protein concentration was 14.4 µM (in 100 mM NaCl, 1 mM EDTA and one of the following buffers covering a pH-range from 3.8 to 11: 20 mM sodium acetate, 20 mM sodium phosphate, 20 mM Tris-HCl, or 20 mM glycine), the DTNB concentration was 100 µM. Reaction rates were monitored by absorbance

(λ = 412 nm), using an SFM-3000S stopped-flow spectrometer (Bio-Logic). Rate constants obtained from three replicates were averaged, plotted against the pH-value, and fitted to the following two-state model (Equation 9), using the OriginPro 2017 software (OriginLab).

Equation 9: Calculation of the pK_a value. k_{app}: experimentally derived apparent rate constant, k_{SH} and k_S: rate constants of the reaction of fully protonated and fully deprotonated cysteines

$$k_{app} = \mathrm{k}_{SH} + \frac{k_{S-} - k_{SH}}{1 + 10^{\mathrm{pK}_a - \mathrm{pH}}}$$

3.12 Mass spectrometry

Mass spectrometry analyses were performed in Prof. Dr. Henning Urlaub´s laboratory (Bioanalytical Mass Spectrometry Group, Max Planck Institute for Biophysical Chemistry, Göttingen, Germany) and analyzed by Dr. Olexandr Dybkov or Uwe Pleßmann.
The mapping of ubiquitination sites in UBE2S by semi-quantitative mass spectrometry is described in [53].
For denaturing intact ESI-MS (electrospray ionization mass spectrometry) analyses, the bBBr-linked UBE2S dimer was purified as described above and the buffer exchanged to 20 mM ammonium acetate, pH 8.0. The sample (20 µl of 28.9 µM) was then diluted with 60 µl of a solution containing 20% acetonitrile and 0.2% formic acid and injected into a LTQ XL mass spectrometer (Thermo Scientific). The measurements were performed using Tune Plus v.2.5.0 (Thermo Scientific) and Spectra were deconvoluted with ProMass for Xcalibur v.2.8 (Thermo Scientific).
For the MS-based mapping of crosslinking sites, the bBBr-crosslinked dimer sample was analyzed by SDS PAGE; the band corresponding to the dimer was cut out and split into two halves. One half was reduced with 10 mM DTT and alkylated with 55 mM iodoacetamide before in-gel digestion with 12.5 mg/l trypsin; the other was digested without reduction and alkylation. Extracted peptides were dissolved in 5% acetonitrile and 0.1% formic acid (FA) and injected into a UHPLC instrument (UltiMateTM 3000 RSLC, Thermo Scientific), in-line desalted and separated on a 28 cm analytical column (packed in-house with C18 1.9 µm Reprosil beads, Dr. Maisch GmbH). The separated peptides were analyzed on-line by ESI-MS using a Q Exactive HF-X mass spectrometer (Thermo Scientific). MS2 was performed for the 40 most abundant precursors observed in the MS1 scan.

To identify protein-protein crosslinks, the raw files were searched with the pLink 2.3.0 software (http://pfind.ict.ac.cn/software/pLink, [183,184]) against a database containing UBE2S as well as 293 common contaminating proteins. Oxidation of methionines and carbamidomethylation of cysteines were considered as variable modifications. The crosslink and monolink mass additions were set to 188.059 and 267.985 Da, respectively.

4. Results and Discussion

4.1 Auto-inhibition mechanism of the ubiquitin-conjugating enzyme UBE2S by auto-ubiquitination

This section is published in ”Autoinhibition Mechanism of the Ubiquitin-Conjugating Enzyme UBE2S by Autoubiquitination,” in Structure (2019) [53]. It describes the structural basis and functional consequences of UBE2S-auto-ubiquitination at a distinct lysine residue (Lys100, hereafter Lys^{+5}) in the catalytic domain ($UBE2S^{UBC}$, residues 1-156) of UBE2S, close to the active site cysteine (Cys95, hereafter Cys^{cat}). Figures are taken and adapted from the publication [53], as permitted by Elsevier.

4.1.1 The active-site region of UBE2S is flexible, allowing a conserved ubiquitination site to come close to the catalytic cysteine

Sequence alignment of the 34 human E2 family members, excluding pseudogenes and E2-like proteins that lack a catalytic cysteine residue (UBE2V1, UBE2V2, AKTIP) reveals that ~25% of the E2s have a conserved lysine residue (Lys^{+5}). Lys^{+5} is located five residues downstream of the catalytic cysteine, whereas the remaining E2s have a Arg, Gln, Glu, Asn, Asp, Ser, Thr, His, or Gly residue at this position (Figure 13). This implies that neither a positive charge nor specifically a lysine is needed at this position to confer catalytic activity. Analysis of proteomic data compiled in the PhosphoSitePlus server for posttranslational modifications [109] highlight Lys^{+5} as a major ubiquitination site in all Lys^{+5}-containing E2 enzymes (Table 13). This raises the question of whether ubiquitination of Lys^{+5} provides the basis for a common regulatory function.

To examine the structural basis as well as functional consequences of Lys^{+5}-ubiquitination, two available crystal structures of $UBC2S^{UBC}$ were compared. These are the crystal structure of *apo* $UBE2S^{UBC}$ WT (PDB: 1ZDN [182], molecule A is shown in grey) and of a $UBE2S^{UBC}$-ubiquitin conjugate (PDB: 5BNB [52], molecule A is shown in cyan), in which the active-site conjugated ubiquitin molecule is not shown. Both structures share the canonical UBC fold (Figure 14A). The only major difference between them is the active-site region (residues 95-103). In the *apo* $UBE2S^{UBC}$ WT structure, the active site region adopts a '*Lys^{+5}-out*' conformation, in which Lys^{+5} and Cys^{cat} are located at opposite sides of a short α-helix (residues 96-100), their side chains thus pointing away from each other. In contrast, the active site region in the crystal structure of the

UBE2S^{UBC}-ubiquitin conjugate adopts a '*Lys^{+5}-in*' in molecule A and D (not shown) (Figure 14A).

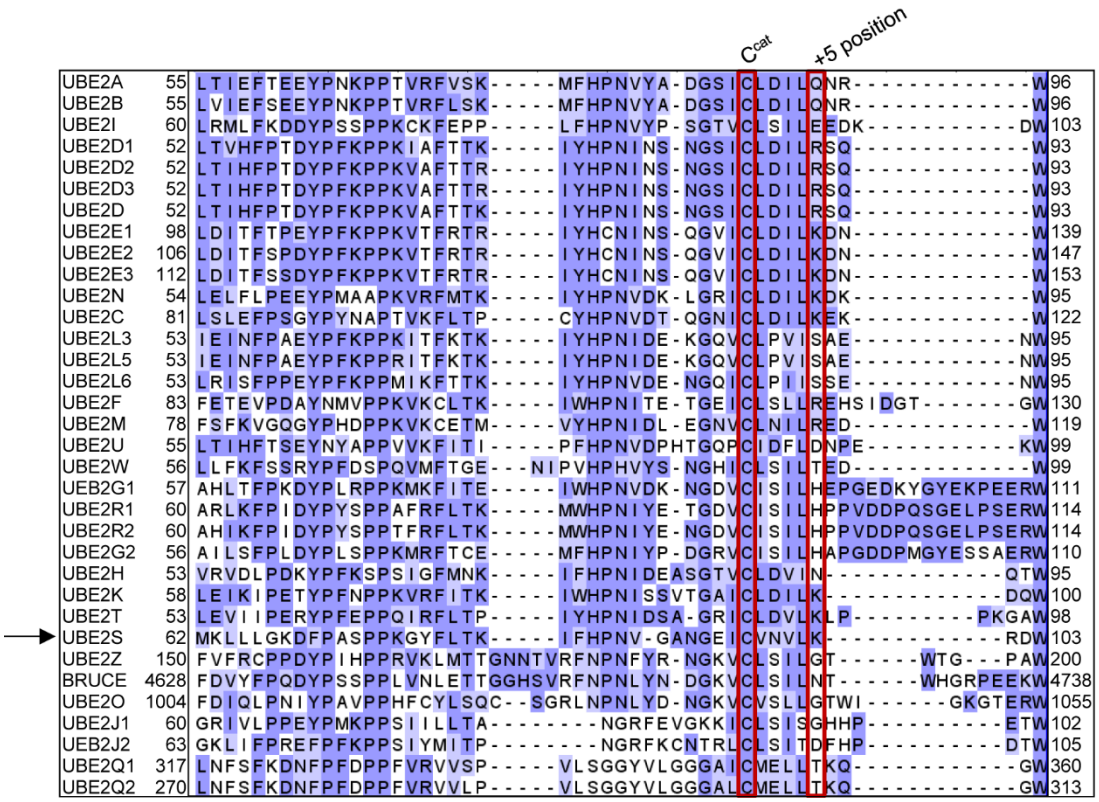

Figure 13: Lys^{+5} is conserved in ~25% of the human E2 enzymes. Sequence alignment of 34 human E2s, focusing on a stretch that contains the active site. The list was compiled with the HUGO Gene Nomenclature Committee (HGNC) [185], excluding pseudogenes and E2-like proteins that do not have a catalytic cysteine residue (UBE2V1, UBE2V2, AKTIP). The amino acid sequences were extracted from UniProt [186], aligned with Clustal Omega [187], illustrated with JalView [188], and colored according to the Blosum62 score [189].C^{cat} and the +5 position are highlighted.

Table 13: Lys^{+5} is an ubiquitination site in human E2s. Proteomic data from the PhosphoSite server [109] were analyzed for Lys^{+5}-ubiquitination.

E2	total # references for all ubiquitination sites	# references for Lys^{+5}-ubiquitination	Is Lys^{+5} the most detected site?
UBE2C	83	69	yes
UBE2E1	64	48	yes
UBE2E2	49	49	yes
UBE2E3	48	48	yes
UBE2K	29	8	yes
UBE2N	537	163	yes
UBE2S	35	25	yes
UBE2T	108	90	yes

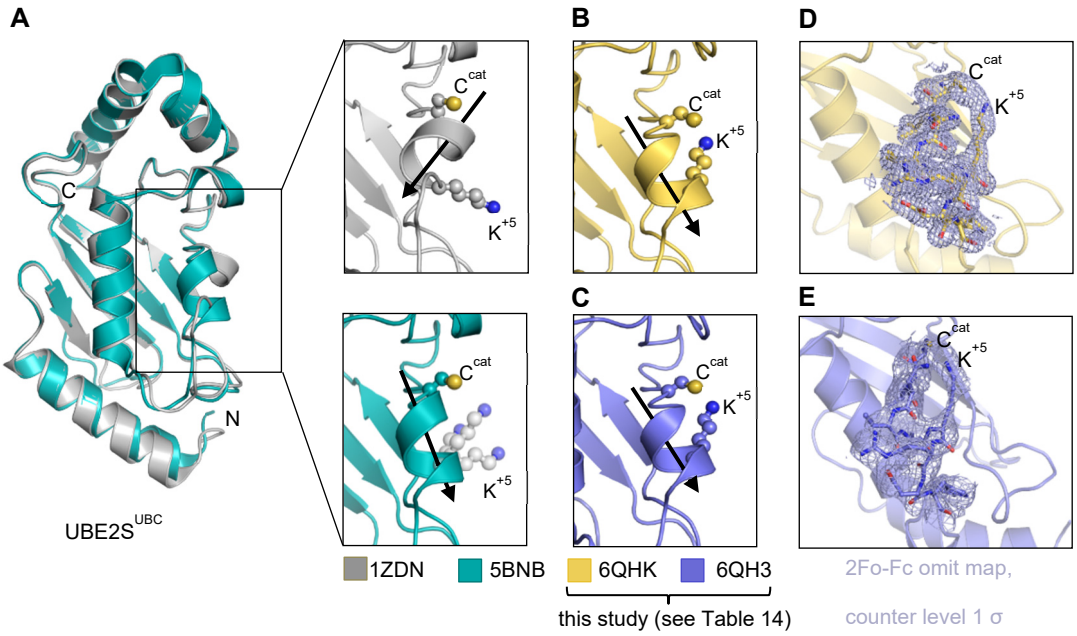

Figure 14: Comparative analysis of four crystal structures of UBE2S^{UBC}. (A) Superposition of two structures of UBE2S^{UBC}: *apo* UBE2S^{UBC} WT, PDB: 1ZDN (molecule A, grey, [182]) and a UBE2S^{UBC}-ubiquitin conjugate, 5BNB (molecule A, cyan, [52]; the Cys^{cat}-linked ubiquitin is not shown) (left). Details of the active-site region, showing the side chains of Cys^{cat} and Lys^{+5} in ball-and-stick representations (right), helical axes are indicated by arrows. For 5BNB, the three likely rotamers of the Lys^{+5} side chain are displayed (white), since the side chain was not modeled unambiguously in the structure. (B, C) Analogous details of the active-site region in the new crystal structures of UBE2S^{UBC} WT (PDB: 6QHK; yellow) and UBE2S^{UBC} C118M (PDB: 6QH3; blue). (D, E) 2Fo-Fc omit map, countered at 1 σ, for the residues 95-103 (active site region) in the UBE2S^{UBC} *apo* structures 6QHK (yellow) and 6QH3 (blue).

Here, the short α-helix of the active site region starts with residue 97 and is tilted by 42° with respect to the *Lys^{+5}-out* state, permitting the ε-amino group of Lys^{+5} to reach the catalytic center (Figure 14A). This rearrangement is likely not induced by ubiquitin bound to Cys^{cat}, as the active site regions of molecules B and C in the same structure are in the *Lys^{+5}-out* conformation. In addition, this is consistent with two new crystal structures of *apo* UBE2S^{UBC} that I determined. These two *apo* structures are UBE2S^{UBC} WT (PDB: 6QHK), in which molecule A is shown in yellow and UBE2S^{UBC} C118M (PDB: 6QH3, chain A is shown in blue) (Figure 14B, D). In the latter structure, Cys118 that is located outside of the active side region is mutated to methionine (Figure 15). Both structures are in the *Lys^{+5}-in* state, with the side chain positions of Cys^{cat} and Lys^{+5} well-defined (Figure 14D, E). The overall fold of the catalytic domain in the new crystal structures is similar to 1ZDN (backbone RMSD-values of 1.17 Å and 1.07 Å). The conformational differences seen in the active-.site regions of the *apo* UBE2S^{UBC} crystal structures do not originate from lattice contacts in this region.

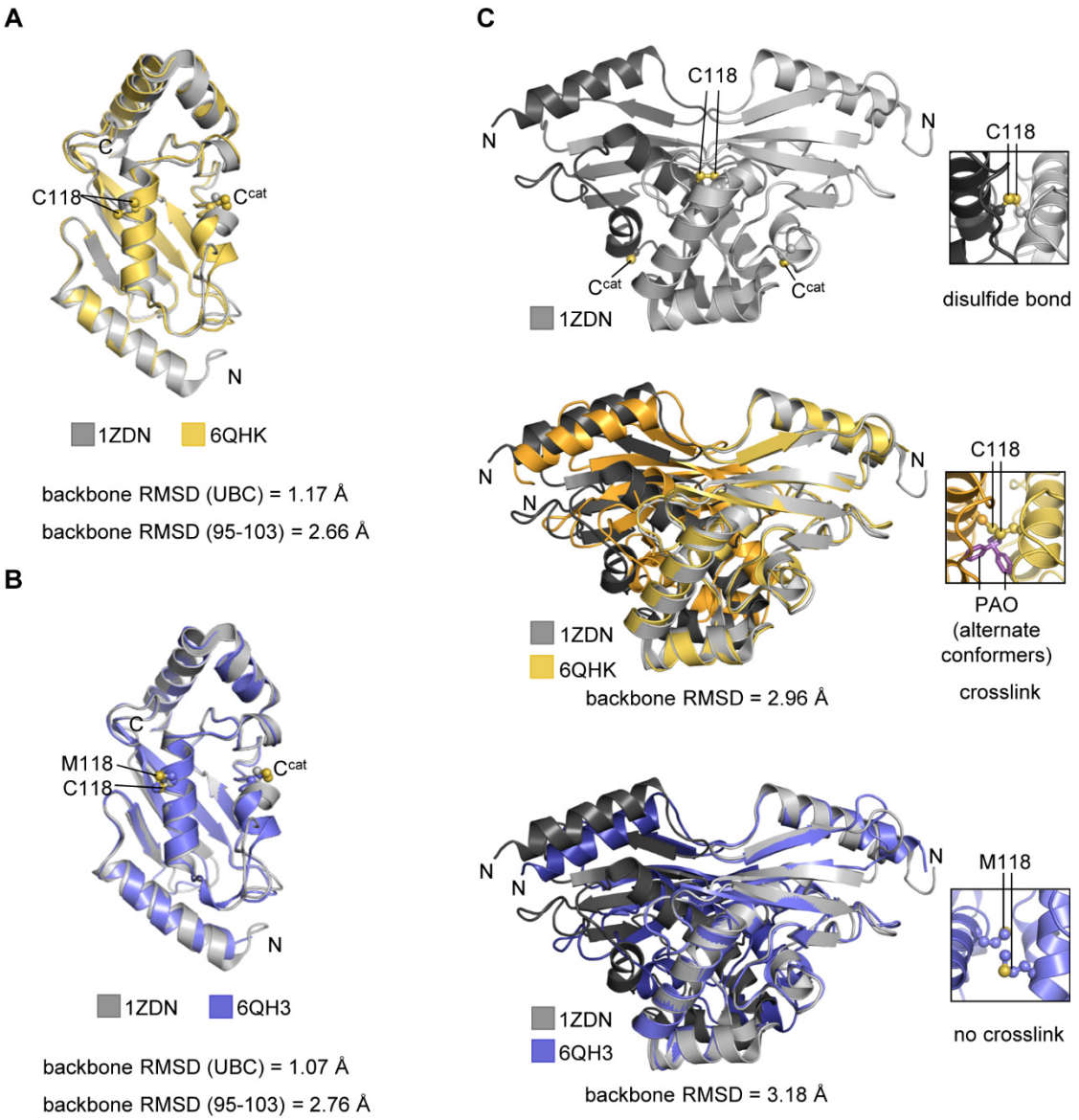

Figure 15: Dimeric arrangement of UBE2S. (A) Superposition of the WT UBE2S^{UBC} crystal structures (PDB: 1ZDN, grey [182] and PDB: 6QHK, yellow). Backbone RMSDs are given for the entire chain and the active-site region, as calculated with CPPTRAJ: Trajectory Analysis, V18.01 [190] (B) Superposition of 1ZDN (UBE2S^{UBC} WT, grey) with the structure of the C118M variant (PDB: 6QH3, blue) and respective backbone RMSDs, calculated as in (A). All backbone RMSDs were calculated by Mathias Diebold. (C) Crystallographic dimers of UBE2S^{UBC} in 1ZDN (top), 6QHK (middle, superposed with 1ZDN), and 6QH3 (bottom, superposed with 1ZDN). Residue 118 at the dimer interface is highlighted. 1ZDN has a cysteine at position 118, which forms a disulfide bond, connecting the subunits; in 6QHK, a covalent crosslinker (phenylarsine oxide, 'PAO') connects the two cysteine residues. It adopts two alternate conformations. In 6QHK, Cys118 is mutated to methionine and therefore the subunits are not linked.

Table 14: X-ray crystallographic data collection and refinement statistics for the structures of UBE2S^{UBC} WT and C118M. Values in parentheses correspond to the highest resolution shell.

	UBE2S^{UBC} WT (PDB: 6QHK)	UBE2S^{UBC} C118M (PDB: 6QH3)
data collection		
wavelength (Å)	0.9680	0.9762
space group	P 6_5	P 6_5
unit cell parameters		
a, b, c (Å)	83.15 83.15 83.13	84.62 84.62 87.83
α, β, γ (°)	90 90 120	90 90 120
total reflections	46726 (4620)	15965 (1589)
unique reflections	23393 (2317)	7984 (795)
R_{pim}	2.32 (28.1)	2.63 (17.29)
completeness (%)	99.72 (99.44)	99.94 (100.00)
I/σ(I)	20.05 (2.64)	21.40 (4.19)
redundancy	2.0 (2.0)	2.0 (2.0)
Wilson B factor	32.04	63.58
CC ½	1 (0.938)	0.999 (0.896)
refinement		
resolution (Å)	19.42 – 1.96 (2.03 – 1.96)	38.12 – 2.90 (3.004 – 2.90)
R_{work} / R_{free}	18.93 / 22.34	18.47 / 22.89
no. of atoms	2364	2270
protein	2253	2270
water	84	
average B-factors	39.11	67.17
protein	39.16	67.17
water	35.65	
RMSD from ideality		
bond lengths (Å)	0.003	0.004
bond angles (°)	0.7	0.80
Ramachandran statistics		
favored (%)	98.63	98.28
disallowed (%)	0.00	0.00
MolProbity clash score	1.77	13.24
MolProbity overall score	0.93	1.63

All UBE2S^{UBC} *apo* structures described here, show a similar crystallographic dimer, albeit UBE2S was found to be active as monomer in solution [4]. In 1ZDN, the two WT subunits are linked via a Cys118-mediated disulfide bond (Figure 15C, top). In 6QHK, a covalent linkage between the two Cys118 is mediated by the cysteine-reactive crosslinker phenylarsine oxide (PAO) (Figure 15C, middle). In 6QH3, a structure of the UBE2S^{UBC} C118M variant, a dimer is formed without any covalent linkage (Figure 15C, bottom).

Despite the differences at position 118, the overall dimeric arrangement of the three crystal structures is similar, as indicated by backbone RMSD-values of 2.96 Å and 3.18 Å with respect to 1ZDN.

This analysis, along with the finding that the dimeric interface is distant from the active-site region, suggests that the mode of dimerization is not causing the particular conformations of the active-site region. To further investigate the flexibility of the active-site region, molecular dynamics (MD) simulations of each of the two molecules in the three UBE2S^{UBC} *apo* crystal structures were performed, using the NAMD 2.12 package [191] with AMBER ff14sb [192] forcefield parameters during 200 ns of simulation time. Considerable motions in the active-site region of UBE2S are observed, as reflected by high backbone root-mean-square fluctuations (RMSFs), plotted as pseudo B-factors (Figure 16A), compared to the surrounding α-helices. This flexibility also manifests itself in the distribution of backbone RMSD-values of the active-site region – the active-site state in 6QH3 and 6QHK changes from a *Lys^{+5}-in* conformation to a *Lys^{+5}-out* conformation in the case of the simulation. Significantly less movement is detected for the active-site region in 1ZDN, where it adopts a *Lys^{+5}-out* conformation (Figure 16B). These observations are visualized by superpositions of the snapshots of the active-site region after equilibration (0 ns, white) and after 100 ns of simulation (colored, Figure 16C). Taken together, the MD data support the idea that the active-site region of UBE2S is flexible and indicate that the *Lys^{+5}-out* state is energetically favored over the *Lys^{+5}-in* state *in silico*.

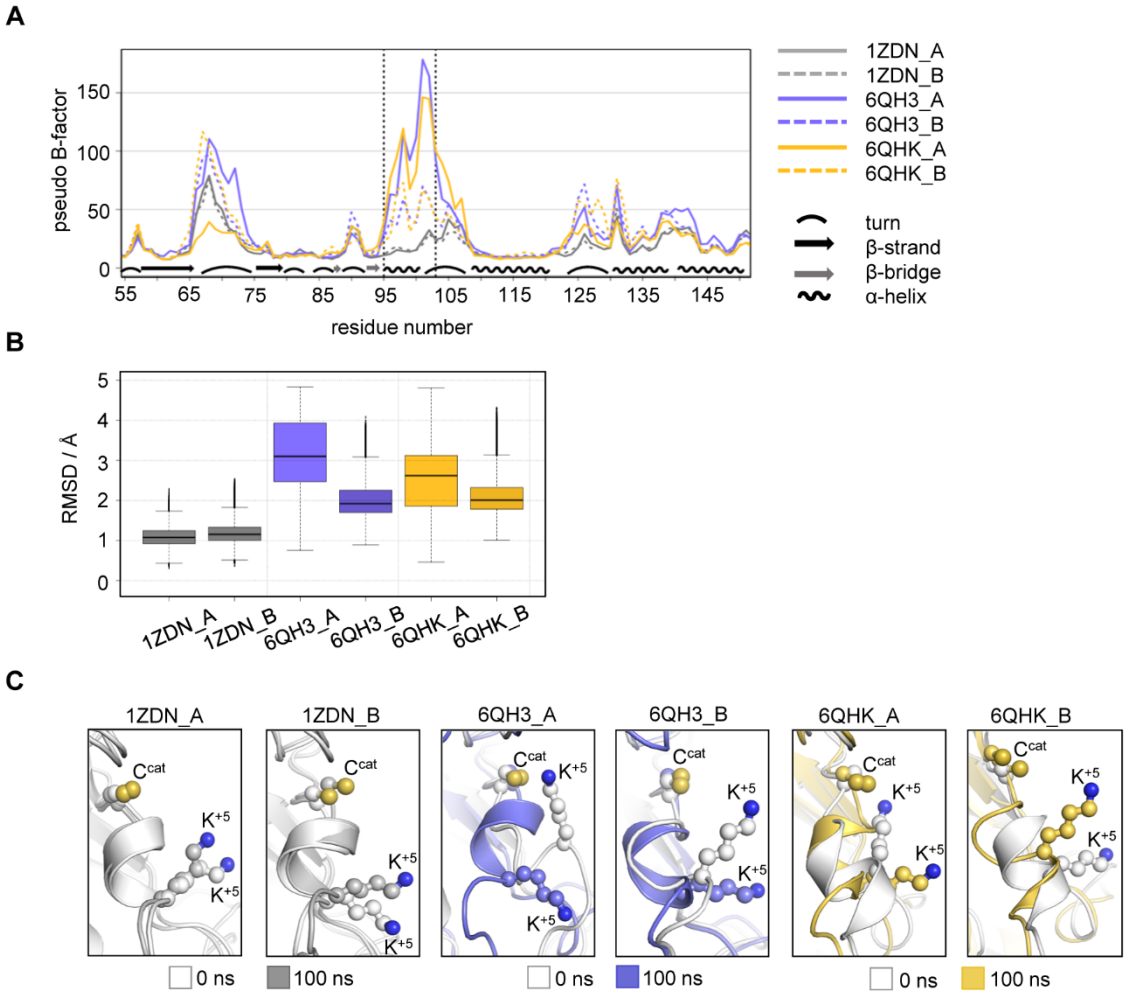

Figure 16: The active-site region of UBE2S is conformationally malleable. (A) MD simulations (200 ns total sampling) with the two unique molecules (A and B) from each of the three *apo* UBE2S^{UBC} crystal structures (PDB: 1ZDN, 6QH3 and 6QHK). Per-residue backbone RMSF-values in relation to the averaged structure are displayed as pseudo B-factors. Residues 95 to 103 (active site region) are marked by dotted lines and secondary structure elements for 1ZDN are indicated and were determined by STRIDE [193]. (B) Distribution of backbone RMSD-values during 200 ns of MD simulation for each of the 6 molecules compared to the corresponding starting structures. (C) Snapshots of the active-site region during the MD simulations, showing superpositions of the equilibrated structures (0 ns; white) and their state after 100 ns of simulation (colored). The side chains of C^{cat} and K^{+5} are presented as ball-and-sticks. All MD simulations were performed in a collaboration with Prof. Dr. Sotriffer, University of Würzburg, Würzburg/Germany and data were kindly provided by Mathias Diebold.

4.1.2 Auto-ubiquitination of UBE2S occurs in *cis*

As noted above, Lys^{+5} is an important ubiquitination site in many E2s. The finding that UBE2S can adopt a *Lys^{+5}-in* conformation motivated the investigation of whether the ubiquitination of this site occurs in *cis*. To test this idea, a *cis-trans* activity assay was performed *in vitro*. Therefore, a hemagglutinin (HA)-tagged, catalytically dead UBE2S

variant (C95A), either full-length UBE2S or UBE2S^{UBC}, was mixed with WT UBE2S/UBE2S^{UBC} in the molar ratios 1:1 or 1:5 and UBE2S-ubiquitination of the HA-tagged variants were detected by anti-HA immunoblotting (Figure 17).

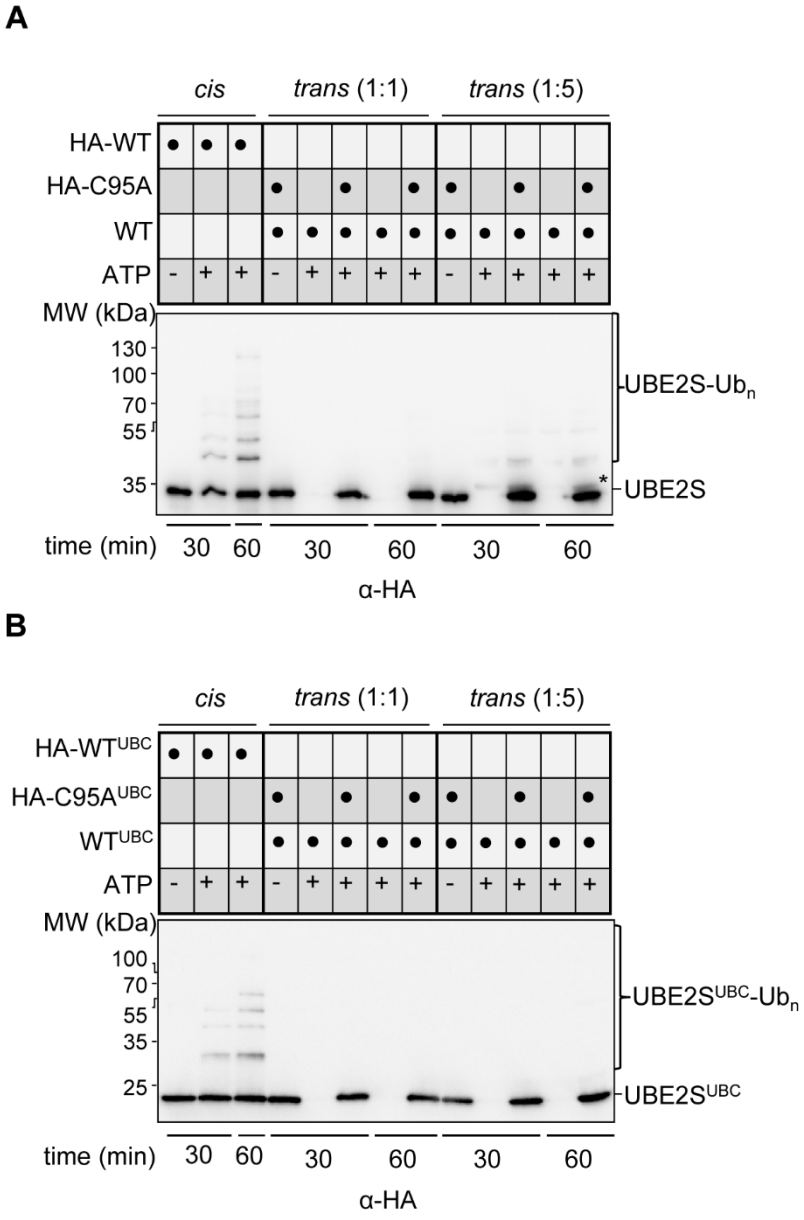

Figure 17: Auto-ubiquitination of UBE2S occurs in *cis*. (A) '*Cis-trans* assay' monitoring the ubiquitination of 1 µM HA-tagged WT (lanes 1-3) UBE2S or catalytically dead UBE2S ('HA-C95A'; lanes 4-13) in the presence of untagged WT UBE2S at molar ratios of 1:1 and 1:5. The assay was performed for 30 and 60 min and visualized by SDS-PAGE and anti-HA immunoblotting. The asterisk marks a background signal from untagged UBE2S. (B) Analogous assay as in (A) using UBE2S^{UBC}.

While an auto-ubiquitination pattern is detected in *cis* (lanes two and three that contain HA-tagged WT UBE2S/UBE2S^{UBC} only), no auto-ubiquitination is detectable in *trans*, even when the wild-type protein is added in a four-fold molar access (Figure 17), in

agreement with previous studies of UBE2S [194]. These experiments demonstrate that UBE2S and UBE2S^{UBC} auto-ubiquitinate in *cis*.

The *in vitro* auto-ubiquitination sites of UBE2S and UBE2S^{UBC} were determined by mass spectrometry (in collaboration with Prof. Dr. Henning Urlaub, Max Planck Institute for Biophysical Chemistry, Göttingen/Germany). These data revealed that Lys^{+5} is a major auto-ubiquitination site in the catalytic domain of UBE2S and is also modified in the full-length protein. In contrast to UBE2S^{UBC}, however, the full-length protein contains the lysine-rich C-terminal extension that is auto-ubiquitinated, e.g. at Lys197 and Lys198, in addition to Lys^{+5} (Table 15). This points to the possibility that the C-terminal extension can reach the active site of UBE2S. Notably, lysines of the C-terminal extension other than Lys197 and Lys198 are likely modified with ubiquitin, but those sites cannot be identified by tryptic digestion-based methods, due to an accumulation of positively charged amino acids in the C-terminal extension.

Table 15: Semi-quantitative mass spectrometric analysis of auto-ubiquitination sites in UBE2S *in vitro*. The analysis is based on a MaxQuant (Tyanova et al., 2015) search against the human SwissProt database [186] for Lys-Gly-Gly modifications, after tryptic digest. The mass spectrum 1 (MS1) intensity typically correlates with the peptide abundance in the samples. The same tendency is detected in the peptide spectrum matches (PSMs), although they do not provide a reliable quantitative read-out. The lysines modified the most (Lys100 (Lys^{+5}'), Lys197, and Lys198) are highlighted in bold.

Gly-Gly-Lys site detected	MS1 intensity		PSMs	
	UBE2S^{UBC}	UBE2S	UBE2S^{UBC}	UBE2S
18	1.94E+08	1.49E+08	2	1
68	2.98E+08	2.64E+08	1	1
76	1.30E+08	1.01E+08	2	2
82	6.06E+07	4.31E+07	2	1
100 (= Lys^{+5})	**8.55E+09**	**7.02E+09**	**47**	**15**
117	9.34E+07	4.45E+07	3	1
197	0	**9.43E+09**	0	**15**
198	0	**9.43E+09**	0	**19**

Consistently, mutating Lys^{+5} to arginine in UBE2S^{UBC} has a drastic effect on the auto-ubiquitination pattern, as shown in *in vitro* auto-ubiquitination assays with UBE2S^{UBC} and wild-type ubiquitin (Figure 18A, left part of the gel); while in the full-length protein, the same mutation does not have a visible effect (Figure 18B, left part of the gel).

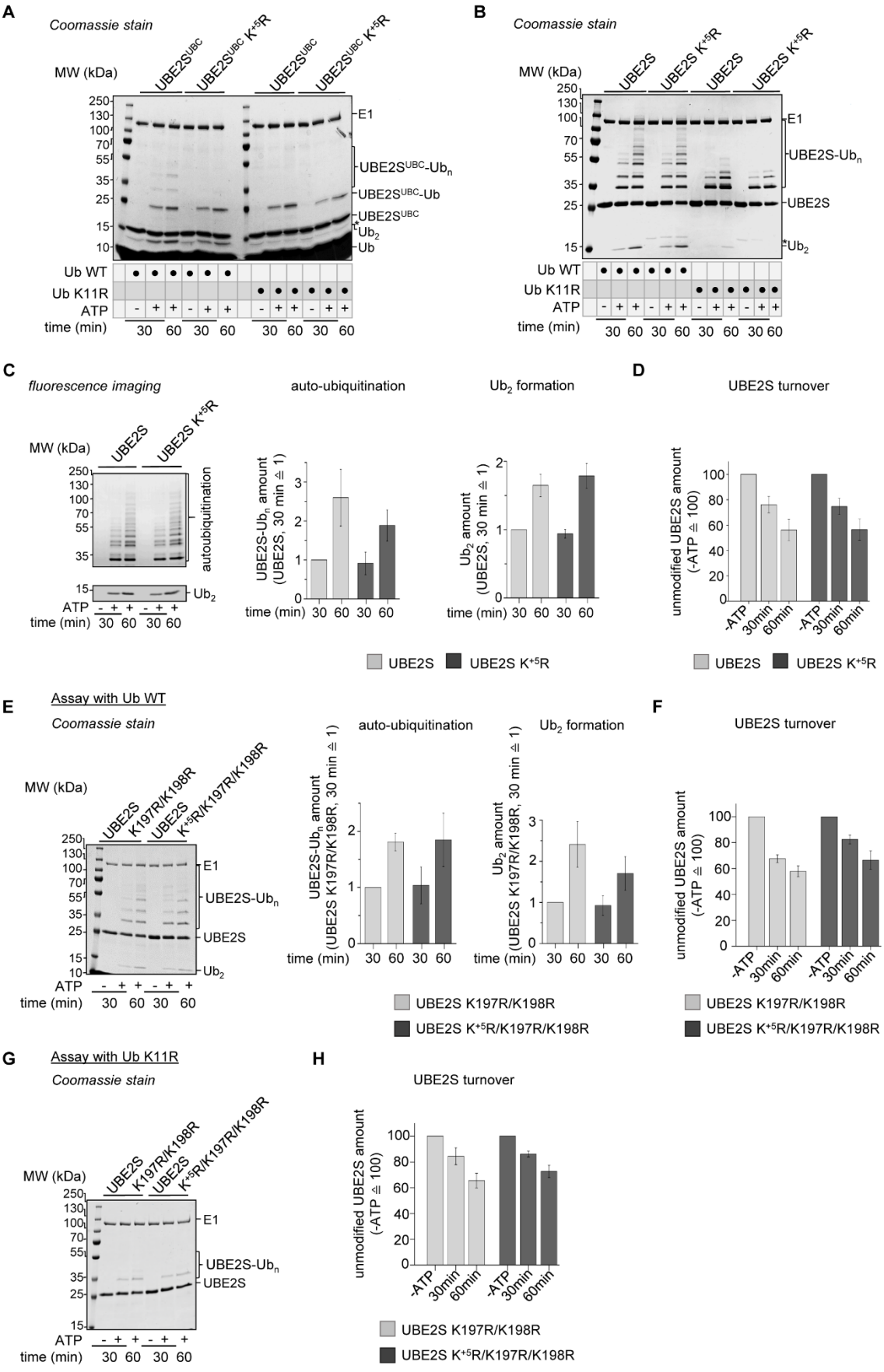

Figure 18: Impact of Lys^{+5} on the auto-ubiquitination of UBE2S^{UBC} and UBE2S. (A) *In vitro* isopetide bond formation assay of UBE2S^{UBC} WT and UBE2S^{UBC} Lys^{+5}, using ubiquitin WT (left part of the gel) and

K11R (right part of the gel) to monitor auto-ubiquitination as well as di-ubiquitin (Ub_2) formation after separation by SDS-PAGE. (B) Analogous assay as in (A) using UBE2S. The asterisk marks a contaminant running at the same height as Ub_2 in (A). (C) *In vitro* isopetide bond formation assay of UBE2S WT and UBE2S $K^{+5}R$, using fluorescently labeled ubiquitin WT to quantify (right) auto-ubiquitination and Ub_2-formation based on fluorescence scanning (left). Note that two images were depicted for the reaction products, because of differences in their relative intensities. The mean and standard deviations (SDs) of the quantified reaction products from three independent experiments were plotted and the amount of reaction product formed by UBE2S WT after 30 min was set to 1. (D) Quantification of the amounts of unmodified UBE2S (WT and $K^{+5}R$) based on SDS-PAGE and Coomassie staining (Figure 18B, left part); the input amount of the enzymes ('minus ATP' lane) was set to 100%. (E) *In vitro* isopetide bond formation assay using UBE2S K197R/K198R and UBE2S K^{+5}/K197R/K198R, supplemented with ubiquitin WT to monitor auto-ubiquitination and Ub_2-formation at two different time points by SDS-PAGE and Coomassie staining (left) for quantification (right). The mean and SDs of the quantified reaction products from three independent experiments were plotted and the amount of reaction product formed by UBE2S K197R/K198R after 30 minutes was set to 1. (F) Analogous quantification of the amount of unmodified E2. The input amount of the enzyme ('minus ATP' lane) was set to 100%. (G) *In vitro* isopetide bond formation assay of UBE2S K197R/K198R and UBE2S K^{+5}/K197R/K198R, using ubiquitin K11R. (H) Quantification of the unmodified E2 enzymes as in (F), the input amount ('minus ATP' lane) was set to 100%.

The auto-ubiquitination and di-ubiquitin (Ub_2) formation activities of UBE2S $K^{+5}R$ are comparable to the ones of UEB2S WT (Figure 18C, D), underlining that the small fraction of auto-inhibited UBE2S is not visible in this *in vitro* setup because the lysine-rich C-terminal extension is the dominant auto-ubiquitination site in UBE2S under these conditions.

To test this hypothesis and enhance the fraction of Lys^{+5}-modified UBE2S, the *in vitro* auto-ubiquitination sites in the C-terminal extensions that were identified by mass spectrometry analysis (Lys197 and Lys198, Table 15) were exchanged by alanine in the wild-type, as well as the $K^{+5}R$ background (Figure 18E-H). Thereafter, an *in vitro* isopetide bond formation assay was performed, and the reaction products and the enzyme turnover were quantified (Figure 18E, F). However, the C-terminal extension still got modified with ubiquitin chains on residues other than Lys^{+5}, hence Lys197 and Lys198 are not the only auto-ubiquitination sites in the C-terminal extension that can accept ubiquitin in this this *in vitro* system. The other acceptor sites escape the detection in the mass spectrometry experiments based on tryptic digest, due to the enrichment of positive charges in the very C-terminus of UBE2S.

In the next step, it was investigated whether the auto-ubiquitination sites including Lys^{+5} can be modified with ubiquitin chains. Ubiquitin K11R does not support the formation of ubiquitin chains by UBE2S, thus only mono- or multi-mono-ubiquitination can be detected in this case. The comparison of $UBE2S^{UBC}$ and UBE2S demonstrate that all

tested proteins, independent of the wild-type or $K^{+5}R$ background, are modified with Lys11-linked chains (Figure 18A, B). At least in the context of $UBE2S^{UBC}$, chains assembled on Lys^{+5} are included. Although this result is in contrast to the finding that auto-ubiquitination occurs in *cis* (Figure 17), our observations imply that auto-ubiquitination of UBE2S is initiated in *cis*, whereas chain elongation can occur in *trans*. The same results were obtained in the K197R/K198R background (Figure 18G, H). These results are in principle consistent with the MD simulations (Figure 16B, C) which have suggested that the Lys^{+5}-*out* state is energetically favored by UBE2S.

To get insights in the interaction of the last 26 C-terminal amino acids of UBE2S with the remaining part of UBE2S (residues 1-196) that should be needed to allow for auto-ubiquitination of the C-terminal lysine residues, the interaction of a peptide comprising of the lysine-rich 26 C-terminal amino acids of UBE2S, and $UBE2S^{1-196}$ were studied by NMR. The peptide contains the C-terminal auto-ubiquitination sites of UBE2S and is predicted to form an α-helix (hereafter referred to as 'C-helix', (Figure 19A)). $^{1}H^{15}N$-HSQC spectra were recorded by titrating the peptide to the ^{15}N-labeled $UBE2S^{1-196}$ construct. The comparison of the $^{1}H^{15}N$-HSQC spectra in the absence and presence of the peptide reveals major chemical shift perturbations around the active site region of UBE2S, including residues 93, 95-97 and 99-101 as well as the nearly residues 127 and 129 (Figure 19B, C). These observations indicate that the C-helix either interact with the active-site region or impacts its conformation allosterically. If the C-helix was, indeed, close to the active site, this could reflect the conformation in which it undergoes auto-ubiquitination.

In summary, these experiments illustrate that Lys^{+5} is also a major auto-ubiquitination site of $UBE2S^{UBC}$ *in vitro*, although auto-ubiquitination of full-length UBE2S occurs not only at Lys^{+5} but dominantly at the C-terminal extension. The C-helix can reach the active-site region, providing a basis for auto-ubiquitination of the lysine residues in the C-helix in *cis*. Nevertheless, Lys^{+5} gets modified with Lys11-linked ubiquitin chains *in vitro*, whereas the first ubiquitin must be attached in *cis*. However, the following ubiquitin molecules of the chain need to be added in *trans* because mono-ubiquitination of Lys^{+5} leads to auto-inhibition of UBE2S, as will be pointed out in the next paragraph.

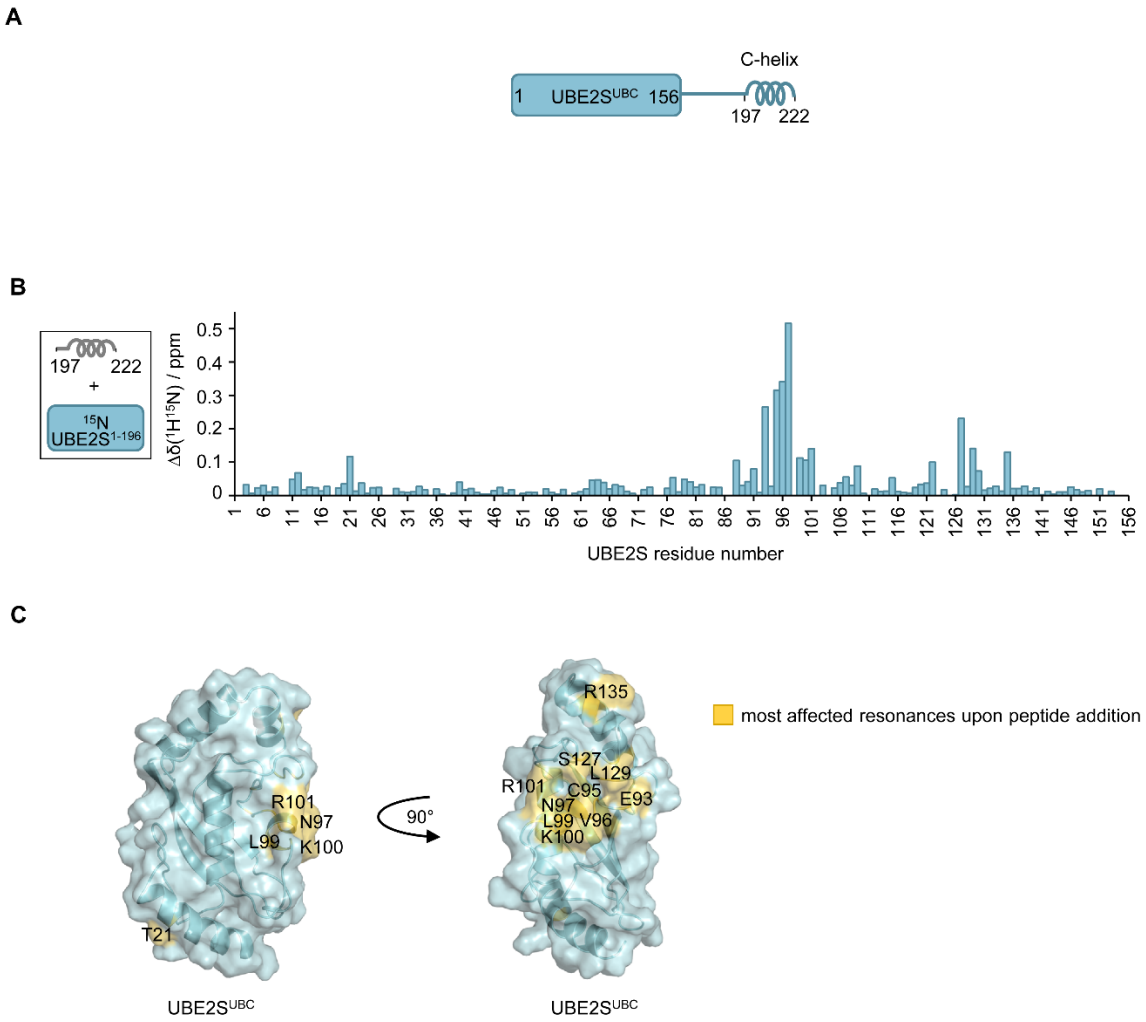

Figure 19: The C-helix can reach the active site region of UBE2S. (A) Schematic representation of the architecture of the UBE2S monomer. The UBC-domain (residues 1-156) represents a structurally studied, folded domain, whereas the C-terminal extension is predicted to be mainly unstructured, besides the last 25 residues that are predicted to form a helix. (B) Weighted combined chemical shift perturbations, $\delta\Delta(^{1}H^{15}N)$, of residues in the catalytic domain upon addition of the C-terminal UBE2S peptide (residues 107-222) to $UBE2S^{1-196}$ resonances. Gaps are due to proline residues (9, 10, 27, 28, 35, 50, 54, 71, 74, 75, and 86) or missing assignments (1, 18, 38, 74, 83, 87, 98, 102, 104, 111, 150). (C) Combined cartoon and surface representation of the crystal structure of $UBE2S^{UBC}$ (PDB: 6S98). Residues that undergo marked chemical shift perturbations ($\delta\Delta(^{1}H^{15}N) \geq 0.1$ ppm) upon peptide addition (C-helix, see B) are highlighted in yellow.

4.1.3 Auto-ubiquitination at Lys^{+5} results in auto-inhibition of UBE2S

The above analyses suggested that the auto-ubiquitination of Lys^{+5} occurs with low efficiency *in vitro*. Therefore, the enzymatically made conjugate of $UBE2S^{UBC}$ and ubiquitin K11R ($UBE2S^{UBC}$-Ub) was isolated by anion-exchange chromatography (Figure 20A), to test the effect of the modification on activity. $UBE2S^{UBC}$ was used instead of UBE2S full-length protein to rule out the effects of UBE2S tail-ubiquitination. The attachment sites of ubiquitin in the conjugate were determined by mass spectrometry (in collaboration with Prof. Dr. Henning Urlaub, Max Planck Institute for Biophysical Chemistry, Göttingen/Germany), confirming that the conjugate was predominantly linked through Lys^{+5}. The ability of $UBE2S^{UBC}$-Ub to accept ubiquitin from the E1 was tested and compared to $UBE2S^{UBC}$ in a thioester-transfer assay. While $UBE2S^{UBC}$ readily forms thioester-linked conjugates with ubiquitin to its active site cysteine, this ability is suppressed by ~85% in the context of the conjugate (Figure 20B). Whether the residual activity of the conjugate (< 15% compared to the WT) resulting in the ($UBE2S^{UBC}$-Ub)~Ub reaction product is indeed formed by the conjugate or stems from the small fraction (5%) of $UBE2S^{UBC}$-Ub conjugate, in which ubiquitin was bound to Lys68 instead remains unclear. However, either way, the attachment of ubiquitin to Lys^{+5} efficiently suppresses thioester formation. Based on this finding, it is expected that auto-ubiquitination at Lys^{+5} also suppresses isopeptide formation by $UBE2S^{UBC}$-Ub. Indeed, this is found in *in vitro* isopeptide formation assays comparing $UBE2S^{UBC}$ and $UBE2S^{UBC}$-Ub: While $UBE2S^{UBC}$ catalyzes auto-ubiquitination and Ub_2-formation efficiently, di-ubiquitin formation was strongly reduced by $UBE2S^{UBC}$-Ub (Figure 20C). Note that this assay does not allow for the detection of auto-ubiquitination of the conjugate, as the conjugate contains ubiquitin K11R to suppress chain formation on UBE2S (Figure 20A).

Thus, the modification of UBE2S with a single ubiquitin molecule at position Lys^{+5} leads to auto-inhibition of UBE2S by interfering with thioester formation and consequently also minimizes the ability to form isopetide-linked ubiquitin chains.

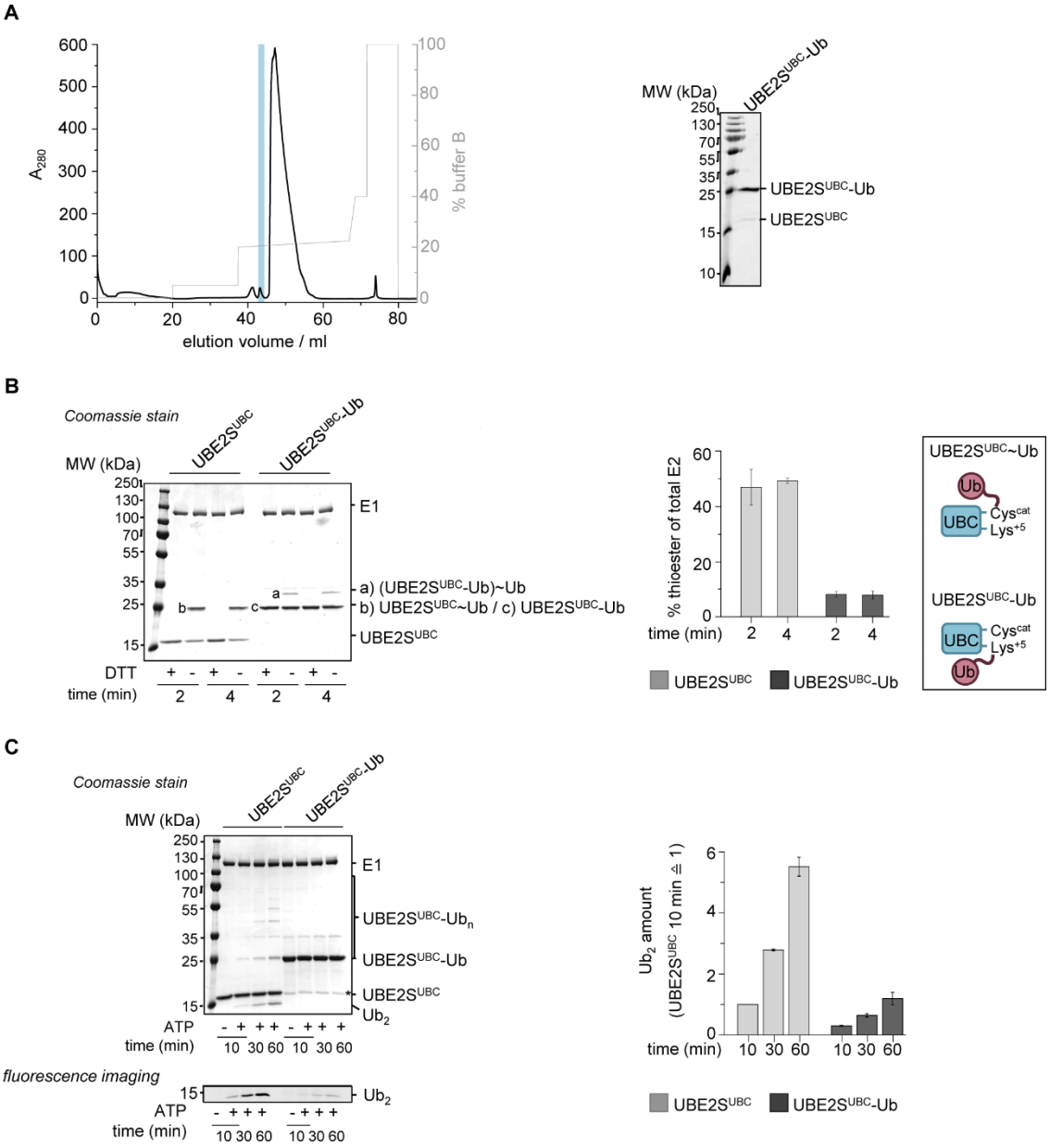

Figure 20: Ubiquitination at position +5 inhibits UBE2S activity. (A) Purification of a UBE2S^{UBC}-Ub conjugate (UBE2S^{UBC} WT and Ub K11R) from an *in vitro* reaction by anion-exchange chromatography (left). The peak containing the conjugate (see SDS-PAGE and Coomassie stain on the right) is highlighted in blue. (B) *In vitro* thioester-bond formation assay comparing UBE2S^{UBC} and UBE2S^{UBC}-Ub, performed at two timepoints. The addition of DTT serves to distinguish thioester (visualized as ~) from isopetide bonds (left). Reaction products were monitored by SDS-PAGE and Coomassie staining, quantified, normalized to the input amount of unmodified enzyme (+DTT) and the mean and standard deviation (SD) of three independent experiments plotted (middle). The cartoon (left) illustrates the differences between the thioester-linked conjugate of UBE2S and ubiquitin (UBE2S^{UBC}~Ub) and the isopeptide-linked conjugate (UBE2S^{UBC}-Ub). (C) *In vitro* isopeptide bond formation assay, comparing UBE2S^{UBC} and UBE2S^{UBC}-Ub, using fluorophore-labeled ubiquitin. Ub_2-formation was monitored at three different time points by SDS-PAGE and Coomassie staining (top left) as well as fluorescence scanning (bottom left). The asterisk marks a minor amount of UBE2S^{UBC} in the UBE2S^{UBC}-Ub preparation. Right: Quantification of Ub_2, followed by fluorescence scanning. The means and SDs of three independent experiments are plotted.

4.1.4 Lys^{+5}-linked ubiquitin can adopt a closed conformation on UBE2S

To study the structural mechanism of UBE2S^{UBC} auto-inhibition by Lys^{+5} modification, NMR experiments on two types of disulfide-linked UBE2S^{UBC}-Ub conjugates were performed, that mimic the isopetide-linked conjugate. Therefore, a variant of UBE2S^{UBC}, UBE2S^{UBC} C95S/C118M/K^{+5}C, was cloned, expressed and purified. In this UBE2S^{UBC} variant, in which Lys100 was mutated to a cysteine for disulfide-formation with a modified ubiquitin variant (Gly76 to Cys). To ensure conjugation of ubiquitin to position +5, the native cysteine residues, Cys95 (≙ Cys^{cat}) and Cys118 were mutated to serine and methionine, respectively. The latter was chosen because it was shown that a methionine at position 118 does not interfere with donor ubiquitin binding in the closed conformation [52]. This conformation is critical for the catalytic activity of UBE2S and a similar interface has been predicted to be important for the thioester transfer of ubiquitin from the E1 to the E2 [54].

In one conjugate, UBE2S^{UBC} was ^{15}N-labeled and ubiquitin unlabeled and in the other UBE2S^{UBC} was unlabeled and ubiquitin ^{15}N-labeled (Figure 21, see 3.2.14) and both could be prepared in feasible amounts for NMR experiments that allow for the detection of the binding mode of Lys^{+5}-linked ubiquitin on UBE2S.

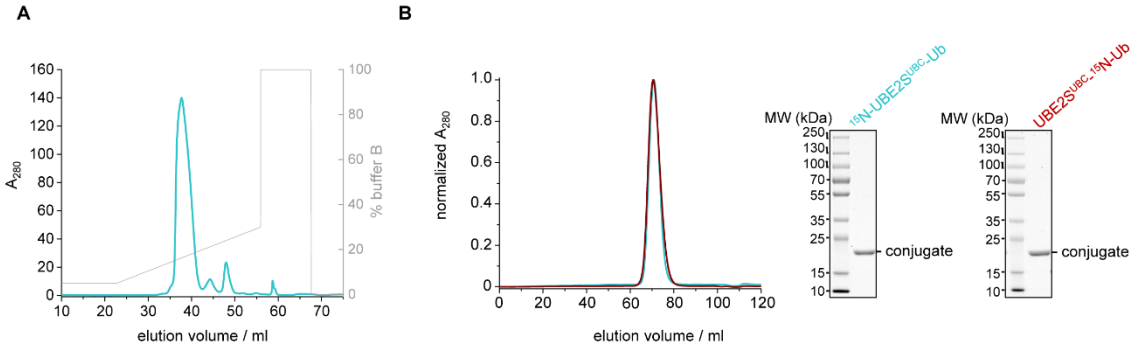

Figure 21: Preparation of a disulfide-linked UBE2S^{UBC} C95S/C118M/K^{+5}C-Ub G76C conjugate for NMR. (A) Anion-exchange chromatography of the disulfide-linked UBE2S^{UBC}-Ub G76C conjugate, in which UBE2S^{UBC} C95S/C118M/K^{+5}C is ^{15}N-labeled. (B) Gel filtration profile for both NMR-conjugates: blue: ^{15}N-labeled UBE2S^{UBC} C95S/C118M/K^{+5}C, red: ^{15}N-labeled ubiquitin G76C (left) and associated SDS-PAGE (right).

Due to the flexibility of the active site region in UBE2S, it is possible that ubiquitin bound to Lys^{+5} can adopt a similar, closed conformation as the donor ubiquitin towards UBE2S. To test this hypothesis, ^{1}H-^{15}N-HSQC spectra of the two conjugates were recorded and compared to the *apo* spectra of ubiquitin and UBE2S^{UBC}. To this end, the backbone chemical shift assignments for ubiquitin and the UBE2S^{UBC}-Ub-conjugate in which

ubiquitin was ^{15}N-labeled, were taken from BMRB Entry 17439 [4], while the assignments of the UBE2S^{UBC} C95S/C118M/K^{+5}C variant and the +5-modified conjugate were generated with the help of triple resonance experiments, performed by Dr. Kristian Schweimer, (University of Bayreuth, Bayreuth/Germany), on double-labeled (^{15}N, ^{13}C) protein that I purified.

The analysis of the weighted combined chemical shift perturbations ($\Delta\delta(^{1}H^{15}N)$) plotted over the ubiquitin residue number reveals that hydrophobic patch of ubiquitin including residues Lys48, His68, Leu71 and Arg72 is needed for UBE2S binding. These residues had also been shown to be functionally critical for the closed UBE2S-donor interface [4,52]. Furthermore in both cases, major chemical shift perturbations can be mapped to the C-terminus of ubiquitin, which is conjugated to the E2 (Figure 22A, B and D; [4]). *Vice versa*, major shift perturbations of UBE2S resonances in the Lys^{+5}-linked UBE2S^{UBC}-Ub-conjugate coincide with the previously defined donor ubiquitin binding site (Figure 22A, C and E). The interface contains functionally-validated key contacts, such as Glu51, Arg101, Asp102, Cys118 and Ser127, needed for appropriate donor ubiquitin binding in the closed conformation [4,52]. The similarity of the two interfaces is further illustrated in Figure 23, comparing the UBE2S^{UBC}-Ub-conjugates mimicking the Lys^{+5}-linked and the thioester-linked (characterized by Dr. Sonja Lorenz) conjugate. This supports the hypothesis that ubiquitin bound to Lys^{+5} can adopt a closed, donor-like conformation on UBE2S.

Note that a second set of chemical shift perturbations specifically induced by Lys^{+5}-linked ubiquitin, is detected opposite to the closed donor binding site (Figure 22E, right). These perturbations are most probably induced by propagated changes in the chemical environment upon linkage of ubiquitin to Lys^{+5}; however, it cannot be ruled out that they reflect a second binding mode of ubiquitin to UBE2S.

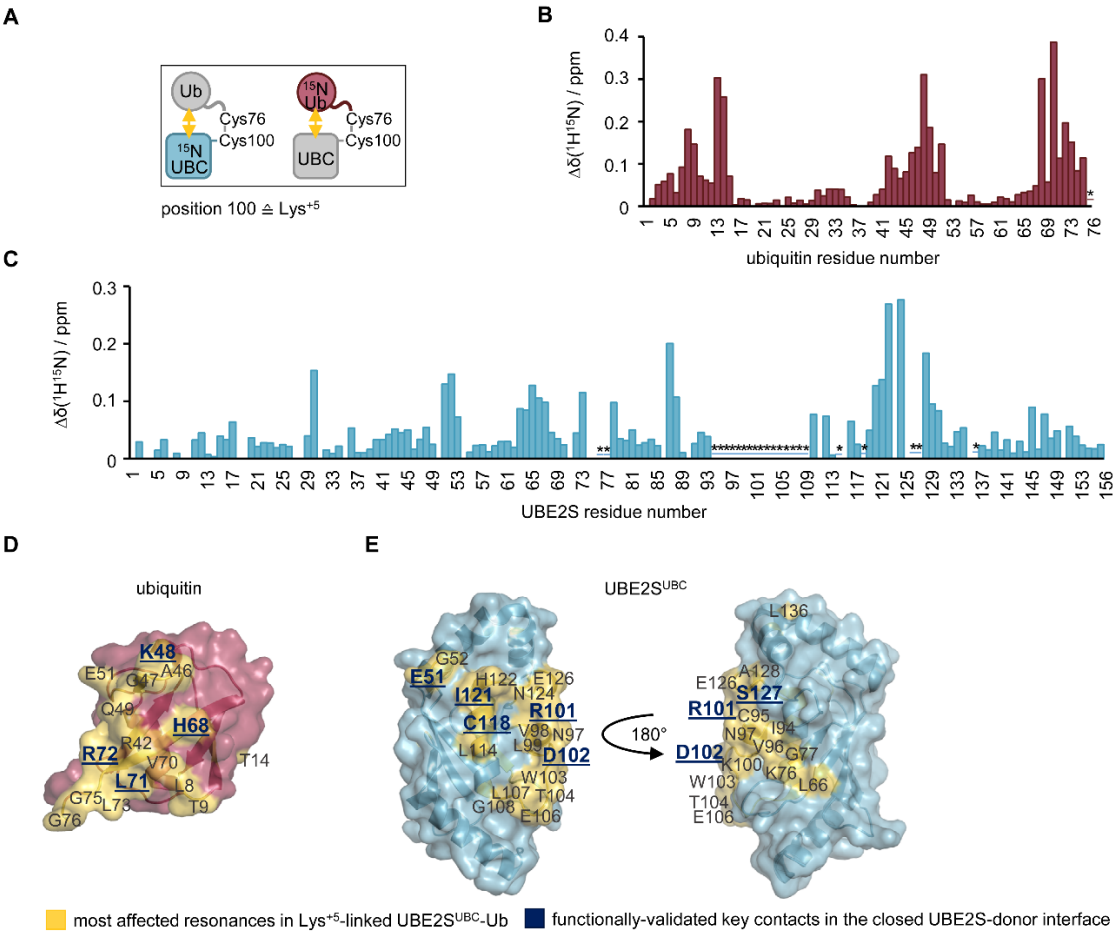

Figure 22: Lys^{+5}-linked ubiquitin adopts a closed conformation on UBE2S^{UBC}. (A) Cartoon representation of the two UBE2S^{UBC} C95S/C118M/K^{+5}C-ub G76C conjugates, mimicking UBE2S^{UBC}, modified with ubiquitin at position +5. In color, ^{15}N-enriched components are highlighted. (B) Weighted combined chemical shift perturbations (Δδ(^{1}H^{15}N)) of ubiquitin resonances in the covalently linked conjugate with UBE2S^{UBC}, compared to the *apo* protein. Δδ(^{1}H^{15}N) is plotted over the ubiquitin residue number and the asterisk marks line broadening. (C) Weighted combined chemical shift perturbations (Δδ(^{1}H^{15}N)) of UBE2S^{UBC} C95S/C118M/K^{+5}C resonances of the covalently linked conjugate with ubiquitin, compared to the *apo* protein. Δδ(^{1}H^{15}N) is plotted over the ubiquitin residue number; the asterisk marks line broadening and/or signal disappearance caused by chemical exchange on the intermediate chemical shift timescale. Gaps result from missing assignments (residues 3, 4, 7, 11, 18, 19, 31, 90, 111, 115, 135 and 150) and prolines (residues 9, 10, 27, 28, 35, 50, 54, 71, 74, 75 and 86). (D) Cartoon and surface representation of the crystal structure of ubiquitin (PDB: 1UBQ, [27]). In yellow, residues that undergo chemical shift perturbations Δδ(^{1}H^{15}N) > 0.1 ppm or line broadening in the context of the conjugate are pointed out. Underlined residue numbers are functionally validated key contacts in the UBE2S^{UBC}-donor ubiquitin interface [4]. (E) Cartoon and surface representation of the crystal structure of UBE2S^{UBC} (PDB: 1ZDN) [182] in two orientations. The color code is analogous to (D), whereas residues with Δδ(^{1}H^{15}N) > 0.12 ppm are labeled.

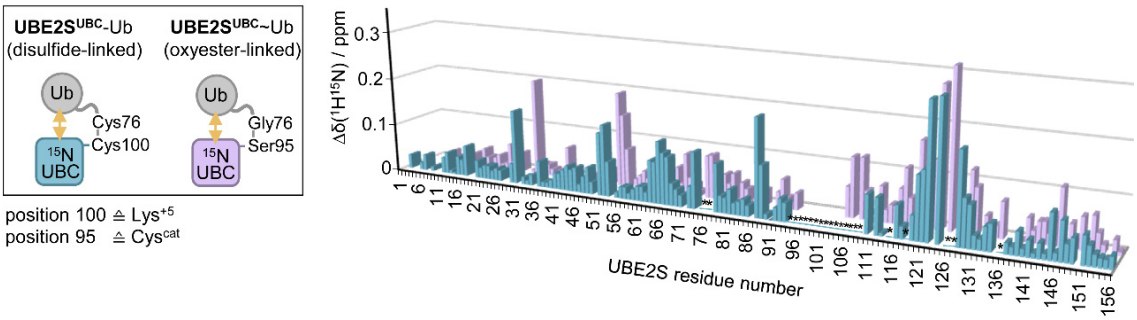

Figure 23: Comparison of the UBE2S^{UBC}-Ub-conjugate mimic and a mimic of the thioester-linked donor conjugate. Cartoon representation of two UBE2S^{UBC}-Ub conjugates for NMR, mimicking the UBE2S^{UBC}-Ub conjugate with ubiquitin bound to position +5 (blue) and the thioester-linked conjugate (purple) by an oxyester bond, as studied previously by Dr. Sonja Lorenz [4] (left). The weighted, combined chemical shift perturbations ($\Delta\delta(^1H^{15}N)$) of the UBE2S^{UBC} C95S/C118M/K^{+5}C-Ub G76C (blue) and the UBE2S^{UBC} C95S-ub conjugate (purple) are plotted over the UBE2S^{UBC} residue number, analogous to Figure 22C (right).

Thus, the NMR data analysis highlights that ubiquitin linked to Lys^{+5} of UBE2S interacts with UBE2S^{UBC} similarly to the closed donor conformation. This provides a structural basis for UBE2S auto-inhibition by Lys^{+5}-auto-ubiquitination, as donor ubiquitin binding and ubiquitin bound to position +5 are mutually elusive.

In summary, this chapter reveals that auto-ubiquitination of Lys^{+5} confers auto-inhibition in UBE2S. Specifically, it was shown that the active-site region of UBE2S is flexible, allowing Lys^{+5} to come in close proximity to the catalytic cysteine (Figure 14 and Figure 16) an allowing Lys^{+5}-auto-ubiquitination in *cis* (Figure 17). When ubiquitin is conjugated to Lys^{+5}, it can adopt a donor ubiquitin-like closed orientation towards UBE2S (Figure 22 and Figure 23). This inhibits the E1-induced thioester-transfer of ubiquitin to the E2 (Figure 20B) and subsequently isopetid bond formation (Figure 20C). This auto-inhibition mechanism may affect substrate ubiquitination by UBE2S in the context of the APC/C and / or UBE2S stability in the cell (Figure 24) – hypotheses that require further investigation.

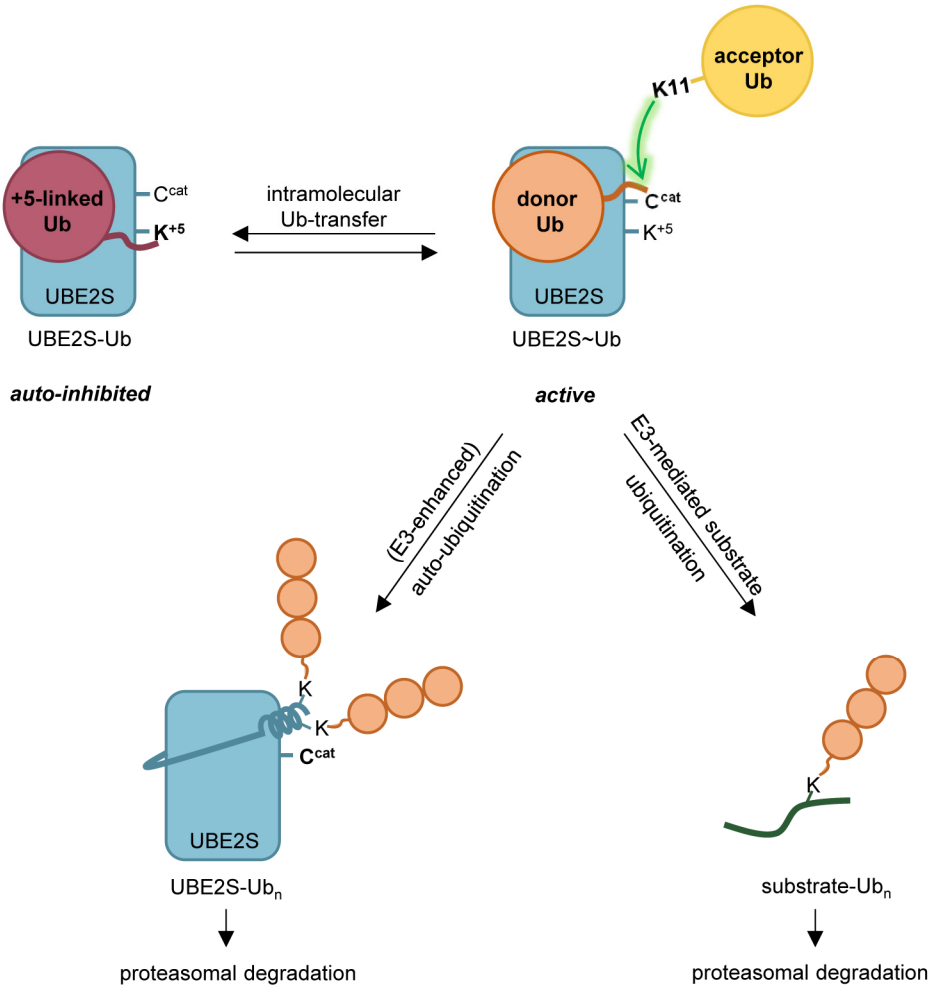

Figure 24: Lys^{+5}-auto-ubiquitination confers auto-inhibition. Model of the active state of UBE2S with donor ubiquitin (orange) thioester-linked to Cys^{cat} and in the closed orientation towards the E2 and the acceptor ubiquitin (yellow) presenting Lys11 for the nucleophilic attack of the thioester bond. Active UBE2S can either perform E3-mediated substrate ubiquitination to promote substrate degradation by the proteasome, or (E3-enhanced) auto-ubiquitination of the C-terminal extension, promoting UBE2S turnover [3]. UBE2S can adopt an auto-inhibited state through intramolecular auto-ubiquitination of Lys^{+5}. Lys^{+5}-linked ubiquitin adopts a closed conformation towards UBE2S, similar than the donor ubiquitin in the active state, thus inhibiting the E2.

4.2 Auto-inhibition of UBE2S by UBE2S dimerization

Parts of this section are going to be published in [175]. It delineates the structural basis and functional consequences of UBE2S dimerization.

4.2.1 UBE2S^{UBC} crystallizes as a dimer

As mentioned in section 4.1, the various crystal structures of UBE2S show a dimeric arrangement (Figure 15). The tendency of UBE2S to crystallize as a dimer is supported by two new crystal structures of UBE2S^{UBC} (Figure 25 and Table 16). The new high resolution crystal structure of UBE2S^{UBC} WT (1.55 Å; PDB: 6S98) adopts the typical canonical α/β-fold with four α-helices and four β-sheets in each of the two subunits and reflects the over-all shape of the crystal structure of UBE2S^{UBC} that was deposited by the Structural Genomics Consortium (PDB: 1ZDN, [182]; Figure 15).
The two subunits are linked by a disulfide bond via Cys118, the catalytic cysteines (Cys95) are oxidized to a sulfoxide, as the crystal was grown in non-reducing conditions. The dimer interface is symmetric, tightly packed and hydrophobic, with an interface area of 1051.1 Å, a solvation free energy gain upon formation of -10.8 kcal/M and a P-value of P = 0.235. The majority of interfacing residues reside in helix αB (residues 109-121), of which the axes are arranged in a 113°angle between the two subunits.
The disulfide bond formed through Cys118 is surrounded by a hydrophobic network including His111, Leu114, Thr115, Cys118, Leu119, Ile121, His122, and Pro123 (Figure 25B). Additional hydrophobic inter-subunit contacts are provided by Pro50, Thr53, Pro54, and the aliphatic side chain portion of Glu51, all of which are located in a turn within the adjacent β-sheet region of UBE2S. With the exception of one flanking hydrogen bond (between Asp102 and Tyr141), the dimer interface is devoid of polar or electrostatic interactions. [170].
Based on the considerable size and hydrophobic nature of the interface, I speculate that its formation may not require an inter-subunit disulfide linkage. To test this idea, a UBE2S^{UBC} variant in which Cys118 was replaced by alanine was crystallized and its structure determined at 2.18 Å resolution (Figure 25C and Table 16; PDB: 6S96). Indeed, this crystal structure contains a dimer, similar to the UBE2S^{UBC} WT structure (backbone RMSD of 1.13 Å), despite the lack of an inter-subunit disulfide bond. This implies that the dimer-formation in UBE2S is not dependent on the disulfide bond, similar to what was observed for UEB2S^{UBC} C118M (Figure 15C).

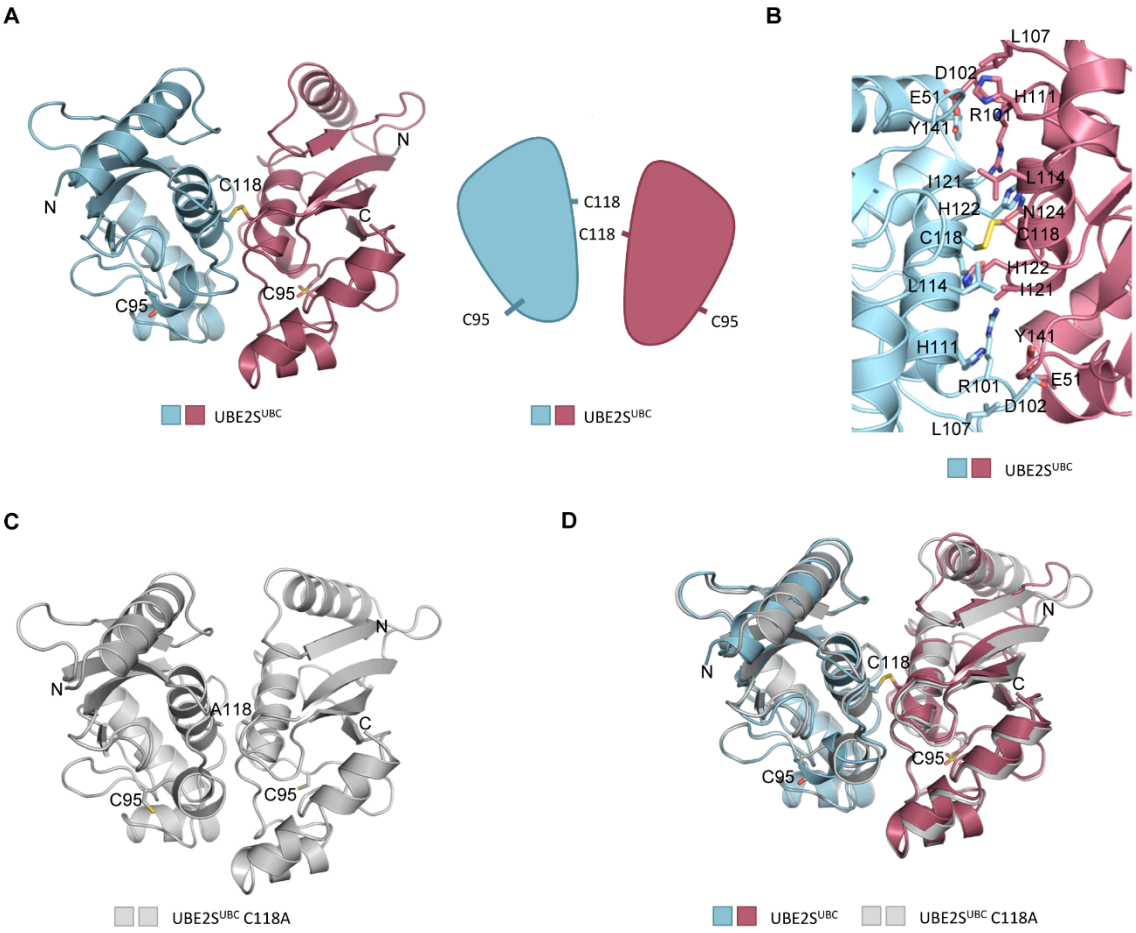

Figure 25: UBE2S^{UBC} crystallizes as a dimer. (A) Crystallographic dimer structure of UBE2S^{UBC} with a resolution of 1.55 Å (Table 16, PDB: 6S98). Each monomer contains one catalytic domain of UBE2S, connected by a disulfide bond via Cys118 (left). Note that the active-site cysteine (C^{cat} = C95) is overoxidized to a sulfoxide in each subunit. Cartoon representation of the dimer (right). (B) Detail of the hydrophobic dimerization interface in the crystal structure of the UBE2S^{UBC} WT shown in (A). Key residue side chains at the subunit interface are illustrated as sticks. (C) Crystal structure of UBE2S^{UBC} C118A (PDB: 6S96). The monomers are not covalently linked in this case. (D) Superposition of the crystallographic dimers formed by UBE2S^{UBC} WT and the C118A variant, demonstrating high overall similarity.

Together, these analyses imply that UBE2S can form a symmetric crystallographic dimer via its catalytic domain, independent of a disulfide linkage at position 118 in the interface.

Table 16: X-ray crystallographic data collection and refinement statistics for the structures of UBE2S^{UBC} WT and C118A. Values in parentheses correspond to the highest resolution shell.

	UBE2S^{UBC} WT (PDB: 6S98)	UBE2S^{UBC} C118A (PDB: 6S96)
data collection		
wavelength (Å)	0.9680	1.033
space group	P 1 21 1	P 61
unit cell parameters		
a, b, c (Å)	44.8 49.05 71.93	120.9 120.9 45.3
α, β, γ (°)	90 106.03 90	90 90 120
total reflections	78466 (7412)	39533 (3800)
unique reflections	43484 (4292)	19810 (1898)
R_{pim}	2.5 (43.0)	4.4 (40.8)
completeness (%)	99.4 (98.9)	98.8 (95.1)
I/σ(I)	14.5 (2.0)	8.6 (1.5)
redundancy	1.8 (1.7)	2.0 (2.0)
Wilson B factor	18.8	44.02
CC ½	0.999 (0.638)	0.997 (0.992)
refinement		
resolution (Å)	42.15 – 1.55 (1.605 – 1.55)	34.91 – 2.18 (2.258 – 2.18)
R_{work} / R_{free}	16.14 / 18.39	20.38 / 24.53
no. of atoms		
protein	2358	2241
water	171	32
average B-factors		
protein	29.5	57.2
water	32.1	49.8
RMSD from ideality		
bond lengths (Å)	0.013	0.014
bond angles (°)	1.35	1.21
Ramachandran statistics		
favored (%)	98.96	98.36
disallowed (%)	0.00	0.00
MolProbity clash score	3.35	9.42
MolProbity overall score	1.22	1.5

4.2.2 UBE2S has the capacity to dimerize *in vitro*.

Together with our collaborators, we demonstrated that UBE2S dimerizes via the crystallographic interface in cells [175]. In this chapter, however, I focus on the associated *in vitro* studies.

First, dimerization in solution was investigated using *in vitro* pull-down experiments with His_6-tagged and HA-tagged variants (either in the UBC or full-length context of UBE2S). A weak self-association of $UBE2S^{UBC}$ could be detected, while it appeared to be enhanced in the full-length protein (Figure 26). UBE2S self-association had previously also been observed by Lim and colleagues [195].

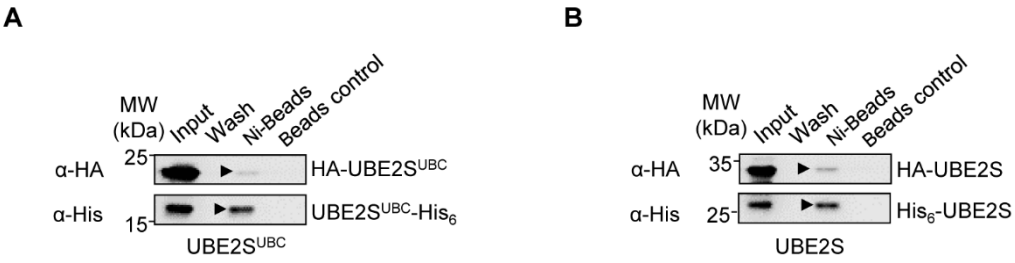

Figure 26: UBE2S dimerizes weakly in solution. (A) *In vitro* pull-down of $UBE2S^{UBC}$, monitored by SDS-PAGE and immunoblotting. The control contains HA-tagged $UBE2S^{UBC}$ only. (B) Pulldown as in (A), using His- and HA-tagged UBE2S.

However, standard biophysical techniques like analytical ultracentrifugation (Figure 27) and SEC-MALS did not show significant dimerization of UBE2S in solution under the conditions used (Figure 29A, B; black curves). This indicates that dimerization of UBE2S occurs transiently.

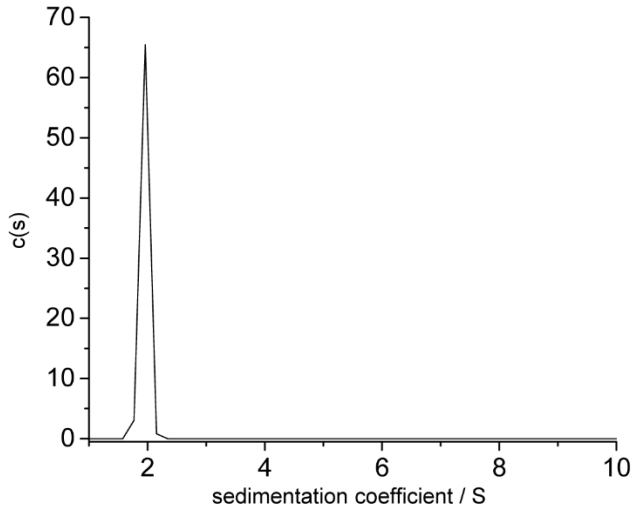

Figure 27: Analytical ultracentrifugation data for UBE2S. The peak at a sedimentation coefficient of ~2 S corresponds to a species with a molecular mass of ~23 kDa.

To be able to capture such transient dimerization events, a crosslinking experiment based on the cysteine-reactive crosslinker dibromobimane (bBBr) was conducted. This assay makes use of the central position of cysteine 118 in the dimeric interface. Thus, bBBr would be able to trap the dimer if it were transiently occupied in solution.

Indeed, incubation of UBE2S^{UBC} with bBBr yielded a second species in SEC experiments. The amount of the second species correlated with the incubation time.

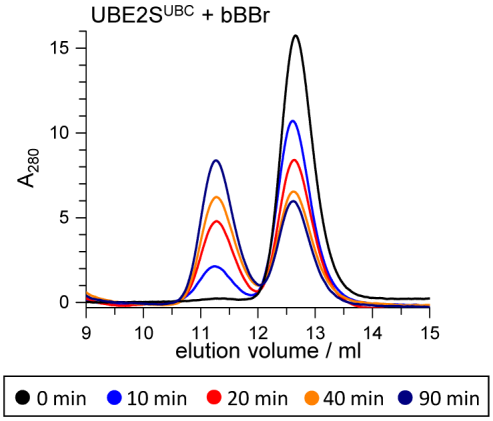

Figure 28: UBE2S crosslinking with bBBr reveals a second protein species. SEC experiments with UBE2S^{UBC} WT (40 µM), crosslinked with bBBr. The reactions were quenched with 5 mM NEM at the indicated time points.

The two species were further characterized by SEC-MALS. UBE2S^{UBC} and UBE2S were incubated with bBBr for 40 min and yielded a dimeric form of UBE2S. The experimentally determined molecular weights of the eluted protein species are 16.5 ± 0.3 and 31.7 ± 0.5 kDa for UBE2S^{UBC} and 26 ± 2 and 47 ± 2 kDa for UBE2S. These molecular weights are in excellent agreement with the expected molecular weights of a UBE2S^{UBC} monomer (17.4 kDa) and dimer (34.7 kDa) and the monomeric and dimeric forms of UBE2S (23.9 and 47.7 kDa), respectively (Figure 29A, B). The results are correlated by the analysis of non-crosslinked and crosslinked samples of the two UBE2S variants by SDS-PAGE: While the non-treated protein samples show a single band at the size of the monomeric protein, an additional band at the size of a UBE2S dimer is detected in the bBBr-treated samples (Figure 29C, D), highlighting that UBE2S dimerizes in solution.

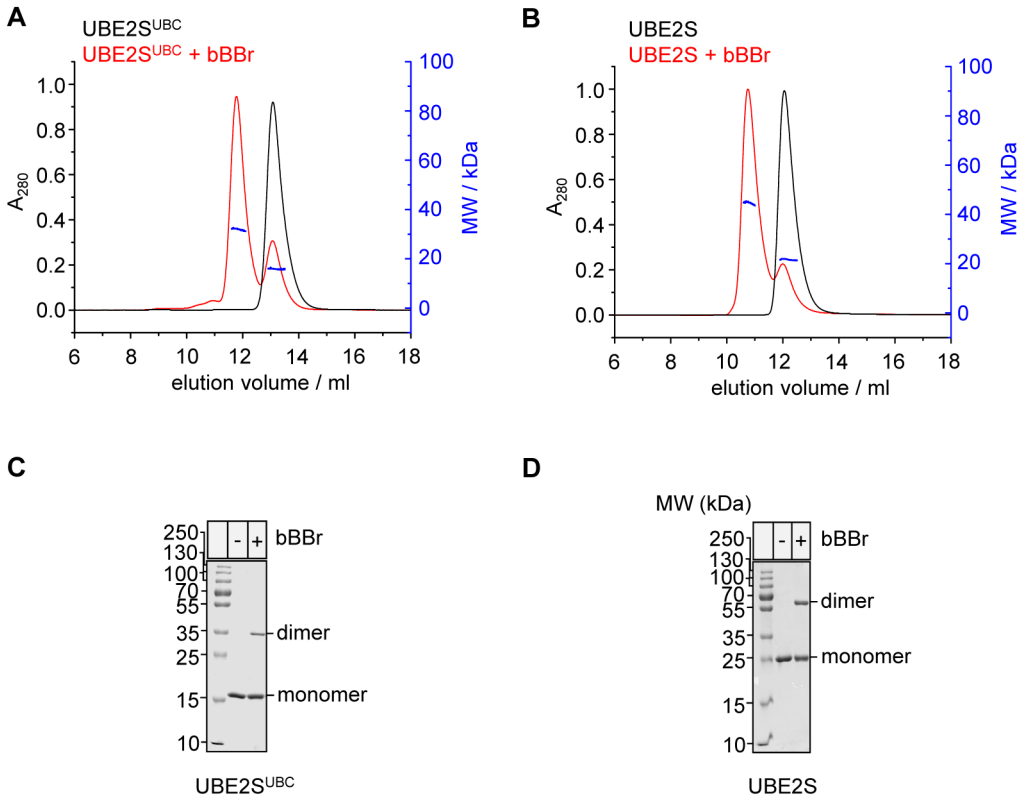

Figure 29: Transient dimerization of UBE2S captured by crosslinking. (A) SEC-MALS experiments of UBE2S^{UBC} (300 µM) with and without bBBr-mediated crosslinking. The proteins were incubated with bBBr for 40 min and thereafter injected onto the gel filtration column. The derived molecular masses are 16.5 ± 0.3 kDa for the UBE2S^{UBC} monomer and 31.7 ± 0.5 kDa for the dimer. (B) SEC-MALS experiments of UBE2S (300 µM) with and without bBBr-mediated crosslinking. The derived molecular masses are 26.2 ± 1.7 kDa for the UBE2S monomer and 47.4 ± 1.4 kDa for the dimer. (C) SDS-PAGE of untreated and bBBr-crosslinked UBE2S^{UBC} (40 µM). (D) SDS-PAGE of untreated and bBBr-crosslinked UBE2S (40 µM).

Since bBBr is a cysteine-reactive crosslinker, these experiments raised the question of whether UBE2S dimerizes in solution via Cys118 or the catalytic cysteine (Cys95), or both. To discriminate between these scenarios, UBE2S^{UBC} WT as well as the single cysteine variants C95S (Cys118 only), C118S (Cys95 only) and the double cysteine variant C95S/C118S were analyzed by size exclusion chromatography: In the absence of the crosslinker, all variants elute in their monomeric form (Figure 30A). Upon incubation with bBBr for 40 min, followed by quenching with N-ethylmaleimide (NEM), WT UBE2S^{UBC} and UBE2S^{UBC} C95S respectively, crosslink with similar efficiencies. In contrast, UBE2S^{UBC} C118S elutes as monomer, just like the cysteine-free variant (UBE2S^{UBC} C95S/C118S (Figure 30B).

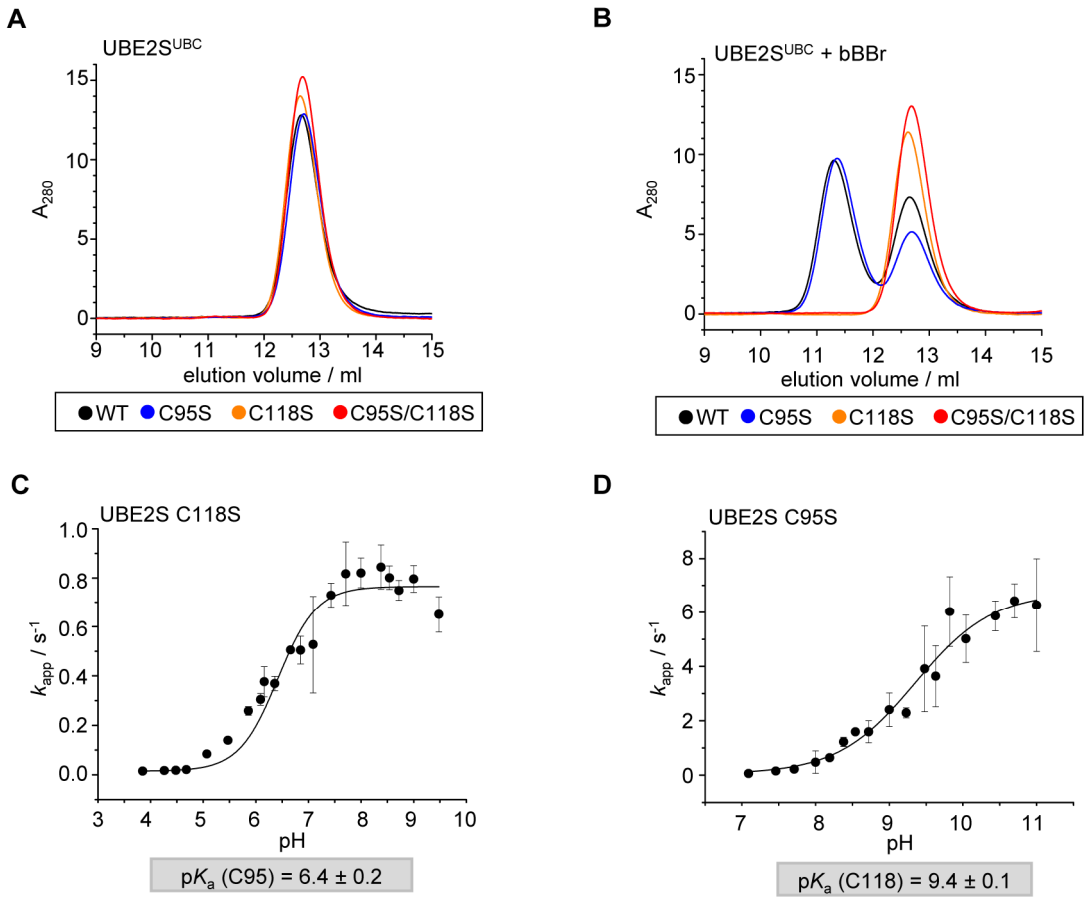

Figure 30: The bBBr-crosslink occurs exclusively via Cys118. (A) SEC experiments with UBE2S^{UBC} WT and three cysteine variants, C95S, C118S, and C95S/C118S (40 µM). (B) SEC experiments with the same proteins as in A, following bBBr-mediated crosslinking. The crosslinking reaction was quenched with 5 mM NEM after 40 min. (C) pK_a determination for the thiol group of Cys95 (Cys^{Cat}) in the single-cysteine variant UBE2S C118S, based on stopped-flow kinetic measurements of the reaction rates towards DTNB. (D) pK_a determination for the thiol group of Cys118 in the single-cysteine variant UBE2S C95S, based on stopped-flow kinetic measurements of the reaction rates towards DTNB. In (C) and (D) the mean and SDs from at least three replicates are plotted. The pK_a determination experiments and analyses were performed by Marie-Annick Letzelter.

The bBBr crosslink is therefore specific to Cys118, in line with the hypothesis that UBE2S transiently dimerizes through the crystallographic interface in solution. Furthermore, this is remarkable, since the catalytic cysteine Cys95 is expected to be more reactive than Cys118. So, if crosslinking was defined by chemical reactivity rather than conformational restrains, it should preferentially occur through Cys95.

Cysteine reactivity towards small-molecule electrophiles is expected to correlate with their p*K*a-value [196] – the lower the p*K*a, the more reactive the respective cysteine residue. Thus, Marie-Annick Letzelter determined the p*K*a-value of Cys95 (C^{cat}; using

UBE2S C118S) and Cys118 (using UBE2S C95S) of UBE2S. The p*K*a of the active site cysteine (Cys95) is 6.4 ± 0.2 and is lower than the one for Cys118 (9.4 ± 0.1), as expected (Figure 30C, D). Nevertheless, crosslinking of UBE2S with bBBr occurs only via Cys118 (Figure 30B). The crosslinking site was additionally verified by mass spectrometry, showing that the crosslinked form of UBE2S is connected via Cys118, while Cys95 was not modified.

Taken together, these experiments demonstrate that UBE2S is crosslinked by bBBr specifically via Cys118, which is part of the dimer interface seen in the crystal structures of UBE2S^{UBC} (Figure 15 and Figure 25). Dimerization via the active-site cysteine, located opposite of the dimerization interface is disfavored, although, it is chemically more reactive. This is in line with the idea that UBE2S forms a transient dimer in solution which resembles the crystallographic one.

4.2.3 The dimerization of UBE2S is concentration-dependent

A second interesting finding is that bBBr-mediated crosslinking is increased at higher UBE2S concentrations, as seen by comparing SEC-MALS experiments at 300 µM protein concentration (Figure 29A, B) with SEC experiments at 40 µM protein concentration (Figure 30A and B). This suggests that UBE2S dimerization is concentration-dependent, as expected from a bimolecular experiment. Therefore, SEC experiments with bBBr-treated UBE2S^{UBC} WT or the full-length protein were performed at different protein concentrations (Figure 31A, B). Increasing UBE2S concentrations result in increased populations of the crosslinked form of the proteins (Figure 31B). This correlates with the SDS-PAGE analysis of the crosslinked samples (Figure 28C, D).

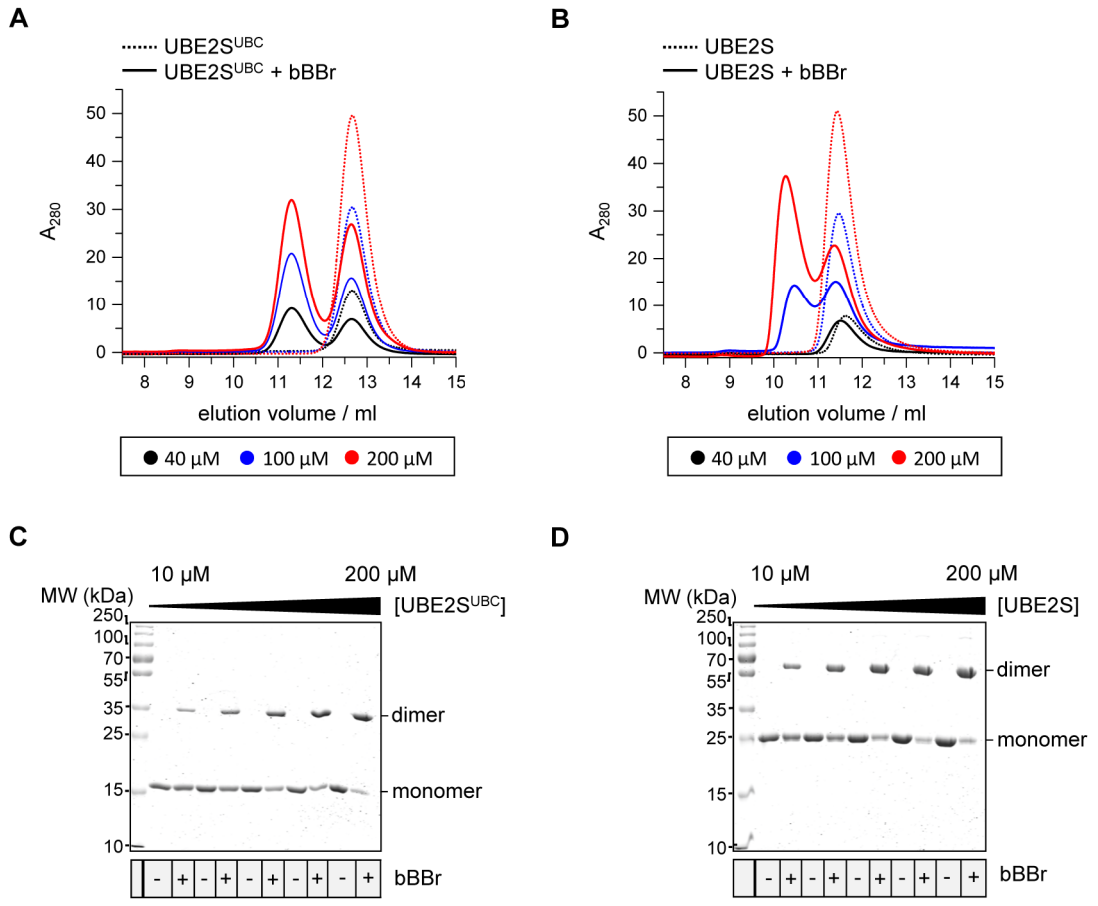

Figure 31: UBE2S crosslinking with bBBr is concentration dependent. (A) SEC experiments with UBE2S^{UBC} WT at indicated concentrations, crosslinked with bBBr in the molar ratio 1:1.5. The reactions were quenched with 5 mM NEM after 60 min of incubation. (B) SEC experiments with UBE2S WT at indicated concentrations, crosslinked with bBBr. The samples were treated as in A. (C) SDS-PAGE analysis of the concentration-dependency of the UBE2S^{UBC}-bBBr crosslink. (D) SDS-PAGE analysis as in (C), using UBE2S.

Another approach capable of detecting weak association events, as used to monitor the dimerization of other E2 enzymes, is NMR [84,197,198]: Concentration-dependent relaxation measurements were performed to derive the average transverse relaxation (R_2) rates of amide protons located in structured regions of UBE2S^{UBC} based on two-point spin echo experiments. The obtained values were 53 ± 8 s^{-1} at 230 µM, 60 ± 8 s^{-1} at 1 mM, and 80 ± 10 s^{-1} at 2.3 mM protein concentration. The same experiments were repeated with full-length UBE2S and revealed the same trend. In this case, the average transverse relaxation (R_2) rates of the amide protons in the structured regions of UBE2S are 70 ± 15 s^{-1} at 200 µM, 83 ± 15 s^{-1} at 1 mM, and 115 ± 23 s^{-1} at 2 mM. The increasing transverse relaxation rates with increasing protein concentrations indicate a

concentration-dependent self-association of both, UBE2S^{UBC} and full-length UBE2S in solution, independent of a crosslinking reagent.

A second NMR approach to detect weak association events is the determination of the average longitudinal (R_1) and transverse (R_2) relaxation rates of the nitrogen nuclei in the structured regions of a protein, as performed by Dr. Kristian Schweimer (University of Bayreuth, Bayreuth/Germany) for UBE2S^{UBC}. The average R_1 and R_2 relaxation rates were 0.93 +/- 0.06 and 15.0 +/- 1.6 s^{-1}, respectively at 200 µM protein concentration and a magnetic field strength of 16.8 T, corresponding to a rotational correlation time of 11 ns. This is in good agreement with the size of a globular protein of ~ 160 amino acids [199], like monomeric UBE2S^{UBC}. The R_2 relaxation rates globally increased by 20 to 30% at 600 µM protein concentration, which is not a result of concentration-dependent structural rearrangements in UBE2S^{UBC}, since the corresponding $^{1}H^{15}N$-HSQC spectra overlay perfectly (Figure 32).

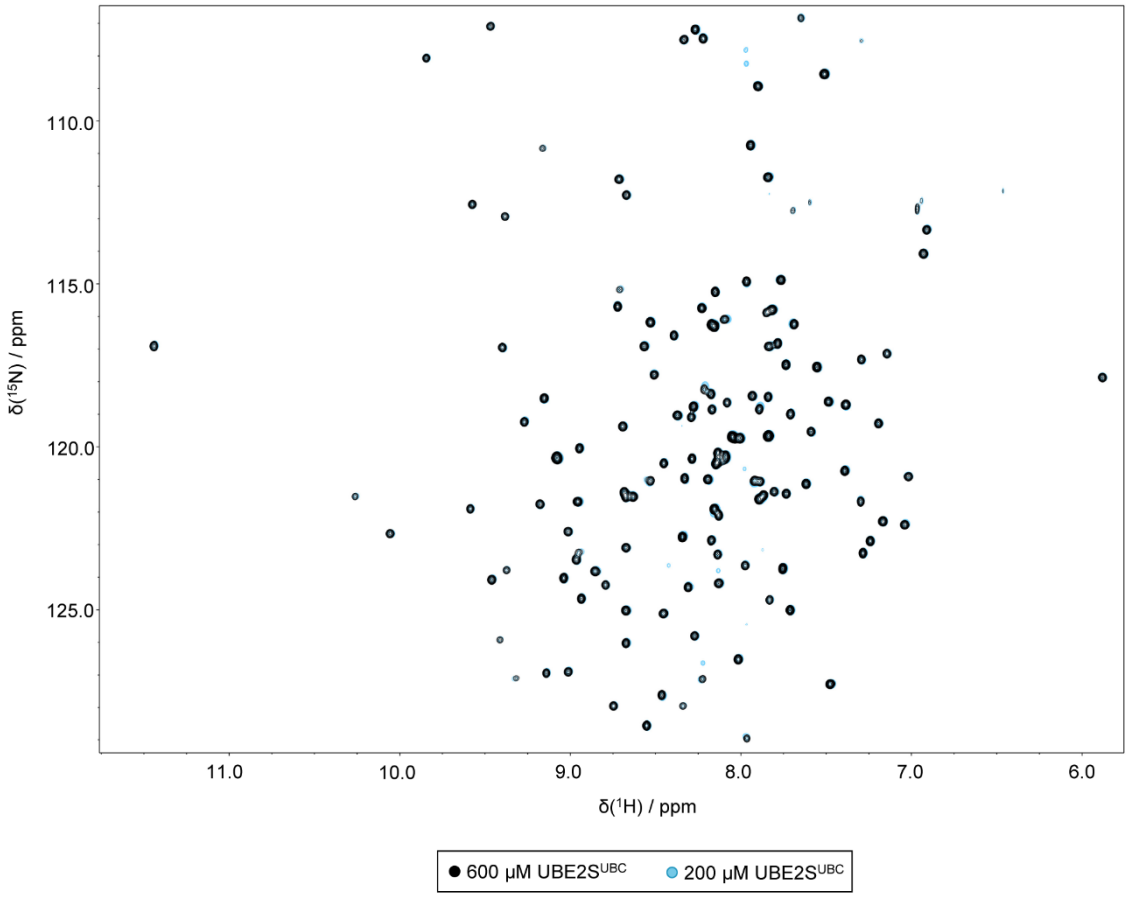

Figure 32: $^{1}H^{15}N$-HSQC spectra of UBE2S^{UBC}. The spectra were recorded at 600 µM (black) and 200 µM (blue) protein concentration.

Based on the knowledge from the crosslinking experiments, this self-association can be assumed to reflect UBE2S dimerization.

4.2.4 The dimerization of UBE2S in solution mirrors the interface seen crystallographically.

As crosslinking of UBE2S occurs only through Cys118, which lies at the center of the dimerization interface, it is likely that the transient dimerization of UBE2S in solution occurs via the same interface that is found in the crystal structures (Figure 25B). To test this, a series of mutations was introduced, individually replacing each key residue in the dimer interface by alanine an glutamate in the case of Leu114, both in the context of UBE2S^{UBC} and the full-length protein. The mutated protein variants were expressed, purified and subjected to crosslinking experiments with bBBr. All UBE2S^{UBC} variants elute in a monomeric form in SEC experiments without bBBr (Figure 33A).
Upon crosslinking, dimeric UBE2S^{UBC} can be detected in the WT as shown in Figure 30B. However, crosslinking is drastically reduced for all mutated variants. Only UBE2S^{UBC} N124A and UBE2S^{UBC} Y141A show crosslinking efficiencies similar to the WT protein (Figure 33B).

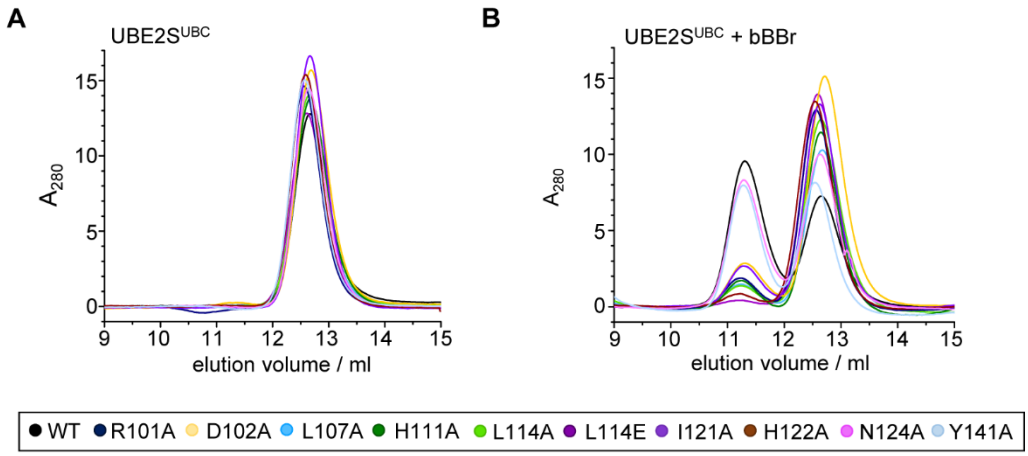

Figure 33: UBE2S^{UBC} dimerizes via the crystallographic interface in solution. (A) SEC experiments with purified UBE2S^{UBC} WT (as in Figure 30A) and the dimer interface variants (40 µM). (B) SEC experiments with UBE2S^{UBC} WT (as in Figure 30B) and the dimer interface variants (40 µM) after incubation with 60 µM bBBr for 40 min. The reactions were quenched with 5 mM NEM before injection on the gel filtration column.

To follow the crosslinking kinetics and provide a quantitative read-out of the dimerization of UBE2S, fluorescence measurements were conducted. Those made use of the fact

that bBBr generates a fluorescent product when both alkylating groups have reacted ([200], Figure 34A).

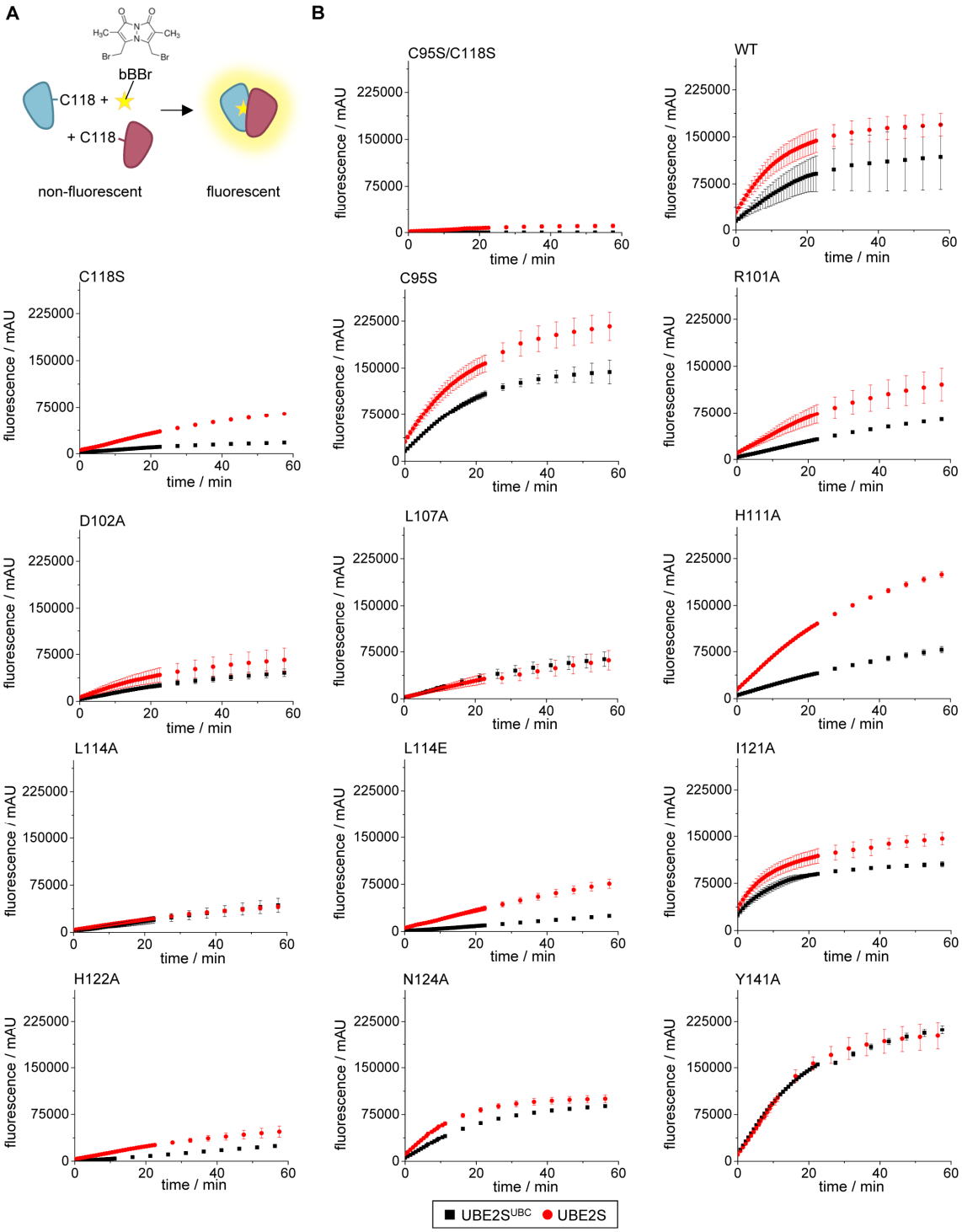

Figure 34: UBE2S^{UBC} / UBE2S crosslinking followed by fluorescence detection. (A) Schematic representation of the fluorescence dimerization assay using bBBr (star) as crosslinking reagent. bBBr is fluorescent after the reaction with two cysteine residues. (B) UBE2S dimerization (plotted as fluorescence) over time for UBE2S WT and the dimer interface variants. For each variant, the experiment was performed with UBE2S and UBE2S^{UBC} in technical triplicates, error bars indicate the standard deviation (SD) of those replicates.

While no significant increase in fluorescence could be measured for the C95S/C118S variant, which serves as negative control as it contains no cysteine residues for crosslinking, an increase of the fluorescence and therefore of the crosslinked, dimeric species is seen for the WT protein. The C95S variant, which contains a substitution of the catalytic cysteine to alanine, shows a comparable pattern to the WT, in line with the previous crosslinking experiments (Figure 30B, Figure 34B). Mutating critical interface residues such as Leu107, Leu114 and Cys118 to alanine leads to a significantly slower increase in the fluorescence.

Notably, all UBE2S variants in the full-length context (black curves) crosslink faster compared to those in the context of the catalytic domain (red curves; Figure 34B).

The dimerization rates were calculated to quantify the impact of mutational effects on the crosslinking propensity of UBE2S. Figure 35 shows that all point mutations in the dimer interface significantly slow down the bBBr-induced dimerization. The only expectations are the I121A and Y141A variants, which still crosslinked as efficiently as the wild-type protein.

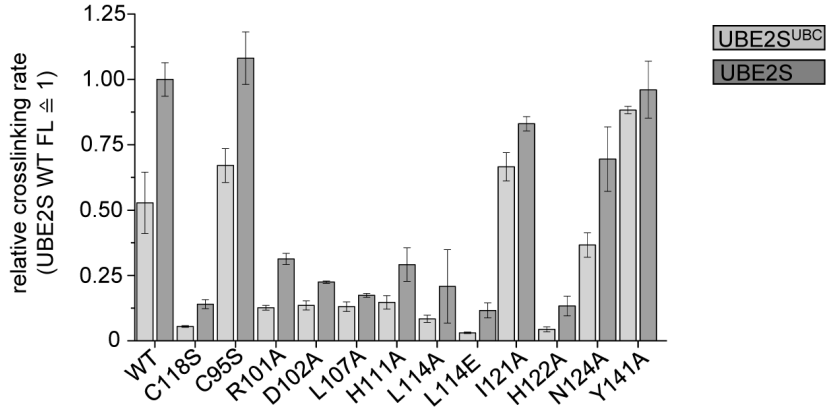

Figure 35: Crosslinking kinetics recapitulate the interface seen in the UBE2S^{UBC} crystal structures. Rates of bBBr-mediated crosslinking of 13 purified variants of UBE2S^{UBC} (light grey) and UBE2S (dark grey), respectively. The mean and SDs from three experiments are plotted. The raw data of one experiment are shown in Figure 34B.

Next, it was investigated whether the UBE2S^{UBC} L114E construct, whose crosslinking capacity is significantly reduced compared to WT still crystallizes as a dimer or as a monomer. Interestingly, I obtained, indeed, the first monomeric crystal structure of *apo* UBE2S^{UBC} (Figure 36A and Table17). In this crystal structure, the cysteine at position 118 is oxidized to a sulfoxide, while the catalytic cysteine is not oxidized. However, the structure does not show major differences in the UBC fold compared to previous

structures. The monomer overlays perfectly with a subunit of the UBE2S^{UBC} dimer (Figure 36B). Interestingly, the L114E variant crystallized in different conditions (see 3.8.1) as a dimer, in which the subunits are tilted compared to the arrangement seen for the WT. This is possibly caused by the larger size and charge of the glutamate side chain compared to leucine (Figure 36C and Table17).

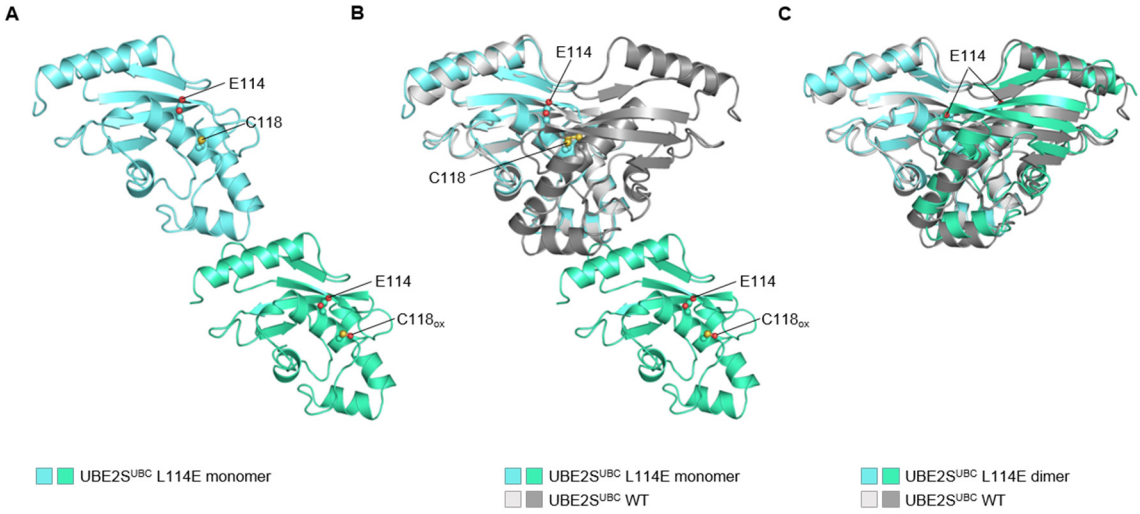

Figure 36: Monomeric and dimeric arrangements of UBE2S^{UBC} L114E in crystal structures. (A) Monomeric UBE2S^{UBC} L114E with Glu114 and Cys118 shown in ball-and-stick representation. Note that Cys118 in chain A (green) is oxidized to sulfoxide. (B) Overlay of monomeric UBE2S^{UBC} L114E with UBE2S^{UBC} WT (PDB: 6S98, grey). (C) Crystal structure of dimeric UBE2S^{UBC} L114E, overlaid with UBE2S^{UBC} WT (PDB: 6S98). Glu114 is shown in ball-and-stick representation.

Overall it appears that the favored state of UBE2S in crystals is the dimer. That one of the structures has the L114E variant also in a dimeric arrangement does not conflict with the crosslinking data because the L114E mutation does not abolish crosslinking and, apparently, the physicochemical parameters during crystallization are different from a solvation-based assay.

In summary, it can be concluded that the transient dimerization of UBE2S in solution, as followed by bBBr-crosslinking, occurs via a similar interface as seen in UBE2S^{UBC} crystal structures. Single amino acid substitutions at the interface to alanine strongly interfere with crosslinking. In addition to the interface formed by the catalytic domain of UBE2S, the unique C-terminal extension of UBE2S, enhances crosslinking.

Table17: X-ray crystallographic data collection and refinement statistics for the structures of UBE2S^{UBC} L114E monomer and dimer. Values in parentheses correspond to the highest resolution shell.

	UBE2S^{UBC} L114E (monomer)	UBE2S^{UBC} L114E (dimer)
data collection		
Wavelength (Å)	0.968	0.968
space group	P 2 21 21	P 1 21 1
unit cell parameters		
a, b, c (Å)	64.08 79.38 82.56	45.32 48.41 70.13
α, β, γ (°)	90 90 90	90 107.07 90
total reflections	157517 (9471)	59830 (5875)
unique reflections	25719 (2513)	15981 (1546)
R_{pim}	3.99 (35.68)	4.69 (31.38)
completeness (%)	99.67 (99.37)	98.8 (95.1)
I/σ(I)	12.12 (1.99)	12.23 (2.31)
multiplicity	6.1 (3.8)	3.7 (3.8)
Wilson B factor	36.80	32.21
CC ½	0.999 (0.941)	0.998 (0.832)
refinement		
resolution (Å)	41.28 – 2.08 (2.159 – 2.08)	43.32 – 2.15 (2.23 – 2.15)
R_{work} / R_{free}	21.32 / 25.91	20.33 / 24.92
no. of atoms		
protein	2378	2218
water	75	22
average B-factors		
protein	50.70	48.04
water	43.49	32.85
RMSD from ideality		
bond lengths (Å)	0.004	0.012
bond angles (°)	0.89	1.40
Ramachandran statistics		
favored (%)	98.98	97.95
disallowed (%)	0.00	0.00
MolProbity clash score	1.04	4.81
MolProbity overall score	0.96	1.77

4.2.5 The C-terminal extension of UBE2S stimulates dimerization.

The finding that full-length UBE2S constructs generally have higher crosslinking rates than UBE2S^{UBC} constructs, motivated further analyses of the C-terminal extension. The C-terminal extension comprises residues 157-222 and is structurally uncharacterized. It is predicted to have no to little secondary structure, except for the C-terminal 22 residues,

which are predicted to form an α-helix (C-helix; Figure 37A). To dissect the role of different regions within the C-terminal extension in dimerization, UBE2S constructs of different length were subjected to crosslinking experiments with bBBr: UEB2S^{UBC} (residues 1-156), UBE2S$^{1-196}$ (residues 1-196) that contains the unstructured part of the C-terminal extension and UBE2S (residues 1-222) that also includes the C-helix. These studies showed that the presence of the unstructured region of the C-terminal extension does not alter the dimerization behavior compared to the catalytic domain. If the C-helix is included, however, a boost in the crosslinking rate is observed (Figure 37B, C). Thus, the C-helix is responsible for the enhanced crosslinking of UBE2S full-length compared to shorter constructs.

Based on these results, a competition experiment was performed, in which a large excess of a peptide comprising the C-terminal 25 amino acids of UBE2S (i.e. including the C-helix) was titrated to UBE2S in *trans*. The addition of the peptide interfered with the crosslinking of UBE2S in a concentration-dependent manner (Figure 37D, E). Thus, the C-helix peptide can interact with UBE2S in *trans*. That a large excess of peptide is required makes sense, because UBE2S already contains the C-helix and thus an intermolecular interaction competes with an intramolecular interaction.

The auto-ubiquitination experiments (see 4.1) confirmed that the C-terminal extension of UBE2S becomes auto-ubiquitinated, in accordance with previous studies [3,194]. It is conceivable that auto-ubiquitination of the C-terminal extension interferes with dimerization. To test this hypothesis, Marie-Annick Letzelter cloned, expressed and purified a construct in which UEB2S$^{1-197}$ is C-terminally fused to ubiquitin. Crosslinking experiments with this fusion protein showed significantly reduces bBBr-induced crosslinking as compared to UBE2S$^{1-196}$ (Figure 37F, G), in line with the idea that the ubiquitination of the C-terminal extension may interfere with dimerization of UBE2S.

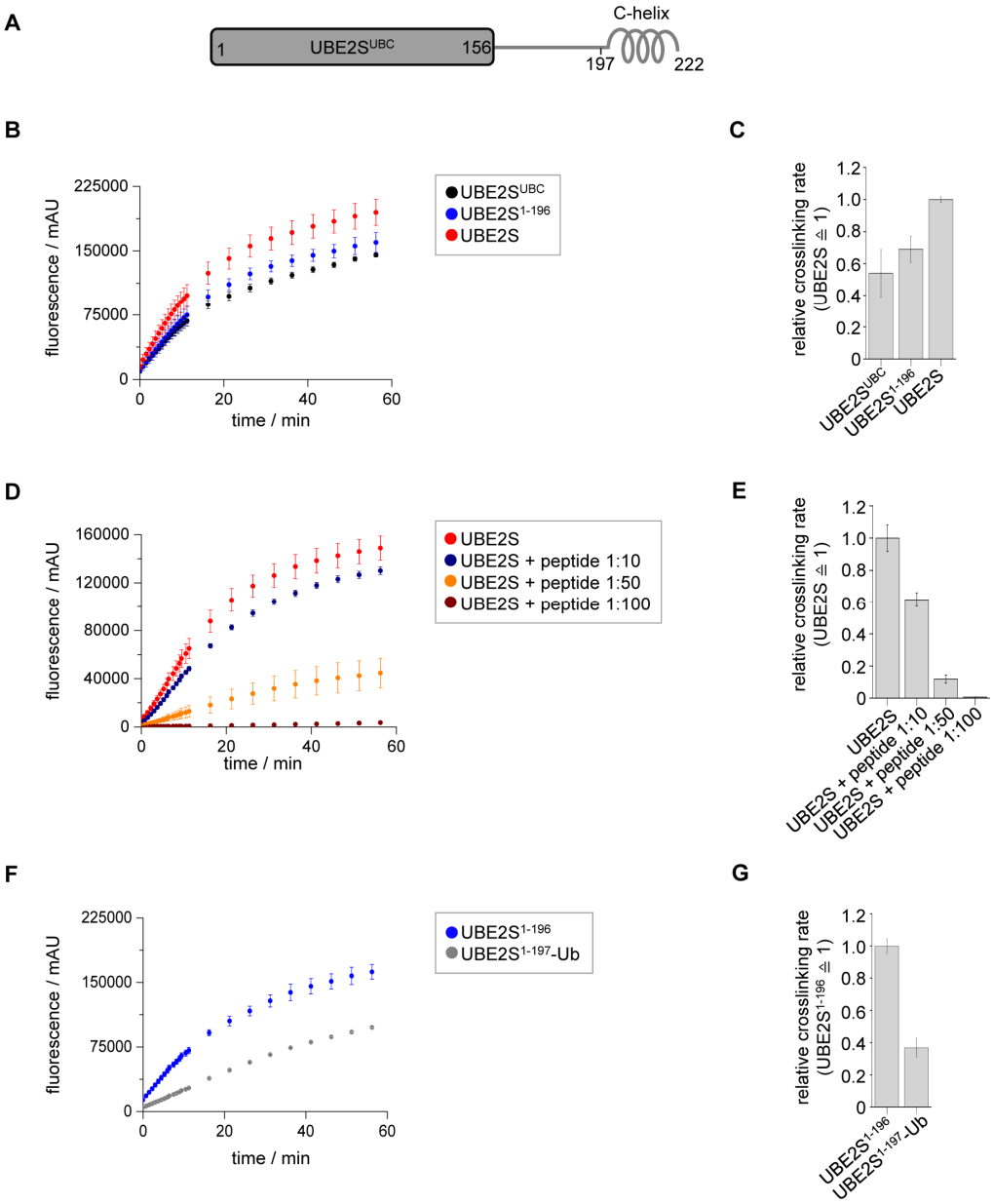

Figure 37: Impact of the C-terminal helix on UBE2S-dimerization. (A) Schematic representation of the architecture of the UBE2S monomer. The catalytic domain (UBE2S^{UBC}) represents a structurally studied, folded domain, whereas the C-terminal extension is predicted to be mainly unstructured, besides the last 25 residues that are predicted to form a helix (C-helix). (B) UBE2S dimerization (plotted as fluorescence) over time for UBE2S and two shortened constructs: UBE2S^{UBC} (residues 1-156) and UBE2S$^{1-196}$ (residues 1-196). For each variant, the experiment was performed in technical triplicates, error bars indicate the SD. (C) Rates of bBBr-mediated crosslinking of the UBE2S constructs shown in B. The mean and SDs from three experiments are plotted. (D) Competition experiment testing the effect of a peptide representing the C-terminal helix (residues 197-222) in indicated ratios, in *trans* on the bBBr-mediated crosslinking kinetics of UBE2S. The experiment was performed in technical duplicates, error bars indicate the SD. (E) Rates of bBBr-mediated crosslinking of UBE2S in the competition experiment in D. The mean and SDs from three experiments are plotted. (F) UBE2S dimerization (plotted as fluorescence) over time for UBE2S$^{1-196}$ and an UBE2S$^{1-197}$-Ub constructs (UBE2S residues 1-197, fused to Ubiquitin at the C-terminus). The experiment was performed in technical triplicates, error bars indicate the SD. (G) Crosslinking rates of the experiment shown in F, the mean and SDs from three experiments are plotted.

Together, these studies are compatible with a model, in which the unmodified C-helix enhances dimerization either by interacting with the UBC domain in *cis* (and thus promote dimerization allosterically) or in *trans* or in a 'cherry-like' assembly (Figure 38). To distinguish between these models requires further analyses. However, based on the NMR titration that showed that the C-helix can interact with the active site region of UBE2S (Figure 19), I favor model A and B.

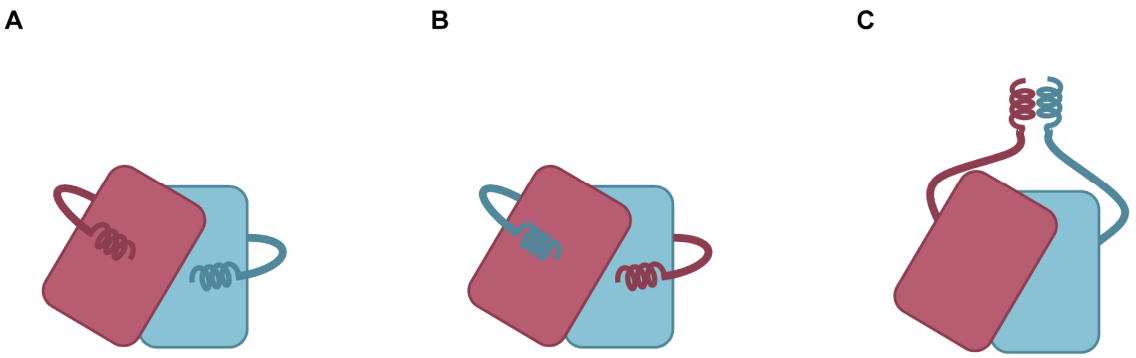

Figure 38: Models for C-helix-enhanced dimerization. (A) Dimerization enhanced by allosteric effects through interactions of the C-helix with the catalytic domain of UBE2S in *cis*. (B) Dimerization enhanced by interactions of the C-helix with the UBC domain in *trans*. (C) Dimerization enhanced by interactions between the C-helices of the two monomers ('cherry-like' assembly).

4.2.6 Dimerization of UBE2S confers auto-inhibition

To elucidate the effect of dimerization on UBE2S activity, three UBE2S variants with point mutations in the dimer interface that reduce the dimerization capacity of UBE2S were chosen for *in vitro* auto-ubiquitination assays. Therefore, it was of importance to choose mutation sites that do not interfere with the binding of the donor ubiquitin in order to monitor only effects caused by diminished dimerization.

As Leu107 and His111 lie outside of and Leu114 peripheral to the donor binding site but their mutation disrupts dimerization (Figure 39A, B), the ^{15}N-labeled mutated variants were purified (UBE2S L107A, UBE2S H111A and UBE2S L114E) and used in chemical shift mapping experiments with unlabeled ubiquitin. Whereas the mutations L107A and H111A leave the interaction between UBE2S and ubiquitin intact, L114E was found to weaken it (Figure 39C).

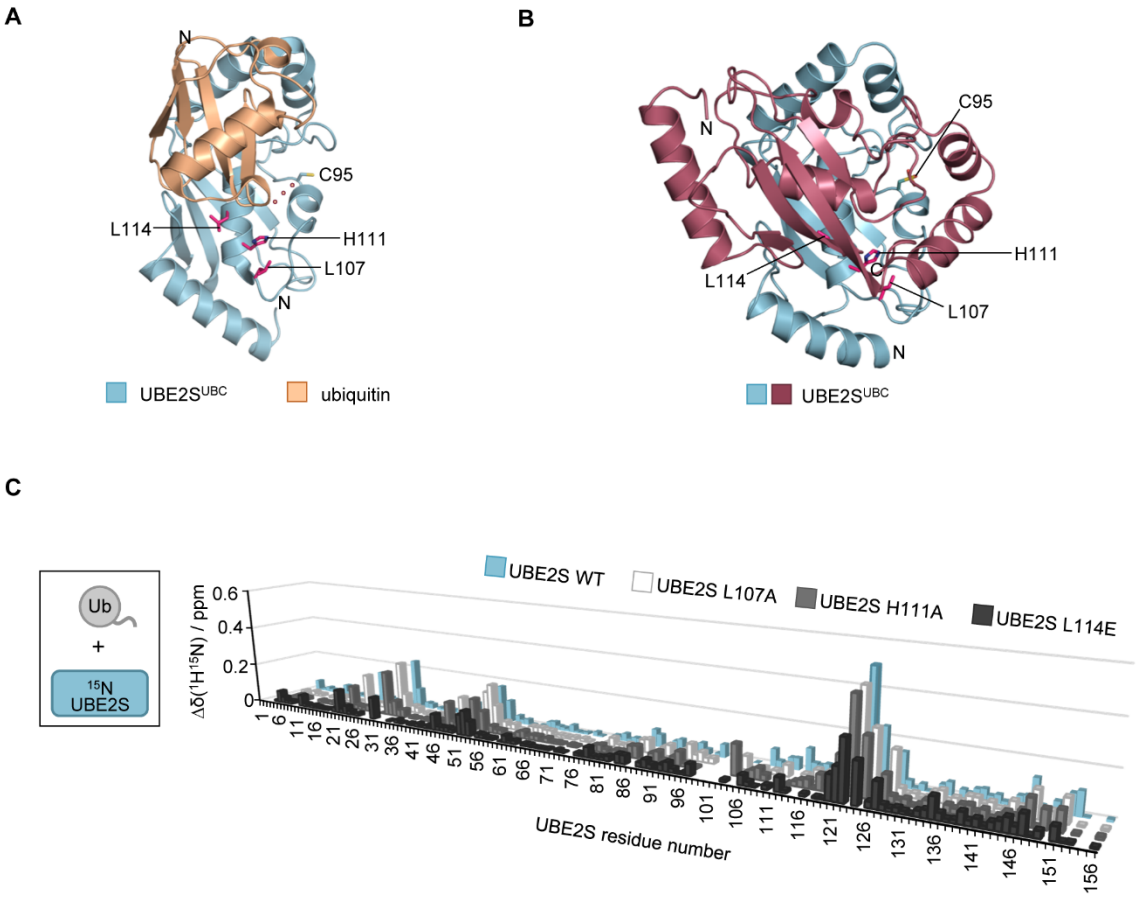

Figure 39: Leu107, His111 and Leu114 are required for dimerization but are dispensable for donor ubiquitin binding. (A) Crystal structure of UBE2S^{UBC} in complex with a donor-like ubiquitin, whereas the interaction in the crystal is formed in *trans* (PDB: 5BNB [52]). The side chains of Cys95 and Leu107, His111 and Leu114 are shown in stick representation. The latter three residues (pink) are part of the dimer interface (see B), but outside or at the rim of the donor ubiquitin interface. (B) Crystal structure of the UBE2S^{UBC} dimer (PDB: 6S98, Table 16), presented as in (A). Here, Cys95 is overoxidized to a sulfoxide. (C) Weighted and combined chemical shift perturbations ($\Delta\delta(^1H^{15}N)$) of resonances of the catalytic domain of UBE2S WT and the three dimer interface variants, induced by donor ubiquitin binding in *trans* (32.5-fold molar excess of ubiquitin).

This is reflected in the NMR-derived K_D-values that are 1.34 ± 0.04 mM for UBE2S WT, 1.43 ± 0.03 mM for UBE2S L107A, 1.84 ± 0.04 mM for UBE2S H111A and 3.3 ± 0.1 mM for UBE2S L114E (Figure 40). This is consistent with Leu107 and His111 being located outside of the donor ubiquitin binding site, while Leu114 is close to it (Figure 39A).

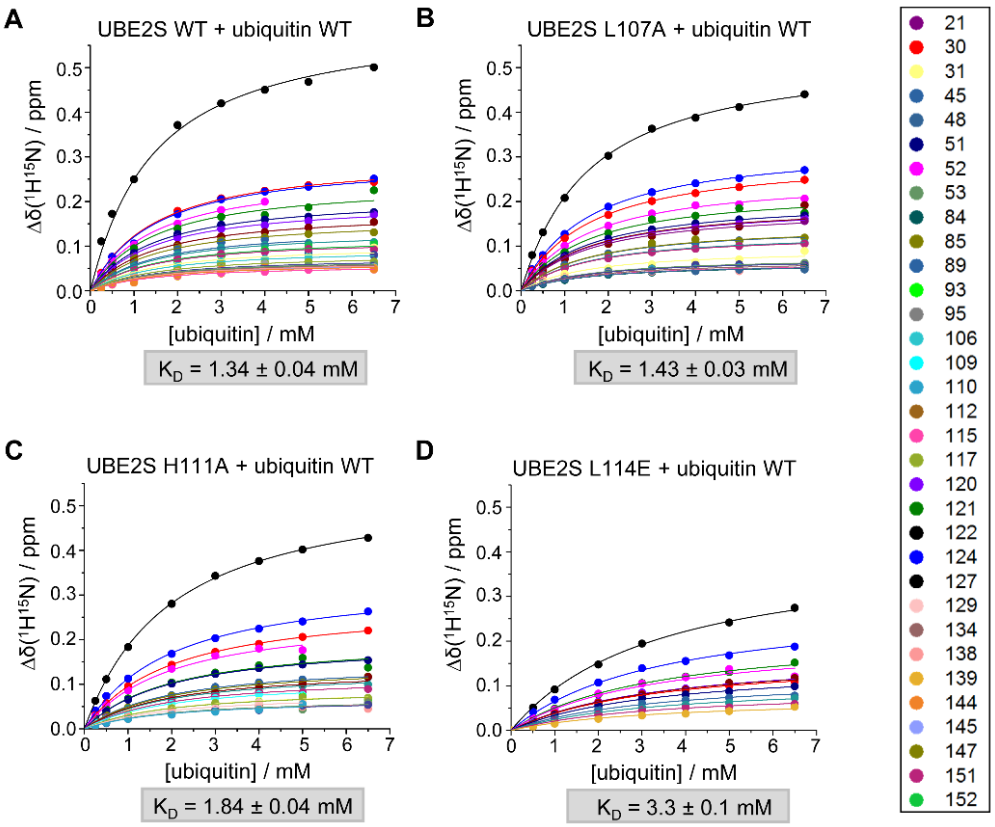

Figure 40: K_D-determination of the interaction of UBE2S with ubiquitin. (A) Ubiquitin-induced weighted, combined chemical shift perturbations, $\delta\Delta(^1H^{15}N)$, of UBE2S WT resonances, plotted over the ubiquitin concentration. The data points were fitted globally to a single-site model including those resonances for which $\delta\Delta(^1H^{15}N)$ was at least 0.048 ppm at the highest ubiquitin concentration. The resonance for Gly52 undergoes line broadening and was thus not included in the fit. (B) Analogous data and fit as in (A) for the UBE2S L107A variant. (C) Analogous data and fit as in (A) for the UBE2S H111A variant. The resonances for Gly52 and Ile109 undergo line broadening and could, therefore, not be included in the fit. (D) Analogous data and fit as in (A) for the UBE2S L114E variant.

Next, the auto-ubiquitination and the di-formation of the UBE2S variants L107A, H111A and L114E were compared with WT UBE2S to possibly uncover a function of UBE2S dimerization. The *in vitro* activity assay did not show a clear trend (Figure 41). Whereas the di-ubiquitin formation and the auto-ubiquitination for UBE2S 107A are reduced, UBE2S H111A and UBE2S L114E show a pattern similar to the WT, with UBE2S L114E being slightly compromised in both read-outs. The trend seen in this assay thus does not strictly recapitulate the ubiquitin binding capacity of this protein variants (Figure 40B). In APC/C-dependent activity assay performed by Alena Kucerova and Dr. Jörg Mansfeld (Technische Universität Dresden, Dresden/Germany) [175], the activities of the mutated proteins were indistinguishable from the WT.

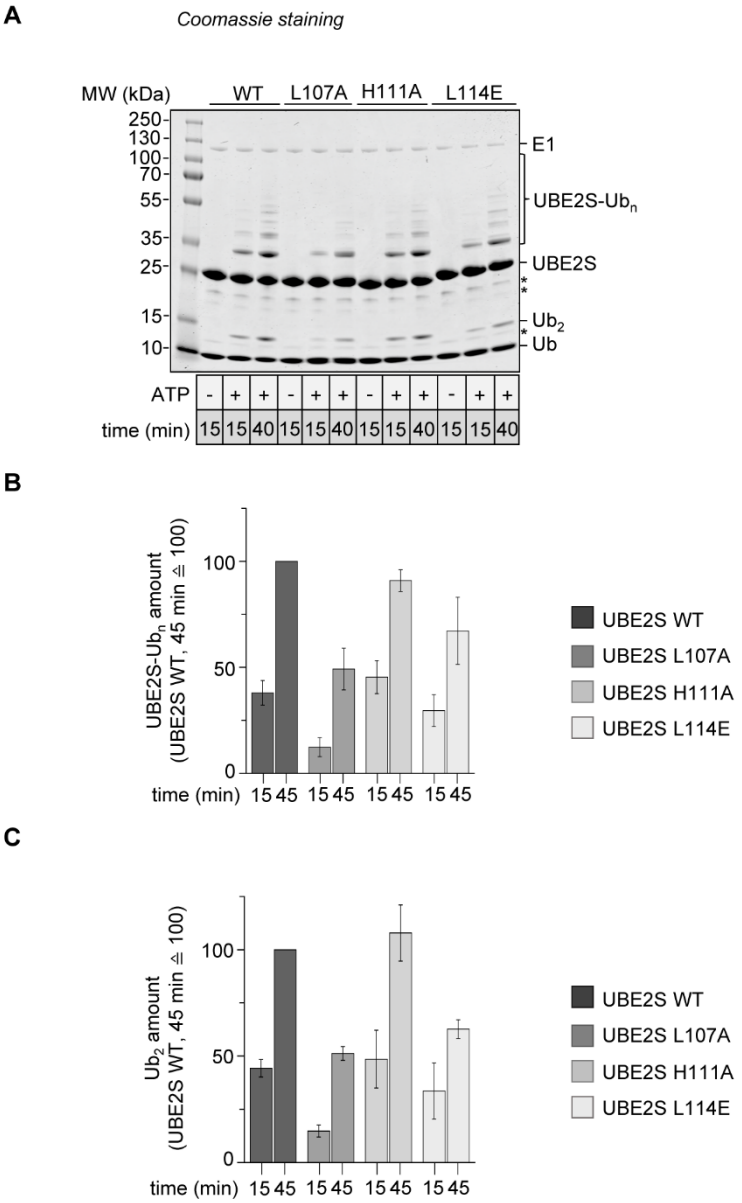

Figure 41: Mutational analysis of the dimer interface variants *in vitro*. (A) Assay, comparing di-ubiquitin formation and auto-ubiquitination of UBE2S variants (WT, L107A, H111A, and L114E), monitored by SDS-PAGE and Coomassie staining. The asterisk (*) denotes contaminations. (B, C) Quantification of Ub_2-formation and UBE2S auto-ubiquitination (UBE2S-Ub_n). The amount of reaction products formed by WT after 45 min was set to 100%. Depicted are the means and the SDs of three independent experiments.

To identify whether the reduced activity of UBE2S L107A is caused by folding defects, circular dichroism (CD) spectra of UBE2S WT and of the dimer interface variants were recorded (Figure 42). CD provides information about the secondary structure elements of a protein because the secondary structure elements absorb right- and left-circularly polarized light at asymmetric optical centers unequally. The signal is dominated by the contributions of the peptide bonds of the chiral amino acids, except for glycine, in the far UV range (170 nm to 260 nm). A maximum at around 192 nm and minima at about

209 nm and 222 nm are characteristics of α-helical structures, whereas a minimum between 210 nm and 225 nm and positive signals in the range of 190 nm to 200 nm characterizes β-strands. Disordered (random coil) or unfolded structures show minima near 200 nm [201].

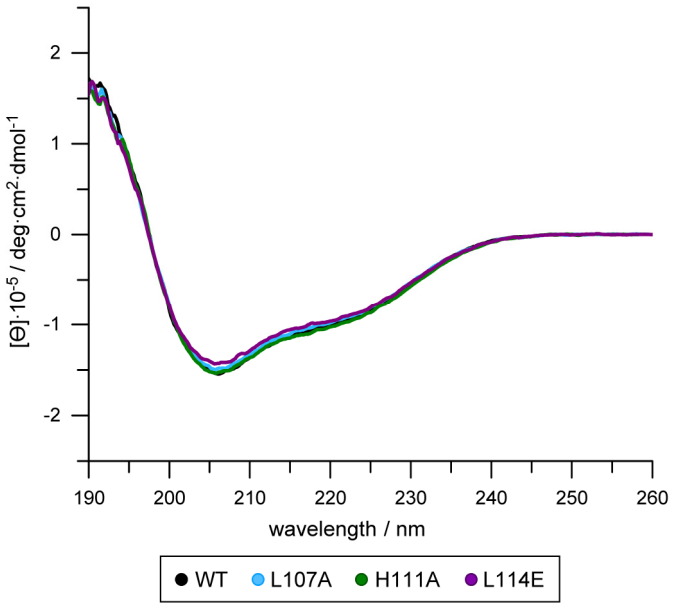

Figure 42: CD spectra of UBE2S WT and the dimer interface variants. For all samples the molar ellipticity was calculated according to Equation 2 (see Methods) and plotted against the wavelength in nm.

The CD spectra of UBE2S WT (black) and the dimer interface variants are nearly identical, showing a maximum at around 190 nm and two minima, one at 206 nm and a less pronounced one at around 225 nm, pointing towards a high content of α-helices and some β-strands. This is in accordance with the crystal structures of the catalytic domain of UBE2S (Figure 14, Figure 15 and Figure 25) and the structural predictions of the full-length protein (Figure 19A and Figure 37A). Taking this into account and the fact that the signal at 200 nm and below is positive, it can be concluded that all UBE2S variants are correctly folded and differences in activity are unlikely to result from structural defects.

The interpretation of the *in vitro* activities with respect to the dimerization of UBE2S is complicated by the fact that dimerization is extremely weak and transient, as demonstrated by the NMR relaxation (Figure 32) and crosslinking experiments (Figure 29). Hence, it is challenging to follow dimerization in solution *in vitro* to determine the functional consequences of dimerization. To overcome these difficulties, the bBBr-crosslinked dimer was isolated. From the same reaction, unmodified, monomeric UBE2S was isolated to ensure an identical treatment of the monomeric and the dimeric protein.

The ability to catalyze the formation of ubiquitin linkages (isopeptide bond formation) and accept ubiquitin from the E1 (thioester formation) of both, monomeric and dimeric UBE2S was compared in an *in vitro* assay.

Dimeric UBE2S was found not to assemble free ubiquitin chains (Ub_2), nor auto-ubiquitinate (Figure 43C). In agreement with the finding that the closed donor ubiquitin conformation is also important for thioester formation by Olsen and Lima [54], thioester formation with ubiquitin is also suppressed, if the UBE2S dimer is formed (Figure 43D). Therefore, dimerization confers auto-inhibition by the ability to prevent donor ubiquitin binding.

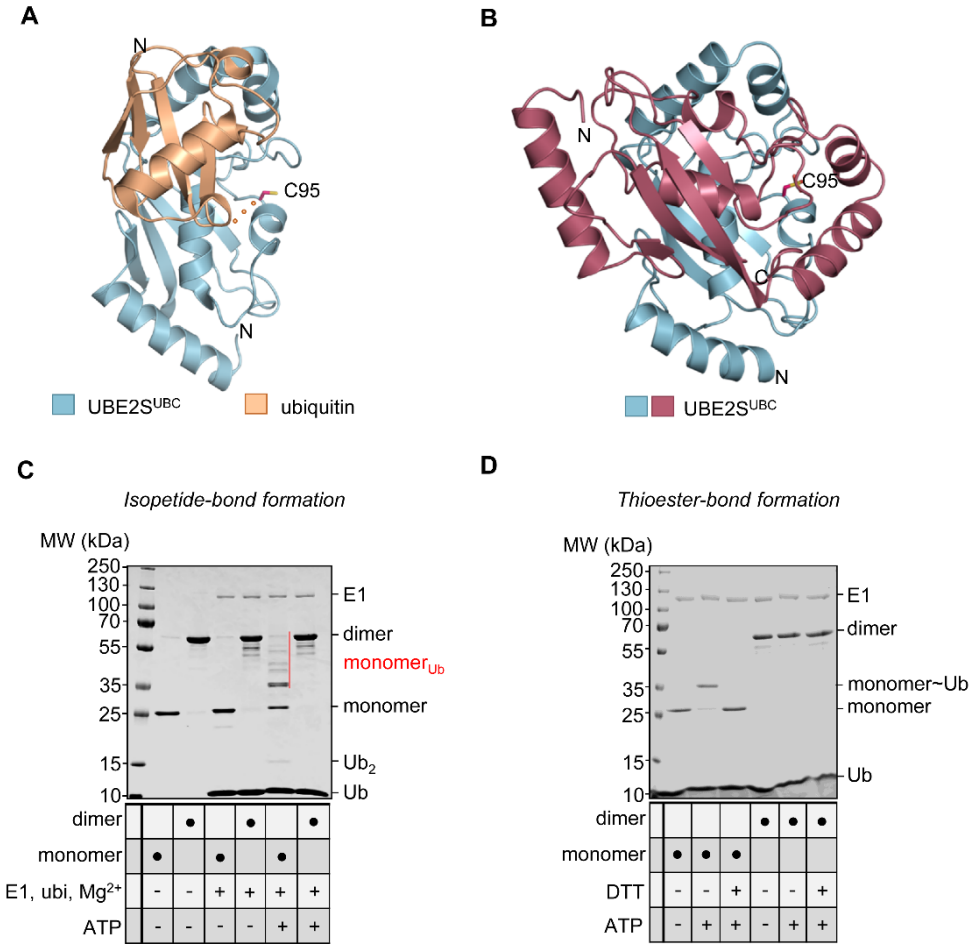

Figure 43: Dimerization causes auto-inhibition of UBE2S. (A) Crystal structure of UBE2S^{UBC} in complex with a donor-like ubiquitin, whereas the interaction in the crystal is formed in *trans* (PDB: 5BNB [52]). The side chain of Cys95 (active site) is highlighted. (B) Crystal structure of the UBE2S^{UBC} dimer (PDB: 6S98, Table 16). Note that Cys95 (highlighted in pink) in this particular structure is overoxidized to a sulfoxide. (C) *In vitro* isopeptide bond formation assay comparing the monomeric state of UBE2S with the purified and crosslinked dimeric state. Auto-ubiquitination ('monomer$_{Ub}$') and free chain formation (Ub_2) can be detected for monomeric UBE2S. (D) *In vitro* thioester formation assay comparing the binding of ubiquitin to the monomeric state of UBE2S and the purified and crosslinked dimeric state. Thioester-linked species are sensitive to reducing agent (DTT) and indicated by '~'. In C and D, the '-ATP' reaction serves as control.

This is in agreement with the analysis of the crystal structures of donor-bound UBE2S^{UBC} and dimeric UBE2S^{UBC}, indicating that UBE2S in its dimeric form represents an auto-inhibited state. Dimerization conflicts with donor ubiquitin binding in the critical closed conformation, because the two binding sites overlap to a considerable degree (Figure 43A, B). Thus, the two interactions should be mutually exclusive.

In summary, it could be shown that UBE2S undergoes a weak self-association in solution (Figure 26). This process can be followed by crosslinking (Figure 29), which reveals that the association mirrors the dimeric arrangement seen in several crystal structures of UBE2S^{UBC} (Figure 33 - Figure 35). Dimerization occurs through the catalytic domain, but is enhanced by the C-helix. Ubiquitination of lysine residues in the C-terminal extension of UBE2S likely diminishes dimerization (Figure 37).
Finally, *in vitro* activity assays with dimeric UBE2S indicate that dimerization confers auto-inhibition. This is consistent with the observation that dimerization and donor ubiquitin binding are mutually exclusive structurally (Figure 43). Thus, auto-inhibition of UBE2S by dimerization presents a third level for the regulation of the UBE2S activity, besides proteasomal degradation of UBE2S by (E3-enhanced) auto-ubiquitination and auto-inhibition by auto-ubiquitination of Lys^{+5} (Figure 44).

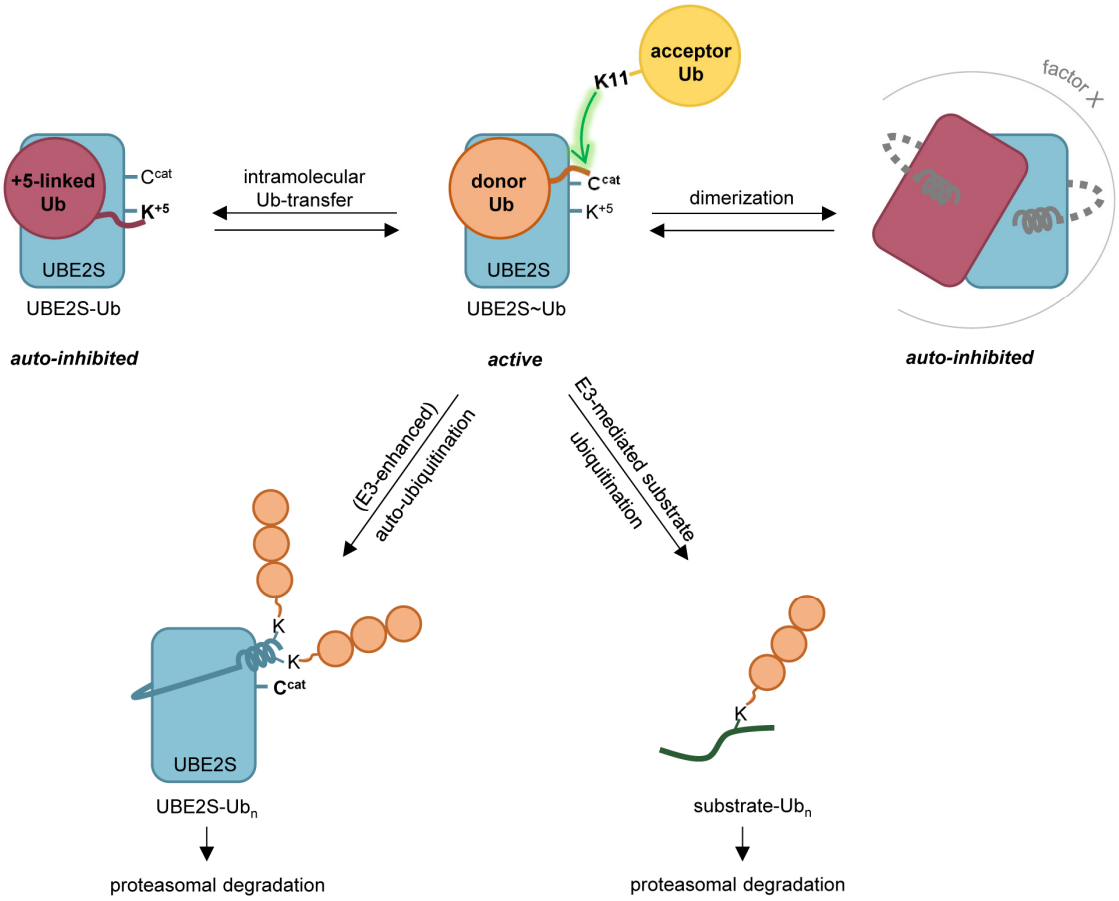

Figure 44: Graphical summary of UBE2S auto-inhibition. Model of the active state of UBE2S with donor ubiquitin (orange) thioester linked to Cys^{cat} in the closed orientation towards the E2 and the acceptor ubiquitin (yellow) presenting Lys11 for the nucleophilic attack of the thioester bond (as shown in Figure 24). The active UBE2S can then either perform E3-mediated substrate ubiquitination what leads to substrate degradation by the proteasome, or (E3-enhanced) auto-ubiquitination of the C-terminal extension that causes the proteasomal degradation of UBE2S [3]. For auto-regulation of UBE2S activity, UBE2S can perform an intramolecular ubiquitin transfer to ubiquitinate Lys^{+5} as elaborated in chapter 4.1 or UBE2S can dimerize via the UBC-domain what is enhanced by the C-helix of UBE2S. It remains to be studied, how the dimerization enhancement is driven by the C-helix (see Figure 38) as indicated by the grey dashed lines. Both, the Lys^{+5}-ubiquitinated as well as the dimeric form of UBE2S present auto-inhibited states of UEB2S.

5. Conclusion and future perspectives

Historically simplified as ‘ubiquitin carriers’, ubiquitin-conjugating enzymes are crucial regulators of ubiquitin-mediated cellular pathways. When interacting with a RING-type E3, they determine linkage specificity in substrate ubiquitination and thereby impact the fate of the substrate. The importance of E2s is underscored by their critical role in human disease.

One E2 associated with poor prognosis and poor response to cancer therapy if overexpressed is UBE2S, which makes it particularly interesting as a biomarker candidate and putative drug-target. UBE2S functions in DNA-repair by promoting non-homologous end-joining (NHEJ) [8] and transcriptional arrest at DNA double-strand breaks [7]. UBE2S has a well understood role in cell cycle regulation. Here, it interacts with the APC/C to elongate or branch ubiquitin chains on primed cell cycle regulators specifically through Lys11-linkages, labeling them for proteasomal degradation and promoting cell cycle progression towards mitotic exit [3–6,18,114,138,139,148]. Although the molecular mechanism of Lys11-linked ubiquitin chain formation is well-studied, the regulation of UBE2S remained to be uncovered. It was known that UBE2S is stabilized by phosphorylation of Thr152 by the RAC-alpha serine/threonine-protein kinase AKT1 in cancer cells [8]. Additionally, UBE2S can undergo auto-ubiquitination at its C-terminal extension [3,194]. This auto-ubiquitination was supposed to be enhanced by the APC/C during G1, when substrates are limiting, leading to the proteasomal degradation of UBE2S [3].

There is growing evidence that E2s are regulated by mechanisms other than auto-ubiquitination-induced turnover [61]. This raises the question of whether UBE2S also has such mechanisms that influence or fine-tune its activity and thereby the activity of the APC/C.

In this thesis, two new regulatory mechanisms of UBE2S are described. Both mechanisms have in common that they block the conserved donor ubiquitin binding site and thereby inhibit thioester formation and isopetide bond formation by the E2, as summarized in Figure 45. Firstly, UBE2S can be auto-inhibited by auto-ubiquitination of a specific lysine residue (Lys^{+5}) close to the catalytic cysteine, which may present a general regulatory mechanism, as Lys^{+5} is found in ~25% of the human E2s and was shown to also confer auto-inhibition in UBE2T upon ubiquitination [67]. Secondly, UBE2S dimerization can render the donor ubiquitin binding site inaccessible. This mechanism is presumably specific for UBE2S, as this particular dimer interface has not been seen in any other human E2 so far.

Together, this work lays the foundation for understanding the different layers of regulation of UBE2S and points out how this important enzyme may be used as a drug target for cancer therapy. Furthermore, this work establishes common principles in E2 regulation, as discussed below.

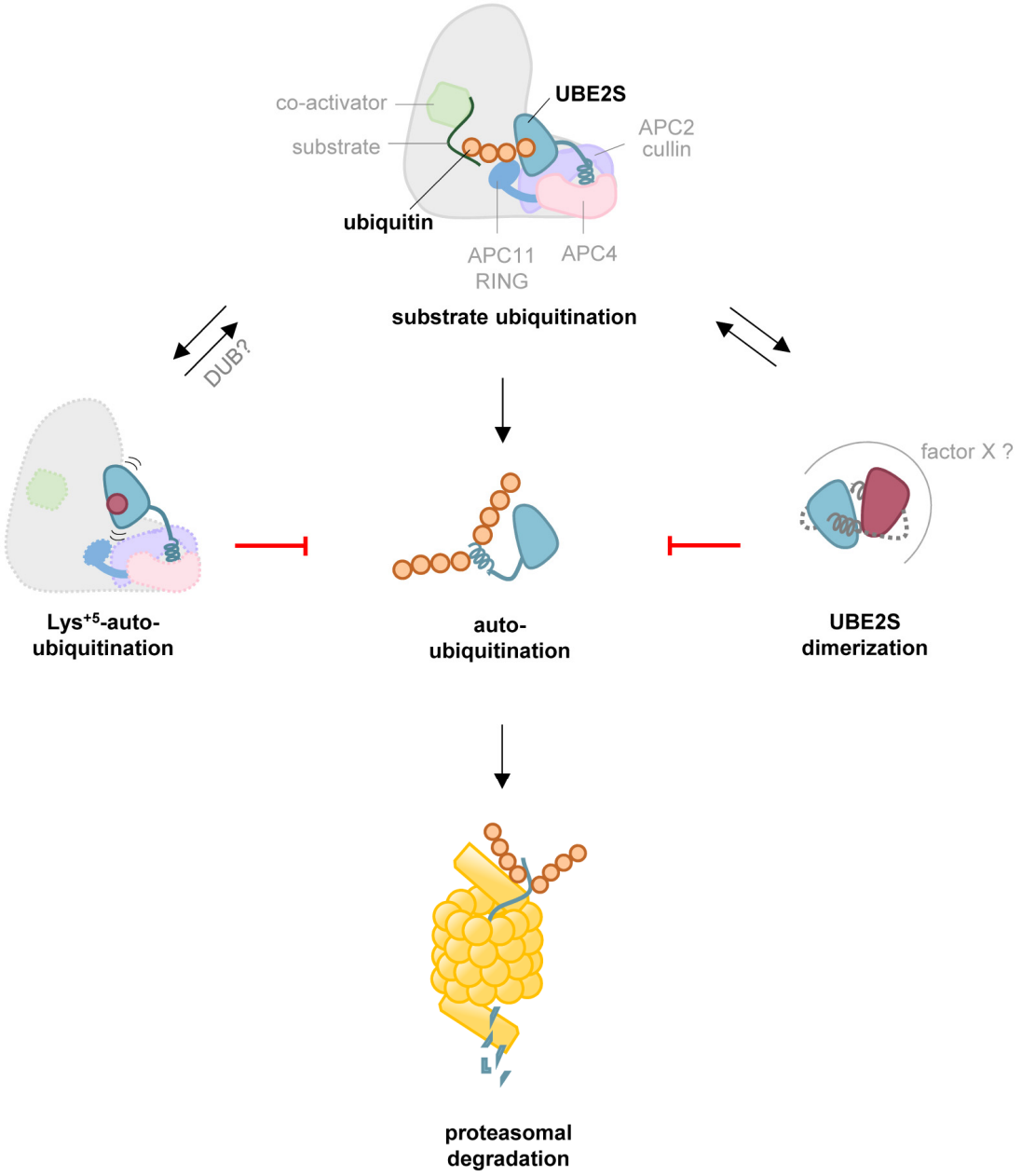

Figure 45: Model of UBE2S auto-inhibition in the context of the APC/C. In the context of the APC/C, UBE2S elongates ubiquitin chains on cell cycle regulators in a Lys11-linked manner to enable mitotic exit by marking the substrates for proteasomal degradation (top) The C-helix of UBE2S is bound in the groove between APC2 and APC4. UBE2S auto-ubiquitination at Lys^{+5} blocks donor binding and thereby auto-inhibits UBE2S activity (left). From a structural perspective, this could happen while the C-helix is attached to the APC/C whereas the UBC-domain is detached for receiving a new ubiquitin molecule from the E1. Auto-inhibition by dimerization (right) involves the C-helix and confers auto-inhibition by blocking donor-ubiquitin binding. UBE2S undergoes (E3-enhanced) auto-ubiquitination at its C-terminal extension, if the C-helix becomes accessible (middle). This induces the proteasomal degradation of UBE2S (bottom).

5.1 Auto-inhibition by auto-ubiquitination

Auto-ubiquitination is a common feature in ubiquitin-conjugating enzymes, linked to proteasomal degradation [3,6,69] or inhibition [67,202]. UBE2S can auto-ubiquitinate its C-terminal extension, which is thought to promote its proteasomal degradation [3]. The catalytic domain contains eight lysine residues, one of which is heavily ubiquitinated in cells [109]. This lysine, Lys^{+5}, is positioned five residues downstream of the catalytic cysteine and is also ubiquitinated *in vitro* (Table 15). Additional crystal structures of the catalytic domain of UBE2S determined here, in combination with MD simulations, unveiled structural flexibility of the active site region, resulting in two extreme conformations, the *Lys^{+5}-in* and the *Lys^{+5}-out* state. In the *Lys^{+5}-in* state, the primary amino group of Lys^{+5} is in close proximity to the catalytic cysteine, whereas it is removed from it in the *Lys^{+5}-out* state (Figure 14). I demonstrated that mono-ubiquitination at Lys^{+5} occurs by intramolecular transfer of the ubiquitin (Figure 17) and inhibits donor ubiquitin binding in the closed conformation (Figure 22) and thus activity (Figure 24). Auto-inhibition occurs at the first step, thioester-bond formation.

Interestingly, Lys^{+5} is found mutated to asparagine in lung adenocarcinoma [203,204], where UBE2S is overexpressed and is required to be active for enhancing the ubiquitination of the tumor suppressor p53 [121]. This may reflect selective pressure to upregulate UBE2S activity in certain cancer settings. This was further addressed in a collaboration with Alena Kucerova and Dr. Jörg Mansfeld (Technische Universität Dresden, Dresden/Germany). Together, we generated a polyclonal antibody against UBE2S that also enabled the detection of mono-ubiquitinated UBE2S. The fraction of mono-ubiquitinated cells amounts to 40% in prometaphase-arrested cells and is significantly diminished 120 min after release from prometaphase-arrest, as monitored by mass spec analyses in collaboration with Dr. Jyoti Choudhary's group (The Institute of Cancer Research, London/UK) [53]. At this timepoint, the levels of UBE2S decrease slightly as well, but this is not connected to Lys^{+5}-modification. Cycloheximide-chase experiments with UBE2S WT and a $K^{+5}R$ variant revealed that mono-ubiquitination of Lys^{+5} does not induce proteasomal degradation [53]. Taken together, these findings imply that Lys^{+5}-auto-ubiquitination presents a cell-cycle regulated auto-inhibition mechanism. This regulation is presumably required as the malleability of the active-site region and the ability to auto-ubiquitinate may otherwise constantly inactivate the enzyme. The cellular factors that influence Lys^{+5+}-auto-ubiquitination are not yet defined and provide an exciting area for further studies.

One possibility is that the E3 impacts E2 regulation. On the APC/C, the C-helix of UBE2S is bound to the APC2/4 groove and the catalytic domain is positioned at the edge of the

complex, interacting with APC2 [112]. As such, the C-helix cannot be auto-ubiquitinated, which may render UBE2S prone to Lys^{+5}-modification. Alternatively, release of the C-helix of UBE2S from the APC2/4 groove may allow for Lys^{+5}-ubiqutination, for example as triggered by the APC/C inhibitor EMI1, which displaces UBE2S by binding to the same groove [142,205]. Lys^{+5}-auto-ubiquitination may thus present a 'safe-lock' to protect UBE2S from auto-ubiquitination at the C-terminal extension and proteasomal degradation. On the other hand, interaction with the APC/C may promote the *Lys^{+5}-out* conformation, thus, keeping the enzyme active. Another possibility to influence the ubiquitination status of UBE2S involve deubiquitinating enzymes (DUBs), as they my cleave ubiquitin off Lys^{+5} or the C-terminal extension. This would ensure that the modification of Lys^{+5} with ubiquitin does not result in a dead-end but presents a dynamic cell cycle regulated mechanism. Finally, the auto-ubiquitination of UBE2S at Lys^{+5} may be influenced by other post-translational modifications, such as phosphorylation. It was already shown that the phosphorylation of Thr152 in UBE2S can enhance its stability in cancer cells [8]. It would be interesting to investigate whether this phosphorylation (or others) occurs also under non-pathogenic conditions and influences the conformation of the active-site region. Intriguingly, Thr152 is only ~6 Å away from a loop adjacent to the active-site region.

A lysine at position +5 is found in ~25% of the human ubiquitin-conjugating enzymes. Therefore, Lys^{+5}-ubiquitination might not only regulate the activity of UBE2S but also of other E2s that contain this lysine. Indeed, in UBE2T, the modification of Lys^{+5} with ubiquitin was found to inactivate the enzyme [67].

Taken together my studies suggest that the auto-ubiquitination of Lys^{+5} provides an auto-inhibition mechanism in UBE2S and presumably other Lys^{+5}-containing E2s. The inhibition is caused by interference with donor ubiquitin binding, thus preventing the E1-mediated first step of ubiquitin transfer to the E2. Therefore, the E2s have the ability to fine-tune their activities and influence substrate ubiquitination. Additionally, in the case of UBE2S I speculate that the Lys^{+5}-modification may crosstalk with the auto-ubiquitination of the C-terminal extension and thus regulate the proteasomal degradation of the enzyme. In this model, Lys^{+5}-modified UBE2S may provide an inactivated 'storage form', that could be reactivated by a DUB. To test this model and identify the putative DUB is the subject of our ongoing studies.

5.2 Auto-inhibition by dimerization

Different crystal structures of the catalytic domain of UBE2S suggest that the donor ubiquitin binding site on UBE2S may also mediate dimerization (Figure 15 and Figure 25). This idea was confirmed in solution by pull-down (Figure 26) and NMR experiments, revealing weak association of UBE2S. However, this association was not detectable by analytical gel filtration (Figure 30A) or analytical ultra-centrifugation (Figure 27). To overcome this challenge, a crosslinking assay was established, which disclosed that dimerization in solution occurs via the same interface as seen in the crystal structures (Figure 35). Crosslinker-induced dimerization was concentration-dependent (Figure 31) and enhanced by the C-helix of UBE2S (Figure 35 and Figure 37). It was further shown by NMR that a C-helix-derived peptide can interact with the active site of UBE2S, suggesting a possible mechanism for this effect. However, clearly, structural studies of the full-length protein are needed to uncover the position of the C-terminal extension of UBE2S and test the different models of dimerization (Figure 38). Since 66 residues of the C-terminal extension are unstructured, crystallizing the full-length protein is challenging. Crystals of full-length UBE2S grew after a minimum of six month, but no density for the bulk of the C-terminal extension could be detected. Only three additional residues after the catalytic domain could be modeled (data not shown). So it remains unclear whether the C-terminal extension has been cleaved in this crystals or was disordered. Further structural analyses of UBE2S may require binding partners to stabilize the extension and/or the entire APC/C.

When interacting with the APC/C, the C-helix is either bound to the coactivator for recruitment [3,131,146] or buried in the APC2/4 groove [112] and thus, cannot promote dimerization at the same time. To enhance dimerization, the C-helix ought to be displaced from the APC/C, for example as mediated the APC/C inhibitor EMI1. EMI1 has a C-terminal region that is highly similar to the one of UBE2S [142] and dislodges UBE2S from the APC2/4 groove.

My activity assays with the cross-linked dimer showed that dimerization inhibits UBE2S activity (Figure 43). However, dimerization is highly transient *in vitro* and the effects of mutating the dimer interface do not manifest themselves in this context. I detected mutations that interfere with crosslinking but not or only weakly with donor ubiquitin binding to UBE2S (Figure 39 and Figure 40) and found that H111A shows a similar activity in di-ubiquitin formation and auto-ubiquitination as the wild-type. L114E, however, is slightly inhibitory, possibly since it is located at the edge of the donor ubiquitin binding site, which might cause a reduction in the affinity of donor ubiquitin binding (Figure 40). Unexpectedly, the activity of UBE2S L107A was strongly reduced in *in vitro*

activity assays, although binding of ubiquitin to the donor binding site of UBE2S in *trans* seems not to be diminished (Figure 40). Together these results highlight that UBE2S activity depends on several interconnected factors and point out the need to test dimerization in the context of the cell.

We thus used proximity-ligation amplification, together with Alena Kucerova and Dr. Jörg Mansfeld (Techische Universität Dresden, Dresden/Germany). These experiments demonstrated that HA- and FLAG-tagged UBE2S co-localize within the same efficiency as UBE2S with ubiquitin. This argues strongly for the self-association of UBE2S in the cell. Intriguingly, this self-association depends on the dimeric interface: HA- and FLAG-tagged point mutations in UBE2S that interfere with dimerization *in vitro*, also disrupt co-localization in the cell [175]. We speculated that UBE2S dimerization in the cell may inhibit C-helix auto-ubiquitination. This was based on the finding that dimerization requires the C-helix. Based on this model, mutations in the dimer interface should decrease the half-life of UBE2S in the cell. Indeed, UBE2S L107A, H111A and L114E were found to have reduced stability compared to the WT, while the effect was strongest for UBE2S H111A [175]. This is in good agreement with the *in vitro* data because UBE2S L107A and L114E showed an impairment in auto-ubiquitination. Additionally, it could be demonstrated that UBE2S H111A is functional in the cell and its expression rescues the delay in mitotic exit caused by dimethylenastron-induced SAC arrest in prometaphase upon UBE2S-depletion. We speculate that dimerization could provide a pool of 'ready-to-use' UBE2S in an inactive storage form that could be activated when APC/C activity rises. This would provide an elegant way to allow for energy saving by hindering UBE2S auto-ubiquitination and thereby its proteasomal degradation.

UBE2S was found to control mitotic slippage [5], a process by which mitotically arrested cells abnormally exit mitosis due to the degradation of cyclin B1, leading to aneuploidy or cell death. Whereas the expression of UBE2S WT (in an UBE2S$^{-/-}$ background) reduced the median duration of taxol-induced arrested cells by ~50%, UBE2S H111A expression only reduced the median duration by ~20%, indicating that this variant does not boost mitotic slippage.

Thus, we speculate that UBE2S H111A is able to release cells from SAC but does not promote mitotic slippage to the same extent as the wild-type as the latter phenomenon is exquisitely sensitive to the concentration of UBE2S. In consequence, the dimeric state could be particularly important in cancer cells, where high levels of UBE2S are needed to promote mitotic slippage after drug-induced mitotic arrest (see 1.3). This would in turn suggest that interfering with the dimerization of UBE2S might provide a new therapeutic window as discussed in chapter 5.4.

Taken together, dimerization provides a second regulatory mechanism in UBE2S – cellular factors initializing dimerization remain to be uncovered.

5.3 What we can learn from UBE2S

E2s share a conserved catalytic domain sufficient for catalysis of the ubiquitin transfer. However, different E2s encode different linkage types, interact with different ubiquitin ligases and perform different types of reactions (Figure 5). The structural basis of this specialization is mostly unknown but thought to be influenced by their diverse N- and C-terminal extensions.

My case studies on UBE2S illustrated several principles that apply broadly to ubiquitin-conjugating enzymes:

1) I showed that the donor-ubiquitin binding site is a conserved regulatory linchpin that controls the first step in catalysis and can be modulated by structurally and functionally diverse mechanisms.

2) I exemplified that the extensions outside of the catalytic domain can serve important regulatory functions. This underscores the need to characterize these extensions structurally, ideally in the context of molecular complexes of E2s.

3) I showed that low-affinities are critical in catalysis and regulation of E2s, in line with previous analyses [4,82,83,113].

Overcoming the challenge of studying such transient, low-affinity interactions will be an important aim for future studies, exploiting chemical biology and other crosslinking tools to reconstitute specific states or complexes and resolve them structurally by cryo-EM. The body of data on the APC/C provide an impressive example of the exceptional level of detail such analyses can reveal.

5.4 UBE2S as a drug target in cancer therapy

Considering the roles of ubiquitin-conjugating enzymes in cancer (see 1.2.2), E2s may serve as potential drug targets. In contrast to the clinically used Bortezomib and Carfilzomib, which are potent proteasome inhibitors that shut down protein degradation

globally, targeting an E2 may provide more specificity to interfere with selected pathways.

In 2011, Ceccarelli and colleagues uncovered a specific UBE2R1 (also called DC34) inhibitor, CC0651. This compound interferes with substrate ubiquitination while promoting UBE2R1 auto-ubiquitination [206]. However, despite a strong interest in developing E2 inhibitors, the number of candidates is limited. A reason for that could be the exposed active site region and the lack of pockets around this site. Therefore, uncovering new regulatory mechanisms in E2s and the roles of the N- or C-terminal extensions might open up new avenues towards understanding E2s structurally and identify targetable vulnerabilities.

An E2 highly expressed in many cancer types is UBE2S. Its overexpression is also connected with unfavorable patient survival [10,118–121], tumor growth and invasion [10,116,118,120,121,123] and poor response to cancer therapy [8,10,118,124]. This is explained by the critical cellular roles of UBE2S in the cell cycle, DNA repair and other key pathways, whose dysregulation lead to tumorigenesis [3–5,7,8,116–121]. In consequence, knockdown or depletion of UBE2S in cancer cells was found to increase the responses to cancer treatments and diminished tumor growth and invasion in most cases [10,118,121,123]. In contrast, UBE2S depletion does not show a phenotype during unperturbed mitosis [5]. This makes UBE2S a promising target for cancer therapy and it would be of great interest to dissect mechanisms to manipulate its activity.

In this thesis, two regulatory mechanism of UBE2S were uncovered that rely on a blockage of donor ubiquitin binding, either by auto-ubiquitination or dimerization. On the one hand, inhibition of UBE2S by these mechanisms may be beneficial for cancer therapy. On the other hand, this may enrich a pool of inactive enzymes, poised to be reactivated, which may be counter-productive. A second challenge might be the conservation of the donor ubiquitin binding site in E2s and the fact that this binding site is hydrophobic and does not contain obvious pockets. Whether the donor binding site can be accessed by small molecules thus requires further investigation.

To overcome the problem of specificity, it may be conceivable to target the interactions of the C-terminal extension. Interfering with the ability of the extension to bind the APC/C may inhibit its role in promoting Lys11-chain formation. Notably, however, Lys11-linked ubiquitin chains can be compensated for by multi-mono-ubiquitination and the formation of short ubiquitin chains by UBE2C and UBE2D in particular settings. Whether modifying the C-terminal extension would also interfere with the ability of UBE2S to interact with RNF8 and thereby blocks its function in transcription arrest at double strand breaks

remains to be elucidated, just as the effect on modifying the tumor suppressors pVHL and p53.

However, manipulation of the C-terminal extension bears another complication: Due to the enrichment in lysines, the C-terminal extension provides auto-ubiquitination sites, which are thought to mediate UBE2S turnover [3]. A putative UBE2S inhibitor should ideally not interfere with this auto-ubiquitination in order to avoid enriching UBE2S in the cell and thus, promote tumorigenesis.

However, dissecting the precise impact of each of the regulatory and conformational states identified here will help provide insights into which function or structural feature may provide useful vulnerabilities.

5.5 Outlook and future directions

UBE2S is an important enzyme, functioning in cell cycle regulation [3–6] and DNA repair [7,8], that is found overexpressed in many cancer types and associated with poor prognosis and diminished response to therapeutics [8–10]. The discovery of UBE2S self-regulation opens up new directions for a detailed understanding of the cellular role of UBE2S in health and disease and possible anti-cancer strategies. For example, it would be important to study the impact of Lys^{+5}-auto-ubiquitination and dimerization in DNA repair. The structural basis of the interactions of UBE2S with KU70 in NHEJ, and of the stabilization of UBE2S by Thr152 phosphorylation require further investigation. It will also be insightful to broadly explore whether phosphorylation has an influence on the conformation and activity status of UBE2S in the DNA repair context. It would be interesting to test whether dimerization and/or Lys^{+5}-modification regulate UBE2S also in DNA repair. Such studies may be able to reveal the missing link between Lys^{+5}-ubiquitination and dimerization. Maybe phosphorylation at Thr152 provides this missing link. Therefore, it should be studied whether phosphorylation of Thr152 occurs also under steady state conditions, when the PI3K/AKT/mTOR signaling pathway is not constantly activated.

Structural analyses of the interaction of RNF8 with UBE2C and UBE2S could uncover whether this interplay to modify histones with Lys11-linked ubiquitin chains works in a similar way as in the context of the APC/C. This could allow for general conclusions about UBE2S-E3 interactions. Does UBE2S generally interact in a non-canonical way with the RING domain or is this APC/C-specific? Is the C-terminal extension needed for this interaction? If RNF8 dimerizes, as seen in several crystal structures [154,207,208], does this allow for UBE2C and UBE2S to bind simultaneously?

Lastly, it is reported that the modification of histone H2A/H2AX [7] and ß-catenin [122] with Lys11-linked ubiquitin chains by UBE2S does not lead to proteasomal degradation and instead stabilizes the substrate. Thus, investigating the role of Lys11-linked ubiquitin chains in these contexts might provide insights into new functions of this chain type beyond degradation, adding an additional facet to the complex kaleidoscope of ubiquitin signaling.

6. References

[1] R. Virchow, Cellular-Pathologie, Archiv für pathologische Anatomie und Physiologie und für klinische Medicin 8 (1855) 3–39. https://doi.org/10.1007/BF01935312.

[2] D. Komander, M. Rape, The Ubiquitin Code, Annu. Rev. Biochem. 81 (2012) 203–229. https://doi.org/10.1146/annurev-biochem-060310-170328.

[3] A. Williamson, K.E. Wickliffe, B.G. Mellone, L. Song, G.H. Karpen, M. Rape, Identification of a physiological E2 module for the human anaphase-promoting complex, Proc. Natl. Acad. Sci. U. S. A. 106 (2009) 18213–18218. https://doi.org/10.1073/pnas.0907887106.

[4] K.E. Wickliffe, S. Lorenz, D.E. Wemmer, J. Kuriyan, M. Rape, The Mechanism of Linkage-Specific Ubiquitin Chain Elongation by a Single-Subunit E2, Cell 144 (2011) 769–781. https://doi.org/10.1016/j.cell.2011.01.035.

[5] M.J. Garnett, J. Mansfeld, C. Godwin, T. Matsusaka, J. Wu, P. Russell, J. Pines, A.R. Venkitaraman, UBE2S elongates ubiquitin chains on APC/C substrates to promote mitotic exit, Nat. Cell Biol. 11 (2009) 1363–1369. https://doi.org/10.1038/ncb1983.

[6] M. Rape, M.W. Kirschner, Autonomous regulation of the anaphase-promoting complex couples mitosis to S-phase entry, Nature 432 (2004) 588–595. https://doi.org/10.1038/nature03023.

[7] A. Paul, B. Wang, RNF8- and Ube2S-Dependent Ubiquitin Lysine 11-Linkage Modification in Response to DNA Damage, Molecular Cell 66 (2017) 458-472.e5. https://doi.org/10.1016/j.molcel.2017.04.013.

[8] L. Hu, X. Li, Q. Liu, J. Xu, H. Ge, Z. Wang, H. Wang, C. Shi, X. Xu, J. Huang, Z. Lin, R.O. Pieper, C. Weng, UBE2S, a novel substrate of Akt1, associates with Ku70 and regulates DNA repair and glioblastoma multiforme resistance to chemotherapy, Oncogene 36 (2017) 1145–1156. https://doi.org/10.1038/onc.2016.281.

[9] S.M. Hosseini, I. Okoye, M.G. Chaleshtari, B. Hazhirkarzar, J. Mohamadnejad, G. Azizi, M. Hojjat-Farsangi, H. Mohammadi, S.S. Shotorbani, F. Jadidi-Niaragh, E2 ubiquitin-conjugating enzymes in cancer: Implications for immunotherapeutic interventions, Clin. Chim. Acta 498 (2019) 126–134. https://doi.org/10.1016/j.cca.2019.08.020.

[10] M.-F. Chen, K.-D. Lee, M.-S. Lu, C.-C. Chen, M.-J. Hsieh, Y.-H. Liu, P.-Y. Lin, W.-C. Chen, The predictive role of E2-EPF ubiquitin carrier protein in esophageal squamous cell carcinoma, J. Mol. Med. 87 (2009) 307–320. https://doi.org/10.1007/s00109-008-0430-3.

[11] A. Hershko, A. Ciechanover, The ubiquitin system for protein degradation, Annu. Rev. Biochem. 61 (1992) 761–807. https://doi.org/10.1146/annurev.bi.61.070192.003553.

[12] A. Hershko, A. Ciechanover, The ubiquitin system, Annu. Rev. Biochem. 67 (1998) 425–479. https://doi.org/10.1146/annurev.biochem.67.1.425.

[13] C.M. Pickart, M.J. Eddins, Ubiquitin: structures, functions, mechanisms, Biochim. Biophys. Acta 1695 (2004) 55–72. https://doi.org/10.1016/j.bbamcr.2004.09.019.

[14] Y. Kulathu, D. Komander, Atypical ubiquitylation - the unexplored world of polyubiquitin beyond Lys48 and Lys63 linkages, Nat. Rev. Mol. Cell Biol. 13 (2012) 508–523. https://doi.org/10.1038/nrm3394.

[15] K. Robzyk, J. Recht, M.A. Osley, Rad6-dependent ubiquitination of histone H2B in yeast, Science 287 (2000) 501–504. https://doi.org/10.1126/science.287.5452.501.

[16] C. Hoege, B. Pfander, G.-L. Moldovan, G. Pyrowolakis, S. Jentsch, RAD6-dependent DNA repair is linked to modification of PCNA by ubiquitin and SUMO, Nature 419 (2002) 135–141. https://doi.org/10.1038/nature00991.

[17] V. Chau, J.W. Tobias, A. Bachmair, D. Marriott, D.J. Ecker, D.K. Gonda, A. Varshavsky, A multiubiquitin chain is confined to specific lysine in a targeted short-lived protein, Science 243 (1989) 1576–1583. https://doi.org/10.1126/science.2538923.

[18] H.-J. Meyer, M. Rape, Enhanced protein degradation by branched ubiquitin chains, Cell 157 (2014) 910–921. https://doi.org/10.1016/j.cell.2014.03.037.

[19] A. Bremm, D. Komander, Emerging roles for Lys11-linked polyubiquitin in cellular regulation, Trends in Biochemical Sciences 36 (2011) 355–363. https://doi.org/10.1016/j.tibs.2011.04.004.

[20] M. Gatti, S. Pinato, A. Maiolica, F. Rocchio, M.G. Prato, R. Aebersold, L. Penengo, RNF168 promotes noncanonical K27 ubiquitination to signal DNA damage, Cell Reports 10 (2015) 226–238. https://doi.org/10.1016/j.celrep.2014.12.021.

[21] Q. Wang, X. Liu, Y. Cui, Y. Tang, W. Chen, S. Li, H. Yu, Y. Pan, C. Wang, The E3 ubiquitin ligase AMFR and INSIG1 bridge the activation of TBK1 kinase by modifying the adaptor STING, Immunity 41 (2014) 919–933. https://doi.org/10.1016/j.immuni.2014.11.011.

[22] C. Fei, Z. Li, C. Li, Y. Chen, Z. Chen, X. He, L. Mao, X. Wang, R. Zeng, L. Li, Smurf1-mediated Lys29-linked nonproteolytic polyubiquitination of axin negatively regulates Wnt/β-catenin signaling, Mol. Cell. Biol. 33 (2013) 4095–4105. https://doi.org/10.1128/MCB.00418-13.

[23] D.V.F. Tauriello, M.M. Maurice, The various roles of ubiquitin in Wnt pathway regulation, Cell Cycle 9 (2010) 3700–3709. https://doi.org/10.4161/cc.9.18.13204.

[24] K. Haglund, I. Dikic, The role of ubiquitylation in receptor endocytosis and endosomal sorting, J. Cell Sci. 125 (2012) 265–275. https://doi.org/10.1242/jcs.091280.

[25] C. Wang, L. Deng, M. Hong, G.R. Akkaraju, J. Inoue, Z.J. Chen, TAK1 is a ubiquitin-dependent kinase of MKK and IKK, Nature 412 (2001) 346–351. https://doi.org/10.1038/35085597.

[26] M. Karin, Y. Ben-Neriah, Phosphorylation meets ubiquitination: the control of NF-kappaB activity, Annu. Rev. Immunol. 18 (2000) 621–663. https://doi.org/10.1146/annurev.immunol.18.1.621.

[27] S. Vijay-Kumar, C.E. Bugg, W.J. Cook, Structure of ubiquitin refined at 1.8 A resolution, J. Mol. Biol. 194 (1987) 531–544. https://doi.org/10.1016/0022-2836(87)90679-6.

[28] A. Ordureau, S.A. Sarraf, D.M. Duda, J.-M. Heo, M.P. Jedrychowski, V.O. Sviderskiy, J.L. Olszewski, J.T. Koerber, T. Xie, S.A. Beausoleil, J.A. Wells, S.P. Gygi, B.A. Schulman, J.W. Harper, Quantitative proteomics reveal a feedforward mechanism for mitochondrial PARKIN translocation and ubiquitin chain synthesis, Molecular Cell 56 (2014) 360–375. https://doi.org/10.1016/j.molcel.2014.09.007.

[29] T. Wauer, K.N. Swatek, J.L. Wagstaff, C. Gladkova, J.N. Pruneda, M.A. Michel, M. Gersch, C.M. Johnson, S.M.V. Freund, D. Komander, Ubiquitin Ser65 phosphorylation affects ubiquitin structure, chain assembly and hydrolysis, EMBO J. 34 (2015) 307–325. https://doi.org/10.15252/embj.201489847.

[30] A. Gärtner, K. Wagner, S. Hölper, K. Kunz, M.S. Rodriguez, S. Müller, Acetylation of SUMO2 at lysine 11 favors the formation of non-canonical SUMO chains, EMBO Rep. 19 (2018). https://doi.org/10.15252/embr.201846117.

[31] J. Qiu, M.J. Sheedlo, K. Yu, Y. Tan, E.S. Nakayasu, C. Das, X. Liu, Z.-Q. Luo, Ubiquitination independent of E1 and E2 enzymes by bacterial effectors, Nature 533 (2016) 120–124. https://doi.org/10.1038/nature17657.

[32] S. Bhogaraju, S. Kalayil, Y. Liu, F. Bonn, T. Colby, I. Matic, I. Dikic, Phosphoribosylation of Ubiquitin Promotes Serine Ubiquitination and Impairs Conventional Ubiquitination, Cell 167 (2016) 1636-1649.e13. https://doi.org/10.1016/j.cell.2016.11.019.

[33] M.J. Clague, S. Urbé, D. Komander, Breaking the chains: deubiquitylating enzyme specificity begets function, Nat Rev Mol Cell Biol 20 (2019) 338–352. https://doi.org/10.1038/s41580-019-0099-1.

[34] X. Huang, V.M. Dixit, Drugging the undruggables: Exploring the ubiquitin system for drug development, Cell Res (2016). https://doi.org/10.1038/cr.2016.31.

[35] D. Chen, M. Gehringer, S. Lorenz, Developing Small-Molecule Inhibitors of HECT-Type Ubiquitin Ligases for Therapeutic Applications: Challenges and Opportunities, Chembiochem 19 (2018) 2123–2135. https://doi.org/10.1002/cbic.201800321.

[36] K.M. Kortuem, A.K. Stewart, Carfilzomib, Blood 121 (2013) 893–897. https://doi.org/10.1182/blood-2012-10-459883.

[37] S.D. Demo, C.J. Kirk, M.A. Aujay, T.J. Buchholz, M. Dajee, M.N. Ho, J. Jiang, G.J. Laidig, E.R. Lewis, F. Parlati, K.D. Shenk, M.S. Smyth, C.M. Sun, M.K. Vallone, T.M. Woo, C.J. Molineaux, M.K. Bennett, Antitumor activity of PR-171, a novel irreversible inhibitor of the proteasome, Cancer Res. 67 (2007) 6383–6391. https://doi.org/10.1158/0008-5472.CAN-06-4086.

[38] L. Meng, R. Mohan, B.H. Kwok, M. Elofsson, N. Sin, C.M. Crews, Epoxomicin, a potent and selective proteasome inhibitor, exhibits in vivo antiinflammatory activity, Proceedings of the National Academy of Sciences 96 (1999) 10403–10408. https://doi.org/10.1073/pnas.96.18.10403.

[39] J. Adams, M. Kauffman, Development of the proteasome inhibitor Velcade (Bortezomib), Cancer Invest. 22 (2004) 304–311. https://doi.org/10.1081/cnv-120030218.

[40] J. Kronke, N.D. Udeshi, A. Narla, P. Grauman, S.N. Hurst, M. McConkey, T. Svinkina, D. Heckl, E. Comer, X. Li, C. Ciarlo, E. Hartman, N. Munshi, M. Schenone, S.L. Schreiber, S.A. Carr, B.L. Ebert, Lenalidomide causes selective degradation of IKZF1 and IKZF3 in multiple myeloma cells, Science 343 (2014) 301–305. https://doi.org/10.1126/science.1244851.

[41] G. Lu, R.E. Middleton, H. Sun, M. Naniong, C.J. Ott, C.S. Mitsiades, K.-K. Wong, J.E. Bradner, W.G. Kaelin JR, The myeloma drug lenalidomide promotes the cereblon-dependent destruction of Ikaros proteins, Science 343 (2014) 305–309. https://doi.org/10.1126/science.1244917.

[42] E.S. Fischer, K. Bohm, J.R. Lydeard, H. Yang, M.B. Stadler, S. Cavadini, J. Nagel, F. Serluca, V. Acker, G.M. Lingaraju, R.B. Tichkule, M. Schebesta, W.C. Forrester, M. Schirle, U. Hassiepen, J. Ottl, M. Hild, R.E.J. Beckwith, J.W. Harper, J.L. Jenkins, N.H. Thoma, Structure of the DDB1-CRBN E3 ubiquitin ligase in complex with thalidomide, Nature 512 (2014) 49–53. https://doi.org/10.1038/nature13527.

[43] I. Churcher, Protac-Induced Protein Degradation in Drug Discovery: Breaking the Rules or Just Making New Ones?, J. Med. Chem. 61 (2018) 444–452. https://doi.org/10.1021/acs.jmedchem.7b01272.

[44] K.G. Coleman, C.M. Crews, Proteolysis-Targeting Chimeras: Harnessing the Ubiquitin-Proteasome System to Induce Degradation of Specific Target Proteins, Annu. Rev. Cancer Biol. 2 (2018) 41–58. https://doi.org/10.1146/annurev-cancerbio-030617-050430.

[45] K.M. Sakamoto, K.B. Kim, A. Kumagai, F. Mercurio, C.M. Crews, R.J. Deshaies, Protacs: chimeric molecules that target proteins to the Skp1-Cullin-F box complex for ubiquitination and degradation, Proceedings of the National Academy of Sciences 98 (2001) 8554–8559. https://doi.org/10.1073/pnas.141230798.

[46] M. Pettersson, C.M. Crews, PROteolysis TArgeting Chimeras (PROTACs) — Past, present and future, Drug Discovery Today: Technologies 31 (2019) 15–27. https://doi.org/10.1016/j.ddtec.2019.01.002.

[47] D. Hormaechea-Agulla, Y. Kim, M.S. Song, S.J. Song, New Insights into the Role of E2s in the Pathogenesis of Diseases: Lessons Learned from UBE2O, Mol. Cells 41 (2018) 168–178. https://doi.org/10.14348/molcells.2018.0008.

[48] D.T. Huang, A. Paydar, M. Zhuang, M.B. Waddell, J.M. Holton, B.A. Schulman, Structural basis for recruitment of Ubc12 by an E2 binding domain in NEDD8's E1, Molecular Cell 17 (2005) 341–350. https://doi.org/10.1016/j.molcel.2004.12.020.

[49] Z.M. Eletr, D.T. Huang, D.M. Duda, B.A. Schulman, B. Kuhlman, E2 conjugating enzymes must disengage from their E1 enzymes before E3-dependent ubiquitin and ubiquitin-like transfer, Nat. Struct. Mol. Biol. 12 (2005) 933–934. https://doi.org/10.1038/nsmb984.

[50] M. Gundogdu, H. Walden, Structural basis of generic versus specific E2–RING E3 interactions in protein ubiquitination, Protein Science 28 (2019) 1758–1770. https://doi.org/10.1002/pro.3690.

[51] A. Plechanovová, E.G. Jaffray, M.H. Tatham, J.H. Naismith, R.T. Hay, Structure of a RING E3 ligase and ubiquitin-loaded E2 primed for catalysis, Nature 489 (2012) 115–120. https://doi.org/10.1038/nature11376.

[52] S. Lorenz, M. Bhattacharyya, C. Feiler, M. Rape, J. Kuriyan, A. Wlodawer, Crystal Structure of a Ube2S-Ubiquitin Conjugate, PLoS ONE 11 (2016) e0147550. https://doi.org/10.1371/journal.pone.0147550.

[53] A.K.L. Liess, A. Kucerova, K. Schweimer, L. Yu, T.I. Roumeliotis, M. Diebold, O. Dybkov, C. Sotriffer, H. Urlaub, J.S. Choudhary, J. Mansfeld, S. Lorenz, Autoinhibition Mechanism of the Ubiquitin-Conjugating Enzyme UBE2S by Autoubiquitination, Structure 27 (2019) 1195-1210.e7. https://doi.org/10.1016/j.str.2019.05.008.

[54] S.K. Olsen, C.D. Lima, Structure of a ubiquitin E1-E2 complex: insights to E1-E2 thioester transfer, Molecular Cell 49 (2013) 884–896. https://doi.org/10.1016/j.molcel.2013.01.013.

[55] H.B. Kamadurai, J. Souphron, D.C. Scott, D.M. Duda, D.J. Miller, D. Stringer, R.C. Piper, B.A. Schulman, Insights into ubiquitin transfer cascades from a structure of a UbcH5B approximately ubiquitin-HECT(NEDD4L) complex, Molecular Cell 36 (2009) 1095–1102. https://doi.org/10.1016/j.molcel.2009.11.010.

[56] J.N. Pruneda, P.J. Littlefield, S.E. Soss, K.A. Nordquist, W.J. Chazin, P.S. Brzovic, R.E. Klevit, Structure of an E3:E2~Ub complex reveals an allosteric mechanism shared among RING/U-box ligases, Molecular Cell 47 (2012) 933–942. https://doi.org/10.1016/j.molcel.2012.07.001.

[57] B.C. Lechtenberg, A. Rajput, R. Sanishvili, M.K. Dobaczewska, C.F. Ware, P.D. Mace, S.J. Riedl, Structure of a HOIP/E2~ubiquitin complex reveals RBR E3 ligase mechanism and regulation, Nature 529 (2016) 546–550. https://doi.org/10.1038/nature16511.

[58] K.K. Dove, B. Stieglitz, E.D. Duncan, K. Rittinger, R.E. Klevit, Molecular insights into RBR E3 ligase ubiquitin transfer mechanisms, EMBO Rep. 17 (2016) 1221–1235. https://doi.org/10.15252/embr.201642641.

[59] X. Wang, R.A. Herr, W.-J. Chua, L. Lybarger, Wiertz, Emmanuel J H J, T.H. Hansen, Ubiquitination of serine, threonine, or lysine residues on the cytoplasmic tail can induce ERAD of MHC-I by viral E3 ligase mK3, J. Cell Biol. 177 (2007) 613–624. https://doi.org/10.1083/jcb.200611063.

[60] X. Wang, R.A. Herr, M. Rabelink, R.C. Hoeben, Wiertz, Emmanuel J H J, T.H. Hansen, Ube2j2 ubiquitinates hydroxylated amino acids on ER-associated degradation substrates, J. Cell Biol. 187 (2009) 655–668. https://doi.org/10.1083/jcb.200908036.

[61] M.D. Stewart, T. Ritterhoff, R.E. Klevit, P.S. Brzovic, E2 enzymes: More than just middle men, Cell Res (2016). https://doi.org/10.1038/cr.2016.35.

[62] P. Coccetti, F. Tripodi, G. Tedeschi, S. Nonnis, O. Marin, S. Fantinato, C. Cirulli, M. Vanoni, L. Alberghina, The CK2 phosphorylation of catalytic domain of Cdc34 modulates its activity at the G1 to S transition in Saccharomyces cerevisiae, Cell Cycle 7 (2008) 1391–1401. https://doi.org/10.4161/cc.7.10.5825.

[63] E. Papaleo, V. Ranzani, F. Tripodi, A. Vitriolo, C. Cirulli, P. Fantucci, L. Alberghina, M. Vanoni, L. de Gioia, P. Coccetti, An acidic loop and cognate phosphorylation sites define a molecular switch that modulates ubiquitin charging activity in Cdc34-like enzymes, PLoS Comput. Biol. 7 (2011) e1002056. https://doi.org/10.1371/journal.pcbi.1002056.

[64] E. Shibata, T. Abbas, X. Huang, J.A. Wohlschlegel, A. Dutta, Selective ubiquitylation of p21 and Cdt1 by UBCH8 and UBE2G ubiquitin-conjugating enzymes via the CRL4Cdt2 ubiquitin ligase complex, Mol. Cell. Biol. 31 (2011) 3136–3145. https://doi.org/10.1128/MCB.05496-11.

[65] B. Sarcevic, A. Mawson, R.T. Baker, R.L. Sutherland, Regulation of the ubiquitin-conjugating enzyme hHR6A by CDK-mediated phosphorylation, EMBO J. 21 (2002) 2009–2018. https://doi.org/10.1093/emboj/21.8.2009.

[66] A. Wood, J. Schneider, J. Dover, M. Johnston, A. Shilatifard, The Bur1/Bur2 complex is required for histone H2B monoubiquitination by Rad6/Bre1 and histone methylation by COMPASS, Molecular Cell 20 (2005) 589–599. https://doi.org/10.1016/j.molcel.2005.09.010.

[67] Y.J. Machida, Y. Machida, Y. Chen, A.M. Gurtan, G.M. Kupfer, A.D. D'Andrea, A. Dutta, UBE2T is the E2 in the Fanconi anemia pathway and undergoes negative autoregulation, Molecular Cell 23 (2006) 589–596. https://doi.org/10.1016/j.molcel.2006.06.024.

[68] F.-R. Schumacher, G. Wilson, C.L. Day, The N-terminal extension of UBE2E ubiquitin-conjugating enzymes limits chain assembly, J. Mol. Biol. 425 (2013) 4099–4111. https://doi.org/10.1016/j.jmb.2013.06.039.

[69] T. Ravid, M. Hochstrasser, Autoregulation of an E2 enzyme by ubiquitin-chain assembly on its catalytic residue, Nat. Cell Biol. 9 (2007) 422–427. https://doi.org/10.1038/ncb1558.

[70] A. Williamson, S. Banerjee, X. Zhu, I. Philipp, A.T. Iavarone, M. Rape, Regulation of ubiquitin chain initiation to control the timing of substrate degradation, Molecular Cell 42 (2011) 744–757. https://doi.org/10.1016/j.molcel.2011.04.022.

[71] A. Pichler, P. Knipscheer, E. Oberhofer, W.J. van Dijk, R. Korner, J.V. Olsen, S. Jentsch, F. Melchior, T.K. Sixma, SUMO modification of the ubiquitin-conjugating enzyme E2-25K, Nat. Struct. Mol. Biol. 12 (2005) 264–269. https://doi.org/10.1038/nsmb903.

[72] P. Knipscheer, A. Flotho, H. Klug, J.V. Olsen, W.J. van Dijk, A. Fish, E.S. Johnson, M. Mann, T.K. Sixma, A. Pichler, Ubc9 sumoylation regulates SUMO target discrimination, Molecular Cell 31 (2008) 371–382. https://doi.org/10.1016/j.molcel.2008.05.022.

[73] C.-W. Ho, H.-T. Chen, J. Hwang, UBC9 autosumoylation negatively regulates sumoylation of septins in Saccharomyces cerevisiae, J. Biol. Chem. 286 (2011) 21826–21834. https://doi.org/10.1074/jbc.M111.234914.

[74] P.S. Brzovic, A. Lissounov, D.E. Christensen, D.W. Hoyt, R.E. Klevit, A UbcH5/ubiquitin noncovalent complex is required for processive BRCA1-directed ubiquitination, Molecular Cell 21 (2006) 873–880. https://doi.org/10.1016/j.molcel.2006.02.008.

[75] R.S. Ranaweera, X. Yang, Auto-ubiquitination of Mdm2 enhances its substrate ubiquitin ligase activity, J. Biol. Chem. 288 (2013) 18939–18946. https://doi.org/10.1074/jbc.M113.454470.

[76] R.C. Page, J.N. Pruneda, J. Amick, R.E. Klevit, S. Misra, Structural insights into the conformation and oligomerization of E2~ubiquitin conjugates, Biochemistry 51 (2012) 4175–4187. https://doi.org/10.1021/bi300058m.

[77] L. Buetow, M. Gabrielsen, N.G. Anthony, H. Dou, A. Patel, H. Aitkenhead, G.J. Sibbet, B.O. Smith, D.T. Huang, Activation of a primed RING E3-E2-ubiquitin complex by non-covalent ubiquitin, Molecular Cell 58 (2015) 297–310. https://doi.org/10.1016/j.molcel.2015.02.017.

[78] R.G. Hibbert, A. Huang, R. Boelens, T.K. Sixma, E3 ligase Rad18 promotes monoubiquitination rather than ubiquitin chain formation by E2 enzyme Rad6, Proc. Natl. Acad. Sci. U. S. A. 108 (2011) 5590–5595. https://doi.org/10.1073/pnas.1017516108.

[79] L. Nguyen, K.S. Plafker, A. Starnes, M. Cook, R.E. Klevit, S.M. Plafker, The ubiquitin-conjugating enzyme, UbcM2, is restricted to monoubiquitylation by a two-fold mechanism that involves backside residues of E2 and Lys48 of ubiquitin, Biochemistry 53 (2014) 4004–4014. https://doi.org/10.1021/bi500072v.

[80] X. Varelas, C. Ptak, M.J. Ellison, Cdc34 self-association is facilitated by ubiquitin thiolester formation and is required for its catalytic activity, Mol. Cell. Biol. 23 (2003) 5388–5400.

[81] W. Li, D. Tu, A.T. Brunger, Y. Ye, A ubiquitin ligase transfers preformed polyubiquitin chains from a conjugating enzyme to a substrate, Nature 446 (2007) 333. https://doi.org/10.1038/nature05542.

[82] W. Li, D. Tu, L. Li, T. Wollert, R. Ghirlando, A.T. Brunger, Y. Ye, Mechanistic insights into active site-associated polyubiquitination by the ubiquitin-conjugating enzyme Ube2g2, Proc. Natl. Acad. Sci. U. S. A. 106 (2009) 3722–3727. https://doi.org/10.1073/pnas.0808564106.

[83] W. Liu, Y. Shang, Y. Zeng, C. Liu, Y. Li, L. Zhai, P. Wang, J. Lou, P. Xu, Y. Ye, W. Li, Dimeric Ube2g2 simultaneously engages donor and acceptor ubiquitins to form Lys48-linked ubiquitin chains, EMBO J. 33 (2014) 46–61. https://doi.org/10.1002/embj.201385315.

[84] Q. Liu, Y.-C. Yuan, B. Shen, D.J. Chen, Y. Chen, Conformational Flexibility of a Ubiquitin Conjugation Enzyme (E2), Biochemistry 38 (1999) 1415–1425. https://doi.org/10.1021/bi981840h.

[85] P. Knipscheer, W.J. van Dijk, J.V. Olsen, M. Mann, T.K. Sixma, Noncovalent interaction between Ubc9 and SUMO promotes SUMO chain formation, EMBO J. 26 (2007) 2797–2807. https://doi.org/10.1038/sj.emboj.7601711.

[86] A.Y. Alontaga, N.D. Ambaye, Y.-J. Li, R. Vega, C.-H. Chen, K.P. Bzymek, J.C. Williams, W. Hu, Y. Chen, RWD Domain as an E2 (Ubc9)-Interaction Module, J. Biol. Chem. 290 (2015) 16550–16559. https://doi.org/10.1074/jbc.M115.644047.

[87] A.F. Alpi, V. Chaugule, H. Walden, Mechanism and disease association of E2-conjugating enzymes: lessons from UBE2T and UBE2L3, Biochem. J. 473 (2016) 3401–3419. https://doi.org/10.1042/BCJ20160028.

[88] J.C. Dorsman, M. Levitus, D. Rockx, M.A. Rooimans, A.B. Oostra, A. Haitjema, S.T. Bakker, J. Steltenpool, D. Schuler, S. Mohan, D. Schindler, F. Arwert, G. Pals, C.G. Mathew, Q. Waisfisz, J.P. de Winter, H. Joenje, Identification of the Fanconi anemia complementation group I gene, FANCI, Cell. Oncol. 29 (2007) 211–218.

[89] A. Smogorzewska, S. Matsuoka, P. Vinciguerra, E.R.3. McDonald, K.E. Hurov, J. Luo, B.A. Ballif, S.P. Gygi, K. Hofmann, A.D. D'Andrea, S.J. Elledge, Identification of the FANCI protein, a monoubiquitinated FANCD2 paralog required for DNA repair, Cell 129 (2007) 289–301. https://doi.org/10.1016/j.cell.2007.03.009.

[90] A.E. Sims, E. Spiteri, R.J. Sims, A.G. Arita, F.P. Lach, T. Landers, M. Wurm, M. Freund, K. Neveling, H. Hanenberg, A.D. Auerbach, T.T. Huang, FANCI is a second monoubiquitinated member of the Fanconi anemia pathway, Nat Struct Mol Biol 14 (2007) 564–567. https://doi.org/10.1038/nsmb1252.

[91] I. Garcia-Higuera, T. Taniguchi, S. Ganesan, M.S. Meyn, C. Timmers, J. Hejna, M. Grompe, A.D. D'Andrea, Interaction of the Fanconi Anemia Proteins and BRCA1 in a Common Pathway, Molecular Cell 7 (2001) 249–262. https://doi.org/10.1016/S1097-2765(01)00173-3.

[92] S.G. Gehrke, H.-D. Riedel, T. Herrmann, B. Hadaschik, K. Bents, C. Veltkamp, W. Stremmel, UbcH5A, a member of human E2 ubiquitin-conjugating enzymes, is closely related to SFT, a stimulator of iron transport, and is up-regulated in

hereditary hemochromatosis, Blood 101 (2003) 3288–3293. https://doi.org/10.1182/blood-2002-07-2192.

[93] Y. Guo, L. An, H.-M. Ng, S.M.H. Sy, M.S.Y. Huen, An E2-guided E3 Screen Identifies the RNF17-UBE2U Pair as Regulator of the Radiosensitivity, Immunodeficiency, Dysmorphic Features, and Learning Difficulties (RIDDLE) Syndrome Protein RNF168, J. Biol. Chem. 292 (2017) 967–978. https://doi.org/10.1074/jbc.M116.758854.

[94] Y. Zhang, X. Zhou, L. Zhao, C. Li, H. Zhu, L. Xu, L. Shan, X. Liao, Z. Guo, P. Huang, UBE2W interacts with FANCL and regulates the monoubiquitination of Fanconi anemia protein FANCD2, Mol. Cells 31 (2011) 113–122. https://doi.org/10.1007/s10059-011-0015-9.

[95] J.-W. Han, H.-F. Zheng, Y. Cui, L.-D. Sun, D.-Q. Ye, Z. Hu, J.-H. Xu, Z.-M. Cai, W. Huang, G.-P. Zhao, H.-F. Xie, H. Fang, Q.-J. Lu, J.-H. Xu, X.-P. Li, Y.-F. Pan, D.-Q. Deng, F.-Q. Zeng, Z.-Z. Ye, X.-Y. Zhang, Q.-W. Wang, F. Hao, L. Ma, X.-B. Zuo, F.-S. Zhou, W.-H. Du, Y.-L. Cheng, J.-Q. Yang, S.-K. Shen, J. Li, Y.-J. Sheng, X.-X. Zuo, W.-F. Zhu, F. Gao, P.-L. Zhang, Q. Guo, B. Li, M. Gao, F.-L. Xiao, C. Quan, C. Zhang, Z. Zhang, K.-J. Zhu, Y. Li, D.-Y. Hu, W.-S. Lu, J.-L. Huang, S.-X. Liu, H. Li, Y.-Q. Ren, Z.-X. Wang, C.-J. Yang, P.-G. Wang, W.-M. Zhou, Y.-M. Lv, A.-P. Zhang, S.-Q. Zhang, D. Lin, Y. Li, H.Q. Low, M. Shen, Z.-F. Zhai, Y. Wang, F.-Y. Zhang, S. Yang, J.-J. Liu, X.-J. Zhang, Genome-wide association study in a Chinese Han population identifies nine new susceptibility loci for systemic lupus erythematosus, Nat. Genet. 41 (2009) 1234–1237. https://doi.org/10.1038/ng.472.

[96] S. Wang, I. Adrianto, G.B. Wiley, C.J. Lessard, J.A. Kelly, A.J. Adler, S.B. Glenn, A.H. Williams, J.T. Ziegler, M.E. Comeau, M.C. Marion, B.E. Wakeland, C. Liang, K.M. Kaufman, J.M. Guthridge, M.E. Alarcon-Riquelme, G.S. Alarcon, J.-M. Anaya, S.-C. Bae, J.-H. Kim, Y.B. Joo, S.A. Boackle, E.E. Brown, M.A. Petri, R. Ramsey-Goldman, J.D. Reveille, L.M. Vila, L.A. Criswell, J.C. Edberg, B.I. Freedman, G.S. Gilkeson, C.O. Jacob, J.A. James, D.L. Kamen, R.P. Kimberly, J. Martin, J.T. Merrill, T.B. Niewold, B.A. Pons-Estel, R.H. Scofield, A.M. Stevens, B.P. Tsao, T.J. Vyse, C.D. Langefeld, J.B. Harley, E.K. Wakeland, K.L. Moser, C.G. Montgomery, P.M. Gaffney, A functional haplotype of UBE2L3 confers risk for systemic lupus erythematosus, Genes Immun. 13 (2012) 380–387. https://doi.org/10.1038/gene.2012.6.

[97] L. Jostins, S. Ripke, R.K. Weersma, R.H. Duerr, D.P. McGovern, K.Y. Hui, J.C. Lee, L.P. Schumm, Y. Sharma, C.A. Anderson, J. Essers, M. Mitrovic, K. Ning, I. Cleynen, E. Theatre, S.L. Spain, S. Raychaudhuri, P. Goyette, Z. Wei, C. Abraham, J.-P. Achkar, T. Ahmad, L. Amininejad, A.N. Ananthakrishnan, V. Andersen, J.M. Andrews, L. Baidoo, T. Balschun, P.A. Bampton, A. Bitton, G. Boucher, S. Brand, C. Buning, A. Cohain, S. Cichon, M. D'Amato, D. de Jong, K.L. Devaney, M. Dubinsky, C. Edwards, D. Ellinghaus, L.R. Ferguson, D. Franchimont, K. Fransen, R. Gearry, M. Georges, C. Gieger, J. Glas, T. Haritunians, A. Hart, C. Hawkey, M. Hedl, X. Hu, T.H. Karlsen, L. Kupcinskas, S. Kugathasan, A. Latiano, D. Laukens, I.C. Lawrance, C.W. Lees, E. Louis, G. Mahy, J. Mansfield, A.R. Morgan, C. Mowat, W. Newman, O. Palmieri, C.Y. Ponsioen, U. Potocnik, N.J. Prescott, M. Regueiro, J.I. Rotter, R.K. Russell, J.D. Sanderson, M. Sans, J. Satsangi, S. Schreiber, L.A. Simms, J. Sventoraityte, S.R. Targan, K.D. Taylor, M. Tremelling, H.W. Verspaget, M. de Vos, C. Wijmenga, D.C. Wilson, J. Winkelmann, R.J. Xavier, S. Zeissig, B. Zhang, C.K. Zhang, H. Zhao, M.S. Silverberg, V. Annese, H. Hakonarson, S.R. Brant, G. Radford-Smith, C.G. Mathew, J.D. Rioux, E.E. Schadt, M.J. Daly, A. Franke, M. Parkes, S. Vermeire, J.C. Barrett, J.H. Cho, Host-microbe interactions have shaped the genetic architecture of inflammatory bowel disease, Nature 491 (2012) 119–124. https://doi.org/10.1038/nature11582.

[98] E.A. Stahl, S. Raychaudhuri, E.F. Remmers, G. Xie, S. Eyre, B.P. Thomson, Y. Li, F.A.S. Kurreeman, A. Zhernakova, A. Hinks, C. Guiducci, R. Chen, L. Alfredsson, C.I. Amos, K.G. Ardlie, A. Barton, J. Bowes, E. Brouwer, N.P. Burtt, J.J. Catanese, J. Coblyn, M.J.H. Coenen, K.H. Costenbader, L.A. Criswell, J.B.A. Crusius, J. Cui, P.I.W. de Bakker, P.L. de Jager, B. Ding, P. Emery, E. Flynn, P. Harrison, L.J. Hocking, T.W.J. Huizinga, D.L. Kastner, X. Ke, A.T. Lee, X. Liu, P. Martin, A.W. Morgan, L. Padyukov, M.D. Posthumus, T.R.D.J. Radstake, D.M. Reid, M. Seielstad, M.F. Seldin, N.A. Shadick, S. Steer, P.P. Tak, W. Thomson, A.H.M. van der Helm-van Mil, I.E. van der Horst-Bruinsma, C.E. van der Schoot, P.L.C.M. van Riel, M.E. Weinblatt, A.G. Wilson, G.J. Wolbink, B.P. Wordsworth, C. Wijmenga, E.W. Karlson, R.E.M. Toes, N. de Vries, A.B. Begovich, J. Worthington, K.A. Siminovitch, P.K. Gregersen, L. Klareskog, R.M. Plenge, Genome-wide association study meta-analysis identifies seven new rheumatoid arthritis risk loci, Nat. Genet. 42 (2010) 508–514. https://doi.org/10.1038/ng.582.

[99] M.-J. Barrera, S. Aguilera, I. Castro, J. Cortes, V. Bahamondes, A.F.G. Quest, C. Molina, S. Gonzalez, M. Hermoso, U. Urzua, C. Leyton, M.-J. Gonzalez, Pro-inflammatory cytokines enhance ERAD and ATF6alpha pathway activity in salivary glands of Sjogren's syndrome patients, J. Autoimmun. 75 (2016) 68–81. https://doi.org/10.1016/j.jaut.2016.07.006.

[100] A. Espinosa, J. Hennig, A. Ambrosi, M. Anandapadmanaban, M.S. Abelius, Y. Sheng, F. Nyberg, C.H. Arrowsmith, M. Sunnerhagen, M. Wahren-Herlenius, Anti-Ro52 autoantibodies from patients with Sjogren's syndrome inhibit the Ro52 E3 ligase activity by blocking the E3/E2 interface, J. Biol. Chem. 286 (2011) 36478–36491. https://doi.org/10.1074/jbc.M111.241786.

[101] F.C. Fiesel, E.L. Moussaud-Lamodiere, M. Ando, W. Springer, A specific subset of E2 ubiquitin-conjugating enzymes regulate Parkin activation and mitophagy differently, J. Cell Sci. 127 (2014) 3488–3504. https://doi.org/10.1242/jcs.147520.

[102] B. Wang, L. Zeng, S.A. Merillat, S. Fischer, J. Ochaba, L.M. Thompson, S.J. Barmada, K.M. Scaglione, H.L. Paulson, The ubiquitin conjugating enzyme Ube2W regulates solubility of the Huntington's disease protein, huntingtin, Neurobiology of Disease 109 (2018) 127–136. https://doi.org/10.1016/j.nbd.2017.10.002.

[103] R. de Pril, D.F. Fischer, R.A.C. Roos, F.W. van Leeuwen, Ubiquitin-conjugating enzyme E2-25K increases aggregate formation and cell death in polyglutamine diseases, Molecular and Cellular Neuroscience 34 (2007) 10–19. https://doi.org/10.1016/j.mcn.2006.09.006.

[104] H. Kadara, L. Lacroix, C. Behrens, L. Solis, X. Gu, J.J. Lee, E. Tahara, D. Lotan, W.K. Hong, I.I. Wistuba, R. Lotan, Identification of gene signatures and molecular markers for human lung cancer prognosis using an in vitro lung carcinogenesis system, Cancer Prev. Res. (Phila) 2 (2009) 702–711. https://doi.org/10.1158/1940-6207.CAPR-09-0084.

[105] T. Qin, G. Huang, L. Chi, S. Sui, C. Song, N. Li, S. Sun, N. Li, M. Zhang, Z. Zhao, L. Li, M. Li, Exceptionally high UBE2C expression is a unique phenomenon in basal-like type breast cancer and is regulated by BRCA1, Biomed. Pharmacother. 95 (2017) 649–655. https://doi.org/10.1016/j.biopha.2017.08.095.

[106] A. Rawat, G. Gopal, G. Selvaluxmy, T. Rajkumar, Inhibition of ubiquitin conjugating enzyme UBE2C reduces proliferation and sensitizes breast cancer

cells to radiation, doxorubicin, tamoxifen and letrozole, Cell. Oncol. (Dordr) 36 (2013) 459–467. https://doi.org/10.1007/s13402-013-0150-8.

[107] Y. Xiong, J. Lu, Q. Fang, Y. Lu, C. Xie, H. Wu, Z. Yin, UBE2C functions as a potential oncogene by enhancing cell proliferation, migration, invasion, and drug resistance in hepatocellular carcinoma cells, Biosci. Rep. 39 (2019). https://doi.org/10.1042/BSR20182384.

[108] I.K. Vila, Y. Yao, G. Kim, W. Xia, H. Kim, S.-J. Kim, M.-K. Park, J.P. Hwang, E. González-Billalabeitia, M.-C. Hung, S.J. Song, M.S. Song, A UBE2O-AMPKα2 Axis that Promotes Tumor Initiation and Progression Offers Opportunities for Therapy, Cancer Cell 31 (2017) 208–224. https://doi.org/10.1016/j.ccell.2017.01.003.

[109] P.V. Hornbeck, B. Zhang, B. Murray, J.M. Kornhauser, V. Latham, E. Skrzypek, PhosphoSitePlus, 2014: mutations, PTMs and recalibrations, Nucleic Acids Research 43 (2014) D512-D520. https://doi.org/10.1093/nar/gku1267.

[110] D.W.A. Buchan, D.T. Jones, The PSIPRED Protein Analysis Workbench: 20 years on, Nucleic Acids Research 47 (2019) W402-W407. https://doi.org/10.1093/nar/gkz297.

[111] D.T. Jones, Protein secondary structure prediction based on position-specific scoring matrices, J. Mol. Biol. 292 (1999) 195–202. https://doi.org/10.1006/jmbi.1999.3091.

[112] N.G. Brown, R. VanderLinden, E.R. Watson, F. Weissmann, A. Ordureau, K.-P. Wu, W. Zhang, S. Yu, P.Y. Mercredi, J.S. Harrison, I.F. Davidson, R. Qiao, Y. Lu, P. Dube, M.R. Brunner, C.R.R. Grace, D.J. Miller, D. Haselbach, M.A. Jarvis, M. Yamaguchi, D. Yanishevski, G. Petzold, S.S. Sidhu, B. Kuhlman, M.W. Kirschner, J.W. Harper, J.-M. Peters, H. Stark, B.A. Schulman, Dual RING E3 Architectures Regulate Multiubiquitination and Ubiquitin Chain Elongation by APC/C, Cell 165 (2016) 1440–1453. https://doi.org/10.1016/j.cell.2016.05.037.

[113] N.G. Brown, E.R. Watson, F. Weissmann, M.A. Jarvis, R. VanderLinden, C.R.R. Grace, J.J. Frye, R. Qiao, P. Dube, G. Petzold, S.E. Cho, O. Alsharif, J. Bao, I.F. Davidson, J. Zheng, A. Nourse, I. Kurinov, J.-M. Peters, H. Stark, B.A. Schulman, Mechanism of polyubiquitination by human Anaphase Promoting Complex: RING repurposing for ubiquitin chain assembly, Molecular Cell 56 (2014) 246–260. https://doi.org/10.1016/j.molcel.2014.09.009.

[114] T. Wu, Y. Merbl, Y. Huo, J.L. Gallop, A. Tzur, M.W. Kirschner, UBE2S Drives Elongation of K11-Linked Ubiquitin Chains by the Anaphase-Promoting Complex, Proc. Natl. Acad. Sci. U. S. A. 107 (2010) 1355–1360.

[115] O.V. Baboshina, A.L. Haas, Novel Multiubiquitin Chain Linkages Catalyzed by the Conjugating Enzymes E2EPF and RAD6 Are Recognized by 26 S Proteasome Subunit 5, J. Biol. Chem. 271 (1996) 2823–2831. https://doi.org/10.1074/jbc.271.5.2823.

[116] C.-R. Jung, K.-S. Hwang, J. Yoo, W.-K. Cho, J.-M. Kim, W.H. Kim, D.-S. Im, E2-EPF UCP targets pVHL for degradation and associates with tumor growth and metastasis, Nat. Med. 12 (2006) 809–816. https://doi.org/10.1038/nm1440.

[117] M. Ohh, pVHL's kryptonite: E2-EPF UCP, Cancer Cell 10 (2006) 95–97. https://doi.org/10.1016/j.ccr.2006.07.016.

[118] J. Liang, H. Nishi, M.-L. Bian, C. Higuma, T. Sasaki, H. Ito, K. Isaka, The ubiquitin-conjugating enzyme E2-EPF is overexpressed in cervical cancer and associates with tumor growth, Oncol. Rep. 28 (2012) 1519–1525. https://doi.org/10.3892/or.2012.1949.

[119] F.C. Roos, A.J. Evans, W. Brenner, B. Wondergem, J. Klomp, P. Heir, O. Roche, C. Thomas, H. Schimmel, K.A. Furge, B.T. Teh, J.W. Thüroff, C. Hampel, M. Ohh, Deregulation of E2-EPF ubiquitin carrier protein in papillary renal cell carcinoma, Am. J. Pathol. 178 (2011) 853–860. https://doi.org/10.1016/j.ajpath.2010.10.033.

[120] Y.-H. Pan, M. Yang, L.-P. Liu, D.-C. Wu, M.-Y. Li, S.-G. Su, UBE2S enhances the ubiquitination of p53 and exerts oncogenic activities in hepatocellular carcinoma, Biochem. Biophys. Res. Commun. 503 (2018) 895–902. https://doi.org/10.1016/j.bbrc.2018.06.093.

[121] Z. Liu, L. Xu, UBE2S promotes the proliferation and survival of human lung adenocarcinoma cells, BMB Rep. 51 (2018) 642–647. https://doi.org/10.5483/BMBRep.2018.51.12.138.

[122] Z. Li, Y. Wang, Y. Li, W. Yin, L. Mo, X. Qian, Y. Zhang, G. Wang, F. Bu, Z. Zhang, X. Ren, B. Zhu, C. Niu, W. Xiao, W. Zhang, Ube2s stabilizes β-Catenin through K11-linked polyubiquitination to promote mesendoderm specification and colorectal cancer development, Cell Death Dis 9 1–13. https://doi.org/10.1038/s41419-018-0451-y.

[123] A. Ayesha, T. Hyodo, E. Asano, N. Sato, M. Mansour, S. Ito, M. Hamaguchi, T. Senga, UBE2S is associated with malignant characteristics of breast cancer cells, Tumor Biol. (2015) 1–10. https://doi.org/10.1007/s13277-015-3863-7.

[124] D. Tedesco, J. Zhang, L. Trinh, G. Lalehzadeh, R. Meisner, K.D. Yamaguchi, D.L. Ruderman, H. Dinter, D.A. Zajchowski, The Ubiquitin-Conjugating Enzyme E2-EPF Is Overexpressed in Primary Breast Cancer and Modulates Sensitivity to Topoisomerase II Inhibition, Neoplasia (New York, N.Y.) 9 (2007) 601–613.

[125] M. Yamaguchi, S. Yu, R. Qiao, F. Weissmann, D.J. Miller, R. VanderLinden, N.G. Brown, J.J. Frye, J.-M. Peters, B.A. Schulman, Structure of an APC3-APC16 complex: insights into assembly of the anaphase-promoting complex/cyclosome, J. Mol. Biol. 427 (2015) 1748–1764. https://doi.org/10.1016/j.jmb.2014.11.020.

[126] D. Hayward, T. Alfonso-Pérez, U. Gruneberg, Orchestration of the spindle assembly checkpoint by CDK1-cyclin B1, FEBS Lett. 593 (2019) 2889–2907. https://doi.org/10.1002/1873-3468.13591.

[127] R.W. King, J.M. Peters, S. Tugendreich, M. Rolfe, P. Hieter, M.W. Kirschner, A 20S complex containing CDC27 and CDC16 catalyzes the mitosis-specific conjugation of ubiquitin to cyclin B, Cell 81 (1995) 279–288. https://doi.org/10.1016/0092-8674(95)90338-0.

[128] J.-M. Peters, The anaphase promoting complex/cyclosome: a machine designed to destroy, Nat Rev Mol Cell Biol 7 (2006) 644–656. https://doi.org/10.1038/nrm1988.

[129] L.-F. Chang, Z. Zhang, J. Yang, S.H. McLaughlin, D. Barford, Molecular architecture and mechanism of the anaphase-promoting complex, Nature 513 (2014) 388–393. https://doi.org/10.1038/nature13543.

[130] L. Chang, Z. Zhang, J. Yang, S.H. McLaughlin, D. Barford, Atomic structure of the APC/C and its mechanism of protein ubiquitination, Nature 522 (2015) 450–454. https://doi.org/10.1038/nature14471.

[131] A. Kelly, K.E. Wickliffe, L. Song, I. Fedrigo, M. Rape, Ubiquitin chain elongation requires E3-dependent tracking of the emerging conjugate, Molecular Cell 56 (2014) 232–245. https://doi.org/10.1016/j.molcel.2014.09.010.

[132] M. Glotzer, A.W. Murray, M.W. Kirschner, Cyclin is degraded by the ubiquitin pathway, Nature 349 (1991) 132–138. https://doi.org/10.1038/349132a0.

[133] C.M. Pfleger, M.W. Kirschner, The KEN box: an APC recognition signal distinct from the D box targeted by Cdh1, Genes Dev. 14 (2000) 655–665.

[134] S. Zhang, L. Chang, C. Alfieri, Z. Zhang, J. Yang, S. Maslen, M. Skehel, D. Barford, Molecular mechanism of APC/C activation by mitotic phosphorylation, Nature 533 (2016) 260–264. https://doi.org/10.1038/nature17973.

[135] Q. Li, L. Chang, S. Aibara, J. Yang, Z. Zhang, D. Barford, WD40 domain of Apc1 is critical for the coactivator-induced allosteric transition that stimulates APC/C catalytic activity, Proc. Natl. Acad. Sci. U. S. A. 113 (2016) 10547–10552. https://doi.org/10.1073/pnas.1607147113.

[136] J. Kernan, T. Bonacci, M.J. Emanuele, Who guards the guardian? Mechanisms that restrain APC/C during the cell cycle, Biochimica et Biophysica Acta (BBA) - Molecular Cell Research 1865 (2018) 1924–1933. https://doi.org/10.1016/j.bbamcr.2018.09.011.

[137] M. Brandeis, T. Hunt, The proteolysis of mitotic cyclins in mammalian cells persists from the end of mitosis until the onset of S phase, EMBO J. 15 (1996) 5280–5289.

[138] L. Jin, A. Williamson, S. Banerjee, I. Philipp, M. Rape, Mechanism of Ubiquitin-Chain Formation by the Human Anaphase-Promoting Complex, Cell 133 (2008) 653–665. https://doi.org/10.1016/j.cell.2008.04.012.

[139] M. Min, T.E.T. Mevissen, M. de Luca, D. Komander, C. Lindon, Efficient APC/C substrate degradation in cells undergoing mitotic exit depends on K11 ubiquitin linkages, Mol. Biol. Cell 26 (2015) 4325–4332. https://doi.org/10.1091/mbc.E15-02-0102.

[140] T. Wild, M.S.Y. Larsen, T. Narita, J. Schou, J. Nilsson, C. Choudhary, The Spindle Assembly Checkpoint Is Not Essential for Viability of Human Cells with Genetically Lowered APC/C Activity, Cell Reports 14 (2016) 1829–1840. https://doi.org/10.1016/j.celrep.2016.01.060.

[141] H. Yu, R.W. King, J.M. Peters, M.W. Kirschner, Identification of a novel ubiquitin-conjugating enzyme involved in mitotic cyclin degradation, Curr. Biol. 6 (1996) 455–466. https://doi.org/10.1016/s0960-9822(02)00513-4.

[142] J.J. Frye, N.G. Brown, G. Petzold, E.R. Watson, C.R.R. Grace, A. Nourse, M.A. Jarvis, R.W. Kriwacki, J.-M. Peters, H. Stark, B.A. Schulman, Electron microscopy structure of human APC/C(CDH1)-EMI1 reveals multimodal

mechanism of E3 ligase shutdown, Nat. Struct. Mol. Biol. 20 (2013) 827–835. https://doi.org/10.1038/nsmb.2593.

[143] N.G. Brown, R. VanderLinden, E.R. Watson, R. Qiao, C.R.R. Grace, M. Yamaguchi, F. Weissmann, J.J. Frye, P. Dube, S. Ei Cho, M.L. Actis, P. Rodrigues, N. Fujii, J.-M. Peters, H. Stark, B.A. Schulman, RING E3 mechanism for ubiquitin ligation to a disordered substrate visualized for human anaphase-promoting complex, Proceedings of the National Academy of Sciences 112 (2015) 5272–5279. https://doi.org/10.1073/pnas.1504161112.

[144] N.V. Dimova, N.A. Hathaway, B.-H. Lee, D.S. Kirkpatrick, M.L. Berkowitz, S.P. Gygi, D. Finley, R.W. King, APC/C-mediated multiple monoubiquitination provides an alternative degradation signal for cyclin B1, Nat. Cell Biol. 14 (2012) 168–176. https://doi.org/10.1038/ncb2425.

[145] L. Chang, D. Barford, Insights into the anaphase-promoting complex: a molecular machine that regulates mitosis, Curr. Opin. Struct. Biol. 29 (2014) 1–9. https://doi.org/10.1016/j.sbi.2014.08.003.

[146] K. Sako, K. Suzuki, M. Isoda, S. Yoshikai, C. Senoo, N. Nakajo, M. Ohe, N. Sagata, Emi2 mediates meiotic MII arrest by competitively inhibiting the binding of Ube2S to the APC/C, Nat Commun 5 1–12. https://doi.org/10.1038/ncomms4667.

[147] D.S. Kirkpatrick, N.A. Hathaway, J. Hanna, S. Elsasser, J. Rush, D. Finley, R.W. King, S.P. Gygi, Quantitative analysis of in vitro ubiquitinated cyclin B1 reveals complex chain topology, Nat. Cell Biol. 8 (2006) 700–710. https://doi.org/10.1038/ncb1436.

[148] R.G. Yau, K. Doerner, E.R. Castellanos, D.L. Haakonsen, A. Werner, N. Wang, X.W. Yang, N. Martinez-Martin, M.L. Matsumoto, V.M. Dixit, M. Rape, Assembly and Function of Heterotypic Ubiquitin Chains in Cell-Cycle and Protein Quality Control, Cell 171 (2017) 918-933.e20. https://doi.org/10.1016/j.cell.2017.09.040.

[149] P. Caron, J. van der Linden, H. van Attikum, Bon voyage: A transcriptional journey around DNA breaks, DNA Repair 82 (2019) 102686. https://doi.org/10.1016/j.dnarep.2019.102686.

[150] R.D. Johnson, M. Jasin, Sister chromatid gene conversion is a prominent double-strand break repair pathway in mammalian cells, EMBO J. 19 (2000) 3398–3407. https://doi.org/10.1093/emboj/19.13.3398.

[151] G.D. Kao, Z. Jiang, A.M. Fernandes, A.K. Gupta, A. Maity, Inhibition of phosphatidylinositol-3-OH kinase/Akt signaling impairs DNA repair in glioblastoma cells following ionizing radiation, J. Biol. Chem. 282 (2007) 21206–21212. https://doi.org/10.1074/jbc.M703042200.

[152] N.K. Kolas, J.R. Chapman, S. Nakada, J. Ylanko, R. Chahwan, F.D. Sweeney, S. Panier, M. Mendez, J. Wildenhain, T.M. Thomson, L. Pelletier, S.P. Jackson, D. Durocher, Orchestration of the DNA-damage response by the RNF8 ubiquitin ligase, Science 318 (2007) 1637–1640. https://doi.org/10.1126/science.1150034.

[153] T. Thorslund, A. Ripplinger, S. Hoffmann, T. Wild, M. Uckelmann, B. Villumsen, T. Narita, T.K. Sixma, C. Choudhary, S. Bekker-Jensen, N. Mailand, Histone H1 couples initiation and amplification of ubiquitin signalling after DNA damage, Nature 527 (2015) 389–393. https://doi.org/10.1038/nature15401.

[154] F. Mattiroli, J.H.A. Vissers, W.J. van Dijk, P. Ikpa, E. Citterio, W. Vermeulen, J.A. Marteijn, T.K. Sixma, RNF168 ubiquitinates K13-15 on H2A/H2AX to drive DNA damage signaling, Cell 150 (2012) 1182–1195. https://doi.org/10.1016/j.cell.2012.08.005.

[155] J.K. Stock, S. Giadrossi, M. Casanova, E. Brookes, M. Vidal, H. Koseki, N. Brockdorff, A.G. Fisher, A. Pombo, Ring1-mediated ubiquitination of H2A restrains poised RNA polymerase II at bivalent genes in mouse ES cells, Nat. Cell Biol. 9 (2007) 1428–1435. https://doi.org/10.1038/ncb1663.

[156] G.S. Stewart, S. Panier, K. Townsend, A.K. Al-Hakim, N.K. Kolas, E.S. Miller, S. Nakada, J. Ylanko, S. Olivarius, M. Mendez, C. Oldreive, J. Wildenhain, A. Tagliaferro, L. Pelletier, N. Taubenheim, A. Durandy, P.J. Byrd, T. Stankovic, A.M.R. Taylor, D. Durocher, The RIDDLE Syndrome Protein Mediates a Ubiquitin-Dependent Signaling Cascade at Sites of DNA Damage, Cell 136 (2009) 420–434. https://doi.org/10.1016/j.cell.2008.12.042.

[157] P.R. Evans, An introduction to data reduction: space-group determination, scaling and intensity statistics, Acta Crystallogr. D Biol. Crystallogr. 67 (2011) 282–292. https://doi.org/10.1107/S090744491003982X.

[158] P.R. Evans, G.N. Murshudov, How good are my data and what is the resolution?, Acta Crystallogr. D Biol. Crystallogr. 69 (2013) 1204–1214. https://doi.org/10.1107/S0907444913000061.

[159] S.A. Shiryev, J.S. Papadopoulos, A.A. Schäffer, R. Agarwala, Improved BLAST searches using longer words for protein seeding, Bioinformatics 23 (2007) 2949–2951. https://doi.org/10.1093/bioinformatics/btm479.

[160] M.D. Winn, C.C. Ballard, K.D. Cowtan, E.J. Dodson, P. Emsley, P.R. Evans, R.M. Keegan, E.B. Krissinel, A.G.W. Leslie, A. McCoy, S.J. McNicholas, G.N. Murshudov, N.S. Pannu, E.A. Potterton, H.R. Powell, R.J. Read, A. Vagin, K.S. Wilson, Overview of the CCP4 suite and current developments, Acta Crystallogr. D Biol. Crystallogr. 67 (2011) 235–242. https://doi.org/10.1107/S0907444910045749.

[161] P. Emsley, K. Cowtan, Coot: Model-building tools for molecular graphics, Acta Crystallogr. D Biol. Crystallogr. 60 (2004) 2126–2132. https://doi.org/10.1107/S0907444904019158.

[162] F. Sievers, A. Wilm, D. Dineen, T.J. Gibson, K. Karplus, W. Li, R. Lopez, H. McWilliam, M. Remmert, J. Söding, J.D. Thompson, D.G. Higgins, Fast, scalable generation of high-quality protein multiple sequence alignments using Clustal Omega, Mol. Syst. Biol. 7 (2011) 539. https://doi.org/10.1038/msb.2011.75.

[163] P. Artimo, M. Jonnalagedda, K. Arnold, D. Baratin, G. Csardi, E. de Castro, S. Duvaud, V. Flegel, A. Fortier, E. Gasteiger, A. Grosdidier, C. Hernandez, V. Ioannidis, D. Kuznetsov, R. Liechti, S. Moretti, K. Mostaguir, N. Redaschi, G. Rossier, I. Xenarios, H. Stockinger, ExPASy: SIB bioinformatics resource portal, Nucleic Acids Research 40 (2012) W597-603. https://doi.org/10.1093/nar/gks400.

[164] M.D. Abramoff, P.J. Magalhães, S.J. Ram, Image processing with ImageJ, Biophotonics international 11 (2004) 36–42.

[165] V.B. Chen, W.B. Arendall, J.J. Headd, D.A. Keedy, R.M. Immormino, G.J. Kapral, L.W. Murray, J.S. Richardson, D.C. Richardson, MolProbity: all-atom structure validation for macromolecular crystallography, Acta Crystallogr. D Biol. Crystallogr. 66 (2010) 12–21. https://doi.org/10.1107/S0907444909042073.

[166] H.M. Berman, J. Westbrook, Z. Feng, G. Gilliland, T.N. Bhat, H. Weissig, I.N. Shindyalov, P.E. Bourne, The Protein Data Bank, Nucleic Acids Research 28 (2000) 235–242. https://doi.org/10.1093/nar/28.1.235.

[167] A.J. McCoy, R.W. Grosse-Kunstleve, P.D. Adams, M.D. Winn, L.C. Storoni, R.J. Read, Phaser crystallographic software, Journal of Applied Crystallography 40 (2007) 658–674. https://doi.org/10.1107/S0021889807021206.

[168] P.D. Adams, P.V. Afonine, G. Bunkoczi, V.B. Chen, I.W. Davis, N. Echols, J.J. Headd, L.-W. Hung, G.J. Kapral, R.W. Grosse-Kunstleve, A.J. McCoy, N.W. Moriarty, R. Oeffner, R.J. Read, D.C. Richardson, J.S. Richardson, T.C. Terwilliger, P.H. Zwart, PHENIX: a comprehensive Python-based system for macromolecular structure solution, Acta Crystallogr. D Biol. Crystallogr. 66 (2010) 213–221. https://doi.org/10.1107/S0907444909052925.

[169] L.A. Kelley, S. Mezulis, C.M. Yates, M.N. Wass, M.J.E. Sternberg, The Phyre2 web portal for protein modeling, prediction and analysis, Nat. Protoc. 10 (2015) 845–858. https://doi.org/10.1038/nprot.2015.053.

[170] E. Krissinel, K. Henrick, Inference of macromolecular assemblies from crystalline state, J. Mol. Biol. 372 (2007) 774–797. https://doi.org/10.1016/j.jmb.2007.05.022.

[171] Z. Lu, PubMed and beyond: a survey of web tools for searching biomedical literature, Database (Oxford) 2011 (2011) baq036. https://doi.org/10.1093/database/baq036.

[172] S.R. Bond, C.C. Naus, RF-Cloning.org: an online tool for the design of restriction-free cloning projects, Nucleic Acids Research 40 (2012) W209-W213. https://doi.org/10.1093/nar/gks396.

[173] P. Schuck, Size-distribution analysis of macromolecules by sedimentation velocity ultracentrifugation and lamm equation modeling, Biophys. J. 78 (2000) 1606–1619. https://doi.org/10.1016/S0006-3495(00)76713-0.

[174] W. Kabsch, XDS, Acta Crystallogr. D Biol. Crystallogr. 66 (2010) 125–132. https://doi.org/10.1107/S0907444909047337.

[175] A.K.L. Liess, A. Kucerova, M.-A. Letzelter, K. Schweimer, D. Schlesinger, O. Dybkov, H. Urlaub, J. Mansfeld, S. Lorenz, Dimerization regulates the human APC/C-associated ubiquitin-conjugating enzyme UBE2S ([submitted]).

[176] F. van den Ent, J. Löwe, RF cloning: A restriction-free method for inserting target genes into plasmids, Journal of Biochemical and Biophysical Methods 67 (2006) 67–74. https://doi.org/10.1016/j.jbbm.2005.12.008.

[177] M.Z. Li, S.J. Elledge, Harnessing homologous recombination in vitro to generate recombinant DNA via SLIC, Nat. Methods 4 (2007) 251–256. https://doi.org/10.1038/nmeth1010.

[178] E. Gasteiger, C. Hoogland, A. Gattiker, S.'e. Duvaud, M.R. Wilkins, R.D. Appel, A. Bairoch, Protein Identification and Analysis Tools on the ExPASy Server, in: J.M. Walker (Ed.), The Proteomics Protocols Handbook, Humana Press Inc, Totowa, NJ, 2005, pp. 571–607.

[179] B.A. Johnson, Using NMRView to visualize and analyze the NMR spectra of macromolecules, Methods Mol. Biol. 278 (2004) 313–352. https://doi.org/10.1385/1-59259-809-9:313.

[180] N.A. Farrow, R. Muhandiram, A.U. Singer, S.M. Pascal, C.M. Kay, G. Gish, S.E. Shoelson, T. Pawson, J.D. Forman-Kay, L.E. Kay, Backbone dynamics of a free and phosphopeptide-complexed Src homology 2 domain studied by 15N NMR relaxation, Biochemistry 33 (1994) 5984–6003. https://doi.org/10.1021/bi00185a040.

[181] A. Favier, B. Brutscher, Recovering lost magnetization: polarization enhancement in biomolecular NMR, J. Biomol. NMR 49 (2011) 9–15. https://doi.org/10.1007/s10858-010-9461-5.

[182] Y. Sheng, J.H. Hong, R. Doherty, T. Srikumar, J. Shloush, G.V. Avvakumov, J.R. Walker, S. Xue, D. Neculai, J.W. Wan, S.K. Kim, C.H. Arrowsmith, B. Raught, S. Dhe-Paganon, A human ubiquitin conjugating enzyme (E2)-HECT E3 ligase structure-function screen, Mol. Cell Proteomics 11 (2012) 329–341. https://doi.org/10.1074/mcp.O111.013706.

[183] S. Lu, S.-B. Fan, B. Yang, Y.-X. Li, J.-M. Meng, L. Wu, P. Li, K. Zhang, M.-J. Zhang, Y. Fu, J. Luo, R.-X. Sun, S.-M. He, M.-Q. Dong, Mapping native disulfide bonds at a proteome scale, Nat. Methods 12 (2015) 329–331. https://doi.org/10.1038/nmeth.3283.

[184] B. Yang, Y.-J. Wu, M. Zhu, S.-B. Fan, J. Lin, K. Zhang, S. Li, H. Chi, Y.-X. Li, H.-F. Chen, S.-K. Luo, Y.-H. Ding, L.-H. Wang, Z. Hao, L.-Y. Xiu, S. Chen, K. Ye, S.-M. He, M.-Q. Dong, Identification of cross-linked peptides from complex samples, Nat. Methods 9 (2012) 904–906. https://doi.org/10.1038/nmeth.2099.

[185] B. Yates, B. Braschi, K.A. Gray, R.L. Seal, S. Tweedie, E.A. Bruford, Genenames.org: the HGNC and VGNC resources in 2017, Nucleic Acids Research 45 (2017) D619-D625. https://doi.org/10.1093/nar/gkw1033.

[186] T. UniProt Consortium, UniProt: the universal protein knowledgebase, Nucleic Acids Research 46 (2018) 2699. https://doi.org/10.1093/nar/gky092.

[187] H. McWilliam, W. Li, M. Uludag, S. Squizzato, Y.M. Park, N. Buso, A.P. Cowley, R. Lopez, Analysis Tool Web Services from the EMBL-EBI, Nucleic Acids Research 41 (2013) W597-600. https://doi.org/10.1093/nar/gkt376.

[188] A.M. Waterhouse, J.B. Procter, D.M.A. Martin, M. Clamp, G.J. Barton, Jalview Version 2—a multiple sequence alignment editor and analysis workbench, Bioinformatics 25 (2009) 1189–1191. https://doi.org/10.1093/bioinformatics/btp033.

[189] S. Henikoff, J.G. Henikoff, Amino acid substitution matrices from protein blocks, Proc. Natl. Acad. Sci. U. S. A. 89 (1992) 10915–10919.

[190] D.R. Roe, T.E. Cheatham, PTRAJ and CPPTRAJ: Software for Processing and Analysis of Molecular Dynamics Trajectory Data, Journal of Chemical Theory and Computation 9 (2013) 3084–3095. https://doi.org/10.1021/ct400341p.

[191] J.C. Phillips, R. Braun, W. Wang, J. Gumbart, E. Tajkhorshid, E. Villa, C. Chipot, R.D. Skeel, L. Kalé, K. Schulten, Scalable molecular dynamics with NAMD, Journal of Computational Chemistry 26 (2005) 1781–1802. https://doi.org/10.1002/jcc.20289.

[192] J.A. Maier, C. Martinez, K. Kasavajhala, L. Wickstrom, K.E. Hauser, C. Simmerling, ff14SB: Improving the Accuracy of Protein Side Chain and Backbone Parameters from ff99SB, Journal of Chemical Theory and Computation 11 (2015) 3696–3713. https://doi.org/10.1021/acs.jctc.5b00255.

[193] M. Heinig, D. Frishman, STRIDE: a web server for secondary structure assignment from known atomic coordinates of proteins, Nucleic Acids Research 32 (2004) W500-2. https://doi.org/10.1093/nar/gkh429.

[194] A. Bremm, Freund, Stefan M V, D. Komander, Lys11-linked ubiquitin chains adopt compact conformations and are preferentially hydrolyzed by the deubiquitinase Cezanne, Nat. Struct. Mol. Biol. 17 (2010) 939–947. https://doi.org/10.1038/nsmb.1873.

[195] J.H. Lim, H.W. Shin, K.-S. Chung, N.-S. Kim, J.H. Kim, H.-R. Jung, D.-S. Im, C.-R. Jung, E2-EPF UCP Possesses E3 Ubiquitin Ligase Activity via Its Cysteine 118 Residue, PLoS ONE 11 (2016) e0163710. https://doi.org/10.1371/journal.pone.0163710.

[196] G. Roos, N. Foloppe, J. Messens, Understanding the pK(a) of redox cysteines: the key role of hydrogen bonding, Antioxid. Redox Signal. 18 (2013) 94–127. https://doi.org/10.1089/ars.2012.4521.

[197] V. Vittal, D.M. Wenzel, P.S. Brzovic, R.E. Klevit, Biochemical and structural characterization of the ubiquitin-conjugating enzyme UBE2W reveals the formation of a noncovalent homodimer, Cell Biochem. Biophys. 67 (2013) 103–110. https://doi.org/10.1007/s12013-013-9633-5.

[198] C. Qi, D.-F. Li, L. Feng, Y. Hou, H. Sun, D.-C. Wang, W. Liu, Biochemical and structural characterization of a novel ubiquitin-conjugating enzyme E2 from Agrocybe aegeria reveals Ube2w family-specific properties, Sci. Rep. 5 (2015) 16056. https://doi.org/10.1038/srep16056.

[199] P. Rossi, G.V.T. Swapna, Y.J. Huang, J.M. Aramini, C. Anklin, K. Conover, K. Hamilton, R. Xiao, T.B. Acton, A. Ertekin, J.K. Everett, G.T. Montelione, A microscale protein NMR sample screening pipeline, J. Biomol. NMR 46 (2010) 11–22. https://doi.org/10.1007/s10858-009-9386-z.

[200] J.S. Kim, R.T. Raines, Dibromobimane as a fluorescent crosslinking reagent, Anal. Biochem. 225 (1995) 174–176. https://doi.org/10.1006/abio.1995.1131.

[201] R. Winter, F. Noll, C. Czeslik, Methoden der biophysikalischen Chemie, 2nd ed., Vieweg + Teubner, Wiesbaden, 2011.

[202] P.A. Banka, A.P. Behera, S. Sarkar, A.B. Datta, RING E3-Catalyzed E2 Self-Ubiquitination Attenuates the Activity of Ube2E Ubiquitin-Conjugating Enzymes, J. Mol. Biol. 427 (2015) 2290–2304. https://doi.org/10.1016/j.jmb.2015.04.011.

[203] E.A. McMillan, M.-J. Ryu, C.H. Diep, S. Mendiratta, J.R. Clemenceau, R.M. Vaden, J.-H. Kim, T. Motoyaji, K.R. Covington, M. Peyton, K. Huffman, X. Wu, L. Girard, Y. Sung, P.-H. Chen, P.L. Mallipeddi, J.Y. Lee, J. Hanson, S. Voruganti, Y. Yu, S. Park, J. Sudderth, C. DeSevo, D.M. Muzny, H. Doddapaneni, A. Gazdar, R.A. Gibbs, T.-H. Hwang, J.V. Heymach, I. Wistuba, K.R. Coombes, N.S. Williams, D.A. Wheeler, J.B. MacMillan, R.J. Deberardinis, M.G. Roth, B.A. Posner, J.D. Minna, H.S. Kim, M.A. White, Chemistry-First Approach for Nomination of Personalized Treatment in Lung Cancer, Cell 173 (2018) 864-878.e29. https://doi.org/10.1016/j.cell.2018.03.028.

[204] J.G. Tate, S. Bamford, H.C. Jubb, Z. Sondka, D.M. Beare, N. Bindal, H. Boutselakis, C.G. Cole, C. Creatore, E. Dawson, P. Fish, B. Harsha, C. Hathaway, S.C. Jupe, C.Y. Kok, K. Noble, L. Ponting, C.C. Ramshaw, C.E. Rye,

H.E. Speedy, R. Stefancsik, S.L. Thompson, S. Wang, S. Ward, P.J. Campbell, S.A. Forbes, COSMIC: the Catalogue Of Somatic Mutations In Cancer, Nucleic Acids Res 47 (2019) D941-D947. https://doi.org/10.1093/nar/gky1015.

[205] W. Wang, M.W. Kirschner, Emi1 preferentially inhibits ubiquitin chain elongation by the anaphase-promoting complex, Nat. Cell Biol. 15 (2013) 797–806. https://doi.org/10.1038/ncb2755.

[206] D.F. Ceccarelli, X. Tang, B. Pelletier, S. Orlicky, W. Xie, V. Plantevin, D. Neculai, Y.-C. Chou, A. Ogunjimi, A. Al-Hakim, X. Varelas, J. Koszela, G.A. Wasney, M. Vedadi, S. Dhe-Paganon, S. Cox, S. Xu, A. Lopez-Girona, F. Mercurio, J. Wrana, D. Durocher, S. Meloche, D.R. Webb, M. Tyers, F. Sicheri, An Allosteric Inhibitor of the Human Cdc34 Ubiquitin-Conjugating Enzyme, Cell 145 (2011) 1075–1087. https://doi.org/10.1016/j.cell.2011.05.039.

[207] S.J. Campbell, R.A. Edwards, C.C.Y. Leung, D. Neculai, C.D. Hodge, S. Dhe-Paganon, J.N.M. Glover, Molecular insights into the function of RING finger (RNF)-containing proteins hRNF8 and hRNF168 in Ubc13/Mms2-dependent ubiquitylation, J. Biol. Chem. 287 (2012) 23900–23910. https://doi.org/10.1074/jbc.M112.359653.

[208] C.D. Hodge, I.H. Ismail, R.A. Edwards, G.L. Hura, A.T. Xiao, J.A. Tainer, M.J. Hendzel, J.N.M. Glover, RNF8 E3 Ubiquitin Ligase Stimulates Ubc13 E2 Conjugating Activity That Is Essential for DNA Double Strand Break Signaling and BRCA1 Tumor Suppressor Recruitment, J. Biol. Chem. 291 (2016) 9396–9410. https://doi.org/10.1074/jbc.M116.715698.

7. Appendix

7.1 List of abbreviations

Prefixes

µ	micro
m	milli
k	kilo
M	mega

Units

°	degree
°C	degree Celsius
A	ampere
Å	Angström
Da	Dalton
g	gram
x g	gravitational force
h	hour
Hz	Hertz
K	Kelvin
l	liter
m	meter
min	minute
M	molar (mol/l)
OD	optical density
rpm	revolutions per minute
s	second
v/v	volume per volume
w/v	weight per volume

Further abbreviations

#	number
α	anti
A	adenine
A	alanine, Ala
A_{280}	measured absorbance at 280 nm
AA	amino acids
AKT1	serin/threonine-protein kinase
AMP	adenosine-5´-monophosphate
Amp	ampicillin
AMPKα2	activated protein kinase alpha 2
APC	anaphase promoting complex subunit
APC/C	anaphase-promoting complex/cyclosome
APS	ammonium persulfate

ATP	adenosine-5´-triphosphate
bBBr	diromobimane
BESSY	Berliner Elektronenspeicherring-Gesellschaft für Synchrotronstrahlung
bp	base pairs
BMRB	Biological Magnetic Resonance Bank
BSA	bovine serum albumin
[c]	concentration
C	cytosine
C	cysteine, Cys
cat	catalytic
CC1/2	correlation coefficient 1/2
CCP4	Collaborative Computational Project, Number 4, 1994
CD	circular dichroism
CDC20	cell division cycle protein 20 homolog
CDC34	Ubiquitin-conjugating enzyme E2-34 kDa from yeast
CDH1	Fizzy-related protein homolog
CRBN	Cereblon
cryo-EM	cryo-electron microscopy
CV	column volume
D	aspartic acid, Asp
D_2O	deuterium oxide
ddH2O	Bi-destilled water
DESY	Deutsches Elektronen-Synchrotron
DMF	dimethylformamide
DMSO	dimethylsulfoxide
DNA	desoxyribonucleic acid
DNA-PKc	DNA-dependent Protein Kinase catalytic subunit
DNase	desoxyribunucelase
DNS	Desoxyribonukleinsäure
dNTP	desoxyribonucleoside-5´-triphosphate (dATP, dCTP, dGTP, dTTP)
DSB	double strand break
DTNB	5,5´-Dithiobis-2-nitrobenzoic acid (Ellman´s reagent)
DTT	dithiothreitol
DUB	deubiquitinating enzyme
E	glutamic acid, Glu
E1	ubiquitin-activating enzyme
E2	ubiquitin-conjugating enzyme
E3	ubiquitin ligase
E. coli	*Escherichia coli*
ECL	enhanced chemiluminescence
EDTA	ethylendiamintetraacetate desoxyribonucleic acid
ESI-MS	electrospray ionization mass spectrometry
ESRF	European Synchrotron Radiation Facility
ER	endoplasmic reticulum
ERAD	endoplasmic-reticulum-associated protein degradation
EtOH	ethanol
F	phenylalanine, Phe
F	forward

FA	Fanconi anemia
FANCD2	Fanconi anemia protein D2
FL	full-length
FPLC	fast protein liquid chromatography
G	guanine
G	glycine, Gly
GST	gluatathione-S-transferase
GTP	guanosine-5´f-triphosphate
H	histidine, His
H_2O	water
HA	human influenza hemagglutinin
HF	high fidelity
HIF-1α	hypoxia-inducible factor 1-alpha
His_6	hexahistidine
HECT	homologous to E6AP C-Terminus
HEPES	2-[4-(2-hydroxyethyl)piperazin-1-yl]ethanesulfonic acid
HPSF	high purity salt free
HR	homologous recombination
HRP	horseradish peroxidase
HSQC	heteronuclear single quantum correlation
I	isoleucine, Ile
IBD	inflammatory bowel disease
IEX	ion exchange chromatography
IgG	Immunoglobulin
IKZF	Ikaros familiy zinc finger protein
IMAC	immobilized metal affinity chromatography
IMiD	immune modulators
IPTG	Isopropyl β-D-1-thiogalactopyranoside
K	lysine, Lys
K_a	acid dissociation constant
Kan	kanamycin
K_D	dissociation constant
KU70	5'-deoxyribose-5-phosphate lyase Ku70
L	leucine, Leu
LB	lysogeny broth
LIG4	DNA Ligase 4
m	mutated
M	methionine, Met
MALS	multi-angle light scattering
MCC	mitotic checkpoint complex
MD	molecular dynamics
MDC1	mediator of DNA damage checkpoint protein 1
B-ME	β-mercapthoethanol
MeOH	Methanol
mHTT	mutated protein huntingtin
MOPS	(3-(N-morpholino)propanesulfonic acid
MR	molecular replacement

MS	mass spectrometry
MS1/2	mass spectrum 1/2
mTOR	mammalian target of rapamycin
MW	molecular weight
MWCO	molecular weight cut-off
N	asparagine, Asn
NEB	New England Biolabs
NEM	N-ethylmaleimide
NF-kB	nuclear factor kappa-light-chain-enhancer of activated B cells
NHEJ	non-homologous end-joining
NMR	nuclear magnetic resonance
NTD	N-terminal domain
NUS	Non-linear sampling
OD_{600}	optical density (= absorbance) measured at a wavelength of 600 nm
P	phosphor
P	proline, Pro
PAGE	polyacrylamide gel electrophoresis
PAO	phenylarsine oxide
PCR	polymerase chain reaction
PDB	protein data bank
PEG	polyethylene glycol
pI	isoelectric point
PINK1	serine/threonine-protein kinase PINK1
POI	protein of interest
PROTAC	Proteolysis Targeting Chimeras
PSMs	peptide spectrum matches
PTEN	Phosphatase and Tensin homolog
PVDF	polyvinylidene difluoride
pVHL	von Hippel-Lindau tumor suppressor protein
R	arginine, Arg
R	reverse
RAD51	DNA repair protein RAD51
RBR	RING-between-RING E3 enzyme
RF	restriction-free
RING	Really Interesting New Gene
RMSD	root-mean-square deviation
RMSF	root-mean-square fluctuation
RNA	ribonucleic acid
RNF	RING-type E3 ubiquitin transferase
ROS	reactive oxygen species
R_{Pim}	precision indicating merging R-factor
RRID	Research Resource Identifier
PROTAC	Proteolysis targeting chimeras
RT	room temperature
S	serine, Ser
SAC	spindle assembly checkpoint
SD	standard deviation
SD	Superdex

SDS	sodium dodecyl sulfate
SEC	size-exclusion chromatography
SGC	Structural Genomics Consortium
SS	Sjörgren´s disease
SUMO	Small ubiquitin-related modifier
T	thymine
T	threonine, Thr
TB	Terrific Broth
TBS-T	Tris-buffered saline with tween 20
TCEP	Tris-(2-carboxymethyl)-phosphine
TEMED	N,N,N´,N´-tetramethylethylendiamine
TEV	Tobacco Etch Virus
TFB	transformation buffer
TM	melting temperature
TRIM21	E3 ubiquitin-protein ligase TRIM21
Tris	Tris-(hydroxymethyl)-aminomethan
U	Uridine
Ub	ubiquitin
UBC	catalytic core domain of ubiquitin-conjugating enzymes
UBC2	Ubiquitin-conjugating enzyme E2 2 from yeast
UBE2	ubiquitin-conjugating enzyme E2
ULP1	ubiquitin-like-specific protease 1
V	valine, Val
W	tryptophane, Trp
Wnt	wingless-type MMTV integration site family member
WT	wild-type
XRCC4	X-ray repair Cross-Complementing protein 4
Y	tyrosine, Tyr
YNB	yeast nitrogen base

7.2 List of figures

7.3 List of tables

7.4 List of publications

A.K.L. Liess, A. Kucerova, K. Schweimer, L. Yu, T.I. Roumeliotis, M. Diebold, O. Dybkov, C. Sotriffer, H. Urlaub, J.S. Choudhary, J. Mansfeld, S. Lorenz, Autoinhibition Mechanism of the Ubiquitin-Conjugating Enzyme UBE2S by Auto-ubiquitination, Structure 27 (2019) 1195-1210.e7.

A.K.L. Liess, A. Kucerova, M-A. Letzelter, K. Schweimer, D. Schlesinger, O. Dybkov, H. Urlaub, J. Mansfeld, S. Lorenz, Dimerization regulates the human APC/C associated ubiquitin-conjugating enzyme UBE2S, *in revision*

L.K. Ries, A.K.L. Liess, C.G. Feiler, D.E. Spratt, E. Lowe, S. Lorenz, Crystal structure of the catalytic C-lobe of the HECT-type ubiquitin ligase E6AP, Protein Science (2020)

7.5 Conference contributions

Poster presentation at the 10th International GSLS Student Symposium “EUREKA! 2015”, October 14-15, 2015, Würzburg/Germany: *Elucidating regulatory mechanisms of the ubiquitin-conjugating enzyme UBE2S*

Poster presentation at the 11th International GSLS Student Symposium “EUREKA! 2016”, October 12-13, 2016, Würzburg/Germany: *Elucidating regulatory mechanisms of the ubiquitin-conjugating enzyme UBE2S*

Poster presentation at the 12th International GSLS Student Symposium “EUREKA! 2017”, October 11-12, 2017, Würzburg/Germany: *Elucidating regulatory mechanisms of the ubiquitin-conjugating enzyme UBE2S*

Poster presentation at the EMBO Workshop “Modularity of signaling proteins and networks”, September 16-21, 2018, Seefeld in Tirol/Austria: *Elucidating the regulation of ubiquitin-conjugating enzymes by auto-ubiquitination*

Oral presentation at the EMBO YIP Sectional Meeting “Structural and RNA Biology”, June 5-6, 2019, Rauischholzhausen/Germany: *Understanding the regulation of the ubiquitin-conjugating enzyme UBE2S*

Poster presentation at the EMBO Workshop “The ubiquitin system: Biology, mechanisms and roles in disease”, September 13-17, 2019, Cavtat/Croatia: *Elucidating regulation mechanisms in the APC/C-associated ubiquitin-conjugating enzyme UBE2S*

7.6 Curriculum vitae

7.7 Acknowledgments

The work on this thesis would not have been possible without those who accompanied and supported me and therefore I would like to express my sincere gratitude towards them.
First of all, I would like to thank my supervisor Dr. Sonja Lorenz for her constant support, the guidance and help throughout this thesis and her positive attitude and enthusiasm towards science, even when others did not (yet) believe in the project. I am very grateful for her advice, the opportunity to present my data at several meetings and conferences and for our music session.
Furthermore, I would like to thank my thesis committee members Dr. Jörg Mansfeld and Prof. Dr. Hermann Schindelin for insightful discussions, constructive criticism and the opportunity to gain from their knowledge.

The success of this thesis is also based on many excellent collaborations. I would like to emphasize Alena Kucerova and Dr. Jörg Mansfeld for supporting the projects depicted in this thesis by performing all cell-based experiments. I would like to thank them for many stimulating discussions and ideas as well as for the great time at our retreat in Königswinter. Additionally, I would like to thank Dr. Bodo Sander, Dr. Christian Feiler and Marie-Annick Letzelter for chairing not only parts of this project but also their enormous experience.
For great experimental support, I would like to thank Dr. Kristian Schweimer from the University of Bayreuth, Dr. Olexandr and Prof. Dr. Henning Urlaub from the Max Planck Institute for Biophysical Chemistry, Göttingen, Dr. Lu Yu, Dr. Theodoros I. Roumeliotis and Dr. Jyoti S Choudhary from the The Institute of Cancer Research, London and Mathias Diebold and Prof. Dr. Christoph Sotriffer from the University of Würzburg.

I would also like to thank all current and past members of the structural biology for creating cheerful and welcoming working atmosphere, especially Dr. Elisabeth Schönwetter, Dr. Lena Ries and Dr. Johanna Bialas, with whom I spent many wonderful hours.

Additionally, I would like to thank Dr. Bernhard Fröhlich and Roland Markert for their excellent technical help, Julia Haubenreißer for excellent maintenance of our lab and Maria Gallant and the GSLS team for their help in administrative issues and the support during the thesis submission.

For financial support, I would like to thank the Emmy Noether Program of the German Research Foundation, the Graduate School of Life Sciences (GSLS) of the University of Würzburg and the GRK 2243 "Understanding Ubiquitylation: From Molecular Mechanisms to Disease".

Lastly, I would like to warmly acknowledge my family and friends who always supported me and knew how to cheer me up. Especially, I would like to appreciate my husband Andreas, who never stopped believing in me and my capabilities, as well as my parents, for their encouragement, wonderful support and love. Without them, all this would not have been possible!

7.8 Affidavit

Affidavit

I hereby confirm that my thesis entitled “Understanding the regulation of the ubiquitin-conjugating enzyme UBE2S” is the result of my own work. I did not receive any help or support from commercial consultants. All sources and/or materials are listed and specified in the thesis.
Furthermore, I confirm that this thesis has not yet been submitted as part of another examination process neither in identical nor in similar form.

Place, Date

Signature

Eidesstattliche Erklärung

Hiermit erkläre ich an Eides statt, die Dissertation „Die Regulation des Ubiquitin-konjugierenden Enzyms UBE2S“ eigenständig, d.h. insbesondere selbstständig und ohne Hilfe eines kommerziellen Promotionsberaters, angefertigt und keine anderen als die von mir angegebenen Quellen und Hilfsmittel verwendet zu haben.
Ich erkläre außerdem, dass die Dissertation weder in gleicher noch in ähnlicher Form bereits in einem anderen Prüfungsverfahren vorgelegen hat.

Ort, Datum

Unterschrift